

**Natural and enhanced retardation of carbon-14 in contaminated  
groundwater**

Aislinn Ann Boylan

Submitted in accordance with the requirements for the degree of  
Doctor of Philosophy

The University of Leeds  
School of Earth and Environment

June 2017

The candidate confirms that the work submitted is her own, except where work which has formed part of jointly-authored publications has been included. The contribution of the candidate and the other authors to this work has been explicitly indicated below. The candidate confirms that appropriate credit has been given within the thesis where reference has been made to the work of others.

Chapter 5: “Mechanisms of inorganic carbon-14 attenuation in contaminated groundwater: Effect of solution pH on isotopic exchange and carbonate precipitation reactions”.

This work has been accepted for publication in *Applied Geochemistry*:

**Boylan, A.A.**, Stewart, D.I., Graham, J.T., Trivedi, D., Burke, I.T., 2016. Mechanisms of inorganic carbon-14 attenuation in contaminated groundwater: Effect of solution pH on isotopic exchange and carbonate precipitation reactions. *Applied Geochemistry*.

Candidate’s contribution – principal author, performed all experimental work, concept development, interpreted data, developed PHREEQC model, prepared the manuscript. D.I. Stewart – concept development, extensive manuscript review. J.T. Graham – concept development, manuscript review. D Trivedi – PHREEQC model development. I.T Burke – initial concept, concept development, extensive review.

Chapter 6: “The behaviour of carbon-14 containing low molecular weight organic compounds in contaminated groundwater under aerobic conditions” presents work that is in preparation to form a jointly authored publication.

Candidate’s contribution – principal author, performed all experimental work, concept development, preparation of manuscript. D.I. Stewart – concept development, manuscript review. J.T. Graham – concept development, manuscript review. I.T Burke – initial concept, concept development, manuscript review.

Chapter 7: “The behaviour of low molecular weight organic carbon-14 containing compounds in contaminated groundwater during denitrification and iron-reduction” presents work that is in preparation to form a jointly authored publication.

Candidate’s contribution – principal author, performed all experimental work, concept development, preparation of manuscript. D.I. Stewart – concept development, manuscript review. J.T. Graham – concept development. I.T Burke – initial concept, concept development, manuscript review.

This copy has been supplied on the understanding that it is copyright material and that no quotation from the thesis may be published without proper acknowledgement.

The right of Aislinn Ann Boylan to be identified as Author of this work has been asserted by her in accordance with the Copyright, Designs and Patents Act 1988.

© 2017 The University of Leeds and Aislinn Ann Boylan

## Acknowledgements

I would like to express my sincere thanks to Ian Burke, Doug Stewart and James Graham for their knowledge, support and most especially for their continued enthusiasm over the past few years. I'd also like to thank Divyesh Trivedi for all his help. A special mention to all the technical staff who have helped me with this project, particularly Andy Connelly and Fiona Keay for battling the AA3. I'd also like to thank EPSRC, NNL and Sellafield Ltd. for funding this project.

A big thank you goes to the Cohen Geochemistry group, past & present, but particularly Burko's Science Club. I have to mention the SCR tribe who have ensured that I had the best time at work, even on the worst days, Becky – for the holidays & the alcohol, Adam – for being ridiculous, Kathy – I can't thank you enough for the dates & the food, Mark – a special thank you for a special person, JT – mainly for the fish pie ...& the flatpack...& the lego, I couldn't have wished for a better housemate, Andy B – I should say for the science, but it's really for the slightly aggressive dancing and finally to Andy, what can I say? Have a nice life.

A huge thank you to Binks for being so supportive, and finally, most importantly, I'd like to say the biggest thank you to the Boylan-Payne's: Mum, Meg, Ed, Mags, Rafa, Doylean, Nic, Nors, Ives, Gezza and James 'Dino' Witts. I couldn't have done it without you.

## **Abstract**

Radiocarbon ( $^{14}\text{C}$ ) is one of the most ubiquitous radionuclide contaminants due to its formation at every stage of the nuclear power generation process. Authorised discharges and accidental release from anthropogenic activity have meant the concentration of this radionuclide at nuclear contaminated sites can be many orders of magnitude higher than the naturally occurring levels of  $^{14}\text{C}$ . It is of interest as a contaminant due to its long half-life ( $5730 \pm 40\text{a}$ ; Godwin, 1962) and bioavailability. This thesis investigates the processes affecting the behaviour of inorganic and organic forms of  $^{14}\text{C}$  in subsurface environments. The first section of this work identified the key attenuation mechanisms of inorganic  $^{14}\text{C}$  in subsurface environments. The precipitation of  $^{14}\text{C}$ -carbonate minerals in subsurface environments is enhanced by the availability of  $\text{Ca}^{2+}$  and by the abundance of nucleation sites. Maximum  $^{14}\text{C}$  removal in solid isotopic exchange experiments occurred after approximately 2 weeks equilibration and the amount of  $^{14}\text{C}$  removed from solution was proportional to the amount of calcite surface area present. These results suggest that if inorganic  $^{14}\text{C}$  is released into subsurface environments, both precipitation and solid phase isotopic exchange can result in non-conservative  $^{14}\text{C}$ -labelled dissolved inorganic carbon transport and so  $^{14}\text{C}$  contamination may persist in groundwater for decades following accidental releases. The results of the experiments using  $^{14}\text{C}$ -labelled low molecular weight organic substances suggest that ubiquitous and diverse bacterial phyla are able to utilise a range of  $^{14}\text{C}$ -containing low molecular weight organic substances very rapidly, and thus such substances are unlikely to persist in aerobic or denitrifying shallow subsurface environments, however under iron reducing conditions there is potential that a proportion of  $^{14}\text{C}$ -formaldehyde and  $^{14}\text{C}$ -methanol may persist for longer in groundwater and therefore spread further in subsurface environments.

## Table of Contents

<b>Acknowledgements</b> .....	<b>v</b>
<b>Abstract</b> .....	<b>vi</b>
<b>Table of Contents</b> .....	<b>vii</b>
<b>List of Tables</b> .....	<b>xii</b>
<b>List of Figures</b> .....	<b>xiv</b>
<b>Abbreviations</b> .....	<b>xviii</b>
<b>Chapter 1 Project relevance and thesis structure</b> .....	<b>1</b>
1.1 Project context and relevance .....	1
1.2 Research goals and approach .....	3
1.3 Thesis structure .....	4
1.4 References .....	6
<b>Chapter 2 Literature Review</b> .....	<b>7</b>
2.1 Overview of Carbon-14 formation .....	7
2.1.1 Forms of <sup>14</sup> C in the environment.....	11
2.2 Biogeochemical cycling of carbon .....	12
2.2.1 Mobility and fate of inorganic <sup>14</sup> C.....	12
2.2.2 Inorganic interactions with solid surfaces .....	14
2.2.3 Mobility and fate of <sup>14</sup> C-containing LMWO compounds .....	18
2.3 The nuclear legacy.....	26
2.3.1 Sellafield reprocessing site, Cumbria, UK .....	27
2.3.2 Geology of Sellafield.....	30
2.3.3 Hydrogeology.....	30
2.3.4 Radionuclide contamination .....	33
2.4 References .....	36
<b>Chapter 3 Methods</b> .....	<b>55</b>
3.1 Sediment collection.....	55
3.2 Sediment and mineral characterisation .....	56
3.2.1 X-ray Diffraction.....	56
3.2.2 Surface area determination.....	57
3.3 Iron analysis by spectrophotometry .....	58
3.3.1 Determination of total aqueous Fe.....	59
3.3.2 Determination of extractable Fe(II) in sediments .....	60
3.4 Determination of nitrate and nitrite by Auto Analyser3 .....	61

3.5	Batch microcosm experiments .....	61
3.5.1	Heat sterilisation .....	62
3.5.2	Microcosm sampling technique.....	62
3.5.3	Carbon-14 spike details.....	63
3.6	Microbiological analysis.....	63
3.7	Statistical analysis.....	64
3.7.1	Standard deviation and relative standard deviation.....	64
3.7.2	Defining microbiological diversity .....	65
3.8	Thermodynamic modelling.....	66
3.9	References .....	68
<b>Chapter 4 Method development – measuring <sup>14</sup>C.....</b>		<b>72</b>
4.1	Description of liquid scintillation.....	72
4.2	Liquid scintillation protocol for all samples and standards.....	74
4.2.1	Statistics of counting .....	75
4.3	Counting aqueous inorganic <sup>14</sup> C.....	76
4.3.1	Cocktail optimisation .....	76
4.3.2	Hionic Fluor counting procedure .....	81
4.4	Counting aqueous organic <sup>14</sup> C.....	82
4.4.1	EcoScint A counting procedure .....	84
4.5	Counting aqueous <sup>14</sup> C-inorganic and <sup>14</sup> C-organic mixed samples.....	85
4.6	Counting <sup>14</sup> CO <sub>2</sub> (g) .....	87
4.7	Summary of approach for <sup>14</sup> C measurement.....	87
4.8	Sequential Extractions .....	88
4.8.1	Permafluor E.....	91
4.9	References .....	92
<b>Chapter 5 Mechanisms of inorganic carbon-14 attenuation in contaminated groundwater: Effect of solution pH on isotopic exchange and carbonate precipitation reactions. ....</b>		<b>94</b>
5.1	Executive Summary .....	94
5.2	Introduction .....	95
5.3	Materials and Methods.....	102
5.3.1	Thermodynamic modelling .....	102
5.3.2	Precipitation experiments.....	102
5.3.3	Isotopic exchange experiments .....	104
5.4	Results .....	106
5.4.1	XRD .....	106

5.4.2	Homogeneous and heterogeneous precipitation.....	108
5.4.3	Solid phase isotopic exchange.....	110
5.4.4	Atmospheric isotopic exchange.....	111
5.5	Discussion.....	114
5.5.1	Effect of seed crystals (nucleation sites) on the precipitation of calcium carbonate.....	114
5.5.2	Contribution of solid phase isotopic exchange to <sup>14</sup> C retardation.....	115
5.5.3	Rate of atmospheric isotopic exchange as a function of solution pH.....	117
5.6	Implications.....	122
5.6.1	Implications for surface release of <sup>14</sup> C-containing water.....	122
5.6.2	Implication for subsurface release of <sup>14</sup> C-containing water.....	123
5.6.3	Historical Release of <sup>14</sup> C to the Subsurface at the UK Sellafield Site.....	125
5.7	Conclusion.....	128
5.8	References.....	129
<b>Chapter 6 The behaviour of carbon-14 containing low molecular weight organic compounds in contaminated groundwater under aerobic conditions .....</b>		<b>139</b>
6.1	Executive Summary.....	139
6.2	Introduction.....	140
6.3	Materials and Methods.....	144
6.3.1	Sediment.....	144
6.3.2	<sup>14</sup> C-DOC partitioning under aerobic incubation (open flasks).....	144
6.3.3	Short term <sup>14</sup> C-DOC partitioning in aqueous fraction (closed bottles).....	146
6.3.4	Amount of <sup>14</sup> C associated with total inorganic carbon (TIC) and total organic carbon (TOC) in sediment from the aerobic incubation experiments.....	147
6.3.5	DNA extraction and sequencing of the V4 hyper-variable region of the 16S rRNA gene.....	149
6.4	Results.....	151
6.4.1	Sediment characterisation.....	151
6.4.2	The partitioning of <sup>14</sup> C-labelled organic compounds under aerobic conditions (open flasks).....	152
6.4.3	Short term <sup>14</sup> C-DOC partitioning in aqueous fraction (closed bottles).....	155
6.4.4	Microbial community analysis.....	157
6.5	Discussion.....	161
6.5.1	The behaviour of <sup>14</sup> C-labelled LMWO substances in solution.....	161
6.5.2	Partitioning of aqueous <sup>14</sup> C-labelled LMWO substances in to solid fraction.....	163

6.5.3	Transformation of aqueous <sup>14</sup> C-labelled LMWO substances to <sup>14</sup> CO <sub>2</sub> (g) by microbial utilisation.....	164
6.5.4	Impact of organic contaminants on natural microbial populations ...	166
6.6	Conclusions .....	167
6.7	References .....	168
<b>Chapter 7 The behaviour of low molecular weight organic carbon-14 containing compounds in contaminated groundwater during denitrification and iron-reduction. ....</b>		<b>176</b>
7.1	Executive Summary .....	176
7.2	Introduction .....	177
7.3	Materials and Methods.....	181
7.3.1	Sediment.....	181
7.3.2	Bioreduction microcosms.....	181
7.3.3	Geochemical methods .....	182
7.3.4	<sup>14</sup> C associated with sediment.....	183
7.3.5	Microbiology .....	184
7.4	Results .....	186
7.4.1	Sediment characterisation.....	186
7.4.2	Microcosm geochemical conditions.....	186
7.4.3	The behaviour of <sup>14</sup> C-labelled LMWO compounds under denitrifying conditions .....	187
7.4.4	The behaviour of <sup>14</sup> C-labelled LMWO compounds under iron-reducing conditions .....	192
7.4.5	Microbial community composition.....	196
7.5	Discussion .....	200
7.5.1	The behaviour of aqueous <sup>14</sup> C-LMWO substances during denitrification .....	200
7.5.2	The behaviour of aqueous <sup>14</sup> C-LMWO substances under iron reducing conditions .....	202
7.5.3	Implications for persistence of <sup>14</sup> C-containing LMWO compounds in anaerobic subsurface environments.....	204
7.6	Conclusions .....	205
7.7	References .....	206
<b>Chapter 8 Conclusions .....</b>		<b>213</b>
8.1	Summary of results.....	213
8.2	Implications.....	215
8.3	Future research .....	217
8.4	References .....	218

<b>Appendix A</b>	<b>Supporting Information for Chapter 5</b>	<b>220</b>
A.1	Tables	220
A.2	Determining the value of the rate constant ( $k_{r2}$ )	220
A.3	Solution compositions for input files for PHREEQC modelling	222
A.4	Calculating the thickness of the calcite surface layer	222
<b>Appendix B</b>	<b>Supporting information for Chapter 6</b>	<b>224</b>
B.1	Experimental results for open flask experiments	224
<b>Appendix C</b>	<b>Supporting information for Chapter 7</b>	<b>225</b>
C.1	Experimental results for complete experimental run	225
C.1.1	Nitrate amended microcosms	225
C.1.2	Iron reducing microcosms	226
C.2	Sterile control figures	227
C.3	Siderite precipitation	229
C.4	References	229
<b>Appendix D</b>	<b>PHREEQC modelling code</b>	<b>230</b>
D.1	Note for users	230
D.2	PHREEQC code	230
D.2.1	To establish the solution compositions required to obtain the desired $SI_{CAL}$ values	230
D.2.2	To investigate the variation of $SI_{CAL}$ with calcium concentration, carbonate alkalinity and pH	232
D.2.3	To model potential leach scenarios relevant to Sellafield Reprocessing site, UK	238
D.2.4	Modelling siderite precipitation	239
D.3	References	240
<b>Appendix E</b>	<b>Presentations</b>	<b>241</b>
E.1	Oral presentations	241
E.2	Poster presentations	242

## List of Tables

Table 2-1 Calcium carbonate mineral formation conditions.....	16
Table 2-2 The associated energy yield with terminal electron accepting processes at pH 7 (Konhauser et al., 2002). .....	21
Table 2-3 Quaternary Drift in the Sellafield Buried Channel, adapted from Cruickshank, 2012.....	31
Table 3-1 Input solution compositions for precipitation experiments to achieve desired range of Saturation Indices. ....	67
Table 3-2 PHREEQC input code for modelling the interaction of silo leachate with groundwater under Sellafield reprocessing site, UK. pH was allowed to equilibrate within the model to achieve charge balance. ....	68
Table 5-1 Solution composition for precipitation experiments. All Na <sub>2</sub> CO <sub>3</sub> solutions equilibrated with atmospheric CO <sub>2</sub> for 72 hours prior to mixing.....	103
Table 5-2 Solution composition for atmospheric isotopic exchange experiments.....	106
Table 6-1 Solution composition for synthetic groundwater, modified from Wilkins et al., (2007). ....	146
Table 6-2 Percentage recovered of organic and inorganic bound <sup>14</sup> C in sediment and <sup>14</sup> C-DOC at the end of the low concentration (10 <sup>-5</sup> M) experiments.....	155
Table 6-3 Concentration of organic <sup>14</sup> C in aqueous pool and gaseous pool (as CO <sub>2</sub> (g)) at 48 hour sampling point in low concentration experiments.....	156
Table 6-4 Alpha-diversity measures, D <sub>0</sub> <sup>α</sup> , species richness, D <sub>1</sub> <sup>α</sup> , exponential of Shannon entropy and concentration, D <sub>2</sub> <sup>α</sup> , inverse of the Simpson concentration. Values displayed to 3 significant figures. Ac – acetate; Fo – formate; Fy – formaldehyde and Me – methanol.....	160
Table 7-1 Solution composition for synthetic groundwater A) unamended and B) high nitrate, both adjusted to pH 7.2 modified from Wilkins et al (2007). ....	182
Table 7-2 Geochemical conditions measured in unaltered microcosms within one hour of establishment. ....	187
Table 7-3 The results of the CO <sub>2</sub> (g) measurement and solid fraction sequential extraction expressed as a percentage of the original activity addition for denitrification experiments. All measurements were based on one sample; where error measurement is recorded this corresponds to the standard deviation of replicate samples taken from an individual gas wash bottle. DIC – dissolved inorganic carbon; TIC – total inorganic carbon; TOC – total organic carbon...	191
Table 7-4 The results of the CO <sub>2</sub> (g) measurement and solid fraction sequential extraction expressed as a percentage of the original activity addition for iron-reducing experiments. All measurements were based on one sample; where error measurement is recorded this corresponds to the standard deviation of replicate samples taken from the gas wash bottle. ....	196

Table 7-5 Alpha-diversity measurements, $D_0^\alpha$ , species richness, $D_1^\alpha$ , exponential of Shannon entropy, $D_2^\alpha$ , inverse of the Simpson index for samples under denitrification (Ac- acetate; Fo- formate; Fy- formaldehyde; Me-methanol).....	200
Table A-1 Input solution compositions for PHREEQC precipitation modelling. ....	220
Table A-2 Calculated values of $kr_2$ using Equation S2 and $k_{obs}$ values. ....	221
Table C-1 Input solution composition for siderite precipitation model.....	229

## List of Figures

Figure 2-1 Speciation of aqueous carbonate species across a range of pH in a simple 0.1 M NaCl solution, modelled using a closed system with a $p\text{CO}_2 = -3.5$ in PHREEQC, $\text{CO}_2 = \text{CO}_2(\text{aq}) + \text{H}_2\text{CO}_3(\text{aq})$ . .....	13
Figure 2-2 The biological pathway from nitrate to nitrogen, facilitated by microbial activity. Purple text highlights the enzymes needed for the reduction to occur... 22	
Figure 2-3 Direct/enzymatic reduction and indirect methods for the reduction of redox active elements by metal reducing bacteria (adapted from Tabak et al., 2005).....	24
Figure 2-4 Aerial photo of the Sellafield site, © Nuclear Management Partners, 2016. 28	
Figure 2-5 Outline map of the Sellafield reprocessing site. The site boundary is outlined in blue, the Separation Area is shown in red. Regional setting of the Sellafield site within the county of Cumbria is shown (inset). Map reproduced from Sellafield Ltd., 2016 groundwater monitoring report.....	29
Figure 2-6 Diagrams showing the groundwater flow through site, reproduced from Sellafield Contaminated Land and Groundwater Management (Cruickshank, 2012). See Table 2-3 for definitions of hydrological units (HU).....	32
Figure 2-7 Sellafield site with $^{14}\text{C}$ concentrations measured in monitoring wells in 2015. The site boundary is outlined in blue, the Separation Area is shown in red. Map reproduced from Sellafield Ltd., 2016 groundwater monitoring report. ....	35
Figure 3-1 Site map showing location of sediment collection. Adapted from Wallace et al. (2012). .....	55
Figure 4-1 Taken from Thomson (2001) showing the pathway from radioactive decay energy emission to the detection of photons by the PMTs. The diagram also highlights the different stages of the energy transfer process which may be impacted by differing types of quench.....	73
Figure 4-2 Efficiency of count against activity in standard, based on 2 mL of standard volume with 10 mL of EcoScint A scintillation cocktail. Dark blue columns represent aliquots prepared with deionised water, light blue columns represent aliquots prepared using a synthetic groundwater composition. ....	77
Figure 4-3 Comparison of EcoScint A and Gold Star scintillation cocktails: determining the impact of increasing matrix pH to retain $^{14}\text{C}$ in scintillant.....	78
Figure 4-4 Comparing the efficiency of EcoScint A (dark blue) and Hionic Fluor (grey) against the activity of $^{14}\text{C}$ across a calibration range. ....	80
Figure 4-5 Comparing the count stability in glass and plastic vials for inorganic carbon-14 after 24 and 48 hours over a calibration range.....	81
Figure 4-6 Calibration for inorganic $^{14}\text{C}$ -labelled sodium carbonate, prepared using 9 mL of Hionic-Fluor with a 100 $\mu\text{L}$ addition of 2M NaOH and 1000 $\mu\text{L}$ of standard in glass vials. $R^2$ value = 0.9988. ....	82
Figure 4-7 Comparison of calibration using EcoScint A and Hionic-Fluor scintillation cocktails. ....	84

Figure 4-8 Calibrations for all organic  $^{14}\text{C}$  labelled compounds, prepared using 10 mL of EcoScint A with 800  $\mu\text{L}$  of standard.  $R^2$  values = 0.9991; 0.9964; 0.9992 and 0.9992 for acetate, formate, formaldehyde and methanol respectively.....85  
86

Figure 4-9 Comparison of the calibration standards in EcoScintA (blue) and Hionic-Fluor (grey) for the mixed calibration.....86

Figure 5-1 X-ray diffraction pattern showing the sample data (black line) and standard fit for kaolinite (red), mica (blue) and quartz (green). ..... 107

Figure 5-2 X-ray diffraction pattern showing the sample data (black line) and calcite standard (red line). ..... 108

Figure 5-3 Homogeneous and heterogeneous precipitation reactions (a) final pH after seven day incubation against the initial predicted saturation index (b) experimental data showing the percentage of  $^{14}\text{C}$  in solution after seven day incubation plotted against the predicted initial calcite saturation index of solution ( $\text{SI}_{\text{CAL}}$ ). Error bars show one standard deviation of triplicate measurements; where not shown, error bars are less than the size of the symbols used. .... 109

Figure 5-4 (a) the amount of  $^{14}\text{C}$  associated with the solid phase against time in hours (b) the amount of  $^{14}\text{C}$  in solid against the surface area of the calcite after two months incubation. Error bars show one standard deviation of triplicate measurements; where not shown, error bars are less than the size of the symbols used. .... 111

Figure 5-5 (a) pH measurement over time in open flask experiments, (b) pH measurement over time in closed bottle experiments, (c) the percentage of  $^{14}\text{C}$  remaining in solution over time in open experiments, (d) the percentage of  $^{14}\text{C}$  remaining in solution over time in closed experiments. Error bars show one standard deviation of triplicate measurements; where not shown, error bars are less than the size of the symbols used. .... 113

Figure 5-6 PHREEQC closed system model predicting the solution compositions necessary for calcite saturation ( $\text{SI} > 0$ , to the right of the blue line) and homogeneous precipitation ( $\text{SI} > 1.5$  to the right of the orange line); (a) at pH 7, (b) at pH 9, and (c) at pH 11..... 114

Figure 5-7 (a) the experimental results showing the percentage of  $^{14}\text{C}$  remaining in solution over time in open system on a log scale (b) experimental data fitted with predicted rate of loss using the derived value of  $k_{z2} = 4500 \text{ hr}^{-1}$  for the rate constant. .... 121

Figure 5-8 Predicted saturation indices for the mixing of two potential leachate plumes with groundwater on Sellafield site (a) surface tank composition from the MAGNOX silo (site data – dotted line) (b) deep tank liquor from the MAGNOX silo (modelled – dashed line). .... 128

Figure 5-9 Schematic model of processes affecting the  $^{14}\text{C}$ -DIC transport in surface and subsurface environments..... 129

- Figure 6-1 The formation of organic  $^{14}\text{C}$  compounds in the nuclear power generation process under varying redox conditions with corresponding ratio of LMWO formation in comparison to formate (McCollom and Seewald, 2007; Kaneko et al., 2003; Wieland and Hummel, 2015). ..... 142
- Figure 6-2 Apparatus for the wet acidification and oxidation of sediment: a)  $\text{N}_2(\text{g})$  inlet line; b) stirrer hotplate; c) water bath; d) 250mL round bottom flask with three inlets; e) sample and reagent addition ; f) 125 mL gas washing tube with frit (porosity 0) containing 100 mL of Carbo-Sorb E for  $^{14}\text{C}$  capture and g) 125 mL gas washing tube with frit (porosity 0) containing 100 mL of 1M NaOH acting as a safety bottle to prevent the release of  $^{14}\text{CO}_2(\text{g})$ . Arrows represent the direction of  $\text{N}_2(\text{g})$  flow through the apparatus..... 148
- Figure 6-3 XRD plot of Calder Bridge sediment..... 152
- Figure 6-5 Data from both open flask (replotted from Figure 6-4) and corresponding closed bottle experiments for: (a)  $^{14}\text{C}$ -acetate amended experiments; (b)  $^{14}\text{C}$ -formate amended experiments; (c)  $^{14}\text{C}$ -formaldehyde amended experiments; and, (d)  $^{14}\text{C}$ -methanol amended experiments. Error bars denote one standard deviation of triplicate measurements; where not shown, error bars are less than the size of the symbols used. .... 156
- Figure 6-6 Bacterial phylogenetic diversity within unaltered sediment (A-C); high concentration systems and low concentration systems (Ac- acetate; Fo- formate; Fy- formaldehyde; Me- methanol). Phyla with relative abundance less than 1% of the total population are grouped as “Other”. Dashed line denotes classes of Proteobacteria descending as follows: unclassified;  $\alpha$ ;  $\beta$ ;  $\gamma$ ;  $\delta$ . .... 159
- Figure 6-7 Two-dimensional non-metric multidimensional scaling (NMDS) ordination for differences in the bacterial community composition distribution based on Bray-Curtis distances of the community (OTUs) by site/sample matrix. Un A, B, C – unaltered sediment samples. Ac – acetate; Fo – formate; Fy – formaldehyde and Me – methanol. H corresponds to high concentration ( $10^{-2}$  M), L to low concentration ( $10^{-5}$  M). The stress value associated with this two dimensional representation is  $<0.05$  which suggests reasonable fit with the data.161
- Figure 7-1 The results of the denitrification experiments a) pH; b) percentage of  $^{14}\text{C}$  in solution; c) concentration of nitrite in solution; d) concentration of nitrate in solution (original nitrate addition = 10mM,  $t=7$  indicates time of  $^{14}\text{C}$  addition). Experiment duration from day 7 to day 14 (acetate and formate) continuing to day 22 for formaldehyde and methanol (data not shown). Error bars denote one standard deviation of triplicate measurements; where not shown error bars are less than the size of the symbol used. .... 190
- Figure 7-2 The results of the iron-reducing experiments a) pH; b) percentage of  $^{14}\text{C}$  remaining in solution; c) fraction of Fe(II) in solids; d) concentration of nitrite; e) concentration of Fe(II) in solution; f) concentration of nitrate. Experiment duration from day 28 to day 35 (acetate and formate) continuing to day 60 for formaldehyde and methanol (data not shown) Error bars denote one standard deviation of triplicate measurements; where not shown error bars are less than the size of the symbol used..... 195

Figure 7-3 Bacterial phylogenetic diversity within the unaltered sediment (A-C) and under denitrification and iron reduction (Ac- acetate; Fo- formate; Fy- formaldehyde; Me-methanol). Phyla with relative abundance less than 1% of the community are grouped as “Other”. Dashed line denotes classes of Proteobacteria descending as follows: unclassified;  $\alpha$ ;  $\beta$ ;  $\gamma$ ;  $\delta$ ..... 199

Figure B 1 Experimental results from open flask experiments showing the evolution of pH and  $^{14}\text{C}$ -DOC activity with time in (a, b)  $^{14}\text{C}$ -acetate amended experiments; (c, d)  $^{14}\text{C}$ -formate amended experiments; (e, f)  $^{14}\text{C}$ -formaldehyde amended experiments and, (g, h)  $^{14}\text{C}$ -methanol amended experiments. Error bars denote one standard deviation of triplicate measurements; where not shown, error bars are less than the size of the symbols used..... 224

Figure C 1 The results of the denitrification experiments a) pH; b) percentage of  $^{14}\text{C}$  in solution; c) concentration of nitrite in solution; d) concentration of nitrate in solution (original nitrate addition = 10mM, t=7 indicates time of  $^{14}\text{C}$  addition). Experiment duration from day 7 to day 14 (acetate and formate) continuing to day 22 for formaldehyde and methanol. Error bars denote one standard deviation of triplicate measurements; where not shown error bars are less than the size of the symbol used. .... 225

Figure C 2 The results of the iron-reducing experiments a) pH; b) percentage of  $^{14}\text{C}$  remaining in solution; c) fraction of Fe(II) in solids; d) concentration of nitrite; e) concentration of Fe(II) in solution; f) concentration of nitrate. Experiment duration from day 28 to day 35 (acetate and formate) continuing to day 60 for formaldehyde and methanol. Error bars denote one standard deviation of triplicate measurements; where not shown error bars are less than the size of the symbol used. .... 226

Figure C-3 The results of the denitrification control experiments a) pH; b) percentage of  $^{14}\text{C}$  in solution; c) concentration of nitrite in solution; d) concentration of nitrate in solution (original nitrate addition = 10mM, t=7 indicates time of  $^{14}\text{C}$  addition). Experiment duration from day 7 to day 14..... 227

Figure C-4 The results of the iron-reducing control experiments a) pH; b) percentage of  $^{14}\text{C}$  remaining in solution; c) fraction of Fe(II) in solids; d) concentration of nitrite; e) concentration of Fe(II) in solution; f) concentration of nitrate. Experiment duration from day 28 to day 35..... 228

## Abbreviations

AOD	Above Ordnance Datum
BET	Brunauer-Emmett-Teller
CANDU	CANada Deuterium Uranium
DIC	Dissolved Inorganic Carbon
DIW	DeIonised Water
DOC	Dissolved Organic Carbon
HDPE	High-Density PolyEthylene
LMWO	Low Molecular Weight Organic
NDA	Nuclear Decommissioning Authority
NMDS	Non-metric Multi-Dimensional Scaling
OTU	Operational Taxonomic Unit
RDP	Ribosomal Database Project
TEA/P	Terminal Electron Acceptors/Accepting Processes
THORP	THermal Oxide Reprocessing Plant
TIC	Total Inorganic Carbon
TOC	Total Organic Carbon
WHO	World Health Organisation
XRD	X-Ray Diffraction

## **Chapter 1 Project relevance and thesis structure**

This introductory chapter presents the rationale and context for this project. It provides a summary of nuclear subsurface contamination, with particular emphasis on the legacy of the UK nuclear industry to highlight the relevance of the work presented in this thesis. In addition it outlines the objectives of this project and provides a brief overview of the structure of the thesis.

### **1.1 Project context and relevance**

Nuclear power has been used for commercial electricity generation for decades, beginning with a series of experimental reactors in the 1940s which used both thorium and uranium as fuel sources. For the majority of the following decades the uranium powered boiling water reactors were the design adopted by most countries (Lillington, 2004). The deployment of nuclear power production has fluctuated over the past decades, decreasing in response to safety concerns over reactor accidents and the release of radionuclides to the environment, and increasing in recognition that a carbon-free, reliable energy source is necessary to mitigate the impacts of climate change. Currently there are 449 nuclear power plants worldwide which are producing energy (NEI, 2017) with increasing investment both in the UK and worldwide in a new fleet of reactors (NAMRC, NiA, 2013).

Many facilities in the UK are nearing the end of their lifetime, contributing further to the existing legacy of nuclear sites that are undergoing decommissioning and remediation (Beresford, 2005). Some of these facilities have discharged radioactivity to the environment, as part of authorised releases and due to accidental leaks (Gray et al., 1995; Hunter et al., 2004). To manage these sites over long timescales it is necessary to begin to define the nature and extent of the contamination and to assess how well we are able to predict the fate and behaviour of the contaminants concerned.

In the UK the responsibility for managing these sites lies with the Nuclear Decommissioning Authority in collaboration with site licence companies (NDA, 2010). Of all the sites in the NDA portfolio this project is primarily concerned with Sellafield reprocessing site in the north-west of England which began operating as a nuclear licensed site in 1947 (NDA, 2017) and is considered one of the most contaminated sites in Western Europe. Originally tasked with generating plutonium for military purposes the site expanded over time and began civil electricity production becoming the site of the world's first nuclear reactor to generate electricity commercially (NDA, 2017; Sellafield Ltd., 2010). The site has suffered some historic leaks and in particular throughout the 1970s a series of accidental leak events caused extensive subsurface contamination (Marshall et al., 2015).

Of the radionuclide contaminants, carbon-14 ( $^{14}\text{C}$ ) has long been considered of less concern due to the assumptions that it was inorganic in nature and would act conservatively in groundwater i.e. moving with groundwater flow off site and being

diluted in the Irish Sea. However recent groundwater monitoring of the site has been extended to include measurements of  $^{14}\text{C}$  activity and the long term retention of this radionuclide in groundwater underlying the site has been revealed (Stamper et al., 2012; Marshall et al., 2015).

This study aims to identify the major mechanisms for retention of aqueous inorganic  $^{14}\text{C}$  and apply these mechanisms to models of Sellafield reprocessing site to evaluate their likelihood. The behaviour of low molecular weight organic (LMWO)  $^{14}\text{C}$ -labelled substances in subsurface environments will be examined as these forms of  $^{14}\text{C}$  are often ignored as contaminants in groundwater environments. This study will also examine the ability of indigenous microbial populations to utilise the  $^{14}\text{C}$ -LMWO compounds under varying redox conditions which are found in the subsurface of many nuclear sites.

## 1.2 Research goals and approach

The principal goal of this thesis was to explore the biogeochemical cycles associated with  $^{14}\text{C}$ -labelled compounds relevant to contaminated groundwater scenarios. This was divided in to two distinct aims which were tested using a range of geochemical and microbiological techniques.

The first aim was to understand the likely transport pathways and fate of inorganic  $^{14}\text{C}$  species in near surface groundwater environments. This has been subdivided in to several objectives:

1. Determine the effect of the presence of cations such as  $\text{Ca}^{2+}$  and the pH of groundwater on the mobility of aqueous, inorganic  $^{14}\text{C}$ .

2. Investigate the extent of  $^{14}\text{CO}_3^{2-}$  isotopic exchange with solid carbonate.
3. Examine the atmospheric isotopic exchange process with stable  $\text{CO}_2(\text{g})$  and the impact of pH on the rate of this exchange.
4. Determine a rate equation for the atmospheric exchange between aqueous  $^{14}\text{C}$  and gaseous  $^{12/13}\text{CO}_2(\text{g})$ .
5. Consider the implications of these retention mechanisms on the behaviour of aqueous  $^{14}\text{C}$  in the subsurface environments of nuclear sites.

The second aim was to investigate the likely persistence of aqueous  $^{14}\text{C}$ -containing LMWO compounds in near surface sediments containing indigenous microbial populations. This aim was broken down in to several objectives:

1. Investigate the removal from aqueous phase and facilitation by microbial utilisation.
2. Examine the generation of gaseous  $^{14}\text{CO}_2(\text{g})$  due to the utilisation of  $^{14}\text{C}$ -LMWO.
3. Determine the extent of retention of  $^{14}\text{C}$  in solid fraction.
4. Study the impact of the electron donor on the composition of the indigenous microbial community.
5. Examine the effect of redox conditions on the behaviour  $^{14}\text{C}$ -LMWO substances.
6. Determine the implications of these results in the event of an accidental leak to subsurface of  $^{14}\text{C}$ -LMWO substances.

### **1.3 Thesis structure**

This thesis contains a general introduction to carbon-14 and the associated biogeochemical cycles, with a brief overview of the nuclear industry with which  $^{14}\text{C}$  is associated. This is followed by method and method development chapters detailing the

techniques used within the study and the development of techniques to measure  $^{14}\text{C}$  in a variety of states. These are followed by three chapters based on experimental work, a summary chapter and appendices.

Chapter 2 contains a literature review detailing the production and behaviour of  $^{14}\text{C}$ , before expanding to look at the associated biogeochemistry as well as an overview of the legacy of nuclear programmes worldwide, with emphasis on the Sellafield reprocessing site, UK.

Chapters 3 & 4 are method chapters with the first summarising all techniques used throughout this study and the second detailing the method development to measure  $^{14}\text{C}$  in a variety of states.

Chapter 5 presents the results of experimental work to establish the mechanisms of inorganic  $^{14}\text{C}$  attenuation in contaminated groundwater: The work aims to describe the behaviour of inorganic  $^{14}\text{C}$  in subsurface environments and models these behaviours using data based around the geochemical conditions at Sellafield site, UK. This work has been published in a paper entitled 'Mechanisms of inorganic  $^{14}\text{C}$  attenuation in contaminated groundwater: Effect of solution pH on isotopic exchange and carbonate precipitation reactions' in *Applied Geochemistry*.

Chapter 6 presents the results of experimental work using sediment of the same drift as Sellafield reprocessing site, UK, and the indigenous microbial population to study the behaviour of four different  $^{14}\text{C}$ -labelled LMWO substances in aerobic systems, using novel techniques to track the partitioning of  $^{14}\text{C}$  across aqueous, gaseous and solid phases.

Chapter 7 presents the results of an investigation in to the behaviour of LMWO  $^{14}\text{C}$  compounds during denitrification and iron-reducing conditions. This chapter uses a

series of microcosm experiments using sediment of the same drift as Sellafield reprocessing site, UK, and the indigenous microbial population with four forms of  $^{14}\text{C}$ -labelled LMWO substances to establish the impact of varying redox conditions on the  $^{14}\text{C}$  behaviour and consider the implications of release of  $^{14}\text{C}$ -labelled LMWO in to subsurface environments dominated by denitrification and iron reduction.

Chapter 8 contains a summary of the work presented in the thesis and suggestions for future work.

## 1.4 References

Beresford, N., 2005. Land contaminated by radioactive materials. *Soil Use and Management* 21, 468-474.

Gray, J., Jones, S., Smith, A., 1995. Discharges to the environment from the Sellafield site, 1951-1992. *Journal of Radiological Protection* 15, 99.

Hunter, J., 2004. SCLS Phase 1 - Conceptual Model of Contamination Below Ground at Sellafield.

Lillington, J. 2004. *The Future of Nuclear Power*, Oxford, Elsevier.

Marshall, A., Coughlin, D., Laws, F., 2015. Groundwater monitoring at Sellafield: Annual data review 2014.

NAMRC. *UK new build plans* [Online]. Available: <http://namrc.co.uk/intelligence/uk-new-build-plans/> [Accessed 19<sup>th</sup> May 2017]

NDA 2017. *NDA: About Us* [Online]. Available: <https://www.gov.uk/government/organisations/nuclear-decommissioning-authority/about#ndas-estate> [Accessed 19<sup>th</sup> May 2017]

NDA, 2010. The 2010 UK Radioactive Waste Inventory.

NiA, 2013. The Essential Guide for the Nuclear New Build Supply Chain. 2<sup>nd</sup> ed.

Sellafield, 2010. *Sellafield: Challenge* [Online]. Available: <http://www.sellafieldsites.com/challenge/> [Accessed 19<sup>th</sup> May 2017]

Stamper, A., McKinlay, C., Coughlin, D., Laws, F., 2012. Land Quality Programme Groundwater Monitoring at Sellafield. Sellafield Ltd.

## Chapter 2 Literature Review

This chapter begins with an overview of carbon-14 ( $^{14}\text{C}$ ) formation. This is followed by a section looking at biogeochemical processes which influence the behaviour of aqueous  $^{14}\text{C}$ , in particular the processes which affect mobility and fate of inorganic  $^{14}\text{C}$  and organic  $^{14}\text{C}$  (as low molecular weight organic compounds) with a review of microbial processes. Finally the chapter will conclude with a summary of the legacy of nuclear power production placing particular emphasis on contamination at Sellafield reprocessing site, UK, to which a large proportion of this thesis is related.

### 2.1 Overview of Carbon-14 formation

Carbon has an atomic number of 6 and is a member of group 14 of the periodic table. It is non-metallic and tetravalent, with four electrons to form covalent bonds. Carbon is present in all known life forms. It has three main isotopes, carbon-12 ( $^{12}\text{C}$ ), carbon-13 ( $^{13}\text{C}$ ) and  $^{14}\text{C}$ .  $^{14}\text{C}$  is a radioactive isotope which decays via beta decay with a long half-life of  $5730 \pm 40$  years (Godwin, 1962). The beta decay takes place at a rate following the law of radioactive decay. The rate is almost entirely independent of external factors such as temperature and pressure. It is dependent only on the nature and energy state of the nuclide (White, 2013). It is impossible to predict the decay of a nucleus, therefore the prediction of the probability of its decay in a given time period is used, this is the decay constant  $\lambda$ . The rate of decay of N nuclides is:

$$\frac{dN}{dT} = -\lambda N \quad \text{Equation 2-1}$$

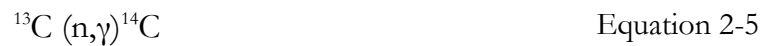
The beta ( $\beta$ ) decay of  $^{14}\text{C}$  is shown below:



The decay of  $^{14}\text{C}$  produces a nitrogen atom as well as an electron and an anti-neutrino. The  $\beta$  emission has a maximum energy of 156 keV (NCRPM, 1978).

$^{14}\text{C}$  is a concern as a radionuclide due to its high biological availability (Baston et al., 2012; Bracke and Müller, 2008; Cook et al., 1998; Evenden et al., 1998; Keogh et al., 2004; Sheppard et al., 1994), particularly as the ingestion pathway is the most significant when looking at human dose (Cook et al., 1998; McCartney et al., 1988; Sheppard et al., 1990).  $^{14}\text{C}$  occurs naturally in the environment through the stratospheric irradiation of  $\text{N}_2$  with an abundance of  $^{14}\text{C}/^{12}\text{C} = 1.2 \times 10^{-12}$  (Cook et al., 1998; Mook, 2006; Yim and Caron, 2006). This forms  $^{14}\text{CO}_2(\text{g})$  with an atmospheric half-life of around 12-16 years in the Northern hemisphere (McNeely, 1994; Kotzer and Watson, 1999), but the naturally occurring levels have been affected by two anthropogenic processes. Firstly the  $^{14}\text{C}$  concentration in the environment has been diluted due to the Suess effect. The process of burning fossil fuels on large scales, primarily for fuel production, has led to an increase in carbon released into the environment. Due to the age of the fossil fuels there is no longer any  $^{14}\text{C}$  remaining in the fuel leading to a dilution of its concentration globally (Suess, 1955). In opposition of and exceeding this dilution effect is the impact of nuclear weapons testing. Nuclear test

explosions were conducted throughout the northern hemisphere between 1945 and 1980. Fallout from the testing increased radiation levels, reaching a peak of around  $0.11 \text{ mSv a}^{-1}$  (total dose) in the 1960's. (UNSCEAR, 2010). Since the ban on nuclear weapons testing was introduced the concentration of  $^{14}\text{C}$  has steadily declined and is almost at pre-1950's levels (UNSCEAR, 2010, McNeely, 1994), therefore authorised and accidental releases of  $^{14}\text{C}$  from nuclear facilities are now the biggest anthropogenic contribution to  $^{14}\text{C}$  levels in the environment (Begg et al., 1992).  $^{14}\text{C}$  is a by-product of nuclear power generation processes: it is commonly formed through three mechanisms from the parent isotopes of nitrogen-14 ( $^{14}\text{N}$ ); oxygen-17 ( $^{17}\text{O}$ ) and  $^{13}\text{C}$ :



where n = neutron, p = proton,  $\alpha$  = alpha and  $\gamma$  = gamma.

$^{14}\text{C}$  has been detected in most parts of the nuclear reactor, it is often produced due to  $^{14}\text{N}$  impurities in spent fuel cladding which can be released in spent fuel pools (Van Konynenburg, 1994; Wilson, 1990). It is also formed in the reactor coolant (Yim and Caron, 2006) and irradiated graphite (Vaitkevičienė et al., 2013). Formation of  $^{14}\text{C}$  in fuel can be due to  $^{14}\text{N}$  impurities within the fuel and  $^{17}\text{O}$  in the  $\text{UO}_2$  matrix, although  $^{14}\text{C}$  associated with fuel is assumed to remain relatively immobile over time (Sakuragi et al., 2016).

Canada's CANDU (CANada Deuterium Uranium) reactors are known to produce twenty times more  $^{14}\text{C}$  than the common light water reactor types due to their dual heavy water circuits which go through the reactor core, one as the coolant and the second as the moderator leading to a greater incidence of  $^{14}\text{C}$  production from the  $^{17}\text{O}$  route ( $^{17}\text{O}(n, \alpha)^{14}\text{C}$ ) (Dayal and Reardon, 1994). As part of efforts to reduce releases of this radionuclide to the environment the  $^{14}\text{C}$  is removed from water, as bicarbonate, using ion exchange resins. Despite this,  $^{14}\text{C}$  is commonly released to the environment through gaseous and liquid discharges as well as through the disposal of solid waste (Liepins and Thomas, 1988; Yim and Caron, 2006).  $^{14}\text{C}$  contamination was first identified in Canada, at the Chalk river site where  $^{14}\text{C}$  was leaching from low level waste trenches with plumes reaching a nearby wetland. This led to a series of studies looking at the cycling of  $^{14}\text{C}$  in a wetland environment (Bird et al., 1999; Caron et al., 1998; Evenden et al., 1998; Killey et al., 1998; Milton et al., 1998; Rao and Killey, 1994) and the dispersion and possible bioaccumulation of  $^{14}\text{C}$  from  $^{14}\text{CO}_2(\text{g})$  (Milton et al., 1995). Since then several monitoring studies have been carried out at different nuclear sites worldwide to examine the local impacts of  $^{14}\text{C}$  contamination, particularly in the form  $^{14}\text{CO}_2(\text{g})$  (Magnusson et al., 2004; Povinec et al., 2015; Roussel-Debet et al., 2006; Xu et al., 2016a; Xu et al., 2016b).

In the UK the main anthropogenic releases to the environment are associated with the reprocessing of spent fuel at Sellafield (Cook et al., 1998). At the Sellafield reprocessing site aqueous and gaseous discharge of  $^{14}\text{C}$  began in the 1950's when site operations began.  $^{14}\text{C}$  gaseous discharges were diverted to the

aqueous discharge route in 1994, leading to an increase in  $^{14}\text{C}$  activity being discharged to the Irish Sea (BNFL, 2002). Sellafield was identified as the biggest contributor of  $^{14}\text{C}$  in the environment on a global scale (Keogh et al., 2004), as most  $^{14}\text{C}$  releases to environment occur when reprocessing spent fuel. There is, however, little data on the fate or form of these aqueous discharges in the environment (Cook et al., 1995; Yim and Caron, 2006).

### 2.1.1 Forms of $^{14}\text{C}$ in the environment

Worldwide only 20-25% of nuclear sites measure and report  $^{14}\text{C}$  emissions (Graven and Gruber, 2011). This lack of site data has led to uncertainty over the form of  $^{14}\text{C}$  upon release to the environment. In previous studies  $^{14}\text{C}$  has been presumed to be present as inorganic species, predominantly bicarbonate ( $\text{HCO}_3^-$ ) (Begg et al., 1992; Eabry et al., 1995) as the  $^{14}\text{C}$  captured on ion exchange resins is predominantly  $\text{HCO}_3^-$  and the  $^{14}\text{C}$  species most commonly found in nuclear waste are  $^{14}\text{CO}_3^{2-}$  and  $\text{H}^{14}\text{CO}_3^-$  (Cline et al., 1985; Dayal and Readson, 1992; Gruhlke et al., 1986; Krupka and Serne, 1998).

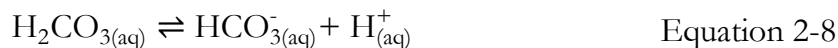
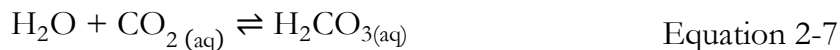
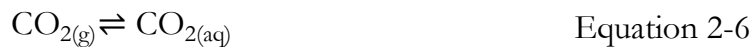
Organic  $^{14}\text{C}$  forms are also present in nuclear waste. Their formation is particularly associated with the pressurised water reactor as this design maintains high concentrations of dissolved hydrogen which are able to combine with  $^{14}\text{C}$  to produce organic compounds such as formaldehyde and methanol (Matsumoto et al., 1994; Petit et al., 2013; Vance et al., 1995). Low molecular weight organic (LMWO) substances are also predicted to form during steel corrosion and from

impurities within fuel cladding (see Figure 6-1; Kaneko et al., 2003; Wieland and Hummel, 2015).

## 2.2 Biogeochemical cycling of carbon

### 2.2.1 Mobility and fate of inorganic <sup>14</sup>C

Inorganic carbon can exist as gaseous CO<sub>2</sub>, aqueous species, sorbed species and solid carbonates. Transitions between these phases are primarily controlled by pH, pCO<sub>2</sub>, the availability of cations in solution and the presence of interfaces (Inskeep and Bloom, 1985; Langmuir, 1997b; van Geen et al., 1994). In aqueous systems there are four inorganic carbon species, carbon dioxide (CO<sub>2</sub>); carbonic acid (H<sub>2</sub>CO<sub>3</sub>); bicarbonate (HCO<sub>3</sub><sup>-</sup>) and carbonate (CO<sub>3</sub><sup>2-</sup>). In systems which are open to atmosphere aqueous CO<sub>2</sub> concentrations equilibrate with atmospheric pCO<sub>2</sub>, see Equations 2-6 to 2-9 (Atkins and De Paula, 2006), however in subsurface environments the bidirectional transfer from aqueous phases to CO<sub>2</sub>(g) is limited due to the structure of the capillary fringe as the soil-gas interface offers resistance to gaseous exchange (Caron et al., 1999; Caron et al., 1994).



(adapted from Greenwood & Earnshaw, 1997)

The speciation of the inorganic carbon species in solution is dependent on the pH of the solution (see Figure 2-1; Langmuir, 1997). The dissociation

constants ( $pK_a$ ) of carbonic acid-bicarbonate-carbonate are 3.6 and 10.3 respectively (at 25°C and zero ionic strength; Plummer and Busenberg, 1982). In open systems, at high pH, high concentrations of aqueous carbonate will be maintained by the continuing equilibrium between atmospheric and dissolved  $CO_2$  (Stumm and Morgan, 1996).

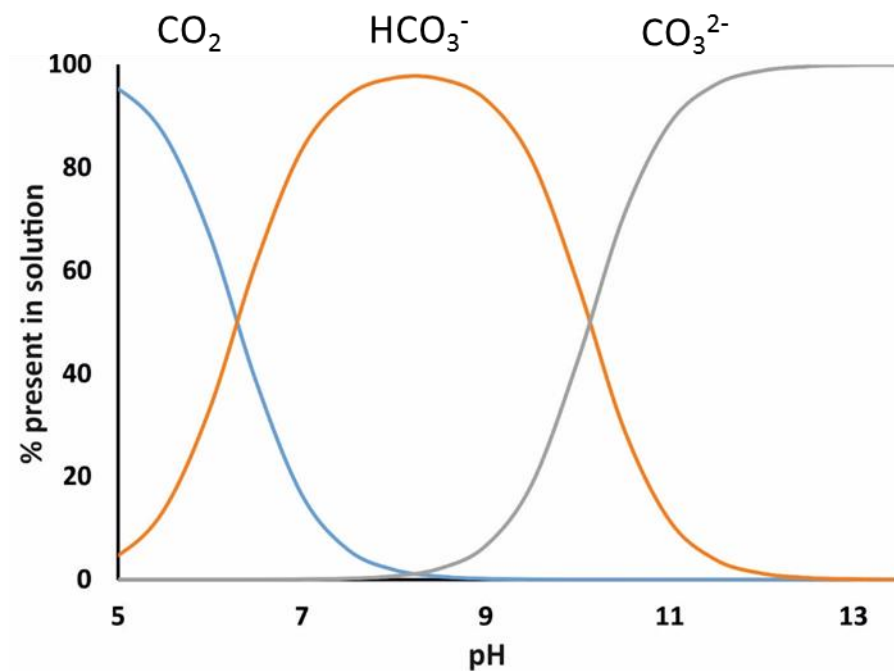


Figure 2-1 Speciation of aqueous carbonate species across a range of pH in a simple 0.1 M NaCl solution, modelled using a closed system with a  $pCO_2 = 3.5$  in PHREEQC,  $CO_2 = CO_2(aq) + H_2CO_3(aq)$ .

In surface water environments the  $^{14}C$  would be diluted with the stable C isotopes when mixed with surface waters (Wang et al., 2014) as evidenced in the Irish Sea where the enriched  $^{14}C$  signal is lost over a short spatial zone after mixing (Ahad et al., 2006).  $^{14}C$  would be expected to behave conservatively and therefore long range transport would be expected.

## 2.2.2 Inorganic interactions with solid surfaces

### 2.2.2.1 Adsorption

There are two forms of adsorption: outer sphere complexation where physical adsorption involving the attachment of an ion/molecule to a surface through intermolecular or van der Waals forces and inner sphere complexation where chemical adsorption where a new chemical bond is formed between the adsorbed species and atoms on the surface of the solid, both of which may affect the movement of a contaminant plume (Chorover et al., 2008).

Aqueous inorganic  $^{14}\text{C}$  species can adsorb to aluminium and iron oxides at circumneutral pH (Su and Suarez, 1997),  $\text{HCO}_3^-$  has been recorded adsorbed to goethite surfaces (pH = 7) as an inner-sphere carbonate surface complex via ligand exchange reaction. This is assumed to be singly coordinated Fe-OH and Al-OH surface groups (Su and Suarez, 1997; Wijnja and Schulthess, 2000). However carbonate species do not sorb to quartz or montmorillonite at circumneutral pH (Garnier, 1985; Sheppard et al., 1998) which suggests that the carbonate species interact poorly with the silica and silicate layers of clays. As the bulk composition of most natural sediments is silicate based it would suggest that sorption of inorganic  $^{14}\text{C}$  species is unlikely to occur in subsurface environments which are typically at circumneutral pH as the anion exchange capacity is typically much smaller than that of the cation (Gu and Schulz, 1991; Sposito, 1989).

### 2.2.2.2 Precipitation of carbonate minerals

In typical aqueous environments precipitation of carbonate minerals is controlled by pH and the concentration of divalent cations (Krauskopf and Bird, 1995). The propensity for precipitation to occur is governed by the ratio of the ion activity products ( $IAP = a_{Me^{2+}(aq)} \cdot a_{CO_3^{2-}(aq)}$ ) to the mineral solubility product at equilibrium (the saturation index,  $SI = \log_{10}(IAP/K_{sp})$ ) for reactions with the form:



Where  $Me^{2+}$  is a divalent metal ion, and  $a$  is the activity of the aqueous ion. When the value of  $SI > 0$  precipitation is thermodynamically favoured, when  $SI < 0$  dissolution is favoured. In oxic natural waters calcium is usually the most abundant divalent cation, followed by magnesium. A variety of other divalent cations are usually only present in trace concentrations (e.g.  $Sr^{2+}$ ;  $Ba^{2+}$ ;  $Fe^{2+}$ ) (Krauskopf and Bird, 1995).

Major carbonate mineral phases are calcite ( $CaCO_3$ ), aragonite ( $CaCO_3$ ) and dolomite ( $CaMg(CO_3)_2$ ). Carbonate minerals tend to be more soluble with decreasing temperature due to the dissolution reaction being slightly exothermic. In addition to an increase in solubility products, carbon dioxide is more soluble at lower temperatures, further favouring carbonate mineral dissolution in lower temperature environments. Carbonic acid concentration is the controlling factor for the solubility of carbonate mineral phases in the environment. Increasing ionic strength can impact the solubility product as the presence of other ions in solution

can act as shields, reducing the interaction of  $\text{Ca}^{2+}$  and  $\text{CO}_3^{2-}$  ions and so precipitation occurring (Langmuir, 1997a).

Table 2-1 Calcium carbonate mineral formation conditions.

Mineral	Log <sub>10</sub> K <sub>sp</sub>	Formation
Calcite CaCO <sub>3</sub>	-8.42 ± 0.07 <sup>a</sup>	At low temperature and pressure calcite is the predominant phase expected to form. It can occur via numerous pathways (Bots et al., 2012; Gebauer et al., 2008; Nielsen et al., 2014). The existence of interfaces reduces the thermodynamic barrier to nucleation (Hu et al., 2012), which is an important mechanism for <sup>14</sup> C retention in subsurface environments due to the number of potential nucleation sites.
Aragonite CaCO <sub>3</sub>	-8.3 <sup>b</sup>	Stable form of calcium carbonate at high pressures, but it is thermodynamically unstable at standard temperature and pressure (Plummer and Busenberg, 1982).
Dolomite CaMg(CO <sub>3</sub> ) <sub>2</sub>	-18 ± 2 <sup>c</sup>	Low-temperature dolomite can occur in natural environments that are rich in organic matter and microbial cell surfaces due to magnesium complexation with carboxyl groups associated with organic matter. It is relatively rare in modern times, but is ubiquitous in the geologic record (Arvidson and Mackenzie, 1999).

<sup>a</sup> Krauskopf and Bird, 1995; <sup>b</sup> Pilsen, 2012; <sup>c</sup> Sherman and Barak, 2000; Stumm and Morgan, 1996.

In groundwater environments the most likely carbonate phase is calcite due to the low temperature and pressures, however the formation of magnesium carbonate phases is also a consideration, particularly within waste storage silos at Sellafield (see section 2.3.4). These silos contain both magnesium alloy waste (from Magnox fuel cladding) and <sup>14</sup>C (formed from <sup>14</sup>N impurities within the fuel cladding). The solid materials are submerged under water for shielding and cooling

purposes leading to the formation of several hydrous magnesium phases. Predicted phases include hydromagnesite; artinite; nesquehonite; and hydrotalcite (Parry et al., 2011; Gregson et al., 2011). Precipitation of these phases and equilibration with the overlying liquor may account for the presence of aqueous  $^{14}\text{C}$  in the deep tank liquor.

### 2.2.2.3 Isotopic equilibrium reactions

There are three mechanisms for isotope fractionation (Krauskopf and Bird, 1995). The first mechanism is dependent on physical properties. For example, this fractionation occurs during evaporation of water, where light isotopes concentrate in the gaseous phase and heavy isotopes in the aqueous phase. The second fractionation occurs due to differences in reaction rates, this separation is particularly noted in reactions catalysed by bacterial activity. For this study there is particular interest in the final mechanism: the exchange reaction to achieve isotopic equilibrium. For example in the aqueous carbonate system at equilibrium there is also an isotopic equilibrium between all four species of carbon in solution i.e. the  $^{14}\text{C}/^{13}\text{C}/^{12}\text{C}$  ratio is equal in all species. When a  $^{14}\text{C}\text{-CO}_3^{2-}$  is added to solution, disequilibrium is created and exchange reactions occur to restore equilibrium among the species of carbonate (Gonfiantini and Zuppi, 2003; Krauskopf and Bird, 1995; Mook et al., 1974; White, 2013; Wigley et al., 1978). There has been a lot of study in this area, for both  $^{13}\text{C}$  and  $^{14}\text{C}$  as tracers, and for  $^{14}\text{C}$  for dating C-containing materials (Doctor et al., 2008; Zhang et al., 1995). Isotopic exchange of inorganic  $^{14}\text{C}$  with mineral carbonates is considered a possible retention mechanism of  $^{14}\text{C}$  in soil (Sheppard and Evenden, 1996).

### 2.2.3 Mobility and fate of <sup>14</sup>C-containing LMWO compounds

Two main processes are believed to govern the availability of LMWO substances in subsurface environments: sorption and microbial utilisation. Sorption between <sup>14</sup>C-organic acids and sediment have been recorded over a range of pH (Fischer and Kuzyakov, 2010; Jones and Brassington, 1998), but it is very limited in cementitious environments (Kaneko et al., 2003; Matsumoto et al., 1994; Wieland et al., 2016) and often occurs at a slower rate than microbial utilisation (Fischer et al., 2010). For anionic species, such as acetate and formate, sorption may be more likely at lower pH where the anion exchange capacity may be increased (Gu and Schulz, 1991; Sposito, 1989).

Microbial utilisation can have a high impact on the behaviour of contaminants in the environment in a variety of ways: firstly the direct impacts of bioaccumulation, which is the sequestration of contaminants within the microbe itself; biosorption where the contaminant complexes with the surface of the microbe and bioreduction where the microbe actively transports electrons from donors to acceptors causing a change in oxidation state (Brown et al., 2000). The impact of microbes can also be indirect, with microbe interactions causing changes to chemical and physical properties of the surrounding environment, for example change in pH (Lovley, 1991; Lovley, 1997). Microbiological processes can be broadly categorised as assimilative: this is a process by which an inorganic compound is reduced for incorporation into organic matter, occurring in the presence or absence of oxygen, or dissimilative: this is the process by which an

inorganic compound such as  $\text{NO}_3^-$  is reduced as it is utilised as an electron acceptor for respiration.

### **2.2.3.1 Terminal Electron Accepting Processes**

Microorganisms obtain energy through the transfer of electrons by coupling the oxidation of an electron donor to the reduction of an electron acceptor (Madigan et al., 2015). Electron donors in subsurface environments are typically the products of the hydrolysis/fermentative breakdown of more complex organic matter. This produces simple organic molecules such as acetate and ethanol and can include inorganic species such as  $\text{H}_2$  (Ehrlich, 1997). Electron acceptors include molecular oxygen, nitrate, manganese (IV), iron (III) oxyhydroxides and sulphate (Chapelle, 2001). In aerobic environments oxygen is utilised, in this reaction electrons are taken from the electron donor and passed along an intracellular electron transport chain of a microorganism to generate energy (ATP) before final transfer to oxygen as the terminal electron acceptor (TEA) (Madigan et al., 2015). By creating a pH gradient and electrical potential across the cell membrane during the electron transfer process, the microorganism can conserve energy for growth from catalysis of these redox reactions. The net energy change, which indicates the favourability of the reaction, is determined by the difference in reduction potentials between the electron donor and the terminal electron acceptor.

For example, coupling the oxidation of acetate with the reduction of oxygen is shown in Equation 2-11 (Konhauser et al., 2002):



$$\Delta G = -854 \text{ kJ mol}^{-1} / \text{mole CH}_3\text{COO}^-$$

In subsurface environments oxygen may be utilised more rapidly than it is replenished due to the slow diffusion of O<sub>2</sub> through the sediment or, if electron donors are available in excess, the available oxygen in the sediment may be utilised prior to consumption of all of the electron donor. This may cause the development of anaerobic conditions. Under these conditions some bacteria are able to utilise alternative terminal electron acceptors other than oxygen. The dominant terminal electron accepting process (TEAP) is a function of the availability of terminal acceptors and the free energy yield of the process (Lovley and Chapelle, 1995). When based upon thermodynamics the TEAP chain begins with oxygen and is followed by nitrate-, manganese (IV)-, iron(III)-, sulfate-reduction and methanogenesis (see Table 2-2; Coates and Achenbach, 2002; Chapelle, 2001; Lovley, 1991). However in subsurface environments the microbial species also effects the TEA used, leading to an overlap in these processes in natural environments where complex and diverse microbial communities exist (Konhauser et al., 2002).

Table 2-2 The associated energy yield with terminal electron accepting processes at pH 7 (Konhauser et al., 2002).

<b>Terminal Electron Accepting Processes</b>	<b><math>\Delta G</math> kJ mol<sup>-1</sup> CH<sub>3</sub>COO<sup>-</sup></b>
$\text{CH}_3\text{COO}^- + 2\text{O}_2 \rightarrow \text{H}_2\text{O} + 2\text{CO}_2 + \text{OH}^-$	-854
$\text{CH}_3\text{COO}^- + 1.6\text{NO}_3^- \rightarrow 2\text{CO}_2 + 0.8\text{N}_2 + 2.6\text{OH}^- + 0.2\text{H}_2\text{O}$	-801
$\text{CH}_3\text{COO}^- + 4\text{MnO}_2 + 3\text{H}_2\text{O} \rightarrow 4\text{Mn}^{2+} + 2\text{HCO}_3^- + 7\text{OH}^-$	-558
$\text{CH}_3\text{COO}^- + 8\text{Fe}(\text{OH})_3 \rightarrow 8\text{Fe}^{2+} + 2\text{HCO}_3^- + 15\text{OH}^- + 5\text{H}_2\text{O}$	-337
$\text{CH}_3\text{COO}^- + \text{SO}_4^{2-} \rightarrow \text{HS}^- + 2\text{HCO}_3^-$	-48
$\text{CH}_3\text{COO}^- + \text{H}_2\text{O} \rightarrow \text{CH}_4 + \text{HCO}_3^-$	-31

Each of these TEAP produces characteristic changes in chemistry which are often used as evidence for its occurrence. For example when iron reduction is occurring the solid phase Fe(III) is reduced and solid and/or aqueous Fe(II) is formed. These are both indicators that Fe(III) reduction is occurring (Chapelle et al., 1995; Jakobsen et al., 1998). It is evident that microbial processes can cause significant changes to the geochemistry of the subsurface environment, particularly in the maintenance of anoxic conditions.

### 2.2.3.2 Denitrification

Nitrate is one of the essential components for microbes in the biosphere as it is one of the thermodynamically favourable electron accepting processes for anaerobic respiration. It is reducible by a large number of microbes that are associated with the oxidation of organic compounds. Several studies have

suggested that addition of nitrate could enhance in situ bioremediation of contaminated sediments by promoting organic C degradation (Cunningham et al., 2001; Hutchins et al., 1998; Xu et al., 2014). Conversely some radionuclide removal is reliant on the establishment of iron-reducing conditions which may be impeded in the presence of high nitrate (DiChristina, 1992; McBeth et al., 2007). Nitrate is often found in the subsurface of nuclear facilities at high concentrations due to the use of nitric acid in a variety of plant operations (Law et al., 2010; Thorpe et al., 2012a). This can lead to areas of nitrate reduction existing in groundwater.

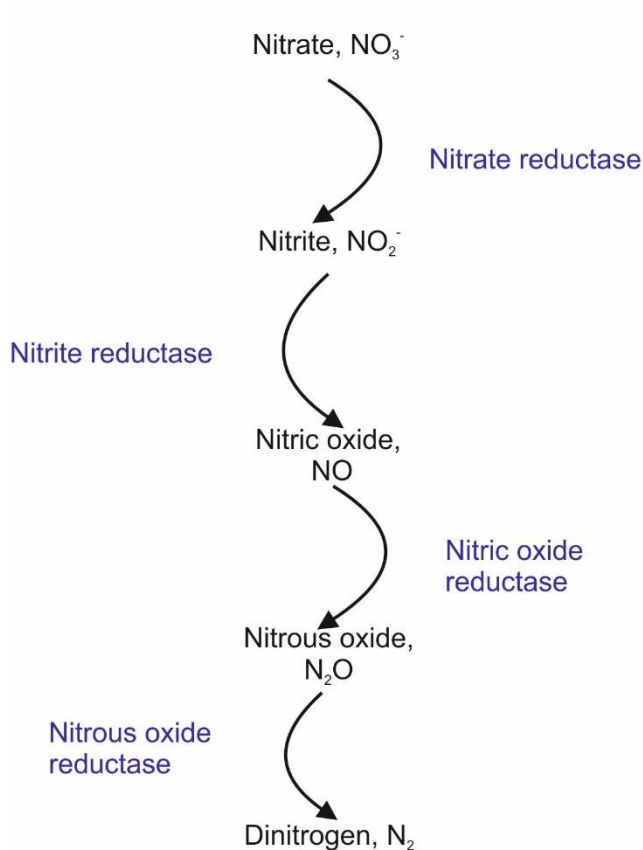


Figure 2-2 The biological pathway from nitrate to nitrogen, facilitated by microbial activity. Purple text highlights the enzymes needed for the reduction to occur.

### 2.2.3.3 Iron reduction

The availability of aqueous Fe(III) is limited in sediment at circumneutral pH where low solubility solid Fe(III) oxyhydroxides phases are the predominant Fe(III) phases present (Weber et al., 2006). Biologically-mediated reduction of Fe(III) is the dominant control on iron cycling in these environments. Dissimilatory Fe(III) reduction can be defined as the use of Fe(III) as an electron acceptor being reduced to Fe(II). This differs from assimilatory reduction as there is no accumulation of Fe inside the cell (Lovley, 1991). This cycling is essential in subsurface environments, oxidising organic compounds (Lloyd et al., 2000; Lovley, 1997). At the onset of anaerobic conditions Fe (III) is usually the most abundant electron acceptor in sedimentary freshwater environments. Studies have shown that Fe(II) accumulation occurs in a wide range of sub-surface environments suggesting that the organic oxidation via Fe(III) may be a common mechanism under a range of conditions, including those of a contaminated groundwater (Canfield, 1989; Lovley, 1997; Lovley and Phillips, 1988; Stumm and Sulzberger, 1992). The indirect interaction shown in Figure 2-3 is the reaction between the Fe(II) formed from the biologically mediated Fe(III) reduction and the redox active species uranium and technetium resulting in the formation of insoluble U(IV) and Tc(IV) phases (Fox et al., 2006; McBeth et al., 2007; Morris et al., 2008; Roh et al., 2015), this process is one of the mechanisms by which bioremediation of radionuclides can occur.

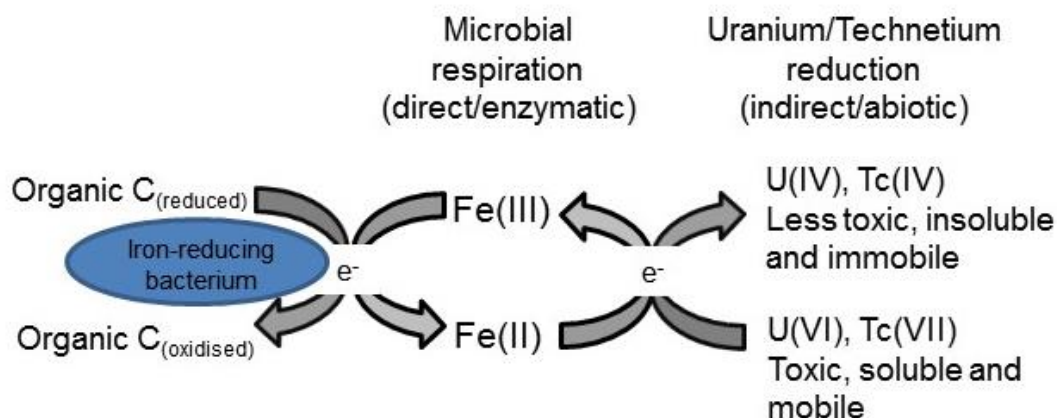


Figure 2-3 Direct/enzymatic reduction and indirect methods for the reduction of redox active elements by metal reducing bacteria (adapted from Tabak et al., 2005)

Reductive dissolution of Fe bearing minerals can also lead to the formation of new minerals, particularly the carbonate-containing mineral siderite ( $\text{FeCO}_3$ ) (Thorpe et al., 2012b; Wieland and Hummel, 2015). In the context of radionuclide behaviour the formation of this mineral has been studied due to the possibility of strontium incorporation as a substitute for Fe (Parmar et al., 2000; Roden et al., 2002), but it has the potential to incorporate  $^{14}\text{C}$  as well. Siderite is expected to form at circumneutral to alkaline pH (Agrawal et al., 2002) and precipitation has been recorded at pH values between 5 and 7 in the presence of microbially induced iron reduction (Sánchez-Román et al., 2014).

#### 2.2.3.4 Sulfate reduction

Sulfate reduction can occur in both natural and anthropogenic groundwater. It serves as a TEA, usually occurring after iron reduction and prior

to methanogenesis (Miao et al., 2012). Dissimilatory sulfate reduction oxidises organic carbon whilst reducing sulfate:



(Canfield, 2001a,b)

Bicarbonate production during this process can have dual impacts on the behaviour of  $^{14}\text{C}$ . Firstly  $^{14}\text{C}$ -labelled organics will be utilised and the  $^{14}\text{C}$  will become part of the inorganic pool, secondly the species generated ( $\text{H}^{14}\text{CO}_3^-$ ) will increase the pH; therefore increasing the potential for carbonate precipitation to occur and remove  $^{14}\text{C}$  from solution.

#### 2.2.3.5 Methanogenesis

Methanogenesis is the mineralisation of organic matter in anaerobic environments where the concentrations of other, more energetically favourable, electron donors are limited. The overall reaction is shown below:



(Le Mer and Roger, 2004)

This reaction requires the successive action of four populations of micro-organisms that degrade the complex substrates in to simpler compounds. Firstly the hydrolysis of biological polymers in to monomers, followed by acidogenesis from monomeric compounds, acetogenesis of the previous metabolites and methanogenesis from the simple compounds which can be utilised by methanogens (particularly  $\text{CO}_2$  and acetate) (Le Mer and Roger, 2001).

Methanogenesis is considered particularly important in the life cycle of  $^{14}\text{C}$  due to its predicted occurrence and associated gas generation under geological disposal conditions (Jefferies, 1990; Jackson and Yates, 2011; Limer et al., 2013; Limer et al., 2011; Marshall et al., 2011).

Both sulfate reduction and methanogenesis are not considered in this project as they are unlikely to be the dominant redox mechanisms in shallow subsurface environments.

### **2.3 The nuclear legacy**

As of April 2017 there are 30 countries with a total of 449 nuclear power plants generating electricity (IAEA, 2017). In 2014 nuclear power provided 11% of the world's electricity production, this was slightly higher for the UK with nuclear power accounting for 19% of electricity (DECC, 2016). The nuclear fuel cycle comprises of six main stages to produce electricity from raw fuel. To mine and mill the ore, purify it, enrich it, utilise the fuel in the reactor, reprocess the fuel and recycle the uranium and plutonium (Wilson, 1996). Every stage of the nuclear fuel cycle produces waste, for reprocessing this waste is categorised by its associated radioactivity in to low level (low activity), intermediate level (can range from mildly to very radioactive) and high level waste (both highly radioactive and heat producing) (Openshaw et al., 1989). Since the commencement of nuclear activity in the UK spent nuclear fuel has been transported to Sellafield site for reprocessing and/or surface storage (McKenzie and McCord, 2010), although the long term strategy is to build a geological disposal facility with formal engagement of potential host communities expected to begin in 2017 (DBEIS, 2017).

The rapid expansion of the nuclear industry has left an extensive legacy of contamination across many sites (Bell et al., 1997; Beresford, 2006; Joyce and Port, 1999). As many nuclear plants reach the end of their lifespan increasingly focus has shifted on to the remediation of these sites (Beresford, 2006). In the UK the responsibility for this process rests with the Nuclear Decommissioning Authority (NDA), a public body created in 2004 which oversees the decommissioning and remediation of the UKs nuclear sites (House of Commons, 2004). Of all sites under NDA management the Sellafield reprocessing site in Cumbria, UK, is the biggest and most complex, housing Europe's largest fuel reprocessing site with an estimated 13-20 million cubic metres of radioactively contaminated land (McKenzie and Armstrong-Pope, 2010).

### **2.3.1 Sellafield reprocessing site, Cumbria, UK**

Sellafield site is located on the northwest coast of England, just outside of the Lake District national park (Gulliver et al., 2007). The site is tasked with remediation and containment of nuclear waste (Cruickshank, 2012; NDA, 2009). The site has been operational since 1947 as a nuclear facility. Calder Hall was the first nuclear power station in the world to generate electricity commercially, operating from 1956 to 2003. A further three reactors were constructed on site, then known as Windscale. Two of these reactors were closed in 1957 after the Windscale fire incident, with the third remaining open till 1981. The extensive history of the site means that it has a very complex radionuclide inventory, with many areas of contamination still too radioactive to remediate. The site operations have been numerous over this time; it currently reprocesses spent fuel, stores

nuclear waste material and fabricates fuel. Spent fuel management occurs in two main facilities: the Thermal Oxide Reprocessing Plant (THORP) which has been operational since 1994 and the Sellafield Mixed Oxide Plant. The plants separate spent fuel used in nuclear reactors, 97% of the spent fuel can be recycled to produce new fuel (NDA, 2009).



Figure 2-4 Aerial photo of the Sellafield site, © Nuclear Management Partners, 2016.

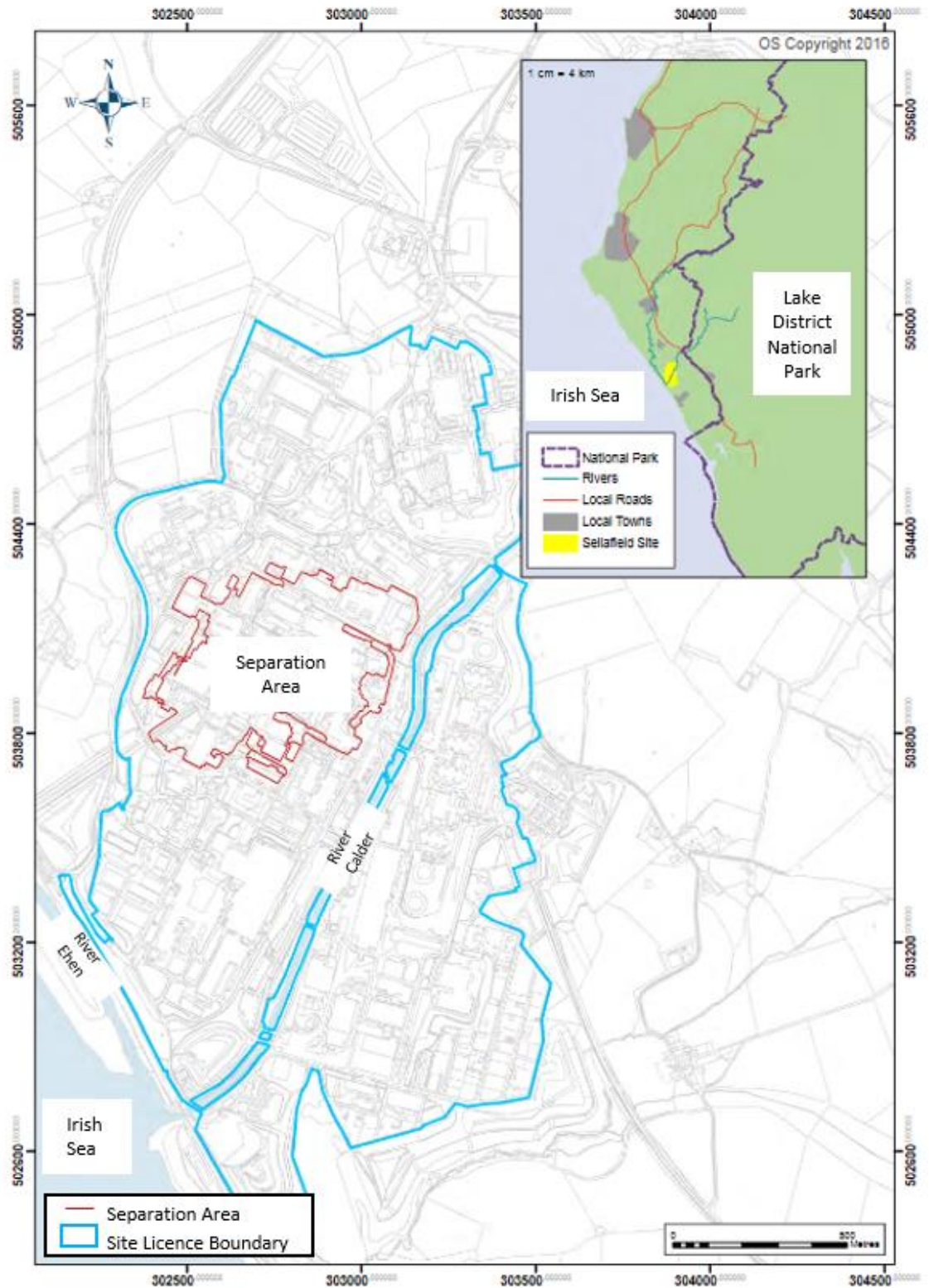


Figure 2-5 Outline map of the Sellafield reprocessing site. The site boundary is outlined in blue, the Separation Area is shown in red. Regional setting of the Sellafield site within the county of Cumbria is shown (inset). Map reproduced from Sellafield Ltd., 2016 groundwater monitoring report.

### **2.3.2 Geology of Sellafield**

The uppermost ground layers at the Sellafield site are known as “Made Ground”. This varies in depth, with an average of around 3m across the site. This ground has been highly disturbed due to site activities (Cruickshank, 2012; Stamper et al., 2012). The natural geology is a sequence of unconsolidated glacial and post glacial sediments, known as superficial deposit, overlying bedrock red sandstone of Triassic age. The composition of the deposit is heterogeneous, but at all depths beneath site it is dominated by sand and gravel. There is a distinct intermediate-depth zone which contains an increased amount of silts and clays which lies within the Sellafield Buried Channel. In the lower depth of the channel the silts and clays are no longer present. The sandstone bedrock is strata of the Sherwood Sandstone Group (Chaplow, 1996). It is comprised of two formations: the Calder and Sellafield Member Sandstones (El-Ghonemy, 2004). These formations are of a predominantly aeolian origin. The sandstone ranges in thickness between 650 and 1150m, averaging around 800m thickness.

### **2.3.3 Hydrogeology**

The sources of the local groundwater are rainfall and surface water that percolate in to the subsurface, forming laterally continuous aquifers within the porous geologic material (Stamper et al., 2012). The depth of groundwater across the site varies from 3 m below ground level (bgl) to the south of Separation Area to approximately 12 m bgl in the northern part of Separation Area. In general this means that groundwater lies below Made Ground across the majority of the site.

Groundwater flows onto the Sellafield site from the north-east within the sandstone, flowing initially to the south-west, see Figure 2-6. Beneath the Separation Area westerly flow occurs within the Sellafield Buried Channel, suggesting high permeability in the deeper deposit. To the south of Separation Area, the south westerly regional flow pattern again becomes dominant. The overall conceptual model for regional hydrogeology is that the groundwater flow is from the Cumbrian Fells towards the coast in a south westerly direction. Recharge occurs through the deposit, and discharge occurs into the Irish Sea (Stamper et al., 2012). The hydraulic conductivity of gravel and sand-dominated sediments in the Quaternary drift is approximately ten times higher than that of silt-dominated sediments. Groundwater CO<sub>2</sub> partial pressures are typically ~ 10-100 times higher than atmospheric, so CO<sub>2</sub> degassing is a consequence of extraction (Cai et al., 2003; Macpherson, 2009).

Table 2-3 Quaternary Drift in the Sellafield Buried Channel, adapted from Cruickshank, 2012

Hydrogeological unit	Elevation	Lithology
HU1a	Base of made ground to +10m Above Ordnance Datum (AOD)	Mainly sands and gravels, 20% silt and clay.
HU2	+10m AOD to -5m AOD	Sands and gravels, 30% silt and clay.
HU3	-5m AOD to top of sandstone bedrock	Reduced proportion of silt and clay. Absent below -16m AOD.

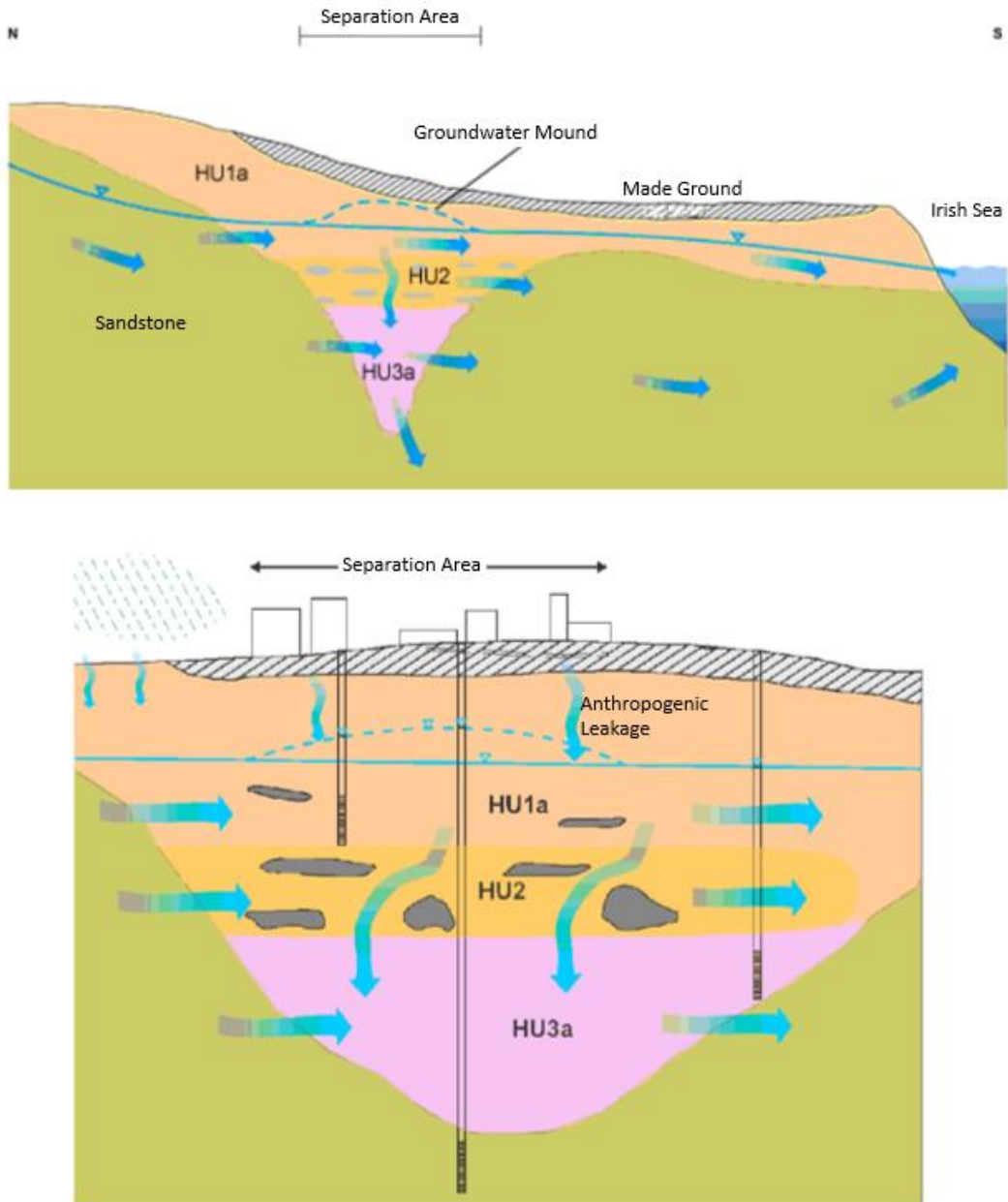


Figure 2-6 Diagrams showing the groundwater flow through site, reproduced from Sellafield Contaminated Land and Groundwater Management (Cruickshank, 2012). See Table 2-3 for definitions of hydrological units (HU).

### 2.3.4 Radionuclide contamination

There are three main pathways from past disposal and unintended leakage routes at Sellafield which have led to contamination of the site. The unlined trenches, constructed in the 1950s which are located in the Separation Area, and the low level waste landfills on site (Cruickshank, 2012; Marshall et al., 2015). However the largest contributor to the contamination is via unauthorised discharges from storage facilities in the Separation Area. The site stores much of its nuclear waste in ponds or silos that have been used beyond the original design lifetime. This has led to historical leaks of radioactive material from storage tanks, which can then be transported to the Irish Sea via groundwater flow (Marshall et al., 2015). In particular the solid waste storage facility and highly active liquor storage tanks are believed to have contributed over 99% of the estimated radionuclide inventory which has been lost to ground. Further significant leaks have been attributed to the Magnox silo and the sludge storage tanks (Hunter, 2004).

The dominant radionuclides making up the Sellafield radioactive contamination are strontium-90 ( $^{90}\text{Sr}$ ), technetium-99 ( $^{99}\text{Tc}$ ), caesium-137 ( $^{137}\text{Cs}$ ), tritium ( $^3\text{H}$ ) and  $^{14}\text{C}$ . This contamination is complicated further by industrial contamination such as fuel, oil, solvents, heavy metals, hydrocarbons and elevated nitrate (Marshall et al., 2015). The monitoring of radioactive contaminants at Sellafield is relatively comprehensive, but only in recent years has this routinely included groundwater monitoring for  $^{14}\text{C}$ .  $^{14}\text{C}$  was expected to have been most likely released to groundwater as dissolved inorganic carbon (chiefly bicarbonate),

which is considered highly mobile in groundwater. Groundwater flow, might therefore, be expected to have dispersed  $^{14}\text{C}$  released in past incidents leading to generally very low in situ  $^{14}\text{C}$  activities. However  $^{14}\text{C}$  activities were high in some areas near to the locations of known previous leaks to ground (Figure 2-7), highlighting the importance of unexpected retention mechanisms in controlling  $^{14}\text{C}$  behaviour at this site.

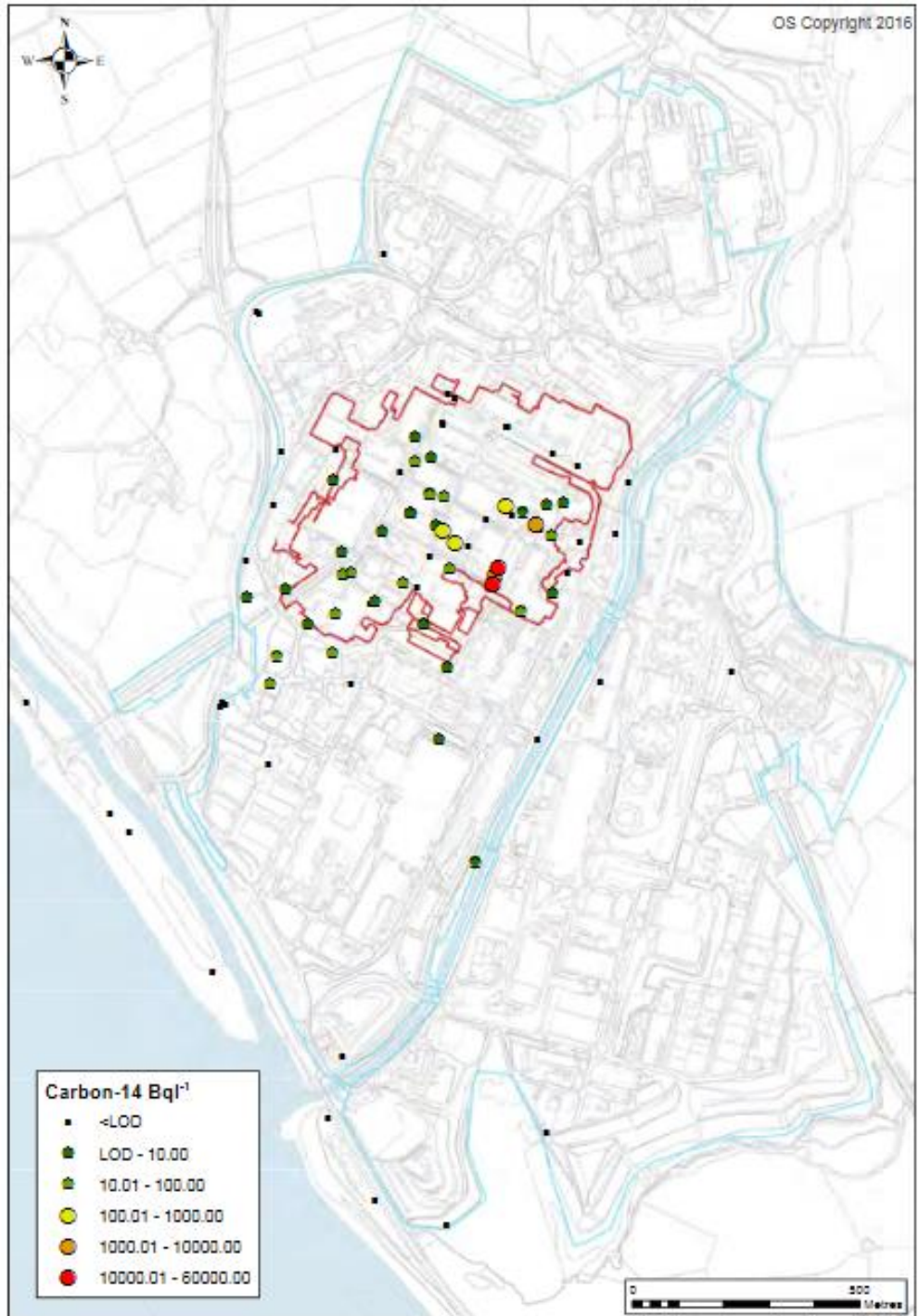


Figure 2-7 Sellafield site with  $^{14}\text{C}$  concentrations measured in monitoring wells in 2015. The site boundary is outlined in blue, the Separation Area is shown in red. Map reproduced from Sellafield Ltd., 2016 groundwater monitoring report.

## 2.4 References

Agrawal, A., Ferguson, W.J., Gardner, B.O., Christ, J.A., Bandstra, J.Z., Tratnyek, P.G., 2002. Effects of carbonate species on the kinetics of dechlorination of 1, 1, 1-trichloroethane by zero-valent iron. *Environmental science & technology* 36, 4326-4333.

Ahad, J.M., Ganeshram, R.S., Spencer, R.G., Uher, G., Gulliver, P., Bryant, C.L., 2006. Evidence for anthropogenic <sup>14</sup>C-enrichment in estuarine waters adjacent to the North Sea. *Geophysical Research Letters* 33.

Arvidson, R.S., Mackenzie, F.T., 1999. The dolomite problem; control of precipitation kinetics by temperature and saturation state. *American Journal of Science* 299, 257-288.

Atkins, P.W., De Paula, J., 2006. *Atkins' Physical Chemistry*. Macmillan Higher Education.

Baston, G.M.N., Marshall, T.A., Otlet, R.L., Walker, A.J., Mather, I.D., Williams, S.J., 2012. Rate and speciation of volatile carbon-14 and tritium releases from irradiated graphite. *Mineralogical Magazine* 76, 3293-3302.

Begg, F.H., Cook, G.T., Baxter, M.S., Scott, E.M., McCartney, M., 1992. Anthropogenic radiocarbon in the eastern Irish Sea and Scottish coastal waters. *Radiocarbon* 34, 707-716.

Beresford, N., 2005. Land contaminated by radioactive materials. *Soil Use and Management* 21, 468-474.

Bird, G.A., Bergström, U., Nordlinder, S., Neal, S.L., Smith, G.M., 1999. Model simulations of the fate of  $^{14}\text{C}$  added to a Canadian shield lake. *Journal of Environmental Radioactivity* 42, 209-223.

Bots, P., Benning, L.G., Rodriguez-Blanco, J.-D., Roncal-Herrero, T., Shaw, S., 2012. Mechanistic Insights into the Crystallization of Amorphous Calcium Carbonate (ACC). *Crystal Growth & Design* 12, 3806-3814.

Bracke, G., Müller, W., 2008. Contribution to a more realistic approach in assessing the release of C-14 from low-level radioactive waste repositories. *Journal of Contaminant Hydrology* 102, 210-216.

Brown, C.J., Schoonen, M.A.A., Candela, J.L., 2000. Geochemical modeling of iron, sulfur, oxygen and carbon in a coastal plain aquifer. *Journal of Hydrology* 237, 147-168.

Cai, W.J., Wang, Y., Krest, J., Moore, W.S., 2003. The geochemistry of dissolved inorganic carbon in a surficial groundwater aquifer in North Inlet, South Carolina, and the Carbon fluxes to the coastal ocean. *Geochimica et Cosmochimica Acta* 67, 631-637.

Canfield, D., 2001a. Biogeochemistry of sulfur isotopes. *Reviews in Mineralogy and Geochemistry* 43, 607-636.

Canfield, D.E., 1989. Reactive iron in marine sediments. *Geochimica et Cosmochimica Acta* 53, 619-632.

Canfield, D.E., 2001b. Isotope fractionation by natural populations of sulfate-reducing bacteria. *Geochimica et Cosmochimica Acta* 65, 1117-1124.

Caron, F., Manni, G., Workman, W., Haas, M., 1998. Soil CO<sub>2</sub> gas–groundwater exchange and migration near Waste Management Area 'C', Chalk River, Ontario. Atomic Energy of Canada Ltd., Chalk River, Ont., Rep. no. RC-2121, COG-98-253i.

Caron, F., Manni, G., Workman, W.J.G., 1999. A large-scale laboratory experiment to determine the mass transfer of CO<sub>2</sub> from a sandy soil to moving groundwater. *Journal of Geochemical Exploration* 64, 111-125.

Caron, F., Wilkinson, S.R., Torok, J., Haas, M.K., Selander, W.N., 1994. CO<sub>2</sub> transport through the capillary fringe in sand. *Waste Management* 14, 421-433.

Chapelle, F., 2001. *Ground-Water Microbiology and Geochemistry*. Wiley.

Chapelle, F.H., McMahon, P.B., Dubrovsky, N.M., Fujii, R.F., Oaksford, E.T., Vroblesky, D.A., 1995. Deducing the distribution of terminal electron-accepting processes in hydrologically diverse groundwater systems. *Water Resources Research* 31, 359-371.

Chaplow, R., 1996. The geology and hydrogeology of Sellafield: an overview. *Quarterly Journal of Engineering Geology and Hydrogeology* 29, S1-S12.

Chorover, J., Choi, S., Rotenberg, P., Serne, R.J., Rivera, N., Strepka, C., Thompson, A., Mueller, K.T., O'Day, P.A., 2008. Silicon control of strontium and cesium partitioning in hydroxide-weathered sediments. *Geochimica et Cosmochimica Acta* 72, 2024-2047.

Clever H. L. and Young C. L., Eds., IUPAC Solubility Data Series, Vol. 27/28, Methane, Pergamon Press, Oxford, England, 1987.

Cline, J., Noyce, J., Coe, L., Wright, K., 1985. Assay of long-lived radionuclides in low-level wastes from power reactors. Science Applications International Corp., Rockville, MD (USA).

Coates, J.D., Achenbach, L.A. The Biogeochemistry of aquifer systems. In: Hurst, C.J., Knudsen, G.R., McInerney, M.J., Stetzenbach, L.D., Walter, M.D., (eds) Manual of environmental microbiology, 2<sup>nd</sup> edn. ASM Press, Washington, DC 2002.

Cook, G.T., Begg, F.H., Naysmith, P., Scott, E.M., McCartney, M., 1995. Anthropogenic <sup>14</sup>C marine geochemistry in the vicinity of a nuclear fuel reprocessing plant. Radiocarbon 37, 459-467.

Cook, G.T., MacKenzie, A.B., Naysmith, P., Anderson, R., 1998. Natural and anthropogenic <sup>14</sup>C in the UK coastal marine environment. Journal of Environmental Radioactivity 40, 89-111.

Cruickshank, J., 2012. Findings of the Sellafield Contaminated Land and Groundwater Management. Sellafield Ltd.

Cunningham, J.A., Rahme, H., Hopkins, G.D., Lebron, C., Reinhard, M., 2001. Enhanced in situ bioremediation of BTEX-contaminated groundwater by combined injection of nitrate and sulfate. Environmental science & technology 35, 1663-1670.

Dayal, R., Readson, E., 1992. Cement-based engineered barriers for carbon-14 isolation. Waste management 12, 189-200.

Dayal, R., Reardon, E., 1994. Carbon-14 behaviour in a cement-dominated environment: Implications for spent candu resin waste disposal. *Waste Management* 14, 457-466.

DBEIS 2017, Geological Disposal Facility (GDF) for higher-activity radioactive waste. Department for Business, Energy and Industrial Strategy.

DECC 2016. UK Energy in Brief 2016. Department of Energy and Climate Change.

DiChristina, T.J., 1992. Effects of nitrate and nitrite on dissimilatory iron reduction by *Shewanella putrefaciens* 200. *Journal of bacteriology* 174, 1891-1896.

Doctor, D.H., Kendall, C., Sebestyen, S.D., Shanley, J.B., Ote, N., Boyer, E.W., 2008. Carbon isotope fractionation of dissolved inorganic carbon (DIC) due to outgassing of carbon dioxide from a headwater stream. *Hydrological Processes* 22, 2410-2423.

Eabry, S., Vance, J.N., Cline, J.E., Robertson, D.E., 1995. Characterization of Carbon-14 Generated by the Nuclear Power Industry: Final Report. Electric Power Research Institute.

Ehrlich, H., 1997. Microbes and metals. *Applied Microbiology and Biotechnology* 48, 687-692.

El-Ghonemy, H., 2004. SCLS Phase 1- Sellafield Groundwater Conceptual Model. Nuclear Sciences and Technology Services.

Evenden, W.G., Sheppard, S.C., Killey, R.W.D., 1998. Carbon-14 and tritium in plants of a wetland containing contaminated groundwater. *Applied Geochemistry* 13, 17-21.

Fischer, H., Ingwersen, J., Kuzyakov, Y., 2010. Microbial uptake of low-molecular-weight organic substances out-competes sorption in soil. *European Journal of Soil Science* 61, 504-513.

Fischer, H., Kuzyakov, Y., 2010. Sorption, microbial uptake and decomposition of acetate in soil: Transformations revealed by position-specific  $^{14}\text{C}$  labeling. *Soil Biology and Biochemistry* 42, 186-192.

Fox, J.R., Mortimer, R.J.G., Lear, G., Lloyd, J.R., Beadle, I., Morris, K., 2006. The biogeochemical behaviour of U(VI) in the simulated near-field of a low-level radioactive waste repository. *Applied Geochemistry* 21, 1539-1550.

Garnier, J.M., 1985. Retardation of dissolved radiocarbon through a carbonated matrix. *Geochimica et Cosmochimica Acta* 49, 683-693.

Gebauer, D., Völkel, A., Cölfen, H., 2008. Stable Prenucleation Calcium Carbonate Clusters. *Science* 322, 1819-1822.

Godwin, H., 1962. Half-life of radiocarbon. *Nature* 195, 984.

Gonfiantini, R., Zuppi, G.M., 2003. Carbon isotope exchange rate of DIC in karst groundwater. *Chemical Geology* 197, 319-336.

Graven, H., Gruber, N., 2011. Continental-scale enrichment of atmospheric  $^{14}\text{C}$   $\text{CO}_2$  from the nuclear power industry: potential impact on the estimation of fossil fuel-derived  $\text{CO}_2$ . *Atmospheric Chemistry and Physics* 11, 12339-12349.

Greenwood, N.N., Earnshaw, A., 1997. Chemistry of the Elements, Second ed. Pergamon Press.

Gregson, C.R., Goddard, D.T., Sarsfield, M.J., Taylor, R.J. 2011. Combined electron microscopy and vibrational spectroscopy study of corroded Magnox sludge from a legacy spent nuclear fuel storage pond. *Journal of Nuclear Materials* 412(1), 145-56.

Gruhlke, J.M., Neiheisel, J., Battist, L., 1986. Estimates of the Quantities, Form and Transport of Carbon-14 in Low-Level Radioactive Waste.

Gu, B., Schulz, R.K., 1991. Anion retention in soil: possible application to reduce migration of buried technetium and iodine. Nuclear Regulatory Commission, Washington, DC (United States). Div. of Regulatory Applications; California Univ., Berkeley, CA (United States). Dept. of Soil Science.

Gu, B., Schulz, R.K., 1991. Anion retention in soil: possible application to reduce migration of buried technetium and iodine. Nuclear Regulatory Commission, Washington, DC (United States). Div. of Regulatory Applications; California Univ., Berkeley, CA (United States). Dept. of Soil Science.

Gulliver, P., Cook, G.T., MacKenzie, A.B., Naysmith, P., Anderson, R., 2007. Sources of anthropogenic (super 14) C to the North Sea.

Hu, Q., Nielsen, M.H., Freeman, C., Hamm, L., Tao, J., Lee, J., Han, T.Y.-J., Becker, U., Harding, J., Dove, P., 2012. The thermodynamics of calcite nucleation at organic interfaces: Classical vs. non-classical pathways. *Faraday Discussions* 159, 509-523.

Hunter, J., 2004. SCLS Phase 1 - Conceptual Model of Contamination Below Ground at Sellafield.

Hutchins, S.R., Miller, D.E., Thomas, A., 1998. Combined laboratory/field study on the use of nitrate for in situ bioremediation of a fuel-contaminated aquifer. *Environmental science & technology* 32, 1832-1840.

IAEA, 2017. *Power Reactor Information System* [Online]. Available <https://www.iaea.org/pris/> [Accessed 21<sup>st</sup> May 2017]

Inskeep, W.P., Bloom, P.R., 1985. An evaluation of rate equations for calcite precipitation kinetics at pCO<sub>2</sub> less than 0.01 atm and pH greater than 8. *Geochimica et Cosmochimica Acta* 49, 2165-2180.

Jackson, C.P., Yates, H., 2011. Key processes and data for the migration of <sup>14</sup>C released from a cementitious repository, Serco Report.

Jakobsen, R., Albrechtsen, H.-J., Rasmussen, M., Bay, H., Bjerg, P.L., Christensen, T.H., 1998. H<sub>2</sub> concentrations in a landfill leachate plume (Grindsted, Denmark): In situ energetics of terminal electron acceptor processes. *Environmental Science & Technology* 32, 2142-2148.

Jefferies, NL, 1990. The evolution of carbon-14 and tritium containing gases in a radioactive waste repository. UK Nirex Ltd Report NSS/R198.

Jones, D.L., Brassington, D.S., 1998. Sorption of organic acids in acid soils and its implications in the rhizosphere. *European Journal of Soil Science* 49, 447-455.

Kaneko, S., Tanabe, H., Sasoh, M., Takahashi, R., Shibano, T., Tateyama, S., 2003. A study on the chemical forms and migration behavior of carbon-14 leached from

the simulated hull waste in the underground condition, Materials Research Society Symposium Proceedings. Warrendale, Pa.; Materials Research Society; 1999, pp. 621-628.

Keogh, S.M., McGee, E.J., Gallagher, D., Mitchell, P.I., 2004. Spatial and temporal impacts of  $^{14}\text{C}$  releases from the Sellafield nuclear complex on the Irish coastline. Radiocarbon 46, 885-892.

Killey, R.W.D., Rao, R.R., Eyvindson, S., 1998. Radiocarbon speciation and distribution in an aquifer plume and groundwater discharge area, Chalk River, Ontario. Applied Geochemistry 13, 3-16.

Konhauser, K.O., Mortimer, R.J., Morris, K., Dunn, V., 2002. The role of microorganisms during sediment diagenesis: implications for radionuclide mobility. Radioactivity in the Environment 2, 61-100.

Kotzer, T., Watson, W., 1999. Spatial and Temporal Distribution of  $^{14}\text{C}$  in Cellulose in Tree Rings in Central and Eastern Canada: Comparison with Long-Term Atmospheric and Environmental Data.

Krauskopf, K.B., Bird, D.K., 1995. Introduction to geochemistry. McGraw-Hill.

Krupka, K., Serne, R., 1998. Effects on radionuclide concentrations by cement/ground-water interactions in support of performance assessment of low-level radioactive waste disposal facilities. Nuclear Regulatory Commission, Division of Waste Management, Washington, DC (United States); Pacific Northwest National Lab., Richland, WA (United States).

Langmuir, D., 1997a. Aqueous Environmental Geochemistry. Prentice Hall.

Langmuir, D., 1997b. Use of laboratory adsorption data and models to predict radionuclide releases from a geological repository: A brief history, Materials Research Society Symposium - Proceedings, pp. [d]769-780.

Law, G.T.W., Geissler, A., Boothman, C., Burke, I.T., Livens, F.R., Lloyd, J.R., Morris, K., 2010. Role of nitrate in conditioning aquifer sediments for technetium bioreduction. *Environmental Science and Technology* 44, 150-155.

Le Mer, J., Roger, P., 2001. Production, oxidation, emission and consumption of methane by soils: A review. *European Journal of Soil Biology* 37, 25-50.

Liepins, L., Thomas, K., 1988. Survey of 14 C literature relevant to a geologic nuclear waste repository. *Radioact. Waste Manage. Nucl. Fuel Cycle* 10, 357-380.

Limer, L., Klos, R., Walke, R., Shaw, G., Nordén, M., Xu, S., 2013. Soil-plant-atmosphere modeling in the context of releases of <sup>14</sup>C as a consequence of nuclear activities. *Radiocarbon* 55, 804-813.

Limer, L.M.C., Thorne, M.C., Cummings, R., 2011. Consideration of canopy structure in modelling <sup>14</sup>C-labelled gas behaviour in the biosphere for human dose assessments. *Radioprotection* 46, S409-S415.

Lloyd, J., Sole, V., Van Praagh, C., Lovley, D., 2000. Direct and Fe (II)-mediated reduction of technetium by Fe (III)-reducing bacteria. *Applied and Environmental Microbiology* 66, 3743-3749.

Lovley, D.R., 1991. Dissimilatory Fe (III) and Mn (IV) reduction. *Microbiological reviews* 55, 259-287.

Lovley, D.R., 1997. Microbial Fe(III) reduction in subsurface environments. *Fems Microbiology Reviews* 20, 305-313.

Lovley, D.R., Chapelle, F.H., 1995. Deep subsurface microbial processes. *Reviews of Geophysics* 33, 365-381.

Lovley, D.R., Phillips, E.J.P., 1988. Novel mode of microbial energy metabolism: organic carbon oxidation coupled to dissimilatory reduction of iron or manganese. *Applied & Environmental Microbiology* 54, 1472-1480.

Macpherson, G.L., 2009. CO<sub>2</sub> distribution in groundwater and the impact of groundwater extraction on the global C cycle. *Chemical Geology* 264, 328-336.

Madigan, M.T., Martinko, J.M., Bender, K.S., Buckley, D.H., Stahl, D.A., 2015. *Brock Biology of Microorganisms*. Pearson Books.

Magnusson, Å., Stenström, K., Skog, G., Adliene, D., Adlys, G., Hellborg, R., Olariu, A., Zakaria, M., Rääf, C., Mattsson, S., 2004. Levels of <sup>14</sup>C in the terrestrial environment in the vicinity of two European nuclear power plants. *Radiocarbon* 46, 863-868.

Marshall, A., Coughlin, D., Laws, F., 2015. *Groundwater monitoring at Sellafield: Annual data review 2014*.

Marshall, T.A., Baston, G.M.N., Otlett, R.L., Walker, A.J., Mather, I.D., 2011. Longer-term release of carbon-14 from irradiated graphite.

Matsumoto, J., Banba, T., Muraoka, S., 1994. Adsorption of carbon-14 on mortar, *MRS Proceedings*. Cambridge Univ Press, p. 1029.

McBeth, J.M., Lear, G., Lloyd, J.R., Livens, F.R., Morris, K., Burke, I.T., 2007. Technetium reduction and reoxidation in aquifer sediments. *Geomicrobiology Journal* 24, 189-197.

McCartney, M., Baxter, M., Scott, E., 1988. Carbon-14 discharges from the nuclear fuel cycle: 1. Global effects. *Journal of environmental radioactivity* 8, 143-155.

McKenzie, H., Armstrong-Pope, N., 2010. *Groundwater Annual Report 2010*. Sellafield Ltd.

McNeely, R., 1994. Long-term environmental monitoring of  $^{14}\text{C}$  levels in the Ottawa region. *Environment International* 20, 675-679.

Miao, Z., Brusseau, M.L., Carroll, K.C., Carreón-Diazconti, C., Johnson, B., 2012. SULFATE REDUCTION IN GROUNDWATER: CHARACTERIZATION AND APPLICATIONS FOR REMEDIATION. *Environmental geochemistry and health* 34, 539-550.

Milton, G., King, K., Sutton, J., Enright, S., 1998. Tracer studies of carbon source utilization in a wetland on the Canadian shield. *Applied geochemistry* 13, 23-30.

Milton, G.M., Kramer, S.J., Brown, R.M., Repta, C.J.W., King, K.J., Rao, R.R., 1995. Radiocarbon dispersion around Canadian nuclear facilities. *Radiocarbon* 37, 485-496.

Mook, W.G., 2006. *Introduction to Isotope Hydrology: Stable and Radioactive Isotopes of Hydrogen, Oxygen and Carbon*. Taylor & Francis.

Mook, W.G., Bommerson, J.C., Staverman, W.H., 1974. Carbon isotope fractionation between dissolved bicarbonate and gaseous carbon dioxide. *Earth and Planetary Science Letters* 22, 169-176.

Morris, K., Livens, F., Charnock, J., Burke, I., McBeth, J., Begg, J., Boothman, C., Lloyd, J., 2008. An X-ray absorption study of the fate of technetium in reduced and reoxidised sediments and mineral phases. *Applied Geochemistry* 23, 603-617.

NCRPM, 1978. A Handbook of radioactivity measurements procedures: with nuclear data for some biomedically important radionuclides. National Council on Radiation Protection and Measurements.

NDA, 2009. Sellafield - the most complex nuclear site in Europe.

Nielsen, M.H., Aloni, S., De Yoreo, J.J., 2014. In situ TEM imaging of CaCO<sub>3</sub> nucleation reveals coexistence of direct and indirect pathways. *Science* 345, 1158-1162.

Nuclear Management Partners, 2016. *Sellafield* [Online]. Available <http://nuclearmanagementpartners.com/sellafield/> [Accessed 21<sup>st</sup> May 2017]

Openshaw, S., Carver, S., Fernie, J., 1989. Britain's nuclear waste: siting and safety.

Parmar, N., Warren, L.A., Roden, E.E., Ferris, F.G., 2000. Solid phase capture of strontium by the iron reducing bacteria *Shewanella alga* strain BrY. *Chemical Geology* 169, 281-288.

Parry, S.A., O'Brien, L., Fellerman, A.S., Eaves, C.J., Milestone, N.B., Bryan, N.D., Livens, F.R., 2011. Plutonium behaviour in nuclear fuel storage pond effluents. *Energy & Environmental Science* 4, 1457-1464.

Petit, L., Bachet, M., Schneider, H., 2013. Study of the speciation of carbon-14 in the primary circuit of pressurized-water reactors. *Journal of Radioanalytical and Nuclear Chemistry* 295, 755-765.

Pilson, M.E.Q., 2012. *An Introduction to the Chemistry of the Sea*. Cambridge University Press.

Plummer, L.N., Busenberg, E., 1982. The solubilities of calcite, aragonite and vaterite in CO<sub>2</sub>-H<sub>2</sub>O solutions between 0 and 90°C, and an evaluation of the aqueous model for the system CaCO<sub>3</sub>-CO<sub>2</sub>-H<sub>2</sub>O. *Geochimica et Cosmochimica Acta* 46, 1011-1040.

Povinec, P., Šivo, A., Ješkovský, M., Svetlík, I., Richtáriková, M., Kaizer, J., 2015. Radiocarbon in the Atmosphere of the Žilkovce Monitoring Station of the Bohunice NPP: 25 Years of Continuous Monthly Measurements. *Radiocarbon* 57, 1-8.

Rao, R., Killely, R., 1994. Quantitative separation and determination of inorganic and organic forms of total carbon and radiocarbon in natural waters and application at a radioactive waste management site. *Radiochimica Acta* 65, 63-74.

Roden, E.E., Leonardo, M.R., Ferris, F.G., 2002. Immobilization of strontium during iron biomineralization coupled to dissimilatory hydrous ferric oxide reduction. *Geochimica et Cosmochimica Acta* 66, 2823-2839.

Roh, C., Kang, C., Lloyd, J.R., 2015. Microbial bioremediation processes for radioactive waste. *Korean J. Chem. Eng* 32, 1720-1726.

Roussel-Debet, S., Gontier, G., Siclet, F., Fournier, M., 2006. Distribution of carbon 14 in the terrestrial environment close to French nuclear power plants. *Journal of Environmental Radioactivity* 87, 246-259.

Runnegar, B., 1985. Shell microstructures of Cambrian molluscs replicated by phosphate. *Alcheringa* 9, 245-257.

Sakuragi, T., Yamashita, Y., Akagi, M., Takahashi, R., 2016. Carbon 14 Distribution in Irradiated BWR Fuel Cladding and Released Carbon 14 after Aqueous Immersion of 6.5 Years. *Procedia Chemistry* 21, 341-348.

Sánchez-Román, M., Fernández-Remolar, D., Amils, R., Sánchez-Navas, A., Schmid, T., Martín-Uriz, P.S., Rodríguez, N., McKenzie, J.A., Vasconcelos, C., 2014. Microbial mediated formation of Fe-carbonate minerals under extreme acidic conditions. *Scientific Reports* 4, 4767.

Sellafield Ltd., 2016. Groundwater monitoring at Sellafield: Annual data review 2015.

Sheppard, M., Sheppard, S., Amiro, B., Schwartz, W., Hawkins, J., Thibault, D., 1990. Soil-to-plant transfer of carbon-14 for environmental assessment of radioactive waste repositories. Electric Power Research Inst., Palo Alto, CA (USA); Atomic Energy of Canada Ltd., Pinawa, MB (Canada). Whiteshell Nuclear Research Establishment.

Sheppard, S.C., Amiro, B.D., Sheppard, M.I., Stephenson, M., Zach, R., Bird, G.A., 1994. Carbon-14 in the biosphere: Modelling and supporting research for the Canadian nuclear fuel waste management program. *Waste Management* 14, 445-456.

Sheppard, S.C., Evenden, W.G., 1996. Retention of inorganic Carbon-14 by isotopic exchange in soils. *Journal of Environmental Quality* 25, 1153-1161.

Sheppard, S.C., Ticknor, K.V., Evenden, W.G., 1998. Sorption of inorganic  $^{14}\text{C}$  on to calcite, montmorillonite and soil. *Applied Geochemistry* 13, 43-47.

Sherman, L.A., Barak, P., 2000. Solubility and Dissolution Kinetics of Dolomite in Ca–Mg–HCO<sub>3</sub>/CO<sub>3</sub> Solutions at 25°C and 0.1 MPa Carbon Dioxide. *Soil Science Society of America Journal* 64, 1959-1968.

Sposito, G., 1989. *The Chemistry of Soils*. Oxford University Press.

Stamper, A., McKinlay, C., Coughlin, D., Laws, F., 2012. *Land Quality Programme Groundwater Monitoring at Sellafield*. Sellafield Ltd.

Stumm, W., Morgan, J.J., 1996. *Aquatic chemistry: chemical equilibria and rates in natural waters*. Wiley.

Stumm, W., Sulzberger, B., 1992. The cycling of iron in natural environments: considerations based on laboratory studies of heterogeneous redox processes. *Geochimica et Cosmochimica Acta* 56, 3233-3257.

Su, C., Suarez, D.L., 1997. In situ infrared speciation of adsorbed carbonate on aluminum and iron oxides. *Clays and Clay Minerals* 45, 814-825.

Suess, H.E., 1955. Radiocarbon concentration in modern wood. *Science* 122, 415-417.

Tabak, H.H., Lens, P., van Hullebusch, E.D., Dejonghe, W., 2005. Developments in bioremediation of soils and sediments polluted with metals and radionuclides–1. Microbial processes and mechanisms affecting bioremediation of metal contamination and influencing metal toxicity and transport. *Reviews in Environmental Science and Biotechnology* 4, 115-156.

Thorpe, C.L., Law, G.T.W., Boothman, C., Lloyd, J.R., Burke, I.T., Morris, K., 2012a. The Synergistic Effects of High Nitrate Concentrations on Sediment Bioreduction. *Geomicrobiology Journal* 29, 484-493.

Thorpe, C.L., Lloyd, J.R., Law, G.T.W., Burke, I.T., Shaw, S., Bryan, N.D., Morris, K., 2012b. Strontium sorption and precipitation behaviour during bioreduction in nitrate impacted sediments. *Chemical Geology* 306-307, 114-122.

UNSCEAR, 2010. UNSCEAR 2008 report to the General Assembly, New York: United Nations.

Vaitkevičienė, V., Mažeika, J., Skuratovič, Ž., Motiejūnas, S., Vaidotas, A., Oryšaka, A., Ovčinnikov, S., 2013. <sup>14</sup>C in Radioactive Waste for Decommissioning of the Ignalina Nuclear Power Plant. *Radiocarbon* 55.

van Geen, A., Robertson, A.P., Leckie, J.O., 1994. Complexation of carbonate species at the goethite surface: Implications for adsorption of metal ions in natural waters. *Geochimica et Cosmochimica Acta* 58, 2073-2086.

Van Konynenburg, R.A., 1994. Behavior of carbon-14 in waste packages for spent fuel in a tuff repository. *Waste Management* 14, 363-383.

Vance, J., Cline, J., Robertson, D., 1995. Characterization of carbon-14 generated by the nuclear power industry. Electric Power Research Institute, TR-105715, Palo Alto.

Wang, Z., Hu, D., Xu, H., Guo, Q., 2014. <sup>14</sup>C Distribution in Atmospheric and Aquatic Environments Around Qinshan Nuclear Power Plant, China. *Radiocarbon* 56, 1107-1114.

Weber, K.A., Achenbach, L.A., Coates, J.D., 2006. Microorganisms pumping iron: anaerobic microbial iron oxidation and reduction. *Nature Reviews Microbiology* 4, 752-764.

White, W., 2013. *Geochemistry*. Wiley-Blackwell.

Wieland, E., Hummel, W., 2015. Formation and stability of <sup>14</sup>C-containing organic compounds in alkaline iron-water systems: Preliminary assessment based on a literature survey and thermodynamic modelling. *Mineralogical Magazine* 79, 1275-1286.

Wieland, E., Jakob, A., Tits, J., Lothenbach, B., Kunz, D., 2016. Sorption and diffusion studies with low molecular weight organic compounds in cementitious systems. *Applied Geochemistry* 67, 101-117.

Wigley, T.M.L., Plummer, L.N., Pearson Jr, F.J., 1978. Mass transfer and carbon isotope evolution in natural water systems. *Geochimica et Cosmochimica Acta* 42, 1117-1139.

Wijnja, H., Schulthess, C.P., 2000. Interaction of carbonate and organic anions with sulfate and selenate adsorption on an aluminum oxide. *Soil Science Society of America Journal* 64, 898-908.

Wilson, C.N., 1990. Results from NNWSI Series 3: Spent Fuel Dissolution Tests. Pacific Northwest Laboratory.

Wilson, P.D., 1996. *The nuclear fuel cycle from ore to wastes*.

Xu, M., Zhang, Q., Xia, C., Zhong, Y., Sun, G., Guo, J., Yuan, T., Zhou, J., He, Z., 2014. Elevated nitrate enriches microbial functional genes for potential

bioremediation of complexly contaminated sediments. *The ISME journal* 8, 1932-1944.

Xu, S., Cook, G.T., Cresswell, A.J., Dunbar, E., Freeman, S.P., Hastie, H., Hou, X., Jacobsson, P., Naysmith, P., Sanderson, D.C., 2016a.  $^{14}\text{C}$  levels in the vicinity of the Fukushima Dai-ichi Nuclear Power Plant prior to the 2011 accident. *Journal of environmental radioactivity* 157, 90-96.

Xu, S., Cook, G.T., Cresswell, A.J., Dunbar, E., Freeman, S.P., Hou, X., Jacobsson, P., Kinch, H.R., Naysmith, P., Sanderson, D.C., 2016b. Radiocarbon Releases from the 2011 Fukushima Nuclear Accident. *Scientific reports* 6.

Yim, M.-S., Caron, F., 2006. Life cycle and management of carbon-14 from nuclear power generation. *Progress in Nuclear Energy* 48, 2-36.

Zhang, J., Quay, P.D., Wilbur, D.O., 1995. Carbon isotope fractionation during gas-water exchange and dissolution of  $\text{CO}_2$ . *Geochimica et Cosmochimica Acta* 59, 107-114.

## Chapter 3 Methods

This chapter describes in detail the sample collection and methods used for experimental and analytical work presented in this thesis, with theoretical background to the techniques employed where appropriate.

### 3.1 Sediment collection

Sediment was collected from the River Calder valley near Calder Bridge, Cumbria, UK (Lat 54°26.3'N, Long 3°28.2'W) in August 2015 and July 2016 (Figure 3-1). This sediment is representative of the glacial/fluvial quaternary deposits that underlie the UK Sellafield nuclear reprocessing plant (Wallace et al., 2012, Law et al., 2010). Sediment was collected in HDPE plastic containers before being transferred to sterile HDPE bags and stored at 4°C. Prior to use the soil was sieved to retain <2 mm fraction.

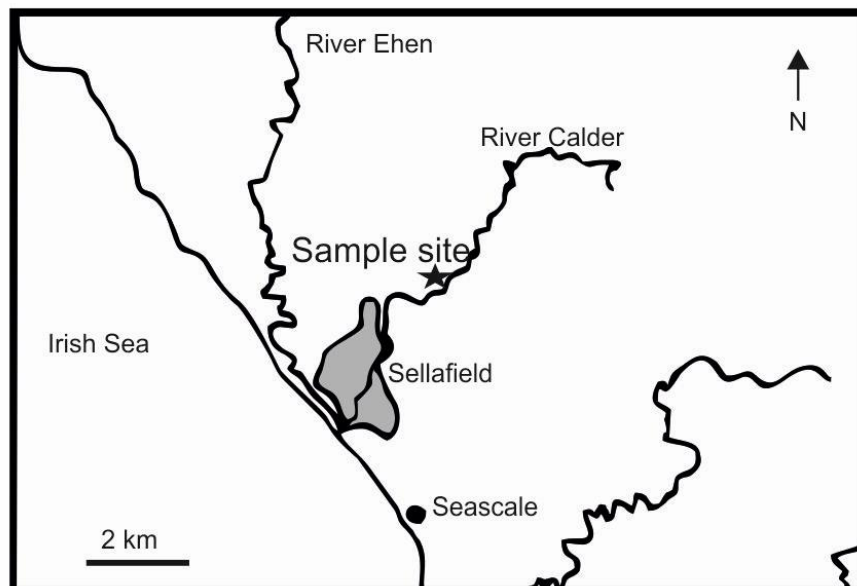


Figure 3-1 Site map showing location of sediment collection. Adapted from Wallace et al. (2012).

## 3.2 Sediment and mineral characterisation

### 3.2.1 X-ray Diffraction

Bulk mineral composition was determined using X-ray diffraction (XRD) (Cu-K alpha radiation) on a Bruker D8 Advance XRD. XRD is a technique using X-ray beams to determine the crystallographic structure of minerals. The x-ray beam is directed at the sample, with x-rays then being reflected from the crystal planes of the mineral. The distance that the X-rays travel in to the crystal before reflection is dependent on the angle of the X-ray beam in relation to the sample ( $\theta$ ) and the spacing between the layers of atoms ( $d$ ). When the reflected X-rays from different layers are in phase with each other they allow X-ray beams to leave the sample, resulting in a diffraction pattern (Brown, 1971). Each spectra is unique for a pure crystal structure and the patterns are produced independently so they are identifiable in mixed samples allowing the identification of the individual minerals. For analysis, all samples were dried and ground to a fine powder (<150 micron) before placing in a sample holder. Diffraction patterns were measured on a Bruker D8 Advance XRD using Cu-K alpha 1 radiation from  $2\theta$  angles of 2-86°. The step size was 0.2° with counting of one step per second. Diffraction peaks are indexed to reference patterns in the EVA software using the International Centre for Diffraction Data Powder Diffraction Files database (PDF-2) to match the full scan or selected peaks against those in the database. The limit of detection is dependent on the crystallinity of the phase but it is able to detect to < 1%, low abundance and non-crystalline phases are not determined in this analysis.

### 3.2.2 Surface area determination

N<sub>2</sub>-specific surface area was measured using the Brunauer-Emmett-Teller method (Brunauer et al., 1938). The volume of gas adsorbed to the surface of the particles is measured at the boiling point of nitrogen (-196°C). The amount of adsorbed gas can then be correlated to the total surface area of the particles including pores in the surface.

Specifically this analysis used the Micrometrics Gemini V Surface Area Analyser with nitrogen used as the adsorbate gas and helium used to measure dead volume. 0.5 g of sample was placed in to a 15 ml pre-weighed glass tube, the tube and sample were then weighed again. The tube was placed in the degasser degassed with nitrogen gas for a minimum of 19 hours at 60°C prior to analysis ensuring the bung was kept in. Sample was then left to cool prior to testing, with N<sub>2</sub>(g) still flowing in the tube. The sample and tube were reweighed prior to analysis. Liquid nitrogen is placed in the measurement Dewar, ensuring that the level was no less than 2 cm from the top. During the sample run an adsorption isotherm is constructed point-by-point by the admission and withdrawal of a known amount of N<sub>2</sub> gas. Adsorption is the adhesion of atoms, ions or molecules from a gas, liquid or dissolved solid to a surface. The BET method is only applicable to adsorption isotherms which are disperse, nonporous, macroporous or mesoporous (pore diameter between 2 and 50 nm). As the gas is pumped in to the sample tube it covers all accessible pores with a complete monolayer of adsorbate. The amount of gas used to create this monolayer can then be calculated from the adsorption isotherm using the BET equations:

$$S_{\text{total}} = (v_m N_s) / V \quad \text{Equation 3-1}$$

$$S_{\text{BET}} = S_{\text{total}} / a \quad \text{Equation 3-2}$$

Where  $v_m$  is in units of volume which are also the units of the monolayer volume of the adsorbate gas,  $N$  is Avogadro's number,  $s$  the adsorption cross section of the adsorbing species,  $V$  the molar volume of the adsorbate gas, and  $a$  the mass of the solid sample/adsorbent.

### **3.3 Iron analysis by spectrophotometry**

The following methods for iron measurement are spectrophotometric methods. The fundamental basis of spectrophotometry is that some compounds absorb radiation at characteristic wavelengths. This means that if a monochromatic light is shone through an aqueous sample of a compound, a portion of the light is absorbed at a characteristic wavelength while the remainder passes through the sample and is detected. There is typically a linear relationship between the amount of radiation absorbed, the thickness of the sample and the concentration of the compound which is described by the Beer-Lambert Law (see Equation 3-3 below):

$$A = \epsilon \cdot b \cdot c$$

Equation 3-3

Where  $A$  = absorbance (no units);  $\epsilon$  = molar absorptivity ( $1 \text{ mol}^{-1} \text{ cm}^{-1}$ );  $b$  = path length of the sample (width of cuvette, cm); and  $c$  = concentration of the compound ( $\text{mol L}^{-1}$ ).

### 3.3.1 Determination of total aqueous Fe

The production of Fe in solution occurs as the microbial reduction of Fe (III) to Fe (II) causes a redistribution of Fe phases between solid and solution leading to Fe (II) in solution. The appearance of the Fe(II) in solution is used as an indicator of Fe (III) reduction occurring (Lovley, 1997; Roden and Urrutia, 1999; Roden and Zachara, 1996) which usually occurs after the appearance of Fe (II) in the solid fraction (Burke et al., 2005; Islam et al., 2004). In these experiments total Fe in solution is assumed to represent the Fe (II) fraction in solution as Fe(III) has limited solubility at circumneutral pH. Total dissolved iron was determined using the ferrozine method of Viollier et al., 2000. In a 1cm path length cuvette 100  $\mu\text{L}$  of sample was diluted to 1 mL using deionised water (DIW). To this 100  $\mu\text{L}$  of ferrozine (0.01 M ferrozine prepared in 0.1 M ammonium acetate) was added with 200  $\mu\text{L}$  of hydroxylamine hydrochloride (1.4 M hydroxylamine hydrochloride in a 2 M hydrochloric acid) and 100  $\mu\text{L}$  of the buffer solution (5 M ammonium acetate adjusted to pH 9.5 with ammonium hydroxide). This mixture is left for 10 minutes to allow full reduction of all Fe (III) before analysis. Ferrozine binds with Fe (II)(aq) to form a purple ligand complex. The buffer is added to ensure the pH is at the optimum range (pH 4-9) for the ligand formation. Absorbance is measured

at 562 nm on a Jenway 6715 UV vis Spectrophotometer. Standards were prepared from 0 – 250 ppb Fe by dilution of Fe certified stock solution (Certipur). Standards were run throughout the experiments and calibration regressions linear  $R^2$  always exceeded 0.99.

### **3.3.2 Determination of extractable Fe(II) in sediments**

The amount of Fe (II) in the sediment is expressed as a percentage of the total Fe in sediment. Fe (II) is extracted using acid extraction based on the method of Lovley and Phillips (1986). This extraction is used to determine the ratio of Fe(II) in the solids which is extracted by 0.5 N HCl to the total amount of Fe(III) in the solids also extracted by 0.5 N HCl. The HCl extractions are used to indicate the formation of solid biogenic Fe(II) from the microbial reduction of Fe(III) containing phase (Lovley and Phillips, 1986; Zachara et al., 1998). 5 mL of 0.5 N HCl was added to sediment (~0.1g) and left for 60 minutes. The solution was passed through a 0.2  $\mu\text{m}$  filter. From this two 100  $\mu\text{L}$  aliquots were taken and placed in 1.5 mL cuvettes. The first sample was diluted to 1 mL using DIW before addition of ferrozine (0.01 M ferrozine prepared in 0.1 M ammonium acetate). This analysis determines the amount of Fe (II) extractable by 0.5 N HCl in the sediment. The second sample was diluted to 1 mL using DIW before addition of 100  $\mu\text{L}$  of ferrozine and 200  $\mu\text{L}$  of hydroxylamine hydrochloride (1.4 M hydroxylamine hydrochloride in a 2 M hydrochloric acid) and 100  $\mu\text{L}$  of ammonium acetate buffer (5 M ammonium acetate adjusted to pH 9.5 with ammonium hydroxide). The samples were left for 10 minutes to allow for

complete reduction in the second sample and colour development in both. The absorbance of the samples was measured at 562 nm and corrected using the absorbance of the reagent-only blank. The percentage of extractable Fe as Fe (II) was then calculated using:

$$\left( \frac{A_{562}^{\text{cuvette1}}}{A_{562}^{\text{cuvette2}}} \right) \times 100 \quad \text{Equation 3-4}$$

### **3.4 Determination of nitrate and nitrite by Auto Analyser3**

The analysis of aqueous nitrate and nitrite is an automated continuous segmented flow procedure which measures nitrite and total nitrogen (by reduction of nitrate)(Armstrong et al., 1967; Grasshoff, 1969). Nitrate reduction is achieved using a copper-cadmium reductor column, the nitrite formed then reacts with sulphanilamide under acidic conditions forming a diazo compound. Finally this compound couples with N-1-naphthylethylene diamine dihydrochloride to form a purple azo dye which is measured spectrophotometrically. In all samples that underwent this analysis the concentration of all oxidising, reducing and interfering metal ions was sufficiently low as to cause no interference.

### **3.5 Batch microcosm experiments**

Methods for individual experiments are detailed in the methods section of the relevant results chapter (Chapters 6 and 7). Below is a general description of methods used for microcosm sterilisation and the sampling technique employed.

### **3.5.1 Heat sterilisation**

Heat sterilisation of soils by autoclaving is a widespread technique due to the availability and ease of use of equipment. The autoclave was set at 121°C and run for 20 minutes, ensuring that the soil layer was not too deep and so the steam was able to fully penetrate the soil (Trevors, 1996). For this work it was decided that one cycle of 121°C would be adequate to eliminate the majority of organisms in the sediment. It has been applied in this way as heat sterilisation has minimal effect on soil pH, organic matter content and cation exchange capacity (Lostrario et al., 1995). The avoidance of Na<sup>+</sup> and Cl<sup>-</sup> leaching and any pH changes to soil were considered crucial to these experiments. Although dry sterilisation (no steam production) can also be used it has limited impact on any spore-forming bacteria so autoclaving has been employed.

### **3.5.2 Microcosm sampling technique**

Sediment and synthetic groundwater slurry (~3 mL) was extracted with a sterile needle (25G x 1" 0.5 mm x 25 mm) from sealed microcosm bottles under oxygen-free nitrogen and placed in to a pre-weighed 50 mL centrifuge tube. Tubes were centrifuged for 10 minutes at 8,000 g (SIGMA 2-16 centrifuge). Supernatant was placed in a clean 50 mL centrifuge tube and the tube plus solid was weighed again. This sediment was used for solid Fe analysis (see 3.3.2). 1 mL of supernatant was filtered (0.2 µm) in to a clean microcentrifuge tube (1.5 mL for determination of Fe in solution (see 3.3.1) and nitrate and nitrite analysis (section 3.4). The pH of the remaining supernatant was measured using Thermo Scientific Orion benchtop multimeter, with a VWR 662-1759 pH electrode calibrated daily at pH 4, 7 and 10,

before an aliquot was removed for liquid scintillation analysis (see Chapter 4 for discussion of liquid scintillation method).

### 3.5.3 Carbon-14 spike details

Inorganic  $^{14}\text{C}$  was added in the form sodium carbonate producing a final activity of  $100 \text{ Bq mL}^{-1}$  ( $4.5 \times 10^{-8} \text{ M } ^{14}\text{CO}_3^{2-}$ ). Organic  $^{14}\text{C}$  was added as acetate (methyl group labelled), formate, formaldehyde and methanol producing a final activity of  $100 \text{ Bq mL}^{-1}$  ( $5 \times 10^{-7} \text{ M}$ ).

## 3.6 Microbiological analysis

For Chapters 6 and 7 nucleotide sequences were determined using Next Generation sequencing. DNA was extracted from soil samples ( $\sim 0.5\text{g}$ ) using the Fast DNA spin kit for soil (MP Bio). DNA fragments in the size range 3 kb to approximately 20 kb were isolated on a 1% agarose “1x” Tris-borate-EDTA (TBE) gel stained with ethidium bromide for viewing under UV light (10x TBE solution supplied by Invitrogen Ltd., UK). The DNA was extracted from the gel using a QIAquick gel extraction kit (QIAGEN Ltd, UK); final elution was by 1/10th strength elution buffer (unless explicitly stated, the manufacturer’s protocols supplied with all kits employed were followed precisely). DNA concentration was quantified fluorometrically using a Qubit dsDNA HS Assay (Thermo Fisher Scientific Inc., USA).

DNA samples ( $1\text{ng}/\mu\text{L}$  in  $20 \mu\text{L}$  aqueous solution) were sent for sequencing at the Centre for Genomic Research, University of Liverpool, where Illumina TruSeq adapters and indices were attached to DNA fragments in a two-

step PCR amplification targeting the 16S rRNA gene. Pooled amplicons were paired-end sequenced on the Illumina MiSeq platform (2x250 bp). Illumina adapter sequences were removed, and the trimmed reads were processed using the UPARSE pipeline (Edgar, 2013) within the USEARCH software (version 9.2) on a Linux platform. Overlapping paired end reads were merged prior to quality filtering and relabelling. The entire sequence run was clustered, with chimeras and singletons removed for generation of the operational taxonomic units (OTUs) which were defined by minimum of 97% sequence identity between the putative OTU members. Taxonomy was defined using a confidence value of more than 0.7 to balance sensitivity and error rate in the prediction using the online Ribosomal Database Project (Wang et al., 2007). The entire set was then allocated to the OTUs and reported in the OTU table with the taxonomy and abundance of the OTUs.

### **3.7 Statistical analysis**

#### **3.7.1 Standard deviation and relative standard deviation**

Standard deviation (SD or  $\sigma$ ) is a measure of the deviation of a set of data from the arithmetic mean of the data. If all measured values across a data set were the same then  $\sigma$  would equal 0; in a data set with a large spread of values  $\sigma$  would be larger than 0.  $\sigma$  is calculated as the square root of variance in a data set. The standard deviation was calculated for most geochemical measurement (where  $n=3$  or larger), unless stated otherwise in the methods sections of individual data chapters, using the equation below:

$$\sigma = \sqrt{\frac{\sum(x-\bar{x})^2}{n-1}} \quad \text{Equation 3-5}$$

For small numbers of replicates the normalcy (i.e. the Gaussian distribution of the data) has been assumed, therefore the data plotted using the mean  $\pm 1$  SD only provides an estimate of the variability in the experimental data.

Relative standard deviation (RSD) is calculated from SD. In this thesis it has been used to express the precision and repeatability of the measurements taken throughout an experiment, especially when measurements were taken on a number of different days, by using the equation below:

$$\%RSD = \frac{\sigma}{\bar{x}} \times 100 \quad \text{Equation 3-6}$$

A lower percentage represents a lower variability in the data set.

### 3.7.2 Defining microbiological diversity

Statistical analysis was performed to determine the bacterial diversity. In this project the alpha diversity was defined using Hill numbers,  $D_q$ , (Hill, 1973; Jost, 2006). Hill numbers define the biodiversity as the reciprocal mean of proportional abundance and compensate for the disproportionate impact of rare taxa by weighting taxa based on abundance. The degree of weighting is controlled by the index  $q$  where increasing  $q$  places progressively more weight on the high-abundance species in a population (Hill., 1973; Jost, 2006, 2007; Kang et al., 2016).  $D_0$  is the unweighted Hill number and is equal to the species richness.  $D_1$  is a measure of the common species and is equivalent to the exponential of Shannon

entropy.  $D_2$  is a measure of the number of dominant species and is equivalent to the inverse of Simpson concentration (Hill, 1973; Jost, 2006, 2007).

$$D_a = \left( \sum_{i=1}^s p_i^a \right)^{\frac{1}{1-a}} \quad (\text{Equation 3-7})$$

The parameter  $a$  defines the special case of the Hill number.

Non-metric Multi-Dimensional Scaling (NMDS) was used to graphically represent the similarity between bacterial assemblages. The aim of this technique is to collapse information from multiple dimensions (in this case samples) in to two dimensions for visualisation. This was done in an optimised two dimensional space using the Bray-Curtis dissimilarity matrix. NMDS was carried out in the package ‘vegan’ (Oksanen et al., 2013) in RStudio v 99.9.9 (RStudio Team, 2015). The microbial community data were input as a matrix of the relative abundance of each OTU.

### **3.8 Thermodynamic modelling**

Geochemical modelling was undertaken using the PHREEQC (version 3) geochemistry program (Parkhurst and Appelo, 2013a) and the Hatches database (version 18) (Cross and Ewart, 1991). PHREEQC is a computer program used to perform aqueous geochemistry calculations. It is based on equilibrium chemistry of aqueous solutions interacting with minerals, gases, solid solutions and sorption surfaces, as well as the ability to model kinetics and one-dimensional transport (Parkhurst and Appelo, 2013b). A database is used to perform the calculations on

a set of user-defined input values. In data chapter one equilibrium geochemical modelling was used to define the solution compositions required for desired values of the  $SI_{CAL}$  in precipitation experiments. It was also used to establish the calcium concentration and carbonate alkalinity required at a given  $SI_{CAL}$  and pH, and to model the potential precipitation of calcite at the Sellafield site in the UK under leak scenarios.

Input parameters for PHREEQC modelling to determine the solution compositions for experiments undertaken in Chapter 5 are shown below.

Table 3-1 Input solution compositions for precipitation experiments to achieve desired range of Saturation Indices.

Predicted Saturation Index	PHREEQC input
+2.92	20°C; pH 9; 0.03 M Na <sub>2</sub> CO <sub>3</sub> equilibrated with atmospheric CO <sub>2</sub> (g), 0.02 M CaCl <sub>2</sub>
+2.51	20°C; pH 9; 0.015 M Na <sub>2</sub> CO <sub>3</sub> equilibrated with atmospheric CO <sub>2</sub> (g), 0.015 M CaCl <sub>2</sub>
+2.12	20°C; pH 9; 0.0075 M Na <sub>2</sub> CO <sub>3</sub> , 0.005 M NaOH equilibrated with atmospheric CO <sub>2</sub> (g), 0.006 M CaCl <sub>2</sub>
+1.58	20°C; pH 9; 0.005 M Na <sub>2</sub> CO <sub>3</sub> , 0.005 M NaOH equilibrated with atmospheric CO <sub>2</sub> (g), 0.0015 M CaCl <sub>2</sub>
+0.96	20°C; pH 9; 0.0025 M Na <sub>2</sub> CO <sub>3</sub> , 0.005 M NaOH equilibrated with atmospheric CO <sub>2</sub> (g), 0.0005 M CaCl <sub>2</sub>
+0.48	20°C; pH 9; 0.0025 M Na <sub>2</sub> CO <sub>3</sub> , 0.005 M NaOH equilibrated with atmospheric CO <sub>2</sub> (g), 0.00015 M CaCl <sub>2</sub>
+0.01	20°C; pH 9; 0.0025 M Na <sub>2</sub> CO <sub>3</sub> , 0.005 M NaOH equilibrated with atmospheric CO <sub>2</sub> (g), 0.00005 M CaCl <sub>2</sub>
-0.98	20°C; pH 9; 0.0025 M Na <sub>2</sub> CO <sub>3</sub> , 0.005 M NaOH equilibrated with atmospheric CO <sub>2</sub> (g), 0.000005 M CaCl <sub>2</sub>

Table 3-1 shows the solution compositions used in precipitation experiments in Chapter 5 to attain the saturation indices defined in the model

output. All models were equilibrated with atmospheric CO<sub>2</sub> to replicate the laboratory conditions as completely as possible.

Table 3-2 PHREEQC input code for modelling the interaction of silo leachate with groundwater under Sellafield reprocessing site, UK. pH was allowed to equilibrate within the model to achieve charge balance.

Composition name	PHREEQC input Units g/L
Surface of Magnox Swarf Storage Silo (MSSS) site data (Sellafield Ltd., 2009)	pH 9; Na 0.31; N 0.57; C 0.12 equilibrated with atmospheric CO <sub>2</sub> (g); S 0.02
Theoretical composition when MSSS liquor equilibrated with MgCO <sub>3</sub> (s)	pH 9; Na 0.31;N 0.57;C 0.18 equilibrated with atmospheric CO <sub>2</sub> (g);S 0.02; Mg 0.03
Groundwater composition of well near to leak source site data (Graham, 2013)	pH 6.5; K 0.0043; Na 0.025;Ca 0.038; Mg 0.005; Cl 0.057; S 0.020; N 0.020; C 0.075 equilibrated with atmospheric CO <sub>2</sub> (g)

Table 3-2 details the solution compositions as input to PHREEQC to model the possibility of calcite precipitation occurring in the subsurface below Sellafield reprocessing site, UK. Two of the compositions are based on site data (surface of MSSS and groundwater near leak site) with PHREEQC used to model the theoretical composition of liquor at greater depth of the tank assuming equilibration with MgCO<sub>3</sub>(s).

### 3.9 References

Armstrong, F.A.J., Stearns, C.R., Strickland, J.D.H., 1967. The measurement of upwelling and subsequent biological process by means of the Technicon Autoanalyzer® and associated equipment. Deep Sea Research and Oceanographic Abstracts 14, 381-389.

- Brown, M.A., 1971. X-ray methods. Merrow; Watford.
- Brunauer, S., Emmett, P.H., Teller, E., 1938. Adsorption of gases in multimolecular layers. *Journal of the American chemical society* 60, 309-319.
- Burke, I.T., Boothman, C., Lloyd, J.R., Mortimer, R.J.G., Livens, F.R., Morris, K., 2005. Effects of progressive anoxia on the solubility of technetium in sediments. *Environmental Science and Technology* 39, 4109-4116.
- Cross, J.E., Ewart, F.T., 1991. Hatches — A Thermodynamic Database And Management System. *Radiochimica Acta* 52-53, 421-422.
- Edgar, R.C., 2013. UPARSE: highly accurate OTU sequences from microbial amplicon reads. *Nature methods* 10, 996-998.
- Graham, J. 2013. ERT Trial Groundwater Analysis – Rounds 16 – 19. NNL Technical Memorandum LP06489/06/10/07.
- Grasshoff, K. 1969. Advances in automated analysis, Technicon International Congress, Vol. II: 147-150.
- Hill, M.O., 1973. Diversity and evenness: a unifying notation and its consequences. *Ecology* 54, 427-432.
- Islam, F.S., Gault, A.G., Boothman, C., Polya, D.A., Charnock, J.M., Chatterjee, D., Lloyd, J.R., 2004. Role of metal-reducing bacteria in arsenic release from Bengal delta sediments. *Nature* 430, 68-71.
- Jost, L., 2006. Entropy and diversity. *Oikos* 113, 363-375.
- Jost, L., 2007. Partitioning diversity into independent alpha and beta components. *Ecology* 88, 2427-2439.

Lothrario, J., Stuart, B., Lam, T., Arands, R., O'Connor, O., Kosson, D., 1995. Effects of sterilization methods on the physical characteristics of soil: implications for sorption isotherm analyses. *Bulletin of environmental contamination and toxicology* 54, 668-675.

Lovley, D.R., 1997. Microbial Fe(III) reduction in subsurface environments. *Fems Microbiology Reviews* 20, 305-313.

Lovley, D.R., Phillips, E.J., 1986. Organic matter mineralization with reduction of ferric iron in anaerobic sediments. *Applied and Environmental Microbiology* 51, 683-689.

Oksanen, J., Blanchet, F.G., Kindt, R., Legendre, P., Minchin, P.R., O'Hara, R.B., Simpson, G.L., Solymos, P., Stevens, M.H.H., and Wagner, H. (2013). *vegan: Community Ecology Package*. R package version 2.0-10 [Online]. Available: <http://CRAN.R-project.org/package=vegan> [Accessed 22<sup>nd</sup> May 2017].

Parkhurst, D., Appelo, C., 2013a. PHREEQC (Version 3)—A computer program for speciation, batch-reaction, one-dimensional transport, and inverse geochemical calculations. US Geological Survey: The United States.

Parkhurst, D.L., Appelo, C.A.J., 2013b. Description of input and examples for PHREEQC version 3- A computer program for speciation, batch-reaction, one-dimensional transport, and inverse geochemical calculations, U.S. Geological Survey Techniques and Methods, p. 497.

Roden, E.E., Urrutia, M.M., 1999. Ferrous iron removal promotes microbial reduction of crystalline iron(III) oxides. *Environmental Science and Technology* 33, 1847-1853.

Roden, E.E., Zachara, J.M., 1996. Microbial reduction of crystalline iron(III) oxides: Influence of oxide surface area and potential for cell growth. *Environmental Science and Technology* 30, 1618-1628.

Sellafield Ltd., 2009. Generic Basis for Inventory Challenge – Legacy Alkaline Sludge Systems, Sellafield Ltd., Cumbria, UK.

RStudio Team (2015). "RStudio: Integrated Development Environment for R". .0.99.486 ed. (Boston, MA: RStudio, Inc). Retrieved from <http://www.rstudio.com/>

Trevors, J., 1996. Sterilization and inhibition of microbial activity in soil. *Journal of Microbiological Methods* 26, 53-59.

Viollier, E., Inglett, P.W., Hunter, K., Roychoudhury, A.N., Van Cappellen, P., 2000. The ferrozine method revisited: Fe(II)/Fe(III) determination in natural waters. *Applied Geochemistry* 15, 785-790.

Wallace, S.H., Shaw, S., Morris, K., Small, J.S., Fuller, A.J., Burke, I.T., 2012. Effect of groundwater pH and ionic strength on strontium sorption in aquifer sediments: Implications for <sup>90</sup>Sr mobility at contaminated nuclear sites. *Applied Geochemistry* 27, 1482-1491.

Wang, Q, G. M. Garrity, J. M. Tiedje, and J. R. Cole. 2007. Naïve Bayesian Classifier for Rapid Assignment of rRNA Sequences into the New Bacterial Taxonomy. *Appl Environ Microbiol.* 73(16), 261-7.

Zachara, J.M., Fredrickson, J.K., Li, S.M., Kennedy, D.W., Smith, S.C., Gassman, P.L., 1998. Bacterial reduction of crystalline Fe<sup>3+</sup> oxides in single phase suspensions and subsurface materials. *American Mineralogist* 83, 1426-1443.

## Chapter 4 Method development – measuring $^{14}\text{C}$

This chapter describes the development of liquid scintillation techniques applied throughout this study to measure  $^{14}\text{C}$  in a variety of forms and phases.

### 4.1 Description of liquid scintillation

Liquid scintillation (LS) is an analytical technique used to measure the activity of radionuclides by converting the energy produced by a radioactive decay event into photons of light and recording the rate of these photon emissions (Kessler, 1989; Passo and Cook, 1994). The radioactive decay event of  $^{14}\text{C}$  releases a beta particle ( $\beta^-$ ) and antineutrino ( $\bar{\nu}$ ). They are released simultaneously and carry the decay energy from the nucleus. For  $^{14}\text{C}$  the maximum decay energy is 156.48 keV, this energy is shared randomly between the  $\beta^-$  and  $\bar{\nu}$ , therefore the  $\beta^-$  particle can possess any energy between 0 and 156.48 keV with an average value of 49.47 keV (NCRPM, 1978). The LS cocktails are typically made up of four components: solvent; primary scintillator; secondary scintillator, and surfactant. In the relatively dense liquid scintillant the beta particle is only able to travel a short distance before all of its kinetic energy is dissipated. Firstly the solvent converts the kinetic energy ( $\beta^-$ ) of radiation in to excitation energy. This excitation energy is transferred to the primary scintillator where it is converted in to photons, which are emitted by the scintillant as it returns to ground state. A secondary scintillator is often employed to shift the light wavelength of the emitted photons to a more optimal range to be detected by the photo multiplier tubes (PMTs). The PMTs then convert the photons into electrical pulses which are quantified by the liquid

scintillation analyser as counts per minute (CPM) (see Figure 4-1). Finally the surfactant is an emulsifier which creates a stable, homogeneous emulsion by forming micelles with aqueous samples and organic solvents ensuring that the samples are held closely with the solvent to ensure the maximum efficiency of energy transfer.

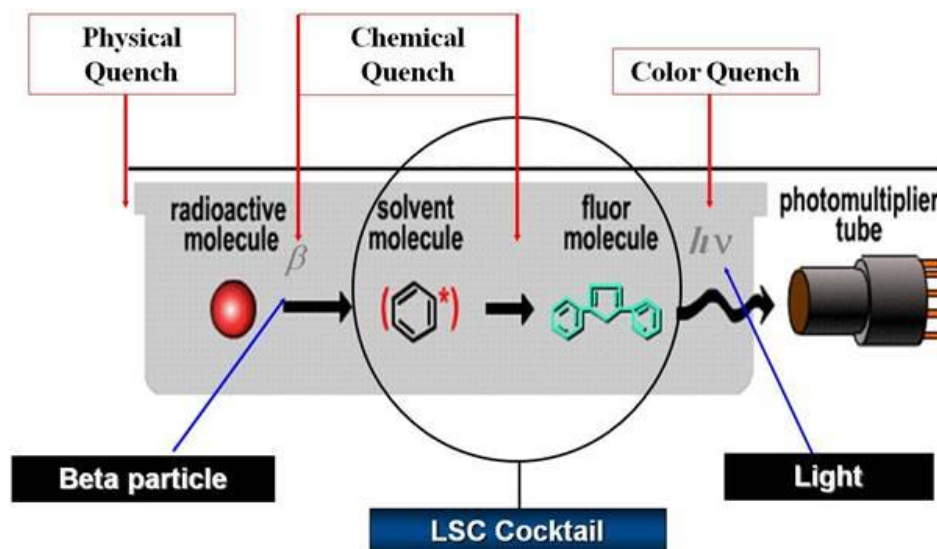


Figure 4-1 Taken from Thomson (2001) showing the pathway from radioactive decay energy emission to the detection of photons by the PMTs. The diagram also highlights the different stages of the energy transfer process which may be impacted by differing types of quench.

This counting procedure relies on the sample and scintillator being dissolved in an aromatic solvent, which allows the energy to be transferred, anything which reduces the efficiency of the energy transfer or causes the photons to be adsorbed before being measured by the PMTs results in quenching of the sample. Quenching is defined as the loss of counts due to sample or cocktail characteristics. It is often divided into physical, chemical and colour quench: physical quench occurs when a barrier reduces the ability of the radioactive sample

and scintillation cocktail to interact, or when photons are absorbed by a solid in the vial; chemical quench effects the transfer of energy from the solvent to the scintillator, reducing the number of photons produced; colour quench is the attenuation of the photons of light, which are absorbed or scattered by the colour in solution. In all forms of quench, the energy of all light pulses is reduced, as well as the total CPM. This leads to an underestimate of the total count and a shift in the energy spectrum of the sample. Another impact on the count efficiency is chemiluminescence, which is caused when a chemical reaction generates an excited product molecule. Upon the decay of that molecule light is emitted. This reaction can be determined by counting the samples twice, with a delay in between counts. The rate of photon production decreases over time, between 2-24 hours the effect of chemiluminescence on the CPM should be almost zero.

## **4.2 Liquid scintillation protocol for all samples and standards**

Defining the energy regions for counts to be collected in:

Region A: 0-1000 keV

Region B: 4-500 keV (all count data used from region B to remove interference from background radiation and tritium ( $^3\text{H}$ ) counts (< 4 keV).

Count time: 10 minutes or until 2 sigma coincidence of 0.5 has been reached.

Quench Indicating Parameter: tSIE transformed Spectral Index of External Standards

tSIE= Barium is used to activate the scintillator and a spectral transform technique is applied to the produced Compton spectrum. The Reverse Spectrum Transform eliminates the spectral distortion due to counting artefacts. A regression technique is used to fit a curve to the transformed spectrum. The tSIE is calculated from the regression coefficients.

The background count is defined by the CPM for the blank standard which is made and measured for each experiment using the matrix compositions of those experiments (solution compositions as defined in the results chapters), the value for each blank standard ( $19 \pm 2$  CPM) is then subtracted from the sample CPM before the  $^{14}\text{C}$  activity is calculated. Reproducibility of  $^{14}\text{C}$  measurements was confirmed by analysis of replicate standards (six replicates with activity of  $100 \text{ Bq mL}^{-1}$ ) throughout experiments to ensure consistent measurement across different  $^{14}\text{C}$  forms and matrices. Certified standard of inorganic  $^{14}\text{C}$  was also checked to ensure the accuracy of the liquid scintillation counter.

#### **4.2.1 Statistics of counting**

Radioactive decay is a random event so the number of decays per set time is variable. Statistics are therefore used to express the probability of measuring a given count within confidence limits (Kessler, 1989). This allows count measurements to be quoted with confidence that they are representative of the true radioactivity contained within the sample. Two statistic values are recorded for each sample counted. The first is the Spectral Index of the Sample (SIS) which is a sample spectrum quench indicating parameter, this index is independent of the count rate which means it does not fluctuate with increasing/decreasing activity.

The second is the Transformed Spectral Index of the External Standard (tSIE) which uses an external standard to calculate the quench. This technique transforms the energy distribution by applying a mathematical technique to correct for spectral distortions. The Packard Tri-carb 2000Ca liquid scintillation analyser uses a  $^{133}\text{Ba}$  external gamma source. Each counting method detailed above has a distinct tSIE value which should remain consistent across the sample counts. Decreases in the value of tSIE suggest an increased level of quench and therefore the sample should be recounted and if tSIE remains inconsistent then the sample is discarded as the count may not be representative of the activity.

### **4.3 Counting aqueous inorganic $^{14}\text{C}$**

The primary stock of inorganic  $^{14}\text{C}$  in the form of sodium bicarbonate ( $\text{NaH}^{14}\text{CO}_3$ ) was received in November 2013 from American Radiolabelled Chemicals (9.25 MBq, ARC Ltd., USA) and a daughter stock was made to create a calibration via dilution with deionised water (DIW).

#### **4.3.1 Cocktail optimisation**

EcoScint A liquid scintillation cocktail is commonly used to measure various beta emitting radionuclides (Fuller et al., 2014; Wallace et al., 2012) and so was the first cocktail used to calibrate the inorganic  $^{14}\text{C}$  stock. Figure 4-2 shows the comparison of the efficiency of the EcoScint A scintillation cocktail using different sample matrices to test the capture efficiency. Efficiency of the scintillant is calculated as shown below:

$$\text{CPM/DPM} \times 100$$

Equation 4-1

Where the counts per minute (CPM) are divided by the decays per minute (DPM) and then multiplied by 100 to give efficiency as a percentage.

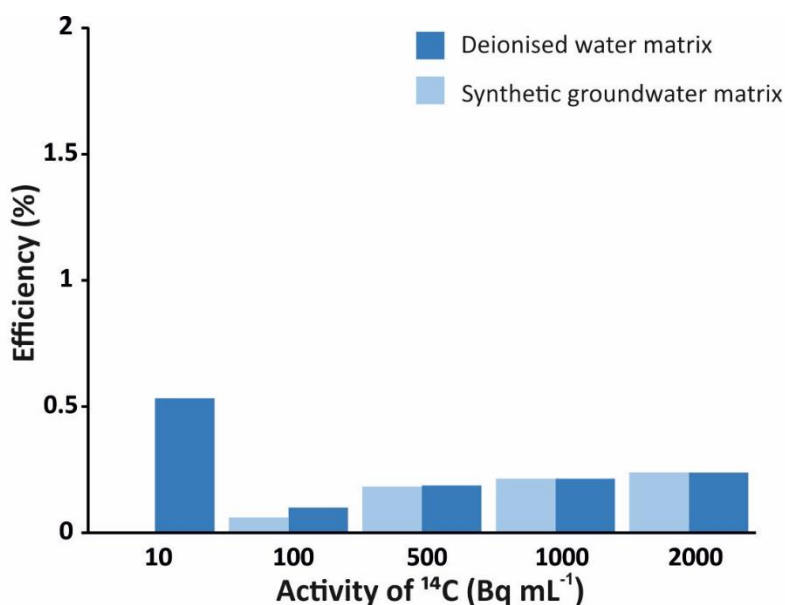


Figure 4-2 Efficiency of count against activity in standard, based on 2 mL of standard volume with 10 mL of EcoScint A scintillation cocktail. Dark blue columns represent aliquots prepared with deionised water, light blue columns represent aliquots prepared using a synthetic groundwater composition.

The results of the initial calibrations show very low efficiency at all <sup>14</sup>C activity levels, this could be due to outgassing of <sup>14</sup>C as <sup>14</sup>CO<sub>2</sub>(g) in to the vial headspace due to the low pH of the scintillation cocktail. Efficiency appears to decrease further when synthetic groundwater is used as the sample carrier suggesting that increasing ionic strength may increase the effect of the quench when counting inorganic <sup>14</sup>C in EcoScint A and so reducing the ability of the solvent to transfer energy to the scintillant.

Following these initial calibration attempts the method was altered whereby 0.1 M NaOH was added to the scintillation cocktail prior to addition of the sample to retain  $^{14}\text{C}$  in solution at a high pH using both EcoScint A and GoldStar scintillation cocktails (see Figure 4-3). These results improved efficiency, but maximum recovery was still only 8% at low activity ( $10 \text{ Bq mL}^{-1}$ ) and close to 2% for activities exceeding  $100 \text{ Bq mL}^{-1}$ . The low efficiency of these measurements across all calibration standards meant that the CPM measurement was already too close to background levels to correct for the high level of quench.

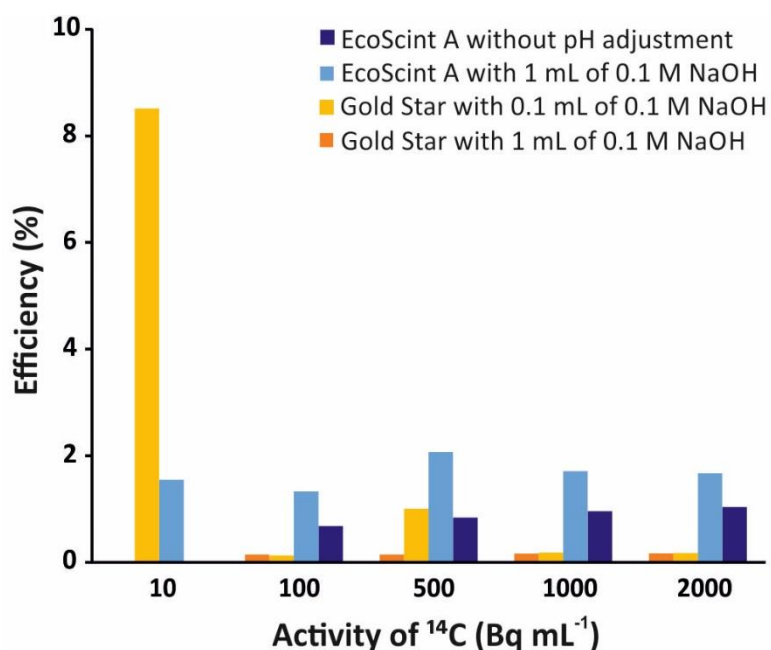


Figure 4-3 Comparison of EcoScint A and Gold Star scintillation cocktails: determining the impact of increasing matrix pH to retain  $^{14}\text{C}$  in scintillant.

Following on from the consideration that outgassing from sample to headspace may be occurring at low pH the primary stock was stabilised by adding

100  $\mu\text{L}$  of  $\sim 20\text{M}$  NaOH which increased the pH to approximately pH 14 where almost all  $^{14}\text{C}$  would be retained in solution as the carbonate anion  $^{14}\text{CO}_3^{2-}$  (see Chapter 2, Figure 2.1). It was therefore necessary to identify a scintillation cocktail with the capability to count highly ionic samples. Hionic-Fluor has been used previously for determination of inorganic  $^{14}\text{C}$  activity in aqueous samples in Caron et al. (2000). It is designed for high pH, high ionic strength samples and so was suitable for use with pH 14 standard solutions for calibration.

The previous work by Caron et al. (2000) had shown a marked increase in efficiency when using Hionic-Fluor with a NaOH addition. To compare the efficiency of this procedure to EcoScint A the method has been applied to both scintillation cocktails across all activities. Figure 4-4 shows that over the complete calibration range Hionic-Fluor give a consistently higher efficiency and this becomes more evident as the activity in the sample decreases. The ability to measure the  $^{14}\text{C}$  at low activity is especially important as this allows  $^{14}\text{C}$  concentration to be tracked over time more accurately and it is easier to distinguish from naturally occurring  $^{14}\text{C}$  radiation. In all experiments the original  $^{14}\text{C}$  addition was equivalent to  $100 \text{ Bq mL}^{-1}$  which has an efficiency of  $\sim 70\%$  in Hionic-Fluor and around  $50\%$  in EcoScint A. At half this activity ( $50 \text{ Bq mL}^{-1}$ ) the efficiency reduces to  $20\%$  for EcoScint A whilst Hionic-Fluor maintains  $\sim 70\%$  efficiency which means that the use of EcoScint A for the measurement of inorganic  $^{14}\text{C}$  could lead to erroneous assumptions regarding its removal from the aqueous phase. Hionic-Fluor has a lower efficiency at an activity of  $10 \text{ Bq mL}^{-1}$ , but it remains higher than the equivalent efficiency for EcoScint A throughout and

also shows more consistency in the efficiency percentage across the complete calibration range.

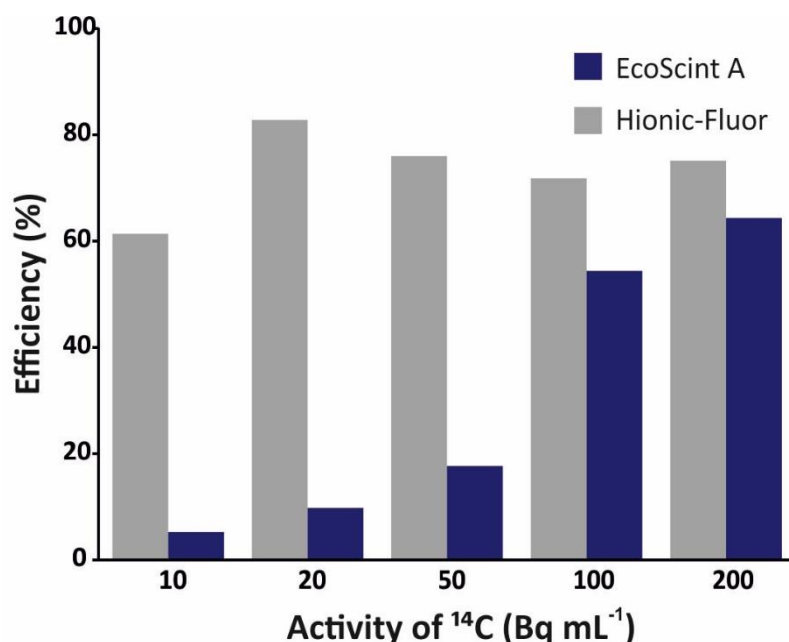


Figure 4-4 Comparing the efficiency of EcoScint A (dark blue) and Hionic Fluor (grey) against the activity of <sup>14</sup>C across a calibration range.

The final consideration for this method is the material of the vial in which the sample is counted. Plastic and glass vials were used following the standard method above across a calibration range (see Figure 4-5). They were counted first at 24 hours after preparation and then again at 48 hours to ascertain the stability of the sample in each container over time. The results show that although plastic vials show a higher CPM at the first count (24 hours after addition) after 48 hours this had dropped by around 3000 CPM for the 200 Bq mL<sup>-1</sup> standard which may be due to the cocktail degrading the vials walls over time. Any samples using plastic vials would need to be counted at exactly the same time point after sample

addition to ensure they were reliable. This is not feasible in an experimental set up. Glass vials reproduce the CPM values at 24 hours at 48 hours almost exactly suggesting that the glass vials do not suffer from degradation of the vial walls over time leading to a greater stability in the sample/cocktail matrix. The CPM measured can be related to the prior experimental samples as it will not be effected if there is some variation in the time prior to counting i.e. there will be no loss of CPM if the sample is left for 24 or 48 hours prior to counting.

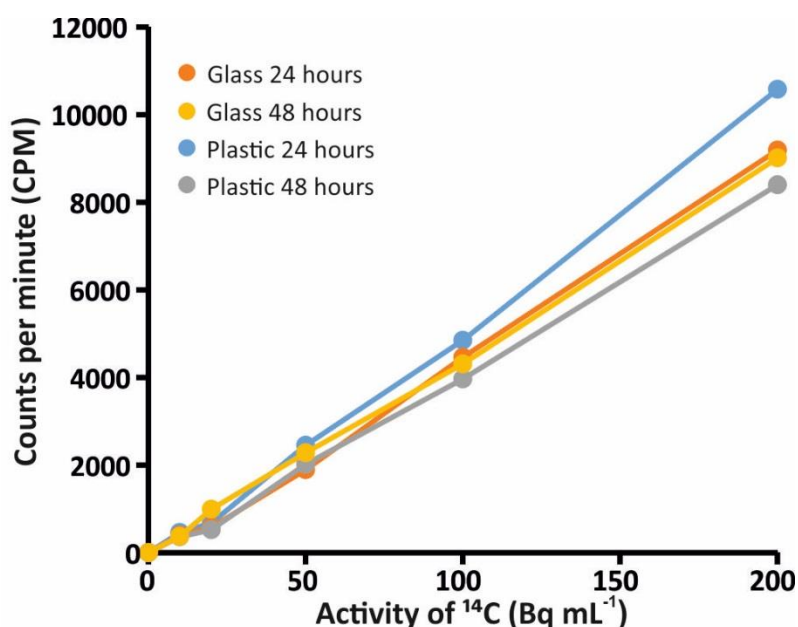


Figure 4-5 Comparing the count stability in glass and plastic vials for inorganic carbon-14 after 24 and 48 hours over a calibration range.

#### 4.3.2 Hionic Fluor counting procedure

The Hionic-Fluor counting procedure is based upon that of Caron et al. (2000). To 9 mL of Hionic Fluor 100  $\mu$ L of 2M NaOH is added prior to the addition of the sample. Calibration standards are set up using 9 mL of Hionic-

Fluor scintillation cocktail to 1 mL standard with concentrations ranged from 200 Bq to 0 Bq giving six standards for calibration (0, 10, 20, 50, 100 and 200 Bq mL<sup>-1</sup>) (see Figure 4-6) . Count time was 10 minutes with a 2s% of 0.5. tSIE was included and regions were set manually to ensure all counts were recorded (CPM for 4-500 keV region used for all activity calculations in data chapters). Calibration gave R<sup>2</sup> = 0.998. All samples and standards were stored for a minimum of 19 hours (overnight) prior to counting to allow any chemiluminescence to reduce.

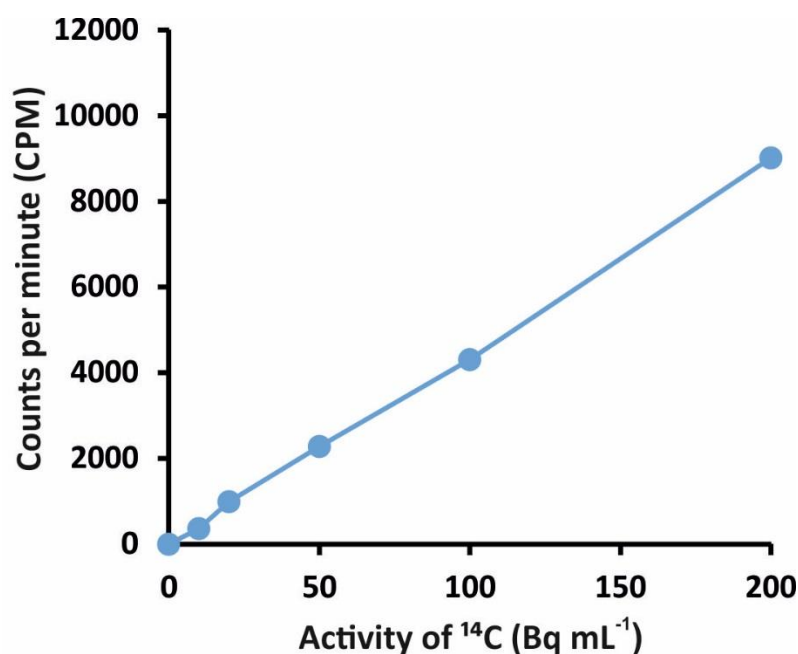


Figure 4-6 Calibration for inorganic <sup>14</sup>C-labelled sodium carbonate, prepared using 9 mL of Hionic-Fluor with a 100 μL addition of 2M NaOH and 1000 μL of standard in glass vials. R<sup>2</sup> value = 0.9988.

#### 4.4 Counting aqueous organic <sup>14</sup>C

Four organic <sup>14</sup>C-labelled stocks were received in June 2015. These were the single carbon compounds of formate, formaldehyde and methanol and the double

carbon compound acetate from ARC Ltd. USA (all 1 MBq activity). Both formate and acetate were received in the sodium salt form with acetate being C<sup>2</sup> (methyl group) labelled. Daughter stocks were made to create the stock calibrations via dilution with deionised water (DIW).

When using organic sources of <sup>14</sup>C the maintenance of high pH is no longer required so the <sup>14</sup>C can be measured using a variety of cocktails. In this case EcoScint A was used due to its high efficiency and decreased environmental impact compared to the classic toluene-containing cocktail Hionic-Fluor. Plastic vials were used as EcoScint A does not degrade the vial walls. Organic sources are able to be counted both by EcoScint A and Hionic Fluor as shown by calibrating acetate using both scintillants (Figure 4-7). The ability of both cocktails to count the organic form means that using a combination of these cocktails does not allow differentiation between organic and inorganic source terms, and due to the slightly lower efficiency of Hionic Fluor it is difficult to determine total <sup>14</sup>C from organic <sup>14</sup>C in aqueous form with any certainty.

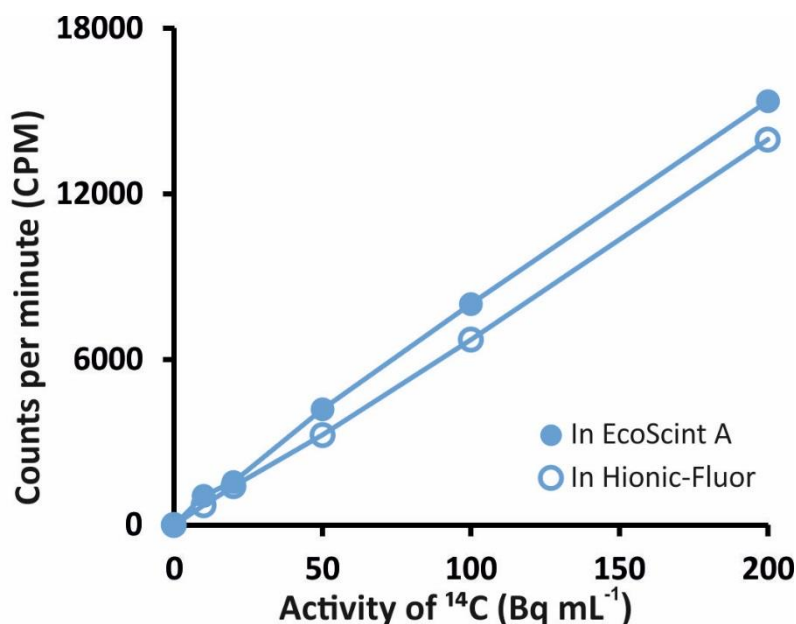


Figure 4-7 Comparison of calibration using EcoScint A and Hionic-Fluor scintillation cocktails.

The calibration in EcoScint A gives an  $R^2 = 0.9991$ , the calibration in Hionic-Fluor gives an  $R^2=0.9994$  which is slightly better, however the efficiency of the Hionic-Fluor count is lower. It varies between 80-95% efficient, improving as the activity decreases. The efficiency in EcoScint A remains  $>95\%$  across the calibration range.

#### 4.4.1 EcoScint A counting procedure

EcoScint A is used to measure the organic  $^{14}\text{C}$  in aqueous samples in Chapters 6 and 7. 10 mL of scintillant is placed in a plastic vial prior to the addition of 800  $\mu\text{L}$  of sample. Concentrations ranged from 200 Bq to 0 Bq using six standards for calibration, activity diluted in DIW. Count time was 10 minutes with a 2s% of 0.5. tSIE was included and regions were set manually to ensure all counts were recorded (CPM for 4-500 keV region used). All samples and

standards were stored for a minimum of 19 hours (overnight) prior to counting to allow any chemiluminescence to reduce.

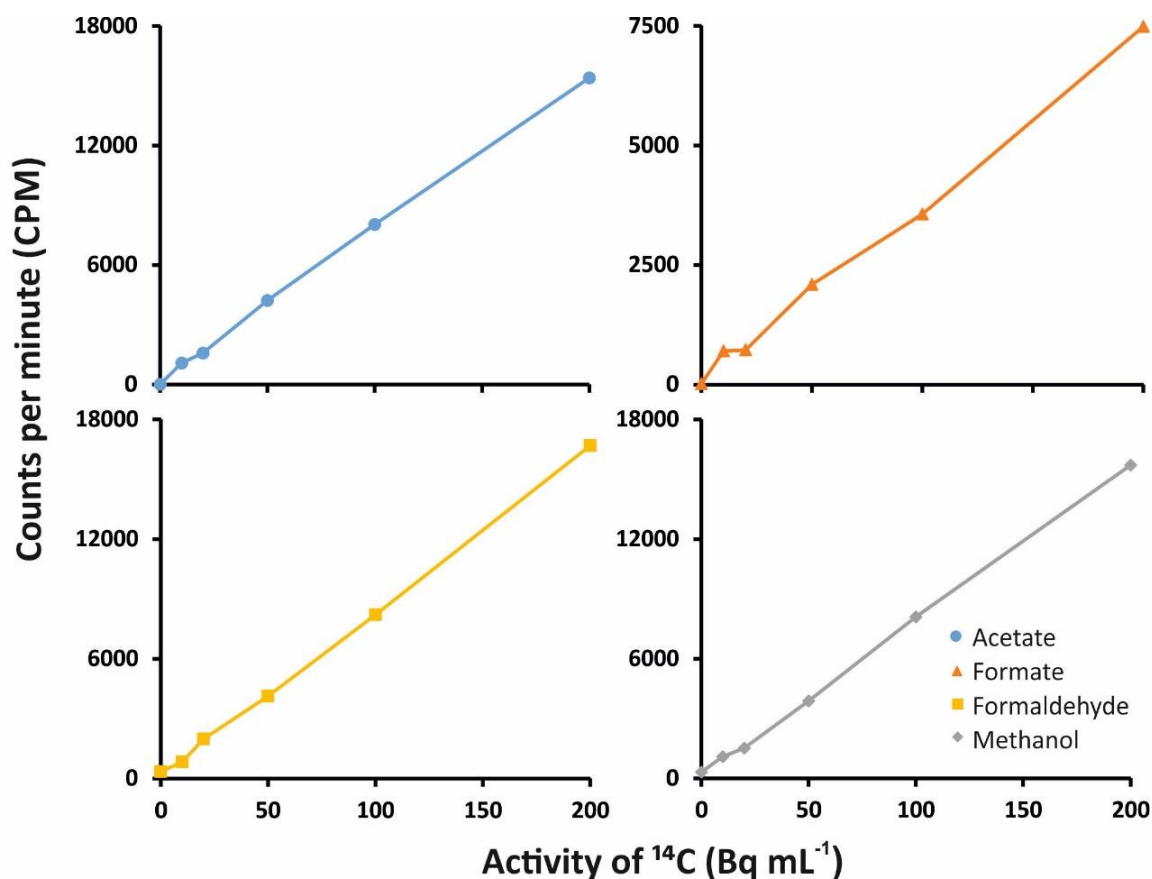


Figure 4-8 Calibrations for all organic <sup>14</sup>C labelled compounds, prepared using 10 mL of EcoScint A with 800  $\mu$ L of standard.  $R^2$  values = 0.9991; 0.9964; 0.9992 and 0.9992 for acetate, formate, formaldehyde and methanol respectively.

#### 4.5 Counting aqueous <sup>14</sup>C-inorganic and <sup>14</sup>C-organic mixed samples

When measuring the <sup>14</sup>C in experimental samples it is necessary to consider the implications of mixed samples, i.e. those which contain inorganic and organic aqueous <sup>14</sup>C. Using the standard protocols for Hionic-Fluor and Eco-Scint A outlined above two sets of calibrations were made with equal activities of <sup>14</sup>C from

the inorganic  $^{14}\text{C}$  (as  $\text{H}^{14}\text{CO}_3^-$ ) and organic  $^{14}\text{C}$  (as  $^{14}\text{CH}_3\text{COO}^-$ ) to give a range of combined activities from 0 to  $200 \text{ Bq mL}^{-1}$  (Figure 4-9).

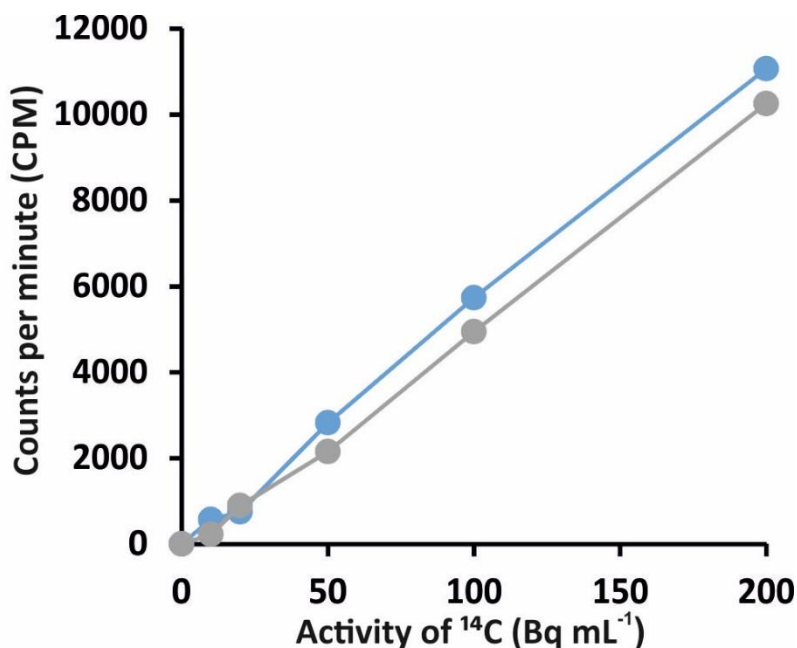


Figure 4-9 Comparison of the calibration standards in EcoScintA (blue) and Hionic-Fluor (grey) for the mixed calibration.

Both scintillation cocktails show a lower total count for the activity of the sample than in the calibration curves for organic/inorganic  $^{14}\text{C}$  alone. This suggests that the mix of the two  $^{14}\text{C}$  compound types may cause a loss of efficiency in the count. As with previous calibrations at high activity there is still good efficiency ( $>60\%$  at  $200 \text{ Bq mL}^{-1}$  for both cocktails), however at lower activity there is a reduction in efficiency. These results show that it is not possible to use these two scintillation cocktails to differentiate between these two forms of  $^{14}\text{C}$  in solution.

#### 4.6 Counting $^{14}\text{CO}_2(\text{g})$

To measure  $^{14}\text{CO}_2(\text{g})$  requires collection of a known volume of gas from the experimental vessel into  $\text{CO}_2(\text{g})$  absorber. This method used Carbosorb E as this is directly compatible with the liquid scintillation cocktail Permafluor E and has a high capacity to absorb  $\text{CO}_2(\text{g})$  ( $4.8 \text{ mmol L}^{-1}$ ). Mixing the Carbosorb E with Permafluor E after gas capture maximises efficiency allowing more precise and accurate measurements of the  $^{14}\text{CO}_2(\text{g})$  (Magnusson, 2007).  $^{14}\text{CO}_2(\text{g})$  was measured directly in Chapters 6 and 7 by removing a known volume of headspace (10 mL) from sealed microcosms and bubbling this slowly through 2 mL of Carbosorb E to maximise  $^{14}\text{CO}_2(\text{g})$  capture. 10 mL of Permafluor E was then added and samples were left overnight (minimum of 19 hours) for counting using the same protocol as the aqueous samples (Caron et al., 2000).

Carbosorb E is designed for only gaseous samples, the addition of Carbosorb E to aqueous standards leads to a quenched count when analysed by the liquid scintillation counter. A blank standard of Permafluor E and Carbosorb E was run using the sample volumes to account for any background interference of the matrix when processing the data (blank =  $28 \pm 2$  CPM).

#### 4.7 Summary of approach for $^{14}\text{C}$ measurement

The initial findings of the method development showed that the measurement of aqueous, inorganic  $^{14}\text{C}$  (DIC) through liquid scintillation counting requires a high pH and a scintillation cocktail which is suitable for highly ionic aqueous samples (see Figure 4-4). In this project the Hionic-Fluor scintillation

cocktail has been used following the method of Caron et al., 2000. It was used to measure  $^{14}\text{C}$ -DIC in Chapter 5 where all  $^{14}\text{C}$  spikes in experiments were in an inorganic  $^{14}\text{CO}_3^{2-}$  form.

When measuring  $^{14}\text{C}$  in an aqueous, organic form (DOC) there is no need to maintain a high pH and therefore the EcoScint A cocktail is used for all measurement of  $^{14}\text{C}$ -DOC. As it counts  $^{14}\text{C}$ -DIC very inefficiently (see Figures 4-2 to 4-4) it can be assumed that all  $^{14}\text{C}$  measured is in a DOC form. This scintillation cocktail is used in Chapters 6 & 7 to measure aqueous  $^{14}\text{C}$  as  $^{14}\text{C}$ -DOC. In these two chapters Carbo-Sorb E and Permafluor E scintillation cocktails are also used to measure  $^{14}\text{C}$  as  $^{14}\text{CO}_2(\text{g})$ . This has allowed the measurement of  $^{14}\text{C}$  in several different phases – gas phase, organic, aqueous phase and solid phases using the sequential extraction detailed below in 4.8.

#### **4.8 Sequential Extractions**

Sequential extractions were used in this project to gain greater understanding of the way that carbon-14 associates with the solid phase. Usually the chemicals used at each stage of the extractions become progressively more 'harsh' to allow differentiation between the phases – the reagent used determines the extractant and most procedures begin with the most weakly bound fraction. Phases extracted later in the process are considered more strongly bound than those which are extracted early. This method is commonly used in metal extractions, but has been modified to perform a simple two step extraction which

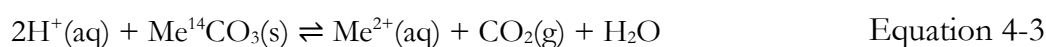
allows continuous capture of the  $^{14}\text{C}$  throughout each stage to improve the recovery efficiency.

In solid form carbon may be associated with inorganic and organic phases. The association of the  $^{14}\text{C}$  in solid phase is important as it has implications for the future behaviour of the isotope and considering its radioactive nature can have implications in terms of dose risk and assessment. In this sequential extraction properties of the solid fraction are exploited to maximise the recovery. The first step is an acid extraction, the retention of solid inorganic carbonate phases are dependent on pH (Stumm and Morgan, 1996). As the pH decreases, increasing dissolution of the inorganic solid phase will occur and if the pH is lowered sufficiently then inorganic aqueous phases will be transformed to  $^{14}\text{CO}_2(\text{g})$  which can then be captured and measured for  $^{14}\text{C}$  content. The second step is an oxidation step which oxidises organic matter again to  $^{14}\text{CO}_2$ , used after the acid extraction ensures that solution pH is already sufficiently low that all  $^{14}\text{CO}_2$  will be in the gaseous phase and trapped via gas capture for  $^{14}\text{C}$  analysis.

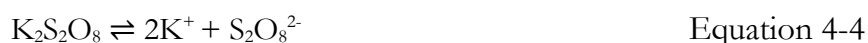
The method used in this project has been adapted from Magnusson et al., 2007, which showed that 85-95% of  $^{14}\text{C}$ -labelled activity (added in inorganic and organic forms) could be recovered by applying a two-step wet oxidation method. The results stated represent the minimum percentage of  $^{14}\text{C}$  present as the capture method is not 100% efficient (Magnusson, 2007).

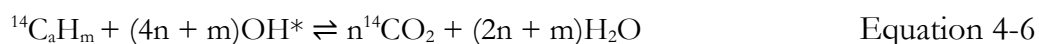
Sediment samples were recovered at the end of experiment (see Chapters 6 & 7) and rinsed with ethanol to stop microbial activity. The sediment was dried overnight and  $\sim 1\text{g}$  was placed in to a round bottom flask (500 mL).  $\text{N}_2(\text{g})$  was

used to flush the system and a flow rate of approximately 40 mL/min was established. 20 mL of 2M H<sub>2</sub>SO<sub>4</sub> was added to the container to achieve a pH ~ 3 when buffered with the sediment. The concentration of H<sub>2</sub>SO<sub>4</sub> added has been reduced from 6M in the original method (Magnusson, 2007) to 2M in this adaptation to ensure that the overlap between the inorganic phase and organic phase recovery is as limited as possible. The system was purged for 30 minutes to allow <sup>14</sup>CO<sub>2</sub>(g) to be captured by Carbo-Sorb E contained in gas washing bottles before being mixed with Permafluor E and analysed using liquid scintillation (see Equation 4-2; Equation 4-3)



The next step is to add 20 mL of 5% potassium persulfate and 4 mL of 4% AgNO<sub>3</sub> whilst heating to ~80°C. K<sub>2</sub>S<sub>2</sub>O<sub>8</sub> is added to the mixture to degrade all organic material and so release <sup>14</sup>C which is then oxidised to <sup>14</sup>CO<sub>2</sub>(g) (see Equation 4-4; Equation 4-5; Equation 4-6), AgNO<sub>3</sub> is used as a catalyst to increase the rate of the reaction. Further additions of the two reagents are made at the same volume after one and two hours of reaction

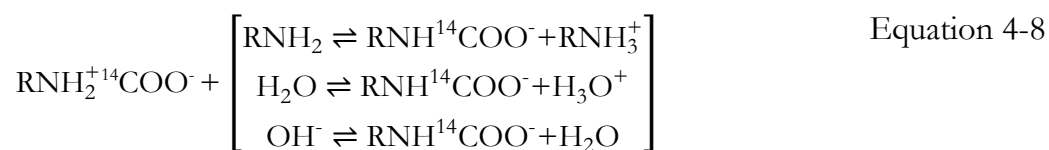




The system was left to react for a further hour before samples were collected for liquid scintillation analysis using the same method as the acidification step with  $^{14}\text{CO}_2(\text{g})$  captured in Carbo-Sorb E prior to mixing with Permafluor E.

#### 4.8.1 Permafluor E

Permafluor E is used in conjunction with Carbosorb E. Carbosorb E traps  $\text{CO}_2(\text{g})$  by absorbing it to the amine groups within it. This creates a zwitterion which reacts with  $\text{H}_2\text{O}$  to form a stable carbonate compound.



This technique was used in Chapters 6 and 7 to quantify the extent of transformation of  $^{14}\text{C}$ -labelled organic compounds to  $^{14}\text{CO}_2(\text{g})$  and to measure the amount of  $^{14}\text{C}$  associated with the solid phase, in both inorganic and organic forms. Approximately 10 mL of sample air is bubbled through 2 mL of Carbo-Sorb E before addition to 10 mL of permafluor E for direct measurement of  $^{14}\text{CO}_2(\text{g})$  in the headspace. For indirect solid fraction sampling 3 x 1 mL aliquots of Carbo-Sorb E were taken from the gas wash bottle and added to 10 mL of

Permafluor E. The calculation to find the amount of  $^{14}\text{C}$  in solid fraction is shown below:

$$\%^{14}\text{C}(s) = \text{CPM}_{(s)} \times 100 \times 10 / \text{CPM}_{(t=0)} \times 100 \quad \text{Equation 4-10}$$

$$\%^{14}\text{C}(s) = \text{CPM}_{(s)} \times 10 / \text{CPM}_{(t=0)} \quad \text{Equation 4-11}$$

Where  $\text{CPM}_{(s)}$  represents the mean CPM recorded from the gas wash bottle samples from one stage of the extraction. This value is multiplied by 100 to correct the dilution of the Carbo-Sorb E volume, and then multiplied by 10 to represent the CPM for the total sediment in the original experiments.  $\text{CPM}_{(t=0)}$  CPM recorded in the aqueous phase at time 0 which is multiplied by 100 to calculate the total activity added to the experiment. This can be simplified to Equation 4-11 and the percentage of  $^{14}\text{C}$  in each solid phase is then calculated.

## 4.9 References

Caron, F., Sutton, J., Benz, M.L., Haas, M.K., 2000. Determination of carbon-14 levels in heavy water and groundwaters. *Analyst* 125, 59-64.

Fuller, A.J., Shaw, S., Peacock, C.L., Trivedi, D., Small, J.S., Abrahamsen, L.G., Burke, I.T., 2014. Ionic strength and pH dependent multi-site sorption of Cs onto a micaceous aquifer sediment. *Applied Geochemistry* 40, 32-42.

Kessler, M.J., 1989. *Liquid Scintillation Analysis: Science and Technology*. Packard Instrument Company.

Magnusson, Å., 2007.  *$^{14}\text{C}$  Produced by Nuclear Power Reactors-Generation and Characterization of Gaseous, Liquid and Solid Waste*. Division of Nuclear Physics Department of Physics Lund University Box 118 SE-221 00 Lund Sweden.

Magnusson, Å., Stenström, K., Aronsson, P.-O., 2007.  $^{14}\text{C}$  in spent ion-exchange resins and process water from nuclear reactors: A method for quantitative determination of organic and inorganic fractions. *Journal of Radioanalytical and Nuclear Chemistry* 275, 261-273.

NCRPM, 1978. A Handbook of radioactivity measurements procedures: with nuclear data for some biomedically important radionuclides. National Council on Radiation Protection and Measurements.

Passo, C.J., Cook, G.T., 1994. Handbook of Environmental Liquid Scintillation Spectrometry: A Compilation of Theory and Methods. Packard Instrument Company.

Stumm, W., Morgan, J.J., 1996. Aquatic chemistry: chemical equilibria and rates in natural waters. Wiley.

Thomson, J., 2001. Use and Preparation of Quench Curves in Liquid Scintillation Counting [Online]. Packard BioScience Company, Meriden, Connecticut.

Retrieved from  
[http://www.perkinelmer.com/liquidsintillation/images/APP\\_Use-and-Preparation-of-Quench-Curves-in-LSC\\_tcm151-171749.pdf](http://www.perkinelmer.com/liquidsintillation/images/APP_Use-and-Preparation-of-Quench-Curves-in-LSC_tcm151-171749.pdf) [Accessed 20/03/2017]

Wallace, S.H., Shaw, S., Morris, K., Small, J.S., Fuller, A.J., Burke, I.T., 2012. Effect of groundwater pH and ionic strength on strontium sorption in aquifer sediments: Implications for  $^{90}\text{Sr}$  mobility at contaminated nuclear sites. *Applied Geochemistry* 27, 1482-1491.

## **Chapter 5 Mechanisms of inorganic carbon-14 attenuation in contaminated groundwater: Effect of solution pH on isotopic exchange and carbonate precipitation reactions.**

### **5.1 Executive Summary**

Radioactive  $^{14}\text{C}$  is a significant contaminant associated with nuclear fuels and wastes that is potentially highly mobile in the environment as dissolved inorganic carbonate species. This study investigated the mechanisms by which dissolved inorganic  $^{14}\text{C}$  is retained in surface and groundwater environments via precipitation and isotopic exchange reactions. Precipitation of calcite in the presence and absence of nucleation sites is considered along with isotopic exchange with both atmospheric  $\text{CO}_2$  and solid carbonates. Precipitation occurs at calcite supersaturation values of  $\text{SI}_{\text{CAL}} > 1.5$  in the absence of nucleation sites and  $\text{SI}_{\text{CAL}} > 0-0.5$  in the presence of nucleation sites, suggesting that precipitation of  $^{14}\text{C}$ -bearing carbonates is much more likely in subsurface environments where nucleation sites are abundant. The maximum  $^{14}\text{C}$  removal in solid isotopic exchange experiments occurred after approximately 2 weeks equilibration. In these experiments the amount of  $^{14}\text{C}$  removed from solution was proportional to the amount of calcite surface area present, and removal from solution was equivalent to rapid equalisation of the isotope ratio in an 8-10 Å active surface layer. Although the reactivity of natural carbonates may be lower than the calcite samples used in this study, these results suggest isotopic exchange with solids will be an important  $^{14}\text{C}$  retardation mechanism in subsurface environments containing only modest TIC concentrations. These results suggest that if inorganic  $^{14}\text{C}$  is released into sub-surface environments, both precipitation and solid phase

isotopic exchange can result in non-conservative  $^{14}\text{C}$ -DIC transport and  $^{14}\text{C}$  contamination may persist in groundwater for decades following accidental releases. In contrast, in experiments open to atmosphere with pH values below 9.3, complete loss of dissolved inorganic  $^{14}\text{C}$  was very rapid and occurred with timescales of 10's of hours.  $^{14}\text{C}$  loss was due to a rapid exchange of dissolved  $^{14}\text{C}$  species with  $^{12}\text{CO}_2$  (g) and the kinetics of  $^{14}\text{C}$  removal increased as pH values were lowered (i.e. atmospheric isotopic exchange was first order with respect to the concentration of carbonic acid present). Thus these results suggest that release of inorganic  $^{14}\text{C}$  to surface waters with pH values  $<9.3$  would result in rapid exchange with  $^{12}\text{CO}_2$  (g) and  $^{14}\text{C}$  would not persist in the aqueous environment, whereas  $^{14}\text{C}$ -DIC released to saturated subsurface environments may persist close to the release site for decades due to precipitation and solid phase exchange reactions preventing/retarding transport with the groundwater.

## 5.2 Introduction

The carbon isotope,  $^{14}\text{C}$ , is a widespread  $\beta$ -emitting radionuclide that is produced both naturally and anthropogenically. It is produced due to stratospheric irradiation of  $^{14}\text{N}$  as well as at each stage of the nuclear power generation process from the parent isotopes  $^{14}\text{N}$ ,  $^{17}\text{O}$  and  $^{13}\text{C}$  (Eabry et al., 1995; Yim and Caron, 2006). Natural and anthropogenic  $^{14}\text{C}$  production are of similar magnitude, however natural production is globally dispersed while anthropogenic sources are highly localised within nuclear sites (Magnusson et al., 2004, Roussel-Debet et al., 2006). At nuclear sites,  $^{14}\text{C}$  is an important radioactive contaminant because of its

long half-life ( $5730 \pm 40a$ ) (Godwin, 1962) and its ability to bioaccumulate in plants and animals (Begg et al., 1992; Cook et al., 1998; Yim and Caron, 2006). Most  $^{14}\text{C}$  formed in nuclear reactors is generated as inorganic species (e.g. carbide and  $^{14}\text{CO}_2$ ) during energy production leading to a large  $^{14}\text{C}$  solid waste inventory for disposal (Yim and Caron, 2006; Boss and Allsop, 1995). As  $^{14}\text{C}$  is a potentially very mobile component of radioactive wastes, many studies have focussed on the expected  $^{14}\text{C}$  behaviour after disposal in deep geological facilities (Yim and Caron, 2006; Bracke and Muller, 2008; Marshall et al., 2011; Baston et al., 2012; NDA, 2012; Doulgeris et al., 2015). Due to the strongly reducing conditions anticipated in repositories, and because aqueous inorganic  $^{14}\text{C}$  ( $^{14}\text{C}$ -DIC) tends to rapidly precipitate as solid carbonates within alkaline cementitious backfills, most studies have concentrated on the production and transport of radiolabelled methane ( $^{14}\text{CH}_4$ ), (e.g. Jackson and Yates, 2011; Limer et al., 2011; Marshall et al., 2011; Limer et al., 2013). Less research has been undertaken on the environmental mobility of inorganic  $^{14}\text{C}$  in shallow subsurface environments, despite the risk of its accidental release to such environments during waste reprocessing and storage.

Due to its ubiquity in the nuclear power generation process  $^{14}\text{C}$ -containing wastes are generated and released at every power station and reprocessing site worldwide, both as regulated discharges to air and water, as well as accidental releases at some sites (Yim and Caron, 2006).  $^{14}\text{C}$  contamination was first identified due to discharge from the low level waste trenches storing  $^{14}\text{C}$  inventory at Chalk River Site, Canada. Historical leaks from this storage area of the facility have led to  $^{14}\text{C}$  plumes reaching the natural environment, particularly a nearby

wetland. This has led to a series of studies into the behaviour of  $^{14}\text{C}$  in natural environments (Evenden et al., 1998; Killey et al., 1998; Bird et al., 1999). In the UK the most significant example of  $^{14}\text{C}$  contamination is associated with the nuclear fuel reprocessing plant at Sellafield, Cumbria (Stamper et al., 2014; Marshall et al., 2015) with the major source being water leaks from the intermediate level waste storage facilities in the 1970's (Marshall et al., 2015). Specifically  $^{14}\text{C}$ -containing liquor was lost from silos holding corroded magnesium alloy (MAGNOX) fuel cladding. The liquor had a pH of 9-11 due to equilibration with the fuel cladding (Wallace et al., 2012, Parry et al., 2011) and  $^{14}\text{C}$  is thought to have been present predominately as the inorganic species  $\text{H}^{14}\text{CO}_3^-$  and  $^{14}\text{CO}_3^{2-}$ .

In soil, inorganic carbon can exist as gaseous carbon dioxide, aqueous species, sorbed species and solid carbonates. Transitions between these phases are controlled by pH,  $\text{pCO}_2$ , the cations in solution, and the presence of interfaces (e.g. Langmuir, 1997, Inskeep et al. 1985; Van Geen et al 1994; Hodkin et al., 2016). In systems open to atmosphere aqueous  $\text{CO}_2$  concentrations reach equilibrium with atmospheric  $\text{pCO}_2$  (Atkins and De Paula, 2006). Dissolved inorganic carbon (DIC) is distributed between  $\text{CO}_2$ , carbonic acid ( $\text{H}_2\text{CO}_3$ ), the bicarbonate anion ( $\text{HCO}_3^-$ ) and carbonate anion ( $\text{CO}_3^{2-}$ ) depending on the solution pH (see equations 5-1 to 5-4 below) (Greenwood and Earnshaw, 1997; Langmuir, 1997). Dissociation constants ( $\text{pK}_a$ ) of carbonic acid – bicarbonate – carbonate are 3.6 and 10.3 respectively (at 25°C and zero ionic strength; Plummer and Busenberg, 1982). In open systems at high pH, therefore, the continuing

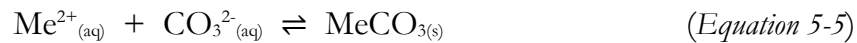
equilibrium between atmospheric and dissolved CO<sub>2</sub> (i.e. CO<sub>2</sub> in gassing) can result in very high DIC values (Stumm and Morgan, 1996).



(adapted from Greenwood & Earnshaw, 1997)

Carbonate species do not sorb to quartz sand or montmorillonite at circumneutral pH (Garnier, 1985; Sheppard et al., 1998), suggesting that carbonate species interact poorly with both silica and the silicate layer of clays. However <sup>14</sup>C-DIC species can adsorb to soil minerals such as aluminium and iron oxides at circumneutral pH values (Su and Suarez, 1997). For example HCO<sub>3</sub><sup>-</sup> was found to adsorb to goethite surfaces at ~pH7 as an inner-sphere carbonate surface complex by a ligand exchange reaction probably with singly coordinated Fe-OH and Al-OH surface groups (Wijnja and Schulthess, 2000; Su and Suarez, 1997). However sediment composition is usually dominated by silicate minerals, so anion exchange is a less effective process than cation exchange (negatively charged surface sites are present at much high densities than positive surface sites; Gu and Schulz, 1991). Therefore in many environments the aqueous transport of DIC is relatively unretarded (i.e. in the absence of precipitation reactions, it will move at approximately the same rate as groundwater flow).

In typical groundwater systems, precipitation of carbonate minerals is controlled by pH and the concentration of divalent cations. The relative propensity for carbonate to precipitate from solution is governed principally by the ratio of the ion activity products ( $IAP = a_{Me^{2+}(aq)} \cdot a_{CO_3^{2-}(aq)}$ ) to the mineral solubility product at equilibrium (the saturation index,  $SI = \log_{10}(IAP/K_{sp})$ ) for reactions with the form:

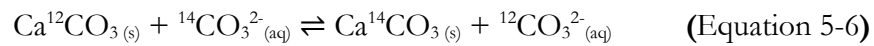


Where  $Me^{2+}_{(aq)}$  is a divalent metal ion, and  $a$  is the activity of the aqueous ion (when  $SI > 0$  precipitation is thermodynamically favoured, and when  $SI < 0$  dissolution is thermodynamically favoured).

In relatively oxic near surface groundwater environments calcium is usually the most abundant divalent cation. Magnesium can also be relatively abundant however, other divalent species (e.g.  $Sr^{2+}$ ;  $Ba^{2+}$ ;  $Fe^{2+}$  etc.) are normally only present as trace components (Krauskopf and Bird, 1995). Although a wide range of different solid carbonate phases are possible (e.g. calcite, aragonite, magnesite and dolomite), at low temperature and pressures, calcite ( $CaCO_3$ ) is the predominant carbonate phase expected. It is often magnesium substituted ( $Ca(Mg)CO_3$ ) where aqueous  $Mg^{2+}$  is present during crystallisation (Mucci and Morse, 1982; Bischoff et al., 1983). In the absence of nucleation sites, calcite will precipitate homogeneously from a supersaturated calcium carbonate solution when the saturation index,  $SI > \sim 1.5$ , and it will occur heterogeneously when  $SI > \sim 0.3$  where solid substrate provides nucleation sites (Ford and Williams, 2007). In the subsurface environment heterogeneous precipitation is likely to be the important

mechanism due to the availability of large numbers of potential nucleation sites. Due to the relatively low solubility of calcite ( $\text{Log } K_{\text{sp}} = -8.42 \pm 0.07$ ; Krauskopf and Bird, 1995), the formation / dissolution of  $^{14}\text{C}$  radiolabelled calcite may potentially be an important control on the mobility of  $^{14}\text{C}$ -DIC at nuclear sites.

In addition to co-precipitation in carbonates,  $^{14}\text{C}$ -DIC can also be removed from solution by isotopic exchange onto calcite surfaces (and other carbonate phases) within the aquifer or soil matrix. Solubility equilibria are dynamic (i.e. dissolution and precipitation rates are equal), so  $^{14}\text{C}$  in solution can replace stable C isotopes in mineral carbonates.



The rate of isotope exchange will depend on the extent of isotope disequilibrium between the solution and carbonate mineral phase, and the dissolution/precipitation kinetics (Sheppard et al., 1997). Pre-existing carbonates will be equilibrated with natural  $^{14}\text{C}$ -DIC concentrations, but where  $^{14}\text{C}$  is present as a contaminant,  $^{14}\text{C}$ -DIC will be present at concentrations far above natural abundance levels, potentially driving rapid exchange kinetics. Indeed, isotope exchange of  $\text{H}^{14}\text{CO}_3^-$  with natural carbonate sand at circumneutral pH was reported to occur on a time scale of only a few days (Garnier, 1985). Isotopic disequilibrium is also the main mechanism in aqueous-gaseous isotopic exchange where disequilibria created by the addition of aqueous  $^{14}\text{C}$  species leads to exchange reactions occurring with atmospheric  $\text{CO}_2$  to restore isotopic equilibrium among all species of carbonate across the aqueous-gaseous pools (Krauskopf and

Bird, 1995; Gonfiantini and Zuppi, 2003; White, 2013). This topic has received extensive academic interest related to the use of both  $^{13}\text{C}$  and  $^{14}\text{C}$  as tracers of carbon flow between environmental reservoirs, and for  $^{14}\text{C}$  for dating carbon-containing material (e.g.; Zhang et al., 1995; Doctor et al., 2008) however, the effect of isotopic equilibrium reactions on  $^{14}\text{C}$  behaviour as an environmental contaminant has received far less attention.

The aim of this study was to investigate the factors controlling the mobility of inorganic  $^{14}\text{C}$  in near-surface geo-environments. The specific objectives were; (1) to determine the conditions under which inorganic  $^{14}\text{C}$  is removed from aqueous solution representative of groundwater by carbonate precipitation reactions; (2) to determine the contribution made by isotopic exchange with calcite in sediments to the loss of inorganic  $^{14}\text{C}$  from groundwater; (3) to investigate the rate at which inorganic  $^{14}\text{C}$  is lost from solution by isotope exchange with atmospheric  $\text{CO}_2$  as a function of aqueous pH, and (4) assess the relative importance of these processes in determining the fate of inorganic  $^{14}\text{C}$  in groundwater at the UK Sellafield nuclear site.

## 5.3 Materials and Methods

### 5.3.1 Thermodynamic modelling

Equilibrium geochemical modelling was undertaken using the PHREEQC (version 3) geochemical speciation program (Parkhurst and Appelo, 2013) and the Hatches database (version 18) (Cross and Ewart, 1991) to establish the solution compositions needed to obtain the desired values of  $SI_{CAL}$  in the precipitation experiments (see Appendix A, Table A-1 for details). Geochemical modelling was also used to investigate the variation of  $SI_{CAL}$  with calcium concentration, carbonate alkalinity and pH and to model potential leach scenarios relevant to the UK Sellafield site (section 5).

### 5.3.2 Precipitation experiments

A series of  $Na_2CO_3$  solutions were prepared aerobically and equilibrated with atmosphere for a minimum of 72 hours by agitation in Erlenmeyer flasks on an orbital shaker (Stuart SSL1; 125 rpm; 16 mm orbit). A series of  $N_2$  purged  $CaCl_2$  solutions were also prepared. 10 mL of the required  $Na_2CO_3$  and  $CaCl_2$  solutions were mixed in 50 mL Oak Ridge tubes under  $N_2(g)$  to produce final solutions ( $20\text{ mL} \pm 0.2\text{ mL}$ ) at a range of saturation indices with respect to calcite ( $SI_{CAL}$ ) from +3 to -1 (see Table 5-1 for details). 20  $\mu\text{L}$  of  $^{14}\text{C}$ -labelled sodium carbonate (pH  $\sim 12$ ) was added to each tube producing a final activity of 100 Bq  $\text{mL}^{-1}$  ( $4.5 \times 10^{-8}\text{ M } ^{14}\text{CO}_3^{2-}$ ). The pH values of the mixtures were adjusted by addition of 5 mM NaOH to maintain the pH value of the  $Na_2CO_3$  solutions used ( $8.9 \pm 0.1$ , see Table 5-1). The mixtures ( $20\text{ mL} \pm 0.2\text{ mL}$ ) were sealed in 50 mL

Oak Ridge tubes with a N<sub>2</sub>(g) filled headspace, and continuously agitated on an end-over-end shaker (Stuart Rotator SB3, 40 rpm). Experiments were prepared in triplicate.

Table 5-1 Solution composition for precipitation experiments. All Na<sub>2</sub>CO<sub>3</sub> solutions equilibrated with atmospheric CO<sub>2</sub> for 72 hours prior to mixing.

Saturation Index	Composition	pH
+3.0	30 mM Na <sub>2</sub> CO <sub>3</sub> , 20 mM CaCl <sub>2</sub>	8.97
+2.5	15 mM Na <sub>2</sub> CO <sub>3</sub> , 15 mM CaCl <sub>2</sub>	9.07
+2.0	7.5 mM Na <sub>2</sub> CO <sub>3</sub> , 6 mM CaCl <sub>2</sub> , 5 mM NaOH	8.89
+1.5	5 mM Na <sub>2</sub> CO <sub>3</sub> , 15 mM CaCl <sub>2</sub> , 5 mM NaOH	9.02
+1.0	2.5 mM Na <sub>2</sub> CO <sub>3</sub> , 0.5 mM CaCl <sub>2</sub> , 5 mM NaOH	8.88
+0.5	2.5 mM Na <sub>2</sub> CO <sub>3</sub> , 0.15 mM CaCl <sub>2</sub> , 5 mM NaOH	8.91
0.0	2.5 mM Na <sub>2</sub> CO <sub>3</sub> , 0.05 mM CaCl <sub>2</sub> , 5 mM NaOH	8.93
-1.0	2.5 mM Na <sub>2</sub> CO <sub>3</sub> , 0.005 mM CaCl <sub>2</sub> , 5 mM NaOH	9.01

After 168 hours, 1.2 mL of sample was removed from each tube and centrifuged for 5 minutes at 14,000g in 1.5 mL centrifuge tubes. After centrifugation, <sup>14</sup>C removal was determined in the supernatant using liquid scintillation counting on a Packard Tri-Carb 2100TR (1 mL sample, 0.1 mL 2 M NaOH, 9 mL PerkinElmer Hionic-Fluor scintillation fluid; count time = 10 min; energy window = 4-156 keV; Caron and Sutton, 2000). Samples were stored for a

24 hour period prior to counting. In all tests the percentage of  $^{14}\text{C}$  remaining in solution was determined by:

$$\%^{14}\text{C}_{\text{aq}} = \frac{A_t}{A_i} \times 100 \quad (\text{Equation 5-7})$$

Where  $A_i$  is the initial activity at time 0 (counts per minute, CPM),  $A_t$  is the activity at a time point (CPM). Solution pH was determined at the beginning and end of experiments using a Thermo Scientific Orion benchtop multimeter, and electrodes calibrated daily at pH 4, 7 and 10.

Seeded precipitation experiments similar to the unseeded precipitation experiments described above were conducted, where  $25 \text{ g L}^{-1}$  kaolinite was added to the empty tubes prior to addition of  $\text{Na}_2\text{CO}_3$  and  $\text{CaCl}_2$  solutions (K-Ga 1b, Clay Mineral Society, Chantilly, USA). Prior to use in experiments, the kaolinite was acid washed (10% HCl) to remove any carbonate impurities, air-dried and de-aggregated by gentle use of a mortar and pestle. The mineralogical purity of kaolinite was confirmed using X-ray powder diffraction (Cu K-alpha radiation) on a Bruker D8 Advance XRD.

### 5.3.3 Isotopic exchange experiments

#### 5.3.3.1 Solid phase isotopic exchange experiments

Equal volumes of  $2.5 \text{ mM Na}_2\text{CO}_3$  and  $0.05 \text{ mM CaCl}_2$  solutions were mixed to give a final solution with a pH of  $8.87 \pm 0.03$  and a calculated  $\text{SI}_{\text{CAL}} = 0$ . In triplicate experiments,  $50 \pm 0.5 \text{ mL}$  aliquots ( $0.2 \text{ }\mu\text{m}$  filtered) of this solution were equilibrated with calcite powder at  $0 \text{ g L}^{-1}$ ,  $5 \text{ g L}^{-1}$ ,  $20 \text{ g L}^{-1}$  and  $50 \text{ g L}^{-1}$  (Sigma-

Aldrich Reagent Plus) in 50 mL glass serum bottles (Wheaton Scientific Ltd, USA) with N<sub>2</sub> filled headspace, sealed with butyl rubber stoppers (Bellco Glass Inc., USA) and Al crimps. The experimental systems were left for one week to allow calcite dissolution/precipitation equilibration to be established prior to addition of <sup>14</sup>C. The bottles were then spiked with 50 µL <sup>14</sup>C-labelled sodium carbonate, giving a final activity of 100 Bq mL<sup>-1</sup>. Periodically 2 mL of solution was removed using sterile, N<sub>2</sub>(g) flushed syringes and analysed for <sup>14</sup>C activity and pH as described above.

The mineralogical purity of the calcite powder was determined using X-ray powder diffraction (Cu K-alpha radiation) on a Bruker D8 Advance XRD. Specific surface area was measured by N<sub>2</sub> gas adsorption using the BET method with a Micrometrics Gemini V Surface Area Analyser (samples degassed with nitrogen gas for a minimum of 19 hours, at 60°C, prior to analysis).

### **5.3.3.2 Atmospheric isotopic exchange experiments**

Triplicate 100 ± 1 mL experiments were established in 500 mL Erlenmeyer flasks using 0.01 M NaCl as the background electrolyte. The pH was altered using a sodium bicarbonate-carbonate-hydroxide buffer system to give range of experimental pH between pH 7.2 and 12.5 (Table 5-2). Flasks were equilibrated with atmosphere (in the dark at 20 ± 1°C) for a minimum of 48 hours by shaking at 125 rpm on an orbital shaker prior to <sup>14</sup>CO<sub>3</sub><sup>2-</sup> addition. 100 µL of <sup>14</sup>C-labelled sodium carbonate was added to each flask, equivalent to 100 Bq mL<sup>-1</sup>. Periodically 1 mL of solution was removed for <sup>14</sup>C analysis, and pH was determined in the flasks. Experiments were continued until either a pH variation of more than ± 0.2

was observed, or less than 5% of initial  $^{14}\text{C}$  activity was measured in solution. Parallel triplicate control experiments were established in 30 ml glass serum bottles (sealed with butyl rubber stoppers and Al crimps) where contact with atmosphere was prevented.

Table 5-2 Solution composition for atmospheric isotopic exchange experiments

Solution pH	Composition
7.2	10 mM NaCl, 0.1 mM $\text{NaHCO}_3$
8.0	10 mM NaCl, 1 mM $\text{NaHCO}_3$
8.8	10 mM NaCl, 10 mM $\text{NaHCO}_3$
9.3	10 mM NaCl, 10 mM $\text{Na}_2\text{CO}_3$
10.5	10 mM NaCl, 100 mM $\text{Na}_2\text{CO}_3$ , 10 mM NaOH
12.5	10 mM NaCl, 10 mM $\text{Na}_2\text{CO}_3$ , 100 mM NaOH

## 5.4 Results

### 5.4.1 XRD

#### 5.4.1.1 XRD for kaolinite

The XRD results for kaolinite (see below) confirms that the kaolinite used is mainly kaolinite, with small quantities of mica and quartz.

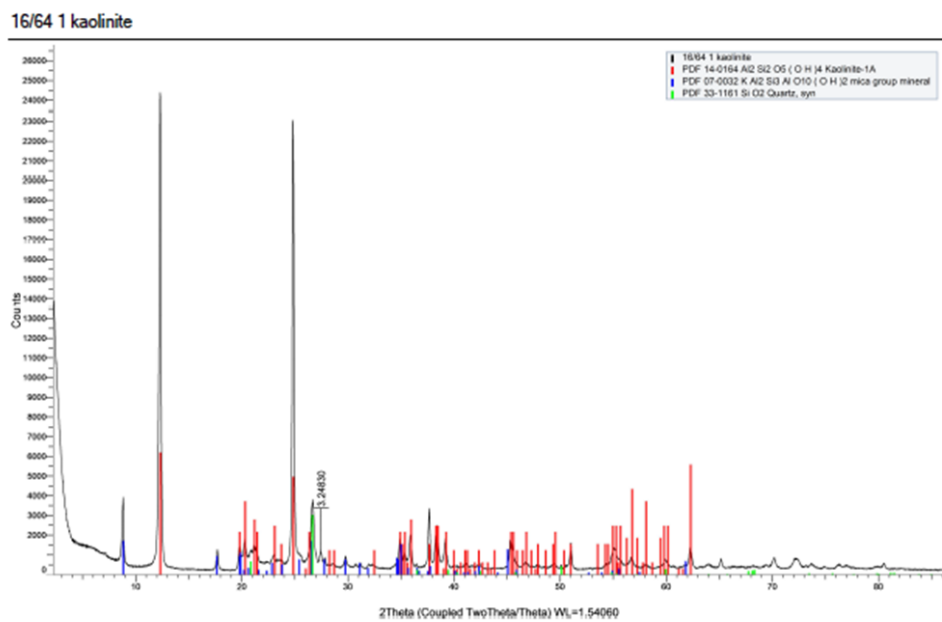


Figure 5-1 X-ray diffraction pattern showing the sample data (black line) and standard fit for kaolinite (red), mica (blue) and quartz (green).

#### 5.4.1.2 XRD for calcite

The XRD for calcite (see below) confirms the mineral purity of the calcite reagent used in the solid isotopic exchange.

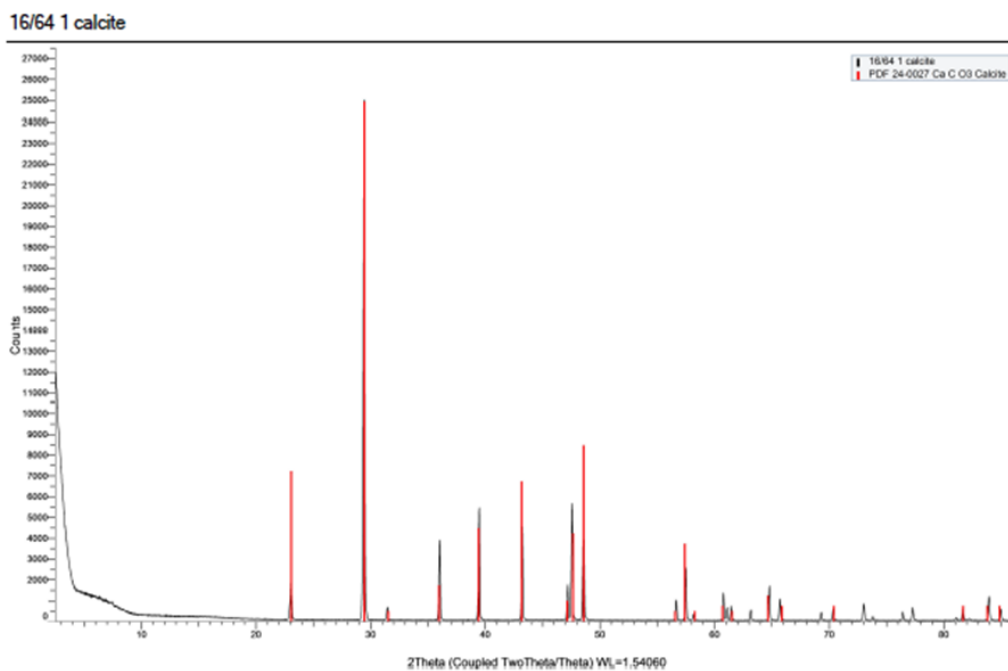


Figure 5-2 X-ray diffraction pattern showing the sample data (black line) and calcite standard (red line).

#### 5.4.2 Homogeneous and heterogeneous precipitation

In the homogeneous precipitation experiments where the calculated  $SI_{CAL}$  was initially between -1.0 and +1.0 there was no change in pH over 7 days (in all cases it remained within 0.1 pH units of the initial value  $8.9 \pm 0.1$ , see Figure 5-3). In these tests the solutions remained visually clear. In the homogeneous precipitation experiments where  $SI_{CAL}$  was initially +1.5, +2.0, +2.5 and +3.0, the pH decreased to 8.4, 7.6, 7.2 and 7.6, respectively, over 7 days. A small amount of white precipitate formed in these solutions.  $^{14}C$  tracer removal from these experiments followed a trend with pH change, with no removal observed over a period of 7 days when the initial  $SI_{CAL} = -1.0$  to +1.0 (Figure 5-3b), and progressively more  $^{14}C$  removal with increasing  $SI_{CAL}$  values from 1.5 to 3.0 (92 – 59% of the  $^{14}C$  remained in solution after 7 days).

The heterogeneous precipitation experiments exhibited similar pH trends over time to the homogeneous precipitation experiments (data also shown in Figure 5-3). The final pH of all experiments where the initial  $SI_{CAL}$  was between -1.0 and +1.0 tests was within 0.1 pH units of the starting value, whereas the final pH of all the experiments where the initial  $SI_{CAL}$  was +1.5 to +3.0 was  $pH\ 7.5 \pm 0.2$ . However the heterogeneous reactions followed a different trend to the homogeneous reactions with respect to  $^{14}C$  removal (Figure 5-3b). Only the  $SI_{CAL} = -1.0$  experiment exhibited no  $^{14}C$  removal after 7 days, the  $SI_{CAL} = 0$  and 0.5 experiments exhibited a small amount of  $^{14}C$  removal, with progressively more occurring as the initial  $SI_{CAL}$  increased to 3.0 (~20-60%  $^{14}C$  was removed from solution).

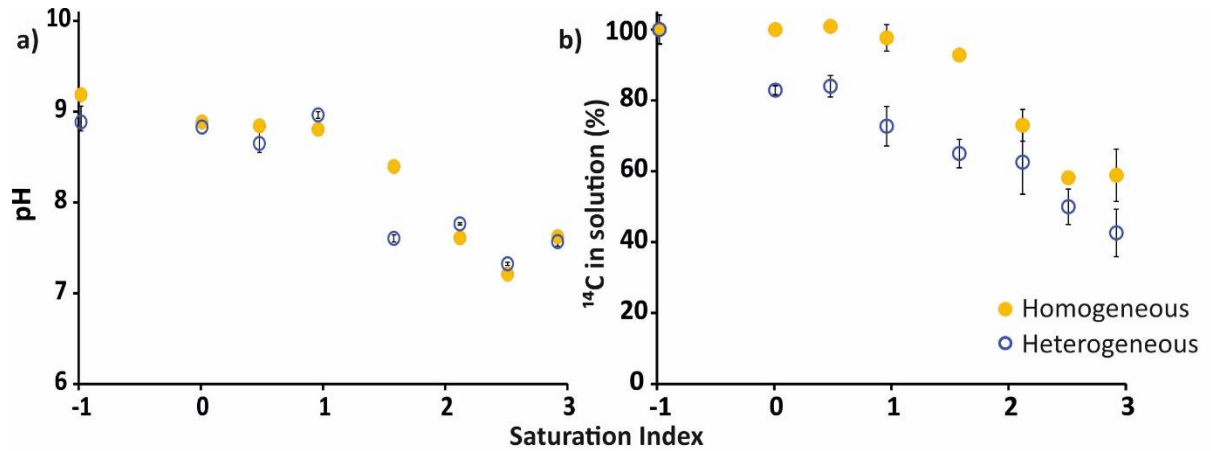


Figure 5-3 Homogeneous and heterogeneous precipitation reactions (a) final pH after seven day incubation against the initial predicted saturation index (b) experimental data showing the percentage of  $^{14}C$  in solution after seven day incubation plotted against the predicted initial calcite saturation index of solution ( $SI_{CAL}$ ). Error bars show one standard deviation of triplicate measurements; where not shown, error bars are less than the size of the symbols used.

### 5.4.3 Solid phase isotopic exchange

When calcite was added to saturated calcium carbonate solutions at pH 9.0 the pH remained  $\pm 0.2$  pH units for the duration of the experiments (1 month incubation). In the calcite-free (0 g) control experiments no  $^{14}\text{C}$  removal occurred over the duration of the experiments (Figure 5-4a). In the 5 g L<sup>-1</sup> calcite ( $\text{SA}_{\text{BET}} = 0.289 \text{ m}^2 \text{ g}^{-1}$ ) experiments there appeared to be a small amount of  $^{14}\text{C}$  removal ( $\sim 2\%$ ) after 1 month, but the amount was within the experimental error. For the experiments amended with 20 g L<sup>-1</sup> calcite there was a removal of 5-6% between 166-334 hours and a 10%  $^{14}\text{C}$  removal at the end of experiments (672 hours). The 50 g L<sup>-1</sup> calcite amended experiments showed a 28% removal at 166 hours, the removal at the end of the experiment was 30% of the initial  $^{14}\text{C}$  addition (672 hours). Overall there was a linear correlation between the total calcite surface area added to each experiment and the observed  $^{14}\text{C}$  removal at the end of the experiment (Figure 5-4b).

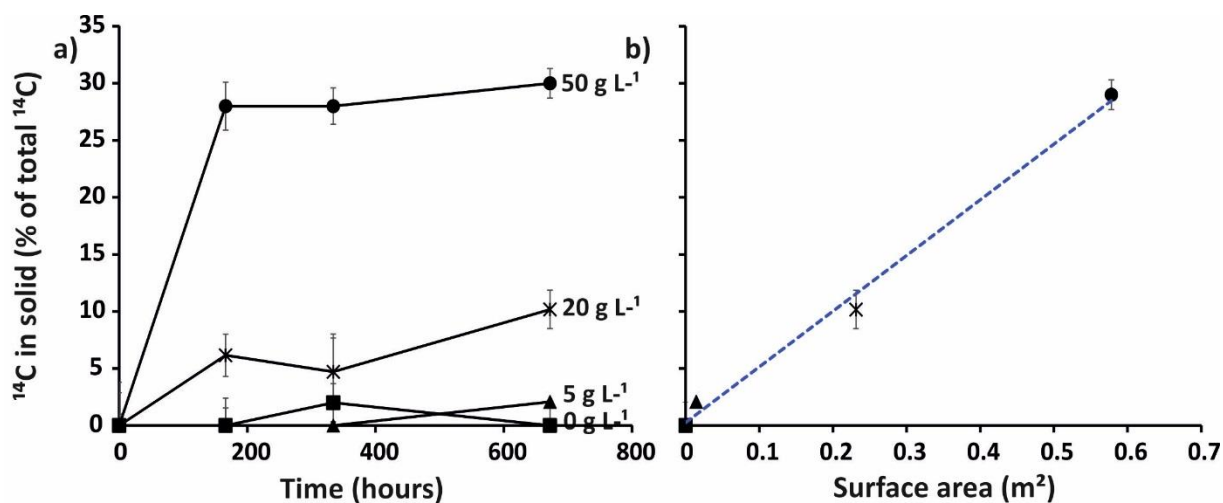


Figure 5-4 (a) the amount of <sup>14</sup>C associated with the solid phase against time in hours (b) the amount of <sup>14</sup>C in solid against the surface area of the calcite after two months incubation. Error bars show one standard deviation of triplicate measurements; where not shown, error bars are less than the size of the symbols used.

#### 5.4.4 Atmospheric isotopic exchange

In the closed controls for the experiments investigating <sup>14</sup>C exchange with atmosphere, the pH remained constant at the initial values ( $\pm 0.2$  pH units) from 0 to 264 hours (data for up to 100 hours is shown in Figure 5-5). The <sup>14</sup>C activity in these experiments decreased by a small amount over the first 24 hours, but ~95 % (pH 11 system) or ~93% (pH 9.5 and 7 systems) of the initial activity remained in solution from 24 hours to the end of the experiment (264 hours).

The pH of the open experiments was slightly less stable than that of the closed systems, so these experiments were terminated when the pH change exceeded 0.2 units to ensure comparability of the systems. In the open experiments at pH 12.5, ~100% of the original <sup>14</sup>C activity remained in solution at

the end of the experiment (48 hours). At pH 10.5, 97% of the initial activity remained in solution at the end of the experiment (96 hours). At pH 9.3, <sup>14</sup>C activity decreased with time (53% remained in solution at 72 hours) with only 5% remaining in solution at the end of the experiment (337 hours). At pH 8.8, 47% of the initial activity remained in solution at 24 hours and only 3% remained in solution at the end of the experiment (121 hours). At pH 7.8, 47% of the initial activity remained in solution at 4 hours and only 6% remained in solution at the end of the experiment (48 hours). At pH 7.0, 48% of the initial activity remained in solution at 1 hour and only 1% remained in solution at the end of the experiment (24 hours).

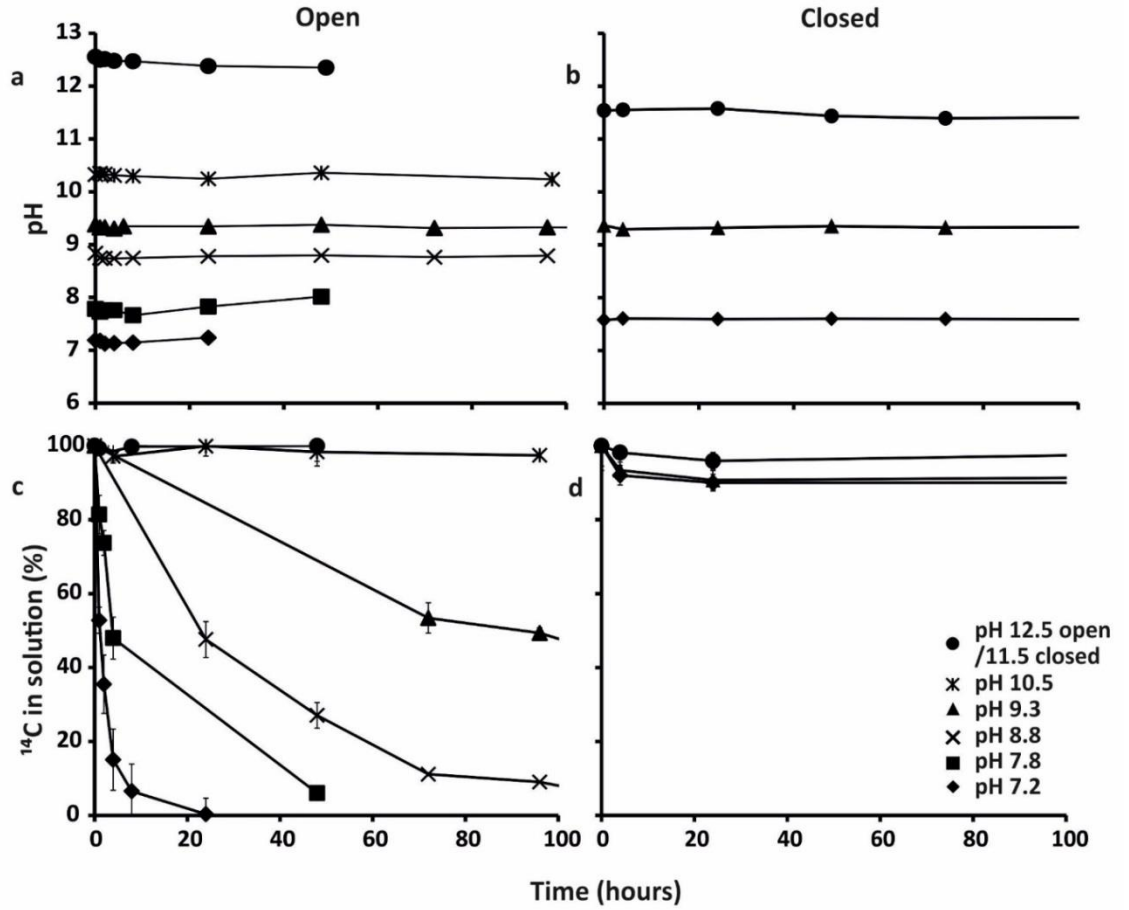


Figure 5-5 (a) pH measurement over time in open flask experiments, (b) pH measurement over time in closed bottle experiments, (c) the percentage of  $^{14}\text{C}$  remaining in solution over time in open experiments, (d) the percentage of  $^{14}\text{C}$  remaining in solution over time in closed experiments. Error bars show one standard deviation of triplicate measurements; where not shown, error bars are less than the size of the symbols used.

## 5.5 Discussion

### 5.5.1 Effect of seed crystals (nucleation sites) on the precipitation of calcium carbonate

In the calcite precipitation experiments removal of the  $^{14}\text{C}$ -DIC tracer indicates that carbonate precipitation occurred in homogeneous systems where the initial  $\text{SI}_{\text{CAL}} \geq 1.5$ , and in heterogeneous systems where initial  $\text{SI}_{\text{CAL}} \geq 0 - 0.5$ . These values closely match published  $\text{SI}_{\text{CAL}}$  values for homogeneous and heterogeneous calcite precipitation of 1.5 and 0.3, respectively. (White, 1997; Dreybrodt et al., 1992, Ford and Williams, 2007) This close agreement suggests that  $^{14}\text{C}$  removal in these experiments was principally controlled by calcite precipitation. Further it suggests that the solution must be significantly over-saturated with respect to calcite ( $\text{SI}_{\text{CAL}} \geq 1.5$ ) for it to precipitate in the absence of suitable nucleation sites.

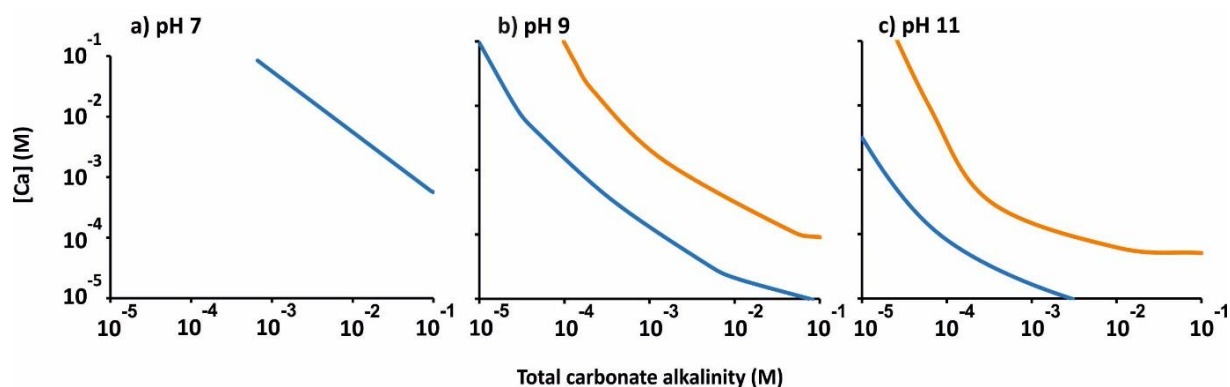


Figure 5-6 PHREEQC closed system model predicting the solution compositions necessary for calcite saturation ( $\text{SI} > 0$ , to the right of the blue line) and homogeneous precipitation ( $\text{SI} > 1.5$  to the right of the orange line); (a) at pH 7, (b) at pH 9, and (c) at pH 11.

The solution composition required for  $\text{SI}_{\text{CAL}} = 0$  and 1.5 at pH values of 7, 9 and 11 has been modelled using PHREEQC (Figure 5-6). These results are

sensitive to pH because of the variation in carbonate speciation (reactions 5-3 and 5-4), and thus higher concentrations of either  $\text{Ca}^{2+}$  or carbonate alkalinity are needed to achieve the required (super)saturation indices at lower pH values. In this simulation only heterogeneous precipitation is predicted at circumneutral pH (and even then only at unrealistically high solution concentrations; see Figure 5-6a); but at high pH both homogeneous and heterogeneous precipitation reactions are predicted to occur at much lower DIC concentration (Figure 5-6b, c) as DIC is mostly speciated as  $\text{CO}_3^{2-}$  at high pH.

### 5.5.2 Contribution of solid phase isotopic exchange to $^{14}\text{C}$ retardation

The solid phase isotope exchange experiments demonstrated that when a solution containing inorganic  $^{14}\text{C}$  comes into contact with non-radiolabelled calcite,  $^{14}\text{C}$  is removed from solution (Figure 5-4) with at least 10%  $^{14}\text{C}$ -DIC removal in experiments with  $\geq 20 \text{ g L}^{-1}$  calcite added. The experimental results show that isotopic exchange reached a pseudo-equilibrium after 334 hours (approximately two weeks), which was similar to that previously reported by Garnier (1985), where isotopic exchange reached an equilibrium with calcareous soils after one week.

In these experiments, it is available calcite surface area that exhibits a primary control on the observed extent of  $^{14}\text{C}$  uptake (Figure 5-4b). The kinetics of  $^{14}\text{C}$  uptake are governed by the rates of the forward and backward reactions during calcite dissolution / precipitation (see Equation 5-5), which at equilibrium are equal leading to no overall change in calcite mass or DIC concentration. Surface mediated isotopic exchange reactions will therefore proceed rapidly until  $^{14}/^{12}\text{C}$

ratio is equilibrated in the active surface layers of the calcite crystals. It is possible to use the data from the 20 and 50 g L<sup>-1</sup> experiments to estimate the depth of the active surface layer based on the number of moles of C that must be exchanged to result in an observed 10 and 30 % <sup>14</sup>C removal (see Appendix A, section A.4 for details). In these calculations, the estimated active surface layer is only 8-10 Å; equating to ~1-2 calcite unit cell thickness (Skinner et al., 1994). This is similar to the theoretical short-term diffusion thickness calculated for <sup>45</sup>Ca<sup>2+</sup> uptake, and the measured thickness for <sup>109</sup>Cd uptake by low-energy electron diffraction (Stipp et al., 1992). Stipp et al. (1992) also determined that slow solid state diffusion exchange can occur on much longer timescales (up to 2 years), effectively increasing the active surface layer to several hundred angstroms. Such diffusion driven <sup>14</sup>C exchange into carbonate grain interiors could therefore constitute significant additional sinks for <sup>14</sup>C-DIC over timescales not observed in these experiments.

Extrapolation of the 20 g L<sup>-1</sup> calcite experimental conditions to a typical aquifer situation (where the solid solution ratio might be closer to 1:1 w/w) suggests that a 2 % w/w calcite concentration in solids is sufficient to reduce the <sup>14</sup>C concentration in groundwater by ~10 % by rapid exchange with the 10 Å active surface layer, and perhaps more by interparticle diffusion of longer timescales. A 2 % calcite concentration is equivalent to a relatively low TIC of 0.24% indicating that isotopic exchange will be an important retardation process in many near-surface environments with pH values > 6 (n.b. the range of natural soil TIC is 0-12%, although it is completely absent in soils below ~pH 6; Walthert et

al., 2010). However, the extent of isotopic exchange will be very sensitive to changes in carbonate surface area, and if carbonates are only present in large detrital grains (with a very low specific surface area), much higher TIC values would be required to cause similar  $^{14}\text{C}$  removal (n.b. the surface area of the calcite crystals used in these experiments was  $0.29 \text{ m}^2 \text{ g}^{-1}$ , which is in the typical range  $0.17 - 8.6 \text{ m}^2 \text{ g}^{-1}$  used in previous studies of calcite; Nancollas and Reddy, 1971; Inskeep and Bloom, 1985; Huang et al., 1991; Dreybrodt et al., 1996; but that does not mean it is typical of that found in natural sediments). Also, if TIC is present as less soluble phases (e.g. dolomite;  $\text{CaMg}(\text{CO}_3)_2$ ;  $\text{Log } K_{\text{sp}} \approx -18 \pm 2$ ; Sherman and Barak, 2000; Stumm and Morgan, 1996), again much slower removal kinetics would be predicted. Therefore, it is very hard to generalise about the specific threshold TIC value where isotopic exchange will become important in the natural environment, and 0.24 % w/w is therefore likely to represent a conservative screening threshold. In this context it is interesting to note that the natural aquifer sediments beneath the UK Sellafield nuclear site have TIC values in the 0-0.6 % range (Dutton et al., 2009; Randall et al. 2004) and up to 4.8 % in made ground (Randall et al., 2004), and thus,  $^{14}\text{C}$  solid isotopic exchange reactions are probably an important retardation mechanism expected to retard  $^{14}\text{C}$ -DIC transport in groundwater at this site (especially for locations dominated by made ground).

### **5.5.3 Rate of atmospheric isotopic exchange as a function of solution pH**

The atmospheric isotopic exchange experiments (Figure 5-5) show that there was significant loss of  $^{14}\text{C}$  from solutions with  $\text{pH} < 9.3$  when there was

contact with atmosphere. This loss did not occur in the closed bottle experiments (the 5-7% loss of  $^{14}\text{CO}_3^{2-}$  activity from solution observed in the closed experiments was probably associated with  $\text{CO}_2$  outgassing into the  $\text{N}_2$ -filled headspaces). In all open experiments, pH was stable ( $\pm 0.2$  units) and solutions were well equilibrated with atmospheric  $\text{CO}_2$  prior to the introduction of  $^{14}\text{C}$  as  $\text{Na}_2\text{CO}_3(\text{aq})$ , therefore, there was minimal net outgassing of  $\text{CO}_2$ . It is reasonable to assume that  $^{14}\text{C}$  loss is by isotopic exchange (at dynamic equilibrium).

Equations 5-4 indicate the steps involved in the exchange of aqueous inorganic carbon species with atmospheric  $\text{CO}_2$ . The equilibrium of these reactions will not have been significantly disturbed by the addition of a small spike of  $^{14}\text{CO}_3^{2-}(\text{aq})$ , but isotopic exchange will have occurred between the inorganic carbon pools because equilibrium is a dynamic state (where the rates of the forward and reverse reaction are equal). If there is a difference in the isotope ratio in the carbon pools driving the forward and reverse reactions, there will be a net transfer of  $^{14}\text{C}$  despite the overall reaction being in equilibrium. Protonation/deprotonation reactions such as equations 5-3 and 5-4 (acid dissociation constants  $K_{a1}$  and  $K_{a2}$ , respectively) tend to be rapid in aqueous solution (Greenwood and Earnshaw, 1997), and therefore it will be assumed that there is rapid transfer of  $^{14}\text{C}$  between the aqueous carbonate pools, and equilibration of their  $^{14}\text{C}$  isotope ratios. If the proportion of an aqueous carbonate species,  $C_{\text{sp}}$  that is  $^{14}\text{C}_{\text{sp}}$  is  $x$  (where  $x$  is a function of  $t$ ) then the following equation can be written for each aqueous carbonate species;

$$[^{14}\text{C}_{\text{sp}}] = x \cdot [\text{C}_{\text{sp}}] \quad (\text{Equation 5-8})$$

At neutral and moderately alkaline pH the outgassing rate of aqueous  $\text{CO}_2(\text{aq})$  (the reverse reaction given by equation 5-1) is thought to be much faster than its hydration of dissolved  $\text{CO}_2$  (the forward reaction given by equation 5-2: Greenwood and Earnshaw, 1997; Appelo and Postma, 2005), so  $^{14}\text{C}$  in the dissolved  $\text{CO}_2$  pool will rapidly equilibrate with the far lower isotope ratio of atmospheric  $\text{CO}_2$ . Thus  $^{14}\text{C}$  that is transferred to the aqueous  $\text{CO}_2$  pool is lost to atmosphere, and the overall rate of  $^{14}\text{C}$  loss from the aqueous system is governed by the dehydration of carbonic acid (the reverse of reaction 5-2). If dehydration is an elementary reaction then the rate equation will have the form:

$$J_{r2} = -d[\text{H}_2\text{CO}_{3(\text{aq})}]/dt = k_{r2} \cdot [\text{H}_2\text{CO}_{3(\text{aq})}] \quad (\text{Equation 5-9})$$

If minor differences in the dehydration rate of different carbon isotopes of carbonic acid are ignored, the overall rate of  $^{14}\text{C}$  loss from the aqueous carbonate pools is given by:

$$-d[^{14}\text{C}_{(\text{aq,carb})}]/dt = -d[\text{H}_2^{14}\text{CO}_{3(\text{aq})}]/dt = k_{r2} \cdot x \cdot [\text{H}_2\text{CO}_{3(\text{aq})}] \quad (\text{Equation 5-10})$$

Where  $x$  decreases with time, but  $[\text{H}_2\text{CO}_{3(\text{aq})}]$  is invariant in a system that is in overall equilibrium with atmospheric  $\text{CO}_2$ . Now:

$$[^{14}\text{C}_{(\text{aq,carb})}] = [\text{H}_2^{14}\text{CO}_{3(\text{aq})}] + [\text{H}^{14}\text{CO}_3^-(\text{aq})] + [^{14}\text{CO}_3^{2-}(\text{aq})] \quad (\text{Equation 5-11})$$

So at equilibrium:

$$[^{14}\text{C}_{(\text{aq,carb})}] = x \cdot [\text{H}_2\text{CO}_{3(\text{aq})}] + x \cdot [\text{HCO}_3^-(\text{aq})] + x \cdot [\text{CO}_3^{2-}(\text{aq})] \quad (\text{Equation 5-12})$$

The acid dissociation constants for equations 5-3 and 5-4 are defined as:

$$K_{a1} = \frac{[H^+_{(aq)}] \cdot [HCO_3^-_{(aq)}]}{[H_2CO_{3(aq)}} \quad \text{and}$$

$$K_{a2} = \frac{[H^+_{(aq)}] \cdot [CO_3^{2-}_{(aq)}]}{[HCO_3^-_{(aq)}}$$

Where  $K_{a1} = 2.5 \times 10^{-4} \text{ mol}\cdot\text{L}^{-1}$  and  $K_{a2} = 4.84 \times 10^{-11} \text{ mol}\cdot\text{L}^{-1}$  (Greenwood and Earnshaw, 1997). This  $K_{a1}$  value is the true dissociation constant for carbonic acid, whereas many published sources combine reactions 5-2 and 5-3 and report the apparent dissociation constant. Equation (12) can be rewritten as:

$$[^{14}C_{(aq,carb)}] = x \cdot [H_2CO_{3(aq)}] \cdot \left( 1 + \frac{K_{a1}}{[H^+]} + \frac{K_{a1}K_{a2}}{[H^+]^2} \right) \quad (\text{Equation 5-13})$$

Which can be substituted in the rate equation (5-10) to yield

$$\frac{-d[^{14}C_{(aq,carb)}]}{dt} = \frac{k_{r2}}{\left( 1 + \frac{K_{a1}}{[H^+]} + \frac{K_{a1}K_{a2}}{[H^+]^2} \right)} \cdot [^{14}C_{(aq,carb)}] \quad (\text{Equation 5-14})$$

The term  $k_{obs} = \frac{k_{r2}}{\left( 1 + \frac{K_{a1}}{[H^+]} + \frac{K_{a1}K_{a2}}{[H^+]^2} \right)}$  is comparable with the experimental rate

constant observed in the atmospheric isotope exchange experiments. Equation 5-14 can be integrated to yield a rate equation that can be fitted to the experimental data (see Figure 5-7):

$$[^{14}C_{(aq,carb)}] = [^{14}C_{(aq,carb)}]_o \cdot e^{-k_{obs} \cdot t} \quad (\text{Equation 5-15})$$

Where  $[^{14}C_{(aq,carb)}]_o$  is the initial concentration of  $^{14}C$  in the aqueous carbonate pool.

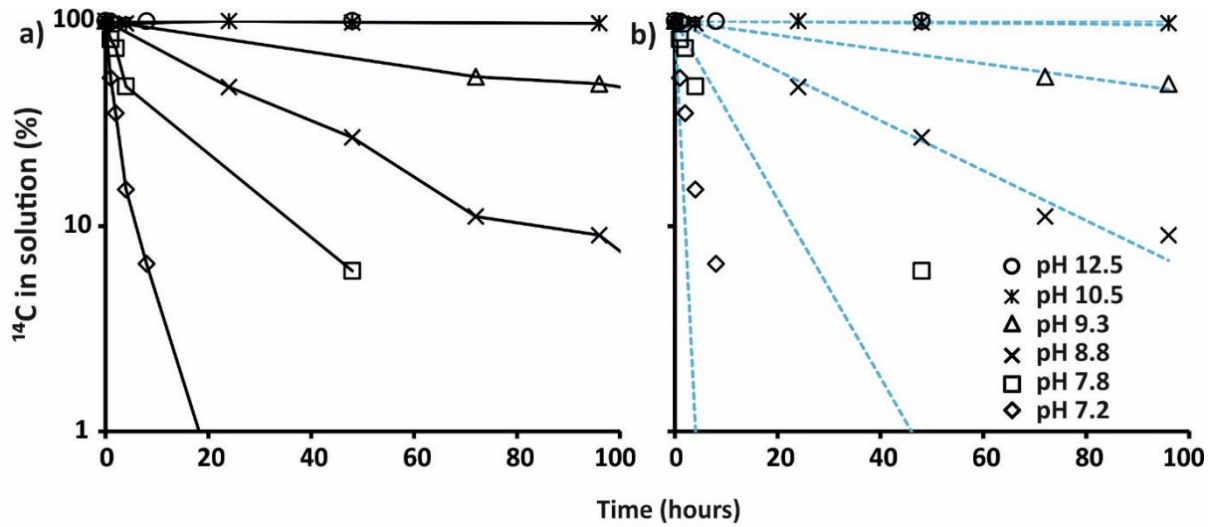


Figure 5-7 (a) the experimental results showing the percentage of  $^{14}\text{C}$  remaining in solution over time in open system on a log scale (b) experimental data fitted with predicted rate of loss using the derived value of  $k_{r2} = 4500 \text{ hr}^{-1}$  for the rate constant.

Equation (5-15) has been fitted to all the data from all the atmospheric isotope exchange data by assuming a single value for the dehydration rate for equation 5-2 of  $k_{r2} = 4500 \text{ hr}^{-1}$  (value derived from fitting experimental data to Equation 5-15, see Appendix A, section A.2). Above pH 8 the prediction and experimental data show good agreement. At pH values below 8 the initial rate of  $^{14}\text{C}$  loss is greater than predicted by the model, whereas the final  $^{14}\text{C}$  concentrations are higher than predicted (the latter error is exaggerated on a log scale and not thought significant). The model explicitly assumes dynamic equilibrium between the DIC pools and atmospheric  $\text{CO}_2$ . Addition of an alkaline  $^{14}\text{CO}_3^{2-}$ -spike to an equilibrated system will have resulted in a brief period of disequilibria, when the out-gassing rate exceeds in-gassing rate. During this period  $^{14}\text{C}$  loss is faster than predicted by the model. This effect will have been negligible

in higher pH systems due to higher initial  $\text{CO}_3^{2-}$  concentrations, but may explain the  $^{14}\text{C}$  loss in systems with a  $\text{pH} < 8$  is faster than predicted by the model.

The linear relationship between the logarithm of  $^{14}\text{C}$  concentration and time (Figure 5-7b) demonstrates that the loss mechanism is pseudo-first order with respect to  $^{14}\text{C}$  concentration. This strongly suggests that the rate of  $^{14}\text{C}$  loss is controlled by an elementary reaction that transforms single  $^{14}\text{C}$ -bearing molecules. The model assumes that the rate limiting step is dehydration of carbonic acid (equation 5-2), an assumption that is well supported by the literature (Greenwood and Earnshaw, 1997; Appelo and Postma, 2005). Conversely the overall reaction described in equations 5-1 to 5-4 would also exhibit pseudo-first order kinetics if equation 5-1 alone (outgassing of dissolved  $\text{CO}_2$ ) was rate limiting (i.e. if reaction 5-2 was fast in comparison with reaction 5-1). However it is unlikely that the reaction conditions reported here were so different from other studies that the dehydration step has no influence on the rate, and so the observed pseudo first order kinetics support the assumption that dehydration is rate limiting. Nonetheless the key finding of this study is that any  $^{14}\text{C}$ -containing water with a  $\text{pH} < 9.3$  that is in contact with atmosphere will rapidly lose  $^{14}\text{CO}_2$  from solution (timescale of 10's of hours) by isotopic exchange with atmospheric  $\text{CO}_2$ .

## **5.6 Implications**

### **5.6.1 Implications for surface release of $^{14}\text{C}$ -containing water**

Authorised discharge or accidental release of  $^{14}\text{C}$ -DIC into surface waters (e.g. at the Sellafield site, UK,  $^{14}\text{C}$ -containing effluents are routinely discharged into

the Irish Sea; NDA, 2014) would require that the  $SI_{CAL}$  values reach +1.5 or greater to initiate  $^{14}C$  removal via homogeneous precipitation reactions. Surface water can contain  $Ca^{2+}$ , but often at a lower concentration in comparison to groundwater, thus except in the rare circumstance where very high calcite supersaturation occurs at the point of discharge and mixing, this would facilitate the dilution and dispersal of  $^{14}C$ -DIC in the environment. Precipitation may also be limited by the circum-neutral pH of many surface water environments. Authorised discharges are limited to pH range of less than 9, typically falling between pH 5.5 and 9 (Mayes et al., 2009). These conditions would favour atmospheric isotopic exchange which occurs rapidly at pH <9.3 due to the lower pH of the surface water and discharges. Under these conditions long range transport of  $^{14}C$ -DIC in surface waters is not expected. Indeed, after mixing with surface waters in the Irish Sea, the  $^{14}C$  enriched signal is lost from DIC over a very short spatial zone (Ahad et al., 2006).

### **5.6.2 Implication for subsurface release of $^{14}C$ -containing water**

The fate of  $^{14}C$ -DIC released to groundwater will depend on the  $SI_{CAL}$  for the combined leak and groundwater. If the mixture remains undersaturated with respect to calcite precipitation, aqueous transport of  $^{14}C$  is very likely to occur, retarded only by isotope exchange with TIC, if present. However, two factors favour the precipitation of calcite in the subsurface. Groundwater often contains  $Ca^{2+}$  and  $Mg^{2+}$  (and they are important exchangeable cations in most soils), and while the typical pH range of groundwater is similar to that of surface waters, heterogeneous precipitation is favoured by the presence of mineral surfaces. Also,

aqueous releases to the subsurface environment are invariably accidental, and therefore the pH value is controlled by the source. If the  $^{14}\text{C}$ -DIC source has a high pH value, precipitation is likely to occur over a large range of  $\text{Ca}^{2+}$  and  $\text{CO}_3^{2-}$  concentrations as shown in Figure 5-6 where the saturation indices are exceeded at much lower  $\text{Ca}^{2+}$  and  $\text{CO}_3^{2-}$  concentrations with increasing pH. However, once aqueous release to the subsurface ceases (i.e. the leak is repaired), any precipitate that has formed is likely to dissolve slowly overtime if the local groundwater is undersaturated with respect to calcite (i.e. the neo-formed calcite will become a secondary source term for  $^{14}\text{C}$ -DIC).

In organic rich near surface soils, oxidation of organic matter can result in pore air with a partial pressure of  $\text{CO}_2(\text{g})$  up to 100 times higher than that of atmosphere (Deutsch and Siegel, 1997). The elevated  $\text{pCO}_2$  value (with respect to atmosphere) indicates that there is poor diffusive  $\text{CO}_2$  mass transfer in the vadose zone, possibly because the air and water phases are discontinuous in the vadose zone and the  $\text{CO}_2$  must cross numerous phase boundaries. The potential to lose  $^{14}\text{C}$  DIC through isotope exchange through the vadose zone, and thence to atmosphere is probably very low (in many situations this isotope exchange must occur against a net TIC flux downwards from the organic rich surface soil). Thus fate of  $^{14}\text{C}$ -DIC released to the subsurface is ultimately to be transported by groundwater flow, but this transport may be significantly more retarded than predicted by simple sorption kinetics if the leak source is alkaline or the soil contains significant TIC.

### 5.6.3 Historical Release of $^{14}\text{C}$ to the Subsurface at the UK Sellafield Site

At the Sellafield reprocessing plant in the UK, there was an accidental discharge of inorganic- $^{14}\text{C}$ -containing leachate from the silos containing corroded MAGNOX fuel cladding into the shallow groundwater approximately 40 years ago (Wallace et al., 2012). The corroded magnesium alloy fuel cladding is dominated by brucite with small amounts of hydrous magnesium carbonates and is stored under water (Parry et al., 2011). Ground conditions at the Sellafield site are 1-5 m of made ground above up to 50 m of unconsolidated fluvio-glacio till (Stamper et al., 2012; Cruickshank, 2012). The local water table is  $\sim 10$  m below ground level, therefore, groundwater flow ( $\sim 200$  m  $\text{a}^{-1}$ ) is predominately within the till and follows the regional hydraulic gradient from east to west across the site (i.e. from the Cumbrian Mountains towards the Irish Sea; Stamper et al., 2012). Groundwater composition varies with location but generally the pH lies between 6 and 8. In the vicinity of the leak the groundwater composition is dominated by Ca-Na-Cl, and the pH is approximately 6.5 (see A3). Currently the  $^{14}\text{C}$ -containing groundwater plume that is associated with the historical leak event is still within the site boundaries and therefore is moving far more slowly than the groundwater.

Two scenarios have been modelled using PHREEQC in order to investigate the potential in situ geochemical conditions during the initial silo leak event. These assume the mixing of either surface or bottom water from within the silos with varying volumes of groundwater. The assumed composition of the water from the surface of the silo is based on site measurements, which showed that it is Na-K- $\text{NO}_3$ - $\text{CO}_3$  dominated with a pH  $\sim 9$  (Sellafield Ltd., 2009). The silo

waters are in contact with atmosphere, so it is assumed for the purposes of modelling the system that this solution was fully equilibrated with atmospheric CO<sub>2</sub> (a pH value of 8.8 was used). The silos contain a significant volume of fine material from the corrosion of magnesium alloy fuel cladding, and therefore the aqueous phase at bottom of the silos may differ significantly from the surface liquor, however, no solution measurements exist for this liquor as it is inaccessible. Therefore this solution has been modelled by assuming it has equilibrated with MgCO<sub>3</sub>(s) as the most stable magnesium carbonate phase (the final corrosion product of magnesium alloy in an aqueous solution in contact with atmosphere) at a pH of 8.9 (pH at equilibrium with MgCO<sub>3</sub>, the full solution compositions used in this modelling are given in Appendix A, section A.3). Modelling with MgCO<sub>3</sub>(s) gives the most conservative DIC for potential mixture of the deep tank liquor with groundwater. Other hydrous magnesium phases (hydromagnesite; artinite; nesquehonite; and hydrotalcite) have all been predicted/measured within these silo environments (Parry et al., 2011; Gregson et al., 2011), and due to their higher solubility with respect to magnesite, would lead to a higher DIC content in deep tank liquor leading to increased SI<sub>CAL</sub> over the mixing range.

The PHREEQC modelling indicates that mixing of silo liquor of either composition with the circumneutral groundwater would allow heterogeneous calcite precipitation at almost all mixing ratios (see Figure 5-8). Thus it is likely that inorganic <sup>14</sup>C in the leak water would be precipitated as calcite. Such calcite precipitation provides a mechanism for retardation of <sup>14</sup>C on this site which can explain the long term retention of <sup>14</sup>C in the vicinity of the leak sites. At Sellafield

the local groundwater has  $SI_{CAL} < 0$  so dissolution of any precipitated calcite and release of  $^{14}C$  to solution is expected over time. The aquifer materials generally contain quite low TIC values of 0-0.6 % w/w (except for locations containing made ground) providing limited potential for further additional  $^{14}C$ -DIC retardation by solid isotopic exchange reactions (depending on local ground TIC values close to the silo leaks). As contact with the atmosphere is also limited there is expected to be little loss via atmosphere exchange (although some boreholes may act as conduits facilitating atmospheric isotopic exchange and therefore increase losses of  $^{14}C$  on a local scale). Therefore, over the long-term,  $^{14}C$  stored initially in calcite precipitates is expected to be slowly remobilised and dispersed into groundwater, which ultimately discharges into surface waters (i.e. the Rivers Calder and Ehen or Irish Sea) where it will be rapidly depleted via dilution and exchange with atmospheric  $^{12}CO_2$ .

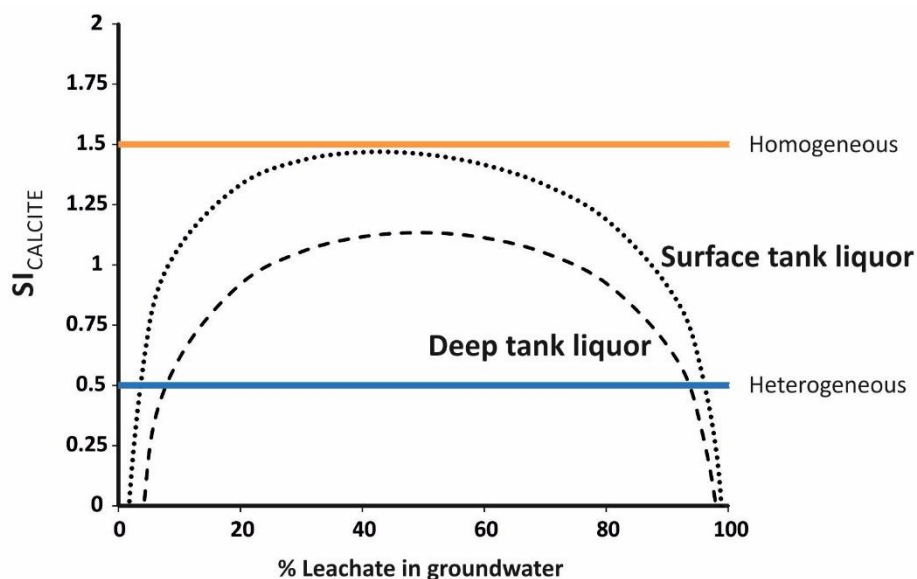


Figure 5-8 Predicted saturation indices for the mixing of two potential leachate plumes with groundwater on Sellafield site (a) surface tank composition from the MAGNOX silo (site data – dotted line) (b) deep tank liquor from the MAGNOX silo (modelled – dashed line).

## 5.7 Conclusion

Figure 5-9 summarises the processes likely to affect  $^{14}\text{C}$ -DIC behaviour as a surface and near surface contaminant. Many surface waters have a circum-neutral pH and are undersaturated with respect to calcium carbonate. In such environments transfer to atmosphere by isotopic exchange with  $^{12}\text{CO}_2(\text{g})$  will be rapid, therefore, if  $^{14}\text{C}$ -DIC is discharged into surface water, it is unlikely to be transported very far with the aqueous flow before being lost to atmosphere. In contrast in subsurface conditions, isolation from the atmosphere will prevent loss by exchange with  $\text{CO}_2(\text{g})$ . Any  $^{14}\text{C}$ -DIC release to this environment can potentially be transported with groundwater flow, but carbonate precipitation reactions are likely to be more favoured (by higher pH and  $\text{Ca}^{2+}$  concentration) and  $^{14}\text{C}$ -DIC may be removed from solution and stored within solid carbonate over long

timescales. In moderately calcareous environments (with TIC > ~0.24 % w/w) isotopic exchange of the  $^{14}\text{C}$ -DIC with  $^{12}\text{C}$ -containing carbonates is also expected to retain  $^{14}\text{C}$  in the solid fraction. Thus, retarded  $^{14}\text{C}$ -DIC transport can be expected in the near field environment at many nuclear sites and  $^{14}\text{C}$  contamination may persist in sub-surface environments for decades following any accidental releases to ground.

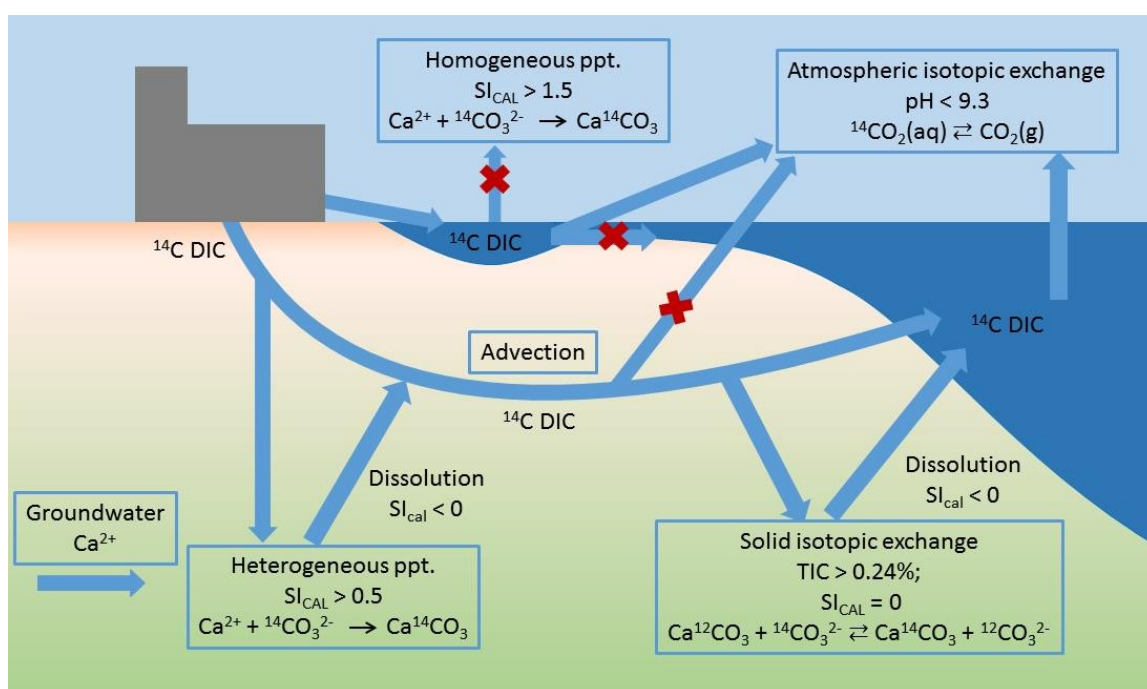


Figure 5-9 Schematic model of processes affecting the  $^{14}\text{C}$ -DIC transport in surface and subsurface environments.

## 5.8 References

Ahad, J.M., Ganeshram, R.S., Spencer, R.G., Uher, G., Gulliver, P., Bryant, C.L. 2006. Evidence for anthropogenic  $^{14}\text{C}$ -enrichment in estuarine waters adjacent to the North Sea. *Geophysical Research Letters*.

Appelo, C.A.J., Postma, D., 2005. *Geochemistry, Groundwater and Pollution*, Second Edition. Taylor & Francis.

Atkins, P.W., De Paula, J., 2006. *Atkins' Physical Chemistry*. Macmillan Higher Education.

Baston, G.M.N., Marshall, T.A., Otlet, R.L., Walker, A.J., Mather, I.D. and Williams, S.J., 2012. Rate and speciation of volatile carbon-14 and tritium releases from irradiated graphite. *Mineralogical Magazine* 76, 3293-3302.

Begg, F.H., Cook, G.T., Baxter, M.S., Scott, E.M., McCartney, M., 1992. Anthropogenic radiocarbon in the eastern Irish Sea and Scottish coastal waters. *Radiocarbon* 34, 707-716.

Bird, G.A., Bergström, U., Nordlinder, S., Neal, S.L., Smith, G.M., 1999. Model simulations of the fate of  $^{14}\text{C}$  added to a Canadian shield lake. *Journal of Environmental Radioactivity* 42, 209-223.

Bischoff, W. D., Bishop, F. C. & Mackenzie, F. T. 1983. Biogenically produced magnesian calcite: inhomogeneities in chemical and physical properties: comparison with synthetic phases. *American Mineralogist*, 68, 1183-1188.

Boss, C., Allsop, P.J., 1995. Radioactive effluents from CANDU 6 reactors during normal operation. Atomic Energy of Canada Ltd.

Boylan, A.A., Stewart, D.I., Graham, J.T., Trivedi, D., Burke, I.T., 2016. Mechanisms of inorganic carbon-14 attenuation in contaminated groundwater: Effect of solution pH on isotopic exchange and carbonate precipitation reactions. *Applied Geochemistry*. <https://doi.org/10.1016/j.apgeochem.2016.12.006>

Bracke, G., Müller, W., 2008. Contribution to a more realistic approach in assessing the release of C-14 from low-level radioactive waste repositories. *Journal of Contaminant Hydrology* 102(3), 210-216.

Caron, F., Sutton, J., Benz, M.L., Haas, M.K., 2000. Determination of carbon-14 levels in heavy water and groundwaters. *Analyst* 125, 59-64.

Cook, G.T., MacKenzie, A.B., Naysmith, P., Anderson, R., 1998. Natural and anthropogenic <sup>14</sup>C in the UK coastal marine environment. *Journal of Environmental Radioactivity* 40, 89-111.

Cross, J.E., Ewart, F.T., 1991. Hatches — A Thermodynamic Database And Management System. *Radiochimica Acta* 52-53, 421-422.

Cruickshank, J. 2012. *Findings of the Sellafield Contaminated Land and Groundwater Management* [Online]. Sellafield Ltd. Available: <http://www.sellafieldsites.com/land/documents/Signpost%20Report.pdf> [Accessed 19/03/2014].

Deutsch, W. J. & Siegel, R. 1997. *Groundwater Geochemistry: Fundamentals and Applications to Contamination*, Taylor & Francis.

Doctor, D.H., Kendall, C., Sebestyen, S.D., Shanley, J.B., Ote, N., Boyer, E.W., 2008. Carbon isotope fractionation of dissolved inorganic carbon (DIC) due to outgassing of carbon dioxide from a headwater stream. *Hydrological Processes* 22, 2410-2423.

Doulgeris, C., Humphreys, P. & Rout, S. 2015. An approach to modelling the impact of <sup>14</sup>C release from reactor graphite in a geological disposal facility. *Mineralogical Magazine*, 79, 1495-1503.

Dreybrodt, W., Buhmann, D., Michaelis, J., Usdowski, E., 1992. Geochemically controlled calcite precipitation by CO<sub>2</sub> outgassing: Field measurements of precipitation rates in comparison to theoretical predictions. *Chemical Geology* 97, 285-294.

Dutton, M.V., Foster, C., Trivedi, D., 2009. Characterisation of Soils from Site Investigation within the Sellafield Separation Area. NNL Commercial.

Eabry, S., Vance, J.N., Cline, J.E., Robertson, D.E., 1995. Characterization of Carbon-14 Generated by the Nuclear Power Industry: Final Report. Electric Power Research Institute.

Evenden, W.G., Sheppard, S.C., Killey, R.W.D., 1998. Carbon-14 and tritium in plants of a wetland containing contaminated groundwater. *Applied Geochemistry* 13, 17-21.

Ford, D., Williams, P.D., 2007. *Karst Hydrogeology and Geomorphology*. Wiley.

Garnier, J.M., 1985. Retardation of dissolved radiocarbon through a carbonated matrix. *Geochimica et Cosmochimica Acta* 49, 683-693.

Godwin, H., 1962. Half-life of radiocarbon. *Nature* 195, 984.

Gonfiantini, R., Zuppi, G.M., 2003. Carbon isotope exchange rate of DIC in karst groundwater. *Chemical Geology* 197, 319-336.

Greenwood, N.N., Earnshaw, A., 1997. *Chemistry of the Elements*, Second ed. Pergamon Press.

Gregson, C.R., Goddard, D.T., Sarsfield, M.J., Taylor, R.J. 2011. Combined electron microscopy and vibrational spectroscopy study of corroded Magnox sludge from a legacy spent nuclear fuel storage pond. *Journal of Nuclear Materials* 412(1), 145-56.

Gu, B., Schulz, R.K., 1991. Anion retention in soil: possible application to reduce migration of buried technetium and iodine. Nuclear Regulatory Commission, Washington, DC (United States). Div. of Regulatory Applications; California Univ., Berkeley, CA (United States). Dept. of Soil Science

Hodkin, D.J., Stewart, D.I., Graham, J.T., Burke, I.T., 2016. Coprecipitation of <sup>14</sup>C and Sr with carbonate precipitates: The importance of reaction kinetics and recrystallization pathways. *Science of The Total Environment* 562, 335-343.

Huang, Y. C., Fowkes, F. M., Lloyd, T. B. & Sanders, N. D. 1991. Adsorption of calcium ions from calcium chloride solutions onto calcium carbonate particles. *Langmuir*, 7, 1742-1748.

Inskeep, W.P., Bloom, P.R., 1985. An evaluation of rate equations for calcite precipitation kinetics at pCO<sub>2</sub> less than 0.01 atm and pH greater than 8. *Geochimica et Cosmochimica Acta* 49, 2165-2180.

Jackson, C.P., Yates, H., 2011. Key processes and data for the migration of <sup>14</sup>C released from a cementitious repository, Serco Report.

Killey, R.W.D., Rao, R.R., Eyvindson, S., 1998. Radiocarbon speciation and distribution in an aquifer plume and groundwater discharge area, Chalk River, Ontario. *Applied Geochemistry* 13, 3-16.

Krauskopf, K.B., Bird, D.K., 1995. *Introduction to geochemistry*. McGraw-Hill.

Langmuir, D., 1997. Use of laboratory adsorption data and models to predict radionuclide releases from a geological repository: A brief history, *Materials Research Society Symposium - Proceedings*, pp. [d]769-780.

Limer, L. M. C., Thorne, M. C., Cummings, R. 2011. Consideration of canopy structure in modelling  $^{14}\text{C}$ -labelled gas behaviour in the biosphere for human dose assessments. *Radioprotection*, 46, S409-S415.

Limer, L., Klos, R., Walke, R., Shaw, G., Norden, M. & Xu, S. 2013. Soil-plant-atmosphere modelling in the context of releases of  $^{14}\text{C}$  as a consequence of nuclear activities. *Radiocarbon*, 55, 804-813.

Magnusson, A., Stenstrom, K., Skog, G., Adliene, D., Adlys, G., Hellborg, R., Olariu, A., Zakaria, M., Raaf, C. and Mattsson, S., 2004. Levels of  $^{14}\text{C}$  in the Terrestrial Environment in the Vicinity of Two European Nuclear Power Plants. *Radiocarbon* 46(2), 863-868.

Marshall, A., Coughlin, D., Laws, F., 2015. *Groundwater monitoring at Sellafield: Annual data review 2014*.

Marshall, T. A., Baston, G. M. N., Otlett, R. L., Walker, A. J. & Mather, I. D. 2011. Longer-term release of carbon-14 from irradiated graphite [Online]. Available:

<http://www.nda.gov.uk/publication/longer-term-release-of-carbon-14-from-irradiated-graphite-october-2011/> [Accessed 31/10/2013].

Mayes, W.M., Johnston, D., Potter, H.A.B., Jarvis, A.P., 2009. A national strategy for identification, prioritisation and management of pollution from abandoned non-coal mine sites in England and Wales. I. Methodology development and initial results. *Science of the Total Environment* 407, 5435-5447.

Mucci, A. & Morse, J. W. 1983. The incorporation of  $Mg^{2+}$  and  $Sr^{2+}$  into calcite overgrowths: influences of growth rate and solution composition. *Geochimica et Cosmochimica Acta*, 47, 217-233.

Nancollas, G.H. and Reddy, M.M., 1971. The crystallization of calcium carbonate. II. Calcite growth mechanism. *Journal of Colloid and Interface Science* 37(4), 824-830.

NDA 2012. Geological Disposal: Carbon-14 Project - Phase 1 Report. Nuclear Decommissioning Authority.

NDA 2014. Monitoring our Environment: Discharges and Environmental Monitoring. Nuclear Decommissioning Authority

Parkhurst, D.L., Appelo, C.A.J., 2013. Description of input and examples for PHREEQC version 3- A computer program for speciation, batch-reaction, one-dimensional transport, and inverse geochemical calculations, U.S. Geological Survey Techniques and Methods, p. 497.

Parry, S.A., O'Brien, L., Fellerman, A.S., Eaves, C.J., Milestone, N.B., Bryan, N.D., Livens, F.R., 2011. Plutonium behaviour in nuclear fuel storage pond effluents. *Energy & Environmental Science* 4, 1457-1464.

Plummer, L.N., Busenberg, E., 1982. The solubilities of calcite, aragonite and vaterite in CO<sub>2</sub>-H<sub>2</sub>O solutions between 0 and 90°C, and an evaluation of the aqueous model for the system CaCO<sub>3</sub>-CO<sub>2</sub>-H<sub>2</sub>O. *Geochimica et Cosmochimica Acta* 46, 1011-1040.

Randall, M.G., Brydie, J., Graham, J., Small, J.S. 2004. SCLS Phase 1: The Geochemistry of the Sellafield Site. BNFL Commercial.

Roussel-Debet, S., Gontier, G., Siclet, F. and Fournier, M., 2006. Distribution of carbon 14 in the terrestrial environment close to French nuclear power plants. *Journal of environmental radioactivity*, 87(3), 246-259.

Sellafield Ltd., 2009. Generic Basis for Inventory Challenge – Legacy Alkaline Sludge Systems, Sellafield Ltd., Cumbria, UK.

Sheppard, M.I., Elrick, D.E., Peterson, S.R., 1997. Review and performance of four models to assess the fate of radionuclides and heavy metals in surface soil. *Canadian Journal of Soil Science* 77, 333-344.

Sheppard, S.C., Ticknor, K.V., Evenden, W.G., 1998. Sorption of inorganic <sup>14</sup>C on to calcite, montmorillonite and soil. *Applied Geochemistry* 13, 43-47.

Sherman, L.A., Barak, P., 2000. Solubility and Dissolution Kinetics of Dolomite in Ca–Mg–HCO<sub>3</sub>/CO<sub>3</sub> Solutions at 25°C and 0.1 MPa Carbon Dioxide. *Soil Science Society of America Journal* 64, 1959-1968.

Skinner, A.J., LaFemina, J.P., Jansen, H.J.F., 1994. Structure and bonding of calcite; a theoretical study. *American Mineralogist* 79 (3-4). 205-214.

Stamper, A., McKinlay, C., Coughlin, D. & Laws, F. 2012. *Land Quality Programme Groundwater Monitoring at Sellafield* [Online]. Sellafield Ltd. Available: <http://www.sellafieldsites.com/land/documents/Groundwater%20Monitoring%20at%20Sellafield%20-%20Annual%20Data%20Review%202012.pdf> [Accessed 19/03 2014].

Stipp, S.L., Hochella, M.F., Parks, G.A. and Leckie, J.O., 1992. Cd<sup>2+</sup> uptake by calcite, solid-state diffusion, and the formation of solid-solution: Interface processes observed with near-surface sensitive techniques (XPS, LEED, and AES). *Geochimica et Cosmochimica Acta*, 56(5), 1941-1954.

Stumm, W., Morgan, J.J., 1996. *Aquatic chemistry: chemical equilibria and rates in natural waters*. Wiley.

Su, C., Suarez, D.L., 1997. In situ infrared speciation of adsorbed carbonate on aluminum and iron oxides. *Clays and Clay Minerals* 45, 814-825.

van Geen, A., Robertson, A.P., Leckie, J.O., 1994. Complexation of carbonate species at the goethite surface: Implications for adsorption of metal ions in natural waters. *Geochimica et Cosmochimica Acta* 58, 2073-2086.

Wallace, S.H., Shaw, S., Morris, K., Small, J.S., Fuller, A.J., Burke, I.T., 2012. Effect of groundwater pH and ionic strength on strontium sorption in aquifer sediments: Implications for <sup>90</sup>Sr mobility at contaminated nuclear sites. *Applied Geochemistry* 27, 1482-1491.

Walthert, L., Graf, U., Kammer, A., Luster, J., Pezzotta, D., Zimmerman, S. & Hagedorn, F. 2010. Determination of organic and inorganic carbon,  $\delta^{13}\text{C}$ , and nitrogen in soils containing carbonates after acid fumigation with HCl. *Journal of Plant Nutrition and Soil Science*, 173, 207-216.

White, W., 1997. Thermodynamic equilibrium, kinetics, activation barriers, and reaction mechanisms for chemical reactions in karst terrains. *Environmental Geology* 30, 46-58.

White, W., 2013. *Geochemistry*. Wiley-Blackwell.

Wijnja, H., Schulthess, C.P., 2000. Interaction of carbonate and organic anions with sulfate and selenate adsorption on an aluminum oxide. *Soil Science Society of America Journal* 64, 898-908.

Yim, M.-S., Caron, F., 2006. Life cycle and management of carbon-14 from nuclear power generation. *Progress in Nuclear Energy* 48, 2-36.

Zhang, J., Quay, P.D., Wilbur, D.O., 1995. Carbon isotope fractionation during gas-water exchange and dissolution of  $\text{CO}_2$ . *Geochimica et Cosmochimica Acta* 59, 107-114.

## **Chapter 6 The behaviour of carbon-14 containing low molecular weight organic compounds in contaminated groundwater under aerobic conditions**

### **6.1 Executive Summary**

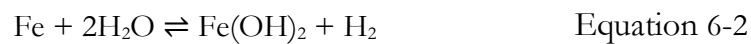
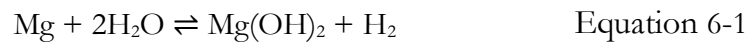
Short chain carbon-14 ( $^{14}\text{C}$ ) containing organic compounds can be formed by oxidation of carbides and impurities within nuclear fuel cladding. During fuel reprocessing and subsequent waste storage there is potential for these organic compounds to leak to shallow subsurface environments. Currently there is little data on the persistence of these compounds in such environments. Four  $^{14}\text{C}$ -labelled compounds (acetate; formate; formaldehyde and methanol) were added to aerobic microcosm experiments that contained glacial outwash sediments and groundwater simulant representative of the UK Sellafield nuclear site. Two concentrations of each electron donor were used, low concentration ( $10^{-5}$  M) to replicate predicted concentrations from an accidental release and high concentration ( $10^{-2}$  M) to study the impact of the individual electron donor on the indigenous microbial community in the sediment. In the low concentration system only  $\sim 5\%$  of initial  $^{14}\text{C}$  remained in solution at the end of experiments in contact with atmosphere ( $\sim 300$  hours). The production of  $^{14}\text{CO}_2(\text{g})$  (measured after 48 hours) suggests microbial utilisation is the primary removal mechanism for these organic compounds, although methanol loss may have been partially by volatilisation. Highest retention of  $^{14}\text{C}$  by the solid fractions was found in the acetate experiment, with 12% being associated with the inorganic fraction, suggesting precipitation as solid carbonate. In the high concentration systems only  $\sim 5\%$  of initial  $^{14}\text{C}$  remains in solution at the end of the experiments for acetate,

formate and methanol. In the formaldehyde experiment only limited loss from solution was observed. The microbial populations of unaltered sediment and those in the low concentration experiments were broadly similar, with highly diverse bacterial phyla present. Under high concentrations of the organic compounds the abundance of common operational taxonomic units was reduced by 66% and the community structure was dominated by Proteobacteria (particularly Betaproteobacteria). The results of this study suggest that many bacterial phyla that are ubiquitous in near surface soils are able to utilise a range of  $^{14}\text{C}$ -containing low molecular weight organic substances very rapidly, and thus such substances are unlikely to persist in aerobic shallow subsurface environments.

## 6.2 Introduction

$^{14}\text{C}$ -labelled low molecular weight organic (LMWO) substances have long been considered a potential source of future  $^{14}\text{C}$  release to deep subsurface environments due to the predicted accumulation of  $^{14}\text{CH}_4$  in underground repositories (Jefferies, 1990; Jackson and Yates, 2011; Limer et al., 2011; Marshall et al., 2011; Limer et al., 2013). Now there is concern that corrosion of activated fuel and fuel cladding may form a range of LMWOs as a by-product (Wieland and Hummel, 2015) providing a source for their potential release to shallow subsurface environments. The formation of  $^{14}\text{C}$  occurs at each stage of the nuclear power generation process (Eabry et al., 1995) from the parent isotopes nitrogen-14 ( $^{14}\text{N}$ ), oxygen-17 ( $^{17}\text{O}$ ) and carbon-13 ( $^{13}\text{C}$ ), especially due to the presence of  $^{14}\text{N}$  impurities in components of the fuel and fuel cladding. During fuel reprocessing the fuel and cladding (e.g. steel encapsulation, Mg-alloy) have historically been

stored in large water filled ponds, often as short term measure before disposal as intermediate level waste (Stamper et al., 2012; NDA, 2014; Morozov et al., 2016). At the free surface of the tanks oxic conditions are expected whereby  $^{14}\text{CO}$  formed from carbides in the fuel cladding would be expected to oxidise to  $^{14}\text{CO}_2$ . At greater depth the oxygen penetration is minimal and corrosion of readily oxidised metals, such as magnesium, uranium and iron, lead to chemically reducing conditions forming within storage ponds (Equation 6-1, Equation 6-2).



This potential redox stratification with oxic conditions at the pond surface becoming more reducing with depth would allow a variety of soluble  $^{14}\text{C}$ -containing organic compounds ( $^{14}\text{C}$ -DOC) to form within the storage silos/ponds. In the past leaks have occurs in storage silos/ponds in Canada and the UK, (Evenden et al., 1998; Killey et al., 1998; Bird et al., 1999; Stamper et al., 2014; Marshall et al., 2015), and thus there is a pathway for  $^{14}\text{C}$ -DOC to enter the shallow subsurface environment.

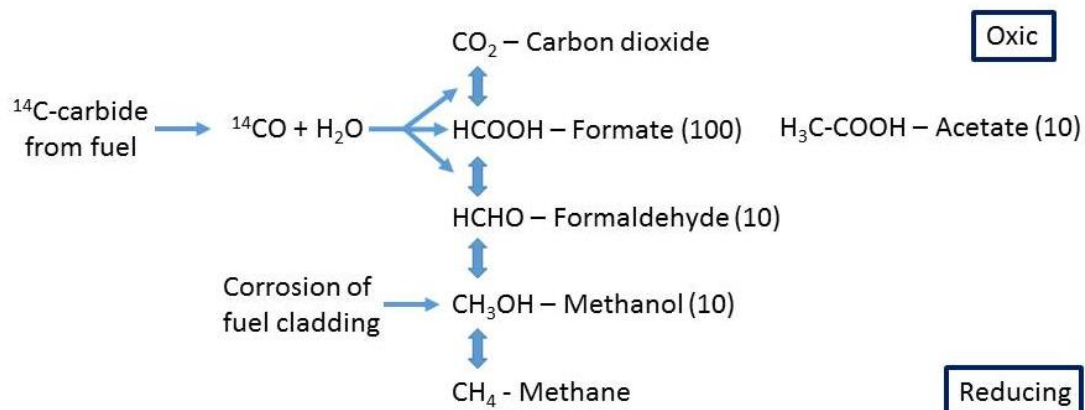
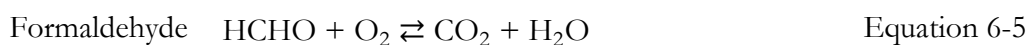


Figure 6-1 The formation of organic  $^{14}\text{C}$  compounds in the nuclear power generation process under varying redox conditions with corresponding ratio of LMWO formation in comparison to formate (McCullom and Seewald, 2007; Kaneko et al., 2003; Wieland and Hummel, 2015).

A range of  $^{14}\text{C}$ -containing LMWO substances can form from oxidation of carbide in spent fuel and corrosion of the fuel cladding (Figure 6-1). The most abundant will be  $\text{CO}_2$  and  $\text{CH}_4$ , whose concentrations are expected to be orders of magnitude higher than any other  $^{14}\text{C}$ -containing molecules produced (Wieland and Hummel, 2015), however  $\text{CO}_2$  and  $\text{CH}_4$  are not expected to persist in aerobic tank environments. At circumneutral pH  $^{14}\text{CO}_2$  would speciate in water as  $\text{H}^{14}\text{CO}_3^-$ , and isotopic exchange reactions with atmospheric  $^{12}\text{CO}_2$  would rapidly deplete  $^{14}\text{C}$ -dissolved inorganic carbon (DIC) concentrations in storage tanks that are open to atmosphere (see Boylan et al., 2016 for full discussion of  $^{14}\text{C}$ -DIC behaviour in surface and groundwater environments).  $^{14}\text{CH}_4$  has very low solubility at surface pressures and temperatures (Clever and Young, 1987) and is therefore expected to strongly partition to the gas phase and is assumed to be present as either pore gas or is released and diluted in atmosphere. Thus acetate, formate, formaldehyde and methanol have been identified as the main chemical forms for aqueous, organic

$^{14}\text{C}$  released to groundwater by leaks from reprocessing waste storage ponds (Kaneko et al., 2003; Wieland and Hummel, 2015). The presence of these different highly soluble  $^{14}\text{C}$ -DOC molecules in groundwater is potentially a mechanism for aqueous  $^{14}\text{C}$  release and transport in the shallow subsurface at nuclear sites.

In the shallow subsurface LMWO molecules can be metabolised by many of the diverse range of microbes found in these environments. Balanced equations for the use of the four most common  $^{14}\text{C}$ -DOC compounds produced from the nuclear power generation process during aerobic metabolism are shown below (Eqn. 6.3-6.6; Lovley et al., 1988). All of these reactions convert organic carbon into inorganic forms (Eqn. 6.3 and 6.4 indicate that oxidation of acetate and formate produce bicarbonate suggesting that these reactions the potential to increase groundwater pH). Further, carboxylates and similar LMWO molecules can sorb to, or become incorporated into soil particulates, which may also contribute to their low natural concentrations (0.1-1000  $\mu\text{M}$ ) in aquifers (van Hees et al., 2002; Fischer and Kuzyakov, 2010).



This study aims to establish the fate of  $^{14}\text{C}$  added as acetate, formate, formaldehyde and methanol in aerobic groundwater systems. These four organic compounds were chosen because they are predicted to be the primary  $^{14}\text{C}$ -DOC

compounds derived from fuel cladding (Kaneko et al., 2003; Wieland and Hummel, 2015). The specific objectives were: 1) to investigate the behaviour of aqueous, organic  $^{14}\text{C}$  in contact with sediment and atmosphere; 2) to establish the extent of the oxidation of organic  $^{14}\text{C}$  to  $^{14}\text{CO}_2(\text{g})$ ; 3) to assess the potential for organic and inorganic  $^{14}\text{C}$  accumulation in sediment; 4) to determine which part of the natural microbial population in the sediment favour the four organic compounds under aerobic conditions; and 5) to assess the implications of these processes for  $^{14}\text{C}$ -DOC release and migration in shallow subsurface environments.

## **6.3 Materials and Methods**

### **6.3.1 Sediment**

Sediment was collected from the River Calder valley near Calder Bridge, Cumbria, UK (Lat  $54^{\circ}26.3'\text{N}$ , Long  $3^{\circ}28.2'\text{W}$ ) in August 2015. This sediment is representative of the glacial/fluvial quaternary deposits that underlie the UK Sellafield nuclear reprocessing plant (Wallace et al., 2012, Law et al., 2010). Sediment was collected in HDPE plastic containers before being transferred to sterile HDPE bags and stored at  $4^{\circ}\text{C}$ . Prior to use the soil was sieved to retain  $<2$  mm fraction. X-ray powder diffraction (Cu K-alpha radiation) using a Bruker D8 Advance XRD was used to characterise the sediment mineralogy. Sediment pH was measured at collection site using standard methodology (ASTM, 2006).

### **6.3.2 $^{14}\text{C}$ -DOC partitioning under aerobic incubation (open flasks)**

Triplicate experiments were established in 500 mL glass Erlenmeyer flasks using 5 g of sediment and  $50 \pm 0.5$  mL of synthetic groundwater. The composition of the synthetic groundwater (Table 6-1) is based on the groundwater

present in similar sediments at the Low Level Waste Repository (LLWR) near Drigg, UK (Wilkins et al., 2007). Flasks were left to equilibrate overnight (minimum 12 hours), and then one of the four organic substances (sodium acetate, sodium formate, formaldehyde or methanol) were added at two concentrations ( $10^{-2}$  M or  $10^{-5}$  M). A small quantity of a  $^{14}\text{C}$ -labelled version of the same organic compound (50  $\mu\text{L}$  of  $4.6 \times 10^{-7}$  M solution with an activity of  $100 \text{ Bq ml}^{-1}$ ; ARC Ltd. USA) was added at the same time (the methyl, or  $\text{C}^2$ , carbon of acetate was labelled). Solution-only control experiments were also established at  $10^{-5}$  M (and  $10^{-2}$  M for methanol) to assess any potential losses of volatile organic compounds to atmosphere (glassware was sterilised at  $160^\circ\text{C}$  for 2 hours, solutions were  $0.2 \mu\text{m}$  filtered). The  $10^{-5}$  M concentration was chosen to represent the low levels predicted to be present in nuclear wastes and assumed to have a limited impact on the microbial community composition in comparison to the microbial community of the unaltered sediment (Kaneko et al., 2003; Wieland and Hummel, 2015). A significantly elevated concentration of  $10^{-2}$  M was used as it would have greater potential to alter the indigenous microbial population and therefore to potentially elucidate the active microbes in each system.

To ensure oxygen was available, flasks were stoppered with foam bungs and incubated on an orbital shaker (Stuart SSL1; 30 rpm; 16 mm orbit) at room temperature in the dark. Periodically 1 mL of solution was removed and centrifuged for 5 minutes at  $14000 g$  in 1.5 mL microcentrifuge tubes. After centrifugation the supernatant was analysed for  $^{14}\text{C}$ -DOC using liquid scintillation counting on a Packard Tri-Carb 2100TR (0.8 mL sample, 10 mL PerkinElmer

EcoScint A scintillation fluid; count time = 10 min; energy window = 4-156 keV). Samples were stored for a 24 hour period prior to counting. Solution pH was also periodically measured in experiments using a Thermo Scientific Benchtop multimeter and electrodes calibrated daily at pH 4, 7 and 10.

Table 6-1 Solution composition for synthetic groundwater, modified from Wilkins et al., (2007).

Compound	g/L in DIW
KCl	0.006
MgSO <sub>4</sub> ·7H <sub>2</sub> O	0.098
MgCl <sub>2</sub> ·6H <sub>2</sub> O	0.081
NaNO <sub>3</sub>	0.028
NaCl	0.0094
NaHCO <sub>3</sub>	0.24

At the end of the experiment sediments from two flasks from each triplicate set were separated by filtering (Whatman 2), washed with DIW and air-dried for further solid phase analysis detailed below. Sediment from the third flask of each triplicate were put in to 50 mL centrifuge tubes and the supernatants were removed. The tubes were immediately placed in a -20°C freezer for microbial DNA analysis.

### 6.3.3 Short term <sup>14</sup>C-DOC partitioning in aqueous fraction (closed bottles)

Triplicate 50 ±0.5 mL experiments were set up in 125 mL serum bottles using 5g of sediment and synthetic groundwater. The open bottles were left to

equilibrate with atmosphere overnight before addition of either, sodium acetate, sodium formate, formaldehyde or methanol. The concentrations of the organic compounds were set to  $10^{-2}$  M and  $10^{-5}$  M and spiked  $^{14}\text{C}$ -labelled organic compound (50  $\mu\text{L}$  of  $4.6 \times 10^{-7}$  M solution with an activity of  $100 \text{ Bq ml}^{-1}$ ; acetate was  $\text{C}^2$  labelled). The experiments were then sealed with butyl rubber stoppers and aluminium crimps, but the large air headspace ensured aerobic conditions were maintained over 48 hours. Aqueous  $^{14}\text{C}$  activity and pH was measured after 48 hours as previously described. A second set of closed experiments were run using the same method to quantify the amount of  $^{14}\text{CO}_2(\text{g})$  in the headspace. A 10 mL gas sample was withdrawn from the headspace and bubbled through 2 mL of Carbo-Sorb E. This was then mixed with 10 mL of PermaFluor E & left to light adjust for at least 24 hours prior to counting.

#### **6.3.4 Amount of $^{14}\text{C}$ associated with total inorganic carbon (TIC) and total organic carbon (TOC) in sediment from the aerobic incubation experiments**

Two gas washing bottles (Drechsel bottle, 125 mL, QuickFit) were attached in series to the reaction vessel (250 mL round bottom flask with three inlets, QuickFit) via the gas outlet line (Figure 6-2); the first gas washing bottle contained 100 mL of Carbo-Sorb E, the second contained 100 mL of 1M NaOH. A sample of  $\sim 1$  g dry weight sediment (recovered at the end of the  $10^{-5}$  M experiments described above) was placed in the reaction vessel with a magnetic stirrer. Carrier gas ( $\text{N}_2$ ) flow rate was 40 mL/min. A two-step method of analysis was used to differentiate between the inorganic carbon fraction (carbonates, CO and  $\text{CO}_2$ ) and organic (hydrocarbons and organic acids). First a volume of 20 mL 2M  $\text{H}_2\text{SO}_4$  was

added to the reaction vessel which resulted in a pH  $\sim$  3. It was then purged for 30 minutes with  $N_2$  and mixed with a magnetic stirrer. Following acid treatment of the sediment the gas washing bottles were exchanged for duplicates. In the second step 20 mL of 5% potassium persulfate and 4 mL of 4%  $AgNO_3$  are added to the reaction vessel and heated to 80-90°. Further additions of  $K_2S_2O_8$  and  $AgNO_3$  at the same concentration and volume were made after one and two hours of reaction. The system was left to react for a further hour to give a total reaction time of 3 hours. Triplicate samples of 1 mL were collected from that gas washing bottles that contained Carbo-Sorb E (Ahn et al., 2013; Magnusson et al., 2007). Each 1 mL Carbo-Sorb E sample was mixed with 10 mL of PermaFluor E and were left to dark adjust for 24 hours prior to counting on the liquid scintillation counter.

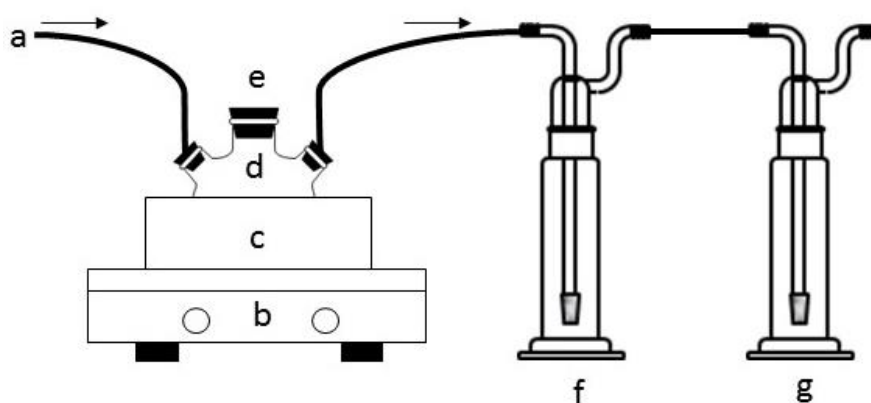


Figure 6-2 Apparatus for the wet acidification and oxidation of sediment: a)  $N_2(g)$  inlet line; b) stirrer hotplate; c) water bath; d) 250mL round bottom flask with three inlets; e) sample and reagent addition ; f) 125 mL gas washing tube with frit (porosity 0) containing 100 mL of Carbo-Sorb E for  $^{14}C$  capture and g) 125 mL gas washing tube with frit (porosity 0) containing 100 mL of 1M NaOH acting as a safety bottle to prevent the release of  $^{14}CO_2(g)$ . Arrows represent the direction of  $N_2(g)$  flow through the apparatus.

### **6.3.5 DNA extraction and sequencing of the V4 hyper-variable region of the 16S rRNA gene**

Bacterial DNA was extracted from eleven sediment samples. These consisted of one sample from each  $10^{-2}$  M LMWO system and one from each  $10^{-5}$  M LMWO system (see Section 2.3) and three samples of the unaltered sediment that was frozen on the day of collection. DNA was extracted from sediment samples (~0.5g of damp sediment) using the Fast DNA spin kit for soil (MP Biomedicals, USA). DNA fragments larger than 3 kb were isolated on a 1% agarose “1x” Tris-borate-EDTA (TBE) gel stained with ethidium bromide for viewing under UV light (10x TBE solution supplied by Invitrogen Ltd., UK). The DNA was extracted from the gel using a QIAquick gel extraction kit (QIAGEN Ltd, UK); final elution was by 1/10th strength elution buffer (unless explicitly stated, the manufacturer’s protocols supplied with all kits employed were followed precisely). DNA concentration was quantified fluorometrically using a Qubit dsDNA HS Assay (Thermo Fisher Scientific Inc., USA).

DNA samples (1ng/ $\mu$ L in 20  $\mu$ L aqueous solution) were sent for sequencing at the Centre for Genomic Research, University of Liverpool, where Illumina TruSeq adapters and indices were attached to DNA fragments in a two-step PCR amplification targeting the 16S rRNA gene (Caporaso et al., 2011). Pooled amplicons were paired-end sequenced on the Illumina MiSeq platform (2x250 bp) generating ~9M clusters of data. Illumina adapter sequences were removed, and the trimmed reads were processed using the UPARSE pipeline (Edgar, 2013) within the USEARCH software (version 9.2; Edgar, 2010) on a Linux platform. Overlapping paired end reads were merged prior to quality

filtering and relabelling. After dereplication, clustering, chimera filtering and singletons removal was performed simultaneously on the dataset. Operational taxonomic units (OTUs) were defined by minimum of 97% sequence identity between the putative OTU members. OTUs were allocated to a taxon using UTEX command and the RDP database (Wang et al., 2007). A confidence value of more than 0.7 was required for classification to balance sensitivity and error rate in the prediction (OTUs not classified to the level of phylum, or classified as archaea were excluded from subsequent analysis). The entire set (~7M reads) was then allocated to the OTUs and reported in the OTU table with the taxonomy and abundance of the OTUs.

Statistical analysis was performed to determine the bacterial diversity. In this paper the alpha diversity was defined using Hill numbers,  $D_q$ , (Hill, 1973; Jost, 2006). Hill numbers define the biodiversity as the reciprocal mean of proportional abundance and compensate for the disproportionate impact of rare taxa by weighting taxa based on abundance, the degree of weighting is controlled by the index  $q$  where increasing  $q$  places progressively more weight on the high-abundance species in a population (Hill, 1973; Jost, 2006, 2007; Kang et al., 2016).  $D_0$  is the unweighted Hill number and is equal to the species richness.  $D_1$  is a measure of the common species and is equivalent to the exponential of Shannon entropy.  $D_2$  is a measure of the number of dominant species and is equivalent to the inverse of Simpson concentration (Hill, 1973; Jost, 2006, 2007). Non-metric Multi-Dimensional Scaling (NMDS) was used to graphically represent the similarity between bacterial assemblages after exposure to different concentrations

of LMWO substances. This was done in an optimised two dimensional space using the Bray-Curtis dissimilarity matrix. NMDS was carried out in the package 'vegan' (Oksanen et al., 2013) in RStudio v 99.9.9 (RStudio Team, 2015). The microbial community data were input as a matrix of the relative abundance of each OTU in each of the samples.

## **6.4 Results**

### **6.4.1 Sediment characterisation**

Sediment from the sampling location has been extensively characterised (e.g. Law et al., 2010; Wallace et al, 2012). Law et al., 2010, describe the sediment as poorly sorted sandy loam with an approximate particle composition of 53% sand, 42% silt, 5% clay. Field observations in this study confirm that the sediment is predominantly fine sand and silt with most/all particles <2mm. XRD spectroscopy (see Figure 6-3) shows that the sediment is dominated by quartz, with some albite and microcline and minor amounts of chlorite and mica. The sediment pH was 5.5.

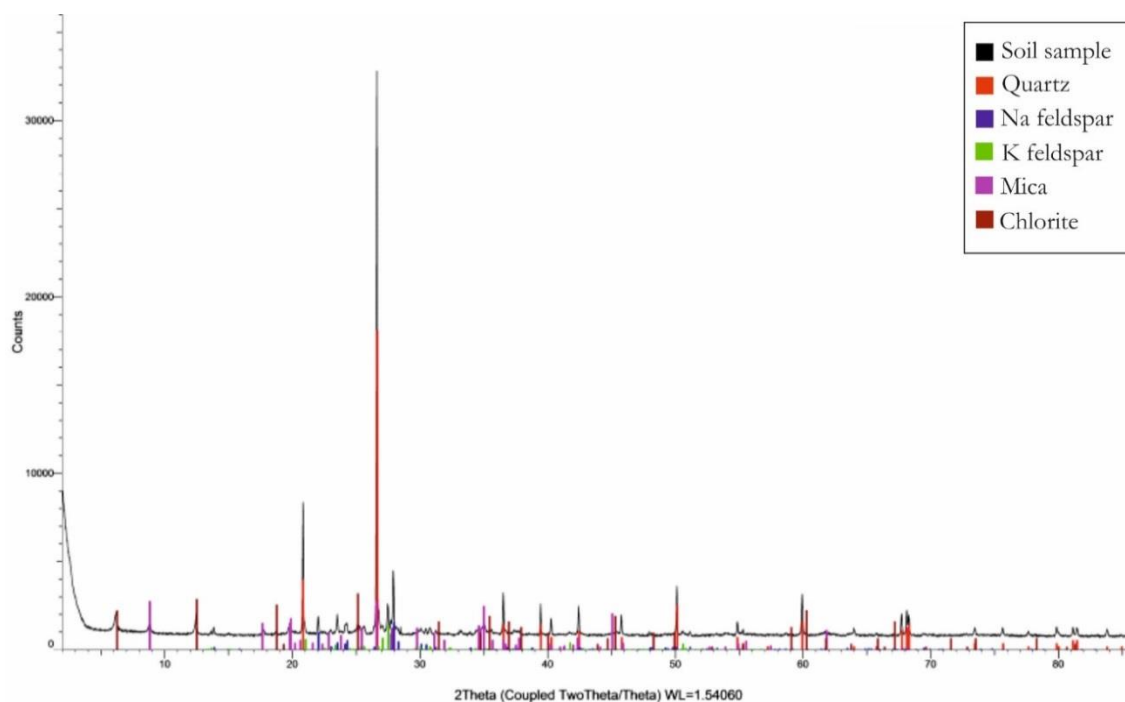


Figure 6-3 XRD plot of Calder Bridge sediment.

#### 6.4.2 The partitioning of $^{14}\text{C}$ -labelled organic compounds under aerobic conditions (open flasks)

The synthetic groundwater had a pH value of 8.7. Addition of sediment to the synthetic groundwater resulted in a solution pH of  $\sim 8.3$ . The pH values of the solution experiments and those containing sediment and low concentration ( $10^{-5}$  M) LMWO did not change significantly over the experimental timescale (which ranged from 238-340 hours, see Appendix B, Figure B1). However, the pH of most of the high concentration LMWO experiments changed with time; the exception was the methanol experiment which remained steady at pH  $\sim 8.3$ . In both the high concentration ( $10^{-2}$  M) acetate and formate experiments the pH increased from  $\sim$ pH 8.3 around to  $\sim$ pH 9.2 at the end of the experiment and the high concentration formaldehyde experiment the pH reduced from  $\sim 8.3$  to  $\sim 7.7$ .

There was rapid and almost complete ( $> 95\%$ ) removal of  $^{14}\text{C}$  in all the low concentration LMWO experiments (Fig 6-4b, d, f &h). No significant removal

( $\pm 10\%$ ) was found in the corresponding solution only experiments, except for the methanol systems where  $^{14}\text{C}$  removal was observed in both control experiments ( $10^{-5}$  and  $10^{-2}$  M). The sediment recovered at the end of the  $10^{-5}$  M experiments retained only small proportion of the  $^{14}\text{C}$  within either the TIC (3-12%) or TOC (2-5%) fractions (Table 6-2).

There also was  $^{14}\text{C}$  removal in all the high concentration LMWO experiments, although there was a lag period at the start of the tests with the carboxylates and formaldehyde before removal started, and the removal was contemporaneous with a change in the solution pH (pH increased with carboxylate removal but decreased with aldehyde removal). In the experiments with the carboxylates and formaldehyde  $^{14}\text{C}$  removal was incomplete after 10 days (particularly formaldehyde where there was only 25% removal was observed). The high concentration methanol experiment lacked an identifiable lag phase, and  $\sim 95\%$  removal was observed after 10 days. Also, the initial rate of  $^{14}\text{C}$  removal was similar to that observed in the equivalent control, suggesting that methanol volatility may have contributed to removal (see discussion).

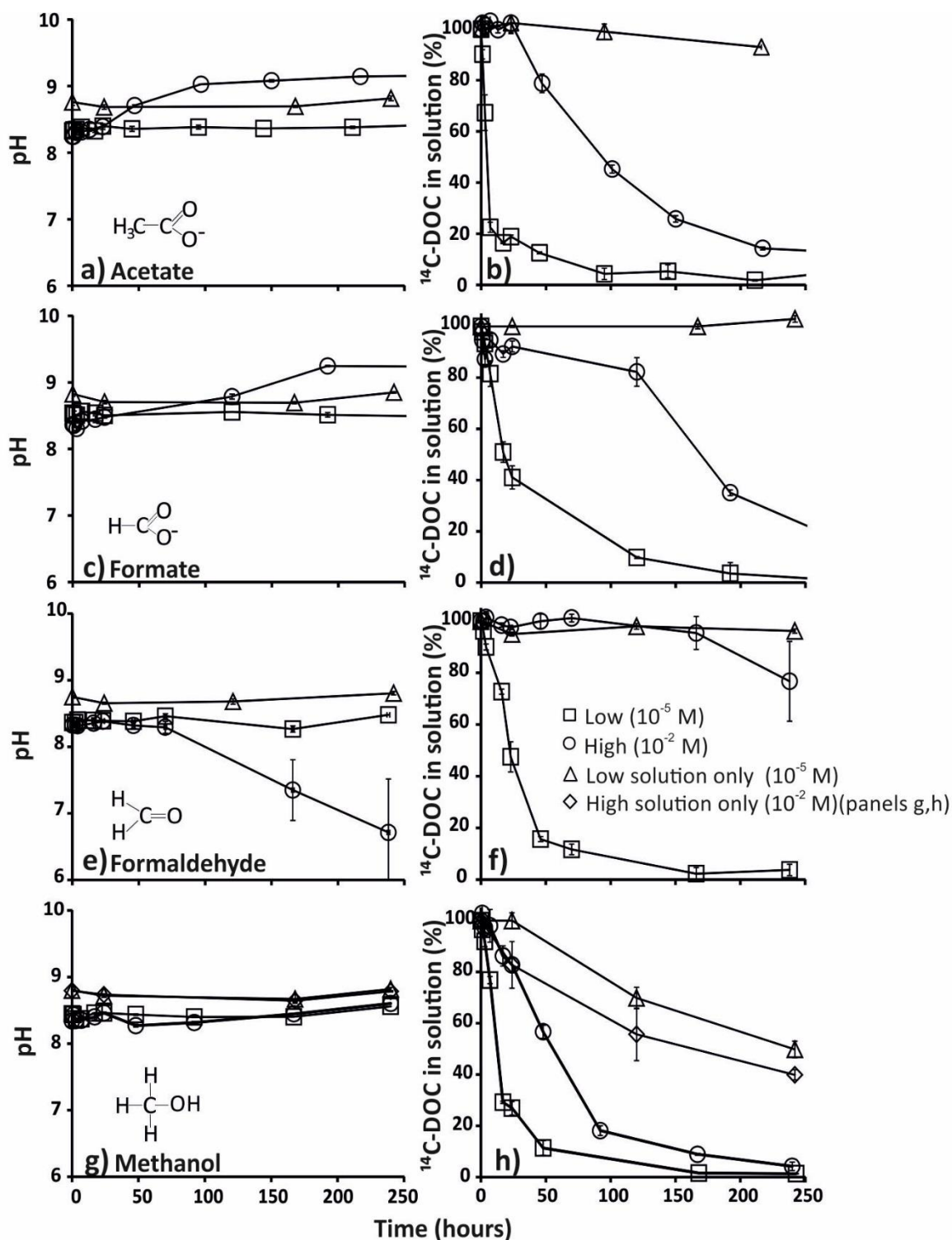


Figure 6-4 Experimental results for first 250 hours of open flask experiments showing the evolution of pH and  $^{14}\text{C}$ -DOC activity with time in (a, b)  $^{14}\text{C}$ -acetate amended experiments; (c, d)  $^{14}\text{C}$ -formate amended experiments; (e, f)  $^{14}\text{C}$ -formaldehyde amended experiments and, (g, h)  $^{14}\text{C}$ -methanol amended experiments. Error bars denote one standard deviation of triplicate measurements; where not shown, error bars are less than the size of the symbols used.

Table 6-2 Percentage recovered of organic and inorganic bound  $^{14}\text{C}$  in sediment and  $^{14}\text{C}$ -DOC at the end of the low concentration ( $10^{-5}$  M) experiments.

	Acetate	Formate	Methanol	Formaldehyde
	316 hours	340 hours	240 hours	238 hours
$^{14}\text{C}$ -TIC	12.3 $\pm$ 5.9%	3.0 $\pm$ 3.5%	6.1 $\pm$ 2.8%	4.0 $\pm$ 1.7%
$^{14}\text{C}$ -TOC	4.9 $\pm$ 1.8%	4.6 $\pm$ 3.3%	1.9 $\pm$ 1.9%	1.7 $\pm$ 1.8%
$^{14}\text{C}$ -DOC	6.8 $\pm$ 0 %	6.0 $\pm$ 3.9%	1.3 $\pm$ 0.1%	3.7 $\pm$ 2.2%
Balance (by difference)	76 $\pm$ 7.7%	86.4 $\pm$ 10.7%	90.7 $\pm$ 4.8%	90.6 $\pm$ 5.7%

\*Balance (by difference) refers to  $^{14}\text{C}$ -DIC and  $^{14}\text{CO}_2(\text{g})$  fractions which are not measured

#### 6.4.3 Short term $^{14}\text{C}$ -DOC partitioning in aqueous fraction (closed bottles)

These short term experiments had a large head space, and were run for only 48 hours to ensure that oxygen in the headspace was not exhausted, to be comparable with the first 48 hours of the corresponding open flask tests described above. Comparison of  $^{14}\text{C}$ -DOC in the closed bottles with that in the open flask tests (Figure 6-5) indicates that parallel experiments behaved similarly. Analysis of gas sampled from the head space of the closed bottles indicates that a measurable fraction (8 – 18 %) of the  $^{14}\text{C}$ -DOC added to the experiments had been converted into  $^{14}\text{CO}_2$  (g) (Table 6-3).

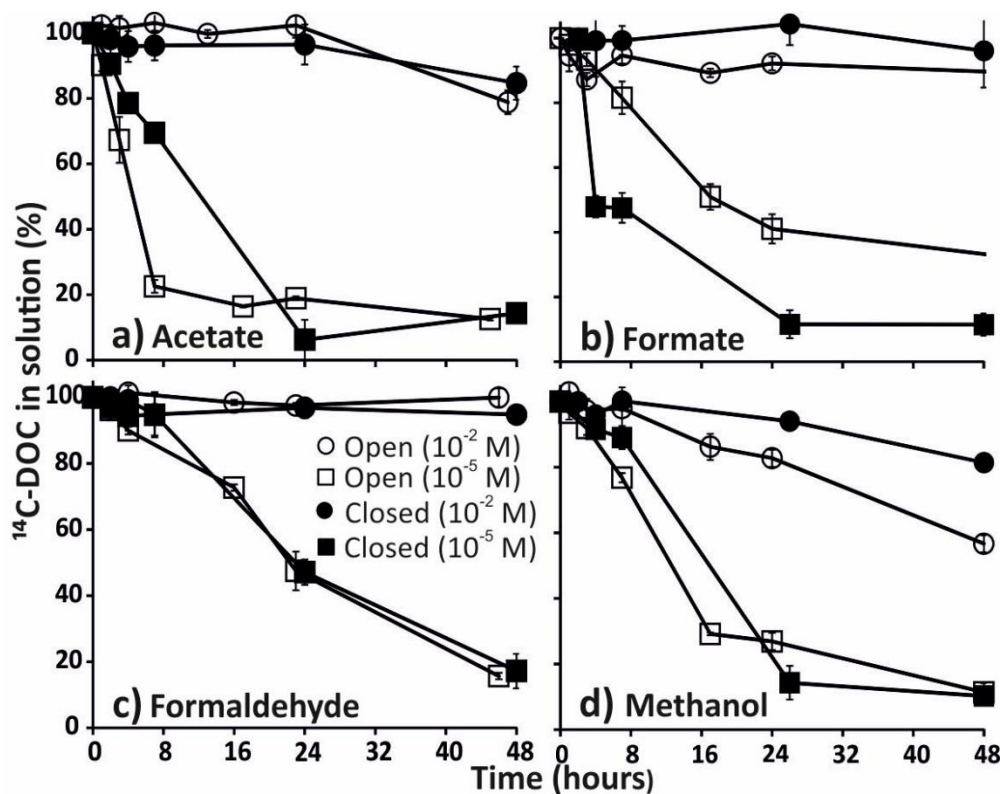


Figure 6-5 Data from both open flask (replotted from Figure 6-4) and corresponding closed bottle experiments for: (a) <sup>14</sup>C-acetate amended experiments; (b) <sup>14</sup>C-formate amended experiments; (c) <sup>14</sup>C-formaldehyde amended experiments; and, (d) <sup>14</sup>C-methanol amended experiments. Error bars denote one standard deviation of triplicate measurements; where not shown, error bars are less than the size of the symbols used.

Table 6-3 Concentration of organic <sup>14</sup>C in aqueous pool and gaseous pool (as CO<sub>2</sub>(g)) at 48 hour sampling point in low concentration experiments.

	Acetate	Formate	Methanol	Formaldehyde
	48 hours	48 hours	48 hours	48 hours
<sup>14</sup> C-DOC	28 ± 3%	52 ± 5%	44 ± 3%	48 ± 1%
<sup>14</sup> CO <sub>2</sub> (g)	8 ± 3%	17 ± 11%	16 ± 4%	18 ± 2%
Balance (by difference)*	64%	31%	40%	34%

\*Balance (by difference) refers to the <sup>14</sup>C-dissolved inorganic carbon (DIC), <sup>14</sup>C-total organic carbon (TOC) and <sup>14</sup>C-total inorganic carbon (TIC) fractions which are not measured.

#### 6.4.4 Microbial community analysis

Sufficient DNA was recovered for high-throughput amplicon sequencing from ten of the eleven samples chosen for analysis (the high concentration formaldehyde system yielded insufficient DNA). For these ten samples the Illumina MiSeq run yielded >100,000 paired-end reads for each sample after quality control. The ten samples in this study were part of a combined pool of 8,763,879 million reads from the sequencing run that passed the chimera check and were used to identify the characteristic OTUs. The combined pool were clustered into OTUs (>97% sequence identity) in the UPARSE pipeline, and assigned to taxonomic groups. OTUs classified as archaea (4% of non-chimeric reads) and bacteria which were not classified at phylum level with a confidence of >0.7 (23% of non-chimeric reads) were excluded from further analysis. This resulted in 7792 OTUs classified to bacteria phylum with a confidence greater than 0.7 which were used to characterise the bacterial populations in the samples from this study.

OTUs classified at the level of a phylum with a confidence >0.7 were grouped to identify phyla that represented <1% of the total number of pair-end reads from of this study. There were 11 phyla that represented more than 1% of the total population (Figure 6-6). At least 10 of these 11 phyla represented > 1% of the population each of the unaltered sediment samples.  $10 \pm 1$  of these phyla represented > 1% of the population of each of the low concentration LMWO samples, whereas only  $7 \pm 1$  of these phyla represented > 1% of the population of each of the high concentration LMWO samples. The most abundant phyla in the

unaltered sediment were Acidobacteria ( $28 \pm 2\%$  of the reads), Proteobacteria ( $28 \pm 1.4\%$ ) and Planctomycetes ( $10 \pm 1\%$ ). The low concentration system showed a similar distribution (Acidobacteria,  $34 \pm 6\%$ ; Proteobacteria,  $31 \pm 5\%$ ; Planctomycetes,  $8 \pm 2\%$ ), however the distribution of OTUs between phyla varied with amendment in the high concentration experiments. In the high acetate system the most abundant phyla are Proteobacteria (64%) and Verrucomicrobia (14%) with Acidobacteria only making up 7%. In the Proteobacteria the most abundant class is Betaproteobacteria (32%) followed by Alphaproteobacteria (17%). The high formate system is dominated by Proteobacteria (45%) and Acidobacteria (23%). Within the Proteobacteria phylum the most abundant class is Betaproteobacteria with 26% of the relative abundance assigned to this class. This is followed by Alphaproteobacteria with 14% abundance. In the high methanol system the most abundant phylum is Proteobacteria (71%), followed by Acidobacteria (13%). Within Proteobacteria over 63% of the abundance is associated with the Betaproteobacteria.

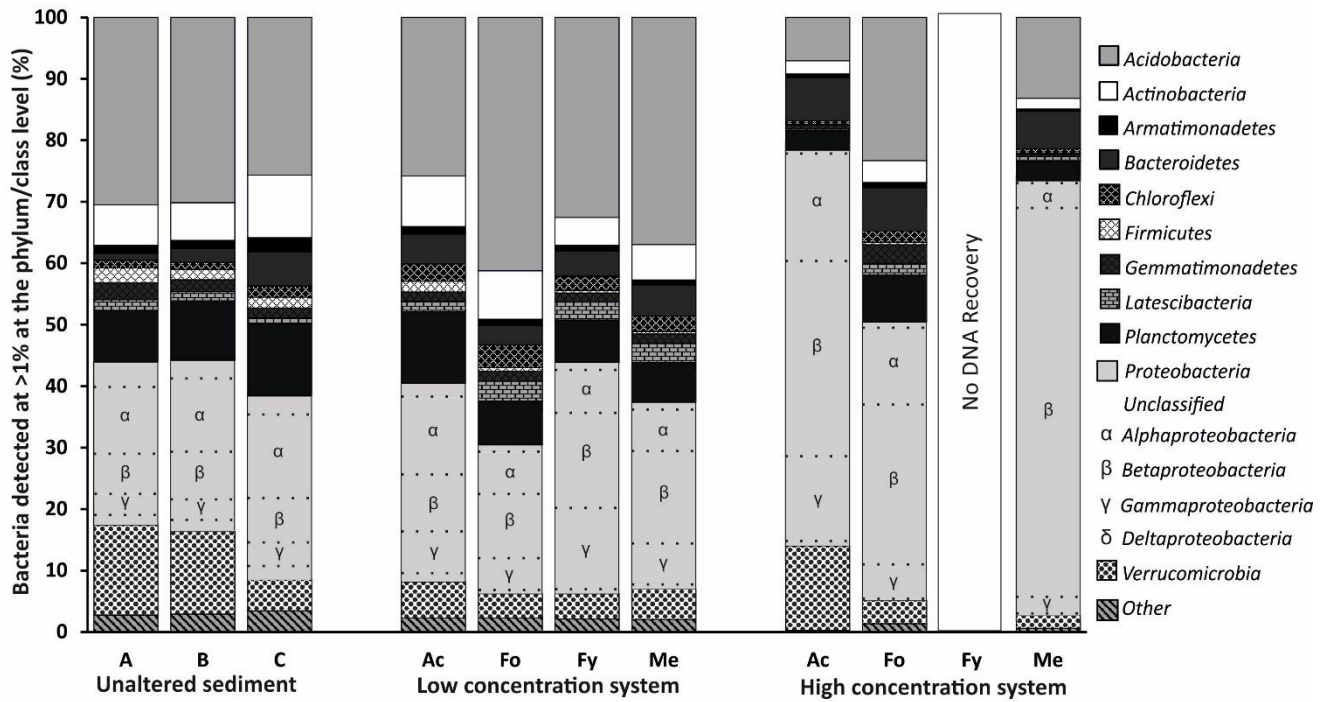


Figure 6-6 Bacterial phylogenetic diversity within unaltered sediment (A-C); high concentration systems and low concentration systems (Ac- acetate; Fo- formate; Fy- formaldehyde; Me- methanol). Phyla with relative abundance less than 1% of the total population are grouped as “Other”. Dashed line denotes classes of Proteobacteria descending as follows: unclassified; α; β; γ; δ.

The OTU richness ( $D_0^\alpha$ ) for each sample is shown in Table 6-4. The average richness for the unaltered sediment is  $6300 \pm 350$  OTUs. The values for richness for the low concentration systems all lie within one standard deviation of the unaltered sediment value. The high concentration systems show slightly lower richness. The species richness takes no account of the relative abundance of the OTUs.  $D_1^\alpha$  for the unaltered sediment is  $895 \pm 219$  OTUs. The  $D_1^\alpha$  values for the low concentration systems are all within one standard deviation of this value. However there are fewer common species in the high concentration systems ( $D_1^\alpha$  varied between 87 OTUs for methanol and 597 OTUs for formate).  $D_2^\alpha$  for the unaltered sediment is  $194 \pm 91$  OTUs, the  $D_2^\alpha$  values for the low concentration systems are all within one standard

deviation of this value. There are fewer dominant species in the high concentration systems where  $D_2^\alpha$  ranged from 7 OTUs for methanol to 107 for formate OTUs. Common OTUs accounted for more than 74% of total sequence reads in all samples, with dominant OTUs accounting for >50% of total reads. The decrease in number of common and dominant OTUs in the high concentration system represent fewer, but more abundant OTUs compared with the low and unaltered samples.

Table 6-4 Alpha-diversity measures,  $D_0^\alpha$ , species richness,  $D_1^\alpha$ , exponential of Shannon entropy and concentration,  $D_2^\alpha$ , inverse of the Simpson concentration. Values displayed to 3 significant figures. Ac – acetate; Fo – formate; Fy – formaldehyde and Me – methanol.

Unaltered sediment				Low concentration system				High concentration system			
A	B	C	Average	Ac	Fo	Fy	Me	Ac	Fo	Fy	Me
$D_0^\alpha$											
6110	6790	5990	±350	6640	6010	6050	6130	4610	3770	n.a.*	5660
$D_1^\alpha$											
616	918	1150	895 ±219	939	891	903	1040	246	597	n.a.*	87
$D_2^\alpha$											
108	153	320	194 ±91	236	196	179	257	63	107	n.a.*	7

\*n.a. = not available

In the two-dimensional NMDS representation of the OTU frequencies in the ten samples (see Figure 6-7) the unaltered sediment shows variation, although two samples have clustered together (UnA, B) sample C shows some dissimilarity. The low concentration samples generally cluster very closely together and tend to lie midway between the unaltered and high concentration systems. The high concentrations are not clustered, the high formaldehyde system is relatively close to the low concentration samples, whereas acetate and methanol are further away from the unaltered, low concentration and each other. NMDS is an indirect gradient analysis which in this case optimises ordination based on a dissimilarity

matrix, the analysis suggests that even at low concentrations there are changes to the bacterial population which are only reflected when examining individual species frequencies.

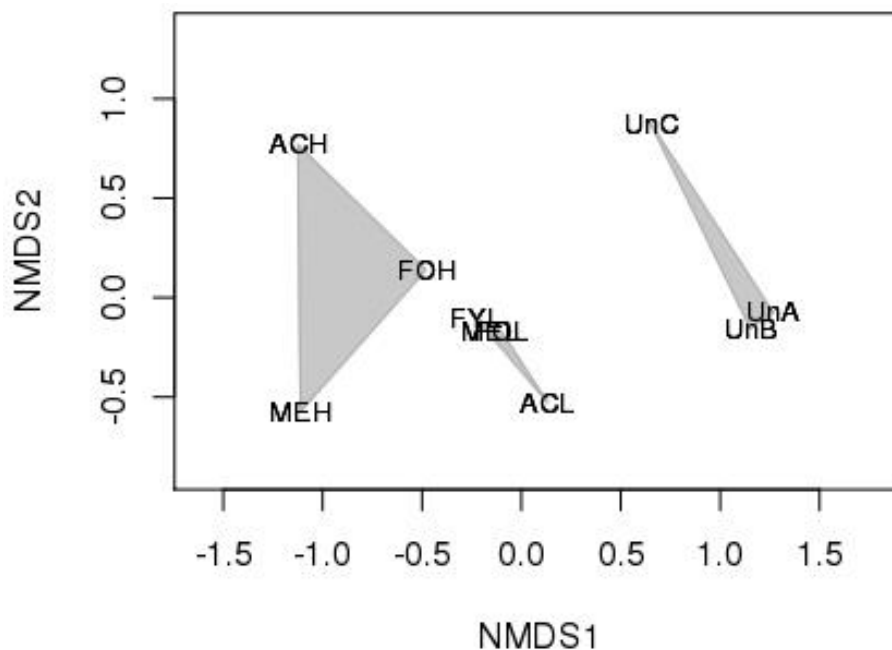


Figure 6-7 Two-dimensional non-metric multidimensional scaling (NMDS) ordination for differences in the bacterial community composition distribution based on Bray-Curtis distances of the community (OTUs) by site/sample matrix. Un A, B, C – unaltered sediment samples. Ac – acetate; Fo – formate; Fy – formaldehyde and Me – methanol. H corresponds to high concentration ( $10^{-2}$  M), L to low concentration ( $10^{-5}$  M). The stress value associated with this two dimensional representation is  $<0.05$  which suggests reasonable fit with the data.

## 6.5 Discussion

### 6.5.1 The behaviour of $^{14}\text{C}$ -labelled LMWO substances in solution

More than 90% of the added  $^{14}\text{C}$  LMWO tracer was removed from solution after 5 days in all experiments amended with  $10^{-5}$  M organics. This  $10^{-5}$  M concentration is indicative of anticipated concentrations in solutions that are in contact with fuel cladding wastes (Wieland and Hummel, 2015), therefore, it is

clear that if released into aerobic sedimentary environments, aqueous  $^{14}\text{C}$ -labelled LMWO substances (such as acetate, formate, methanol and formaldehyde) are unlikely to persist in groundwater for more than a few days. Removal did not occur without contact with sediments (with the exception of methanol, see discussion below), and so it is inferred that sediment interaction was responsible for the removal. At the pH of these experiments (pH  $\sim$  8.5), the four LMWO substances tested in this study are predicted to only very weakly sorb to sediments as the anion exchange capacity would be very limited (Gu and Schulz, 1991; Sposito, 1989), hence the removal is attributed to microbial respiration. This is supported by the pH data from the high concentration ( $10^{-2}$  M) tests, where trends were either upwards in the case of acetate and formate coinciding with the production of  $\text{HCO}_3^-$  (Equations 6-3, 6-4), or, downwards in the case of formaldehyde with the production of  $\text{CO}_2$  (Equation 6-5).

The high concentration acetate and formate tests had a distinct lag phase lasting between 1- 4 days with no significant  $^{14}\text{C}$  removal occurring, it is likely that the indigenous microbial population utilised these electron donors at the same rate as the low concentration tests, but due to the higher overall concentration of LMWO substances the utilisation of  $^{14}\text{C}$  was not seen in the first 4 days. The concentration of  $^{14}\text{C}$ -formaldehyde remained high after 250 hours ( $\sim$ 76%) with increasing standard deviation between replicates suggesting that there may be a sterilisation effect at this concentration which is leading to toxicity and impeding the ability of the microbial population to utilise  $^{14}\text{C}$ -formaldehyde, this is supported by the lack of extractable DNA recovered from the sediment sample.

In contrast to the other systems studied, up to 50% of  $^{14}\text{C}$ -methanol was lost after 10 days in the solution only experiments performed at both high and low concentrations ( $10^{-2}$  and  $10^{-5}$  M). This suggests that some  $^{14}\text{C}$ -methanol was volatilised directly from solution even in the lower concentration experiment. Therefore, if discharged to open surface waters,  $^{14}\text{C}$ -methanol and possibly other  $^{14}\text{C}$ -labelled alcohols (e.g. ethanol, propanol) are likely to be depleted by volatilisation with the potential to form gaseous  $^{14}\text{C}$  (Hoch, 2014), but any  $^{14}\text{C}$ -methanol would be highly diluted in atmosphere, and is likely to be oxidised in a number of days to  $^{14}\text{CO}_2(\text{g})$  (Grosjean, 1997). In sub-surface environments with poor connectivity to atmosphere volatilisation is limited, the generation of  $^{14}\text{CO}_2(\text{g})$  after 48 hours in the  $10^{-5}$  M  $^{14}\text{C}$ -methanol closed experiments ( $16 \pm 4\%$  of total  $^{14}\text{C}$  activity) suggests that microbial respiration also plays a role in  $^{14}\text{C}$ -methanol removal in these experiments. Thus, microbial respiration is also likely to provide a  $^{14}\text{C}$ -methanol removal mechanism (i.e. in most sub-surface aquifer environments; Boylan et al., 2016).

### **6.5.2 Partitioning of aqueous $^{14}\text{C}$ -labelled LMWO substances in to solid fraction**

The amount of  $^{14}\text{C}$  associated with inorganic and organic solid fractions was low (1-12%) in all experiments with the measurements of formate TIC, methanol TOC and formaldehyde TOC results all lying within one standard deviation of 0% recovery. For acetate and formate the TOC results show that there is a modest amount of  $^{14}\text{C}$  association with the organic solid fraction (<5% of activity added) and therefore there may be potential for retardation of acetate and formate in a subsurface. Previous work by Fischer and Kuzyakov (2010)

suggests that the carboxyl group is less likely to be assimilated than other functional groups therefore formate assimilation into microbial biomass is unlikely. Sorption between organic acids and sediment has been previously recorded over a range of pH (Jones and Brassington, 1998) suggesting the formate in the organic solid fraction may be due to sorption of the formate anion on sediment surfaces which is removing it from the aqueous pool.

Acetate shows the highest amount of  $^{14}\text{C}$  associated with TIC ( $12 \pm 6\%$  of total  $^{14}\text{C}$  activity). Once utilised by microbes the transformation to  $\text{CO}_2(\text{g})$  in subsurface environments adds to the DIC pool. This increase in carbonate concentration in solution allows adsorption and precipitation reactions to occur which lead to the accumulation of  $^{14}\text{C}$  in the solid inorganic phase, particularly in association with divalent cations as carbonate minerals. This occurrence may be particularly likely at higher pH ( $>8$ ) as can be found in alkali leachate plumes which exist underneath nuclear reprocessing facilities (Marshall et al., 2015; Parry et al., 2011).

### **6.5.3 Transformation of aqueous $^{14}\text{C}$ -labelled LMWO substances to $^{14}\text{CO}_2(\text{g})$ by microbial utilisation**

The electron donors considered in this study, especially formate and acetate, are readily utilised by microbes. Three of these electron donors contain single carbon atoms that are not readily assimilated by microbes, so most will be oxidised to  $\text{CO}_2$  which will either be retained as aqueous  $\text{HCO}_3^-$ , precipitated as solid carbonates, or released as  $\text{CO}_2(\text{g})$ . The amount of  $^{14}\text{CO}_2(\text{g})$  produced in the closed, low concentration systems was measured after 48 hours with all experiments producing low, but measurable quantities, this is consistent with

organic matter oxidation during microbially mediated aerobic respiration. With increasing time, increasing  $^{14}\text{CO}_2(\text{g})$  production would be expected as more  $^{14}\text{C}$ -organics are utilised (Ishii et al., 2015). In surface environments this  $^{14}\text{CO}_2(\text{g})$  would be quickly dispersed and diluted in the much larger stable isotope  $\text{CO}_2(\text{g})$  pool in the atmosphere. In subsurface environments there is limited connectivity to atmosphere and often a high partial pressure of  $\text{CO}_2(\text{g})$  which would mean that the  $^{14}\text{CO}_2$  produced would join the dissolved inorganic carbon (DIC) pool and speciate according to the pH of the groundwater. In this instance its behaviour would be governed by pH and the availability of divalent cations as discussed in previous studies (Langmuir, 1997, Inskeep et al. 1985; Van Geen et al 1994; Hodkin et al., 2016; Boylan et al., 2016).

Combining the  $^{14}\text{C}$  activities recovered for the aqueous and gaseous phase does not account for the total  $^{14}\text{C}$  activity added to the original samples, this is likely to be due to two factors. Firstly and most importantly there is no measurement of the DIC pool which may account for some  $^{14}\text{C}$  in the closed system bottles where  $\text{CO}_2$  will equilibrate across the aqueous and gaseous phases.  $^{14}\text{C}$ -DIC could potentially be measured by acidifying a known quantity of solution and capturing the  $^{14}\text{CO}_2(\text{g})$  released. The measurement of  $\text{CO}_2(\text{g})$  is consistent across three organics, formate; formaldehyde; and methanol, but slightly lower for the acetate system, this is expected due to the higher association with the TIC fraction and may also suggest that there has been assimilation of  $^{14}\text{C}$  in to microbial biomass.

#### **6.5.4 Impact of organic contaminants on natural microbial populations**

The microbial community characterised from the unaltered and low concentration system show a diverse range of bacterial phyla similar to previous studies which sampled Sellafield sediment directly (Newsome et al., 2014). The NMDS (Figure 6-7) does imply differences in OTU frequency between the unaltered, low and high concentration systems. This suggests there may be some impact even at low concentration of the addition of LMWO substances on the microbial community. The NMDS also suggests that the unaltered indigenous microbial community is heterogeneous evidenced by the distance between samples. The composition of the microbial community is altered under the high concentration conditions, where diversity is reduced, with an average reduction of 66% in common OTUs compared to the unaltered sediment community. There is an increase in the relative abundance of the Betaproteobacteria class for all electron donors at high concentration, with the most abundant order for acetate and formate being Burkholderiales. With methanol as the electron donor the most abundant order is Methylophilales (>55% of total reads) which are ubiquitous in natural environments (Vorobev et al., 2013). Methylophilales are capable of utilising C1 compounds (i.e. those containing no carbon-carbon bonds) (Anthony, 1982; Baev et al., 1992), and are known for their role in the utilisation of both formaldehyde and methanol. If the indigenous community is representative of that which underlies the Sellafield reprocessing site, UK, this suggests that this microbial community is able to utilise a range of <sup>14</sup>C-LMWO substances, removing them from solution rapidly in low concentration systems. Under high concentration conditions the population has shifted, allowing bacterial orders such

as Methylophilales to dominate the community structure, for acetate, formate and methanol this shift in population structure still results in rapid removal from solution of the  $^{14}\text{C}$ -LMWOs. Formaldehyde is utilised rapidly at low concentration, presumably by members of the indigenous microbial community; but at high concentration it was not possible to extract any DNA for analysis, suggesting that this concentration sterilises the sediment and so there is limited, if any microbial activity under this condition (Manchee et al., 1983; Trevors, 1996; Weir et al., 1996).

## 6.6 Conclusions

This study shows there is minimal persistence of  $^{14}\text{C}$ -labelled LMWO substances in solution in the presence of sediment with an active microbial population under aerobic conditions. For  $^{14}\text{C}$ -methanol, volatilisation may also contribute to its removal from solution in surface waters, but would be limited in subsurface environments due to poor connectivity to atmosphere. Production of  $^{14}\text{CO}_2(\text{g})$  is assumed to be due to the utilisation of the LMWO molecules by the microbial populations found in sediment. At low concentration there is very little  $^{14}\text{C}$  retention in the solid fraction, the only exception to this is acetate which is measured at higher percentages compared to the other LMWO substances in this study in both organic and inorganic fractions (5 & 12% respectively, Table 6.1) suggesting that limited amounts of longer chain organic molecules may be retained in solid fraction. The indigenous microbial community detected in the sediment samples in this study represent a diverse mix of bacterial phyla which are ubiquitous in terrestrial environments and are therefore likely to be similar to

those found in the subsurface below Sellafield reprocessing site. In high concentration systems there is evidence for increasing dominance of Betaproteobacteria, with the order Burkholderiales being most abundant with acetate and formate electron donors and Methylophilales being the most abundant when methanol was the electron donor. Any  $^{14}\text{C}$ -LMWO substances, particularly C1 compounds, are therefore unlikely to persist or bioaccumulate in their organic forms when in contact with microbial populations (i.e. subsurface environments) where they are rapidly utilised and transformed to  $\text{CO}_2(\text{g})$ .

## 6.7 References

Ahn, H.J., Song, B.C., Sohn, S.C., Lee, M.H., Song, K., Jee, K.Y., 2013. Application of a wet oxidation method for the quantification of  $^3\text{H}$  and  $^{14}\text{C}$  in low-level radwastes. *Applied Radiation and Isotopes* 81, 62-66.

Anthony, C., 1982. *The biochemistry of methylotrophs*. Academic Press.

ASTM, 2006. D4972-01: standard test method for pH of soils. In: *Annual Book of ASTM Standards*. American Society for Testing and Materials, pp. 963–965.

Baev, M., Schklyar, N., Chistoserdova, L., Chistoserdov, A., Polanuer, B., Tsygankov, Y., Sterkin, V., 1992. Growth of the obligate methylotroph *Methylobacillus flagellatum* under stationary and nonstationary conditions during continuous cultivation. *Biotechnology and bioengineering* 39, 688-695.

Bird, G.A., Bergström, U., Nordlinder, S., Neal, S.L., Smith, G.M., 1999. Model simulations of the fate of  $^{14}\text{C}$  added to a Canadian shield lake. *Journal of Environmental Radioactivity* 42, 209-223.

- Boylan, A.A., Stewart, D.I., Graham, J.T., Trivedi, D., Burke, I.T., 2016. Mechanisms of inorganic carbon-14 attenuation in contaminated groundwater: Effect of solution pH on isotopic exchange and carbonate precipitation reactions. *Applied Geochemistry*. <https://doi.org/10.1016/j.apgeochem.2016.12.006>.
- Caporaso, J.G., Lauber, C.L., Walters, W.A., Berg-Lyons, D., Lozupone, C.A., Turnbaugh, P.J., Fierer, N., Knight, R., 2011. Global patterns of 16S rRNA diversity at a depth of millions of sequences per sample. *Proceedings of the National Academy of Sciences*, **108**(Supplement 1), pp.4516-4522.
- Clever H. L. and Young C. L., Eds., IUPAC Solubility Data Series, Vol. 27/28, Methane, Pergamon Press, Oxford, England, 1987.
- Eabry, S., Vance, J.N., Cline, J.E., Robertson, D.E., 1995. Characterization of Carbon-14 Generated by the Nuclear Power Industry: Final Report. Electric Power Research Institute.
- Edgar, R.C., 2010. Search and clustering orders of magnitude faster than BLAST. *Bioinformatics* 26, 2460-2461.
- Edgar, R.C., 2013. UPARSE: highly accurate OTU sequences from microbial amplicon reads. *Nature methods* 10, 996-998.
- Evenden, W.G., Sheppard, S.C., Killey, R.W.D., 1998. Carbon-14 and tritium in plants of a wetland containing contaminated groundwater. *Applied Geochemistry* 13, 17-21.

Fischer, H., Kuzyakov, Y., 2010. Sorption, microbial uptake and decomposition of acetate in soil: Transformations revealed by position-specific  $^{14}\text{C}$  labeling. *Soil Biology and Biochemistry* 42, 186-192.

Grosjean, D., 1997. Atmospheric chemistry of alcohols. *Journal of the Brazilian Chemical Society* 8, 433-442.

Gu, B., Schulz, R.K., 1991. Anion retention in soil: possible application to reduce migration of buried technetium and iodine. Nuclear Regulatory Commission, Washington, DC (United States). Div. of Regulatory Applications; California Univ., Berkeley, CA (United States). Dept. of Soil Science.

Hill, M.O., 1973. Diversity and evenness: a unifying notation and its consequences. *Ecology* 54, 427-432.

Hoch, A.R., 2014. Uptake of Gaseous Carbon-14 in the Biosphere: Development of an assessment model.

Hodkin, D.J., Stewart, D.I., Graham, J.T., Burke, I.T., 2016. Coprecipitation of  $^{14}\text{C}$  and Sr with carbonate precipitates: The importance of reaction kinetics and recrystallization pathways. *Science of The Total Environment* 562, 335-343.

Inskeep, W.P., Bloom, P.R., 1985. An evaluation of rate equations for calcite precipitation kinetics at  $\text{pCO}_2$  less than 0.01 atm and pH greater than 8. *Geochimica et Cosmochimica Acta* 49, 2165-2180.

Ishii, N., Tagami, K., Uchida, S., 2015. The  $^{14}\text{C}$  partitioning of [1, 2- $^{14}\text{C}$ ] sodium acetate in three phases (solid, liquid, and gas) in Japanese agricultural soils. *Journal of Radioanalytical and Nuclear Chemistry* 303, 1389-1392.

Jackson, C.P., Yates, H., 2011. Key processes and data for the migration of <sup>14</sup>C released from a cementitious repository, Serco Report.

Jefferies, N.L., 1990. The evolution of carbon-14 and tritium containing gases in a radioactive waste repository. UK Nirex Ltd Report NSS/R198.

Jones, D.L., Brassington, D.S., 1998. Sorption of organic acids in acid soils and its implications in the rhizosphere. *European Journal of Soil Science* 49, 447-455.

Jost, L., 2006. Entropy and diversity. *Oikos* 113, 363-375.

Kaneko, S., Tanabe, H., Sasoh, M., Takahashi, R., Shibano, T., Tateyama, S., 2003. A study on the chemical forms and migration behavior of carbon-14 leached from the simulated hull waste in the underground condition, *Materials Research Society Symposium Proceedings*. Warrendale, Pa.; Materials Research Society; 1999, pp. 621-628.

Killey, R.W.D., Rao, R.R., Eyvindson, S., 1998. Radiocarbon speciation and distribution in an aquifer plume and groundwater discharge area, Chalk River, Ontario. *Applied Geochemistry* 13, 3-16.

Langmuir, D., 1997. Use of laboratory adsorption data and models to predict radionuclide releases from a geological repository: A brief history, *Materials Research Society Symposium - Proceedings*, pp. [d]769-780.

Law, G.T.W., Geissler, A., Boothman, C., Burke, I.T., Livens, F.R., Lloyd, J.R., Morris, K., 2010. Role of nitrate in conditioning aquifer sediments for technetium bioreduction. *Environmental Science and Technology* 44, 150-155.

Limer, L., Klos, R., Walke, R., Shaw, G., Nordén, M., Xu, S., 2013. Soil-plant-atmosphere modeling in the context of releases of <sup>14</sup>C as a consequence of nuclear activities. *Radiocarbon* 55, 804-813.

Limer, L.M.C., Thorne, M.C., Cummings, R., 2011. Consideration of canopy structure in modelling <sup>14</sup>C-labelled gas behaviour in the biosphere for human dose assessments. *Radioprotection* 46, S409-S415.

Lovley, D.R., Phillips, E.J.P., 1988. Novel mode of microbial energy metabolism: organic carbon oxidation coupled to dissimilatory reduction of iron or manganese. *Applied & Environmental Microbiology* 54, 1472-1480.

Magnusson, Å., 2007. <sup>14</sup>C Produced by Nuclear Power Reactors-Generation and Characterization of Gaseous, Liquid and Solid Waste. Division of Nuclear Physics Department of Physics Lund University Box 118 SE-221 00 Lund Sweden.

Manchee, R.J., Broster, M., Anderson, I.S., Henstridge, R., Melling, J., 1983. Decontamination of *Bacillus anthracis* on Gruinard Island? *Nature* 303, 239-240.

Marshall, A., Coughlin, D., Laws, F., 2015. Groundwater monitoring at Sellafield: Annual data review 2014.

Marshall, T.A., Baston, G.M.N., Otlett, R.L., Walker, A.J., Mather, I.D., 2011. Longer-term release of carbon-14 from irradiated graphite.

McCollom, T.M., Seewald, J.S., 2007. Abiotic synthesis of organic compounds in deep-sea hydrothermal environments. *Chemical Reviews* 107, 382-401.

Morozov, M., Pierce, S.G., Dobie, G., Bolton, G.T., Bennett, T., 2016. Robotic ultrasonic testing of AGR fuel cladding. *Case Studies in Nondestructive Testing and Evaluation* 6, Part A, 26-31.

NDA, 2014. *Monitoring our Environment: Discharges and Environmental Monitoring*. Nuclear Decommissioning Authority

Newsome, L., Morris, K., Trivedi, D., Atherton, N., Lloyd, J.R., 2014. Microbial reduction of uranium(VI) in sediments of different lithologies collected from Sellafield. *Applied Geochemistry* 51, 55-64.

Oksanen, J., Blanchet, F.G., Kindt, R., Legendre, P., Minchin, P.R., O'Hara, R.B., Simpson, G.L., Solymos, P., Stevens, M.H.H., and Wagner, H. (2013). *vegan: Community Ecology Package*. R package version 2.0-10 [Online]. Available: <http://CRAN.R-project.org/package=vegan> [Accessed 22<sup>nd</sup> May 2017].

Parry, S.A., O'Brien, L., Fellerman, A.S., Eaves, C.J., Milestone, N.B., Bryan, N.D., Livens, F.R., 2011. Plutonium behaviour in nuclear fuel storage pond effluents. *Energy & Environmental Science* 4, 1457-1464.

RStudio Team (2015). "RStudio: Integrated Development Environment for R". .0.99.486 ed. (Boston, MA: RStudio, Inc). Retrieved from <http://www.rstudio.com/>

Sposito, G., 1989. *The Chemistry of Soils*. Oxford University Press.

Stamper, A., McKinlay, C., Coughlin, D., Laws, F., 2012. *Land Quality Programme Groundwater Monitoring at Sellafield*. Sellafield Ltd.

Trevors, J., 1996. Sterilization and inhibition of microbial activity in soil. *Journal of Microbiological Methods* 26, 53-59.

van Geen, A., Robertson, A.P., Leckie, J.O., 1994. Complexation of carbonate species at the goethite surface: Implications for adsorption of metal ions in natural waters. *Geochimica et Cosmochimica Acta* 58, 2073-2086.

van Hees, P.A.W., Jones, D.L., Godbold, D.L., 2002. Biodegradation of low molecular weight organic acids in coniferous forest podzolic soils. *Soil Biology and Biochemistry* 34, 1261-1272.

Vorobev, A., Beck, D.A., Kalyuzhnaya, M.G., Lidstrom, M.E., Chistoserdova, L., 2013. Comparative transcriptomics in three Methylophilaceae species uncover different strategies for environmental adaptation. *PeerJ* 1, e115.

Wallace, S.H., Shaw, S., Morris, K., Small, J.S., Fuller, A.J., Burke, I.T., 2012. Effect of groundwater pH and ionic strength on strontium sorption in aquifer sediments: Implications for <sup>90</sup>Sr mobility at contaminated nuclear sites. *Applied Geochemistry* 27, 1482-1491.

Wang, Q, G. M. Garrity, J. M. Tiedje, and J. R. Cole. 2007. Naïve Bayesian Classifier for Rapid Assignment of rRNA Sequences into the New Bacterial Taxonomy. *Appl Environ Microbiol.* 73(16), 261-7.

Weir, S., Lee, H., Trevors, J., 1996. Survival of free and alginate-encapsulated *Pseudomonas aeruginosa* UG2Lr in soil treated with disinfectants. *Journal of Applied Microbiology* 80, 19-25.

Wieland, E., Hummel, W., 2015. Formation and stability of <sup>14</sup>C-containing organic compounds in alkaline iron-water systems: Preliminary assessment based

on a literature survey and thermodynamic modelling. *Mineralogical Magazine* 79, 1275-1286.

Wilkins, M.J., Livens, F.R., Vaughan, D.J., Beadle, I., Lloyd, J.R., 2007. The influence of microbial redox cycling on radionuclide mobility in the subsurface at a low-level radioactive waste storage site. *Geobiology* 5, 293-301.

## **Chapter 7 The behaviour of low molecular weight organic carbon-14 containing compounds in contaminated groundwater during denitrification and iron-reduction.**

### **7.1 Executive Summary**

Aqueous low molecular weight organic carbon-14 ( $^{14}\text{C}$ ) substances can be formed by the oxidation of carbides and impurities within nuclear fuel cladding. During the subsequent reprocessing and interim storage there is potential for these  $^{14}\text{C}$ -labelled organic compounds to leak in to the shallow subsurface environments of nuclear facilities where complex geochemical conditions exist, such as denitrification and iron reduction, due to historic leaks. The persistence of  $^{14}\text{C}$ -organic compounds under such biogeochemical conditions is unknown. Four  $^{14}\text{C}$ -labelled organic compounds (acetate, formate, formaldehyde and methanol) were used as electron donors (concentration  $10^{-5}$  M) in a series of microcosm experiments, under both denitrification and iron reduction, using glacial outwash sediments and groundwater composition representative of the Sellafield reprocessing site, UK. In microcosms posed at the denitrification state, only  $\sim 5\%$  of the initial  $^{14}\text{C}$  remained in solution after 15 days irrespective of which  $^{14}\text{C}$ -containing electron donor was supplied.  $^{14}\text{CO}_2(\text{g})$  production measured at the end of the experiments and the lack of removal in sterile controls support the assumption that microbial utilisation is the primary mechanism of removal for the  $^{14}\text{C}$ -organics. Under iron-reducing conditions both the  $^{14}\text{C}$ -carboxylates were removed from solution rapidly, but some formaldehyde and methanol remained in solution after 32 days. For both redox conditions the microbial population showed decreases in the values of both common and dominant OTUs, generally with the

community structures becoming more dominated by Proteobacteria, and especially the Betaproteobacteria class. The results of this study suggest that the ubiquitous and diverse indigenous bacterial phyla are able to utilise  $^{14}\text{C}$ -organics very rapidly under denitrification conditions, but under iron reducing conditions there is potential that a proportion of  $^{14}\text{C}$ -formaldehyde and  $^{14}\text{C}$ -methanol may persist for longer in groundwater and therefore spread further in subsurface environments.

## 7.2 Introduction

Contamination of groundwater is common at nuclear sites where historic leaks of radionuclides to subsurface environments including carbon-14 ( $^{14}\text{C}$ ), technetium-99 ( $^{99}\text{Tc}$ ), strontium-90 ( $^{90}\text{Sr}$ ) and uranium (U) are co-located with contaminants such as nitrate (from nitric acid) and organic acids (Thorpe et al., 2012; Law et al., 2010; McKenzie and Armstrong-Pope, 2010). Similar groundwater contamination has been recorded at US nuclear licensed sites such as Oak Ridge, TN (Edwards et al., 2007 ; Istok et al., 2004; McBeth et al., 2007), San Juan Shiprock, NM (Finneran et al., 2002) and Hanford WA (Singleton et al., 2005). These sites are often typified by their extremes in pH, with high nitrate and in some cases significant naturally occurring iron(III) oxyhydroxide phases that support a variety of redox conditions existing in the subsurface (Fredrickson et al., 2004; Istok et al., 2004; Begg et al., 2007; Edwards et al., 2007; McBeth et al., 2007; McKenzie and Armstrong-Pope, 2010; Law et al., 2010; Stamper et al., 2012).

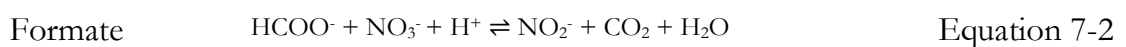
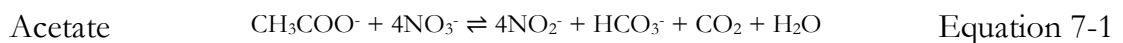
The existence of such geochemical conditions can lead to localised reducing zones in subsurface environments. Under iron reducing conditions the radionuclides Tc and U can be reduced to their insoluble, low-valence forms

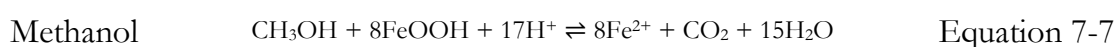
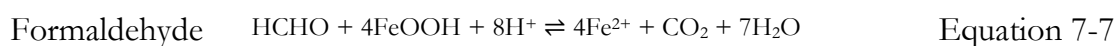
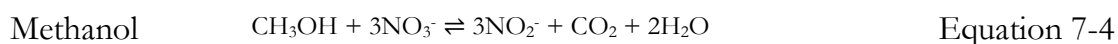
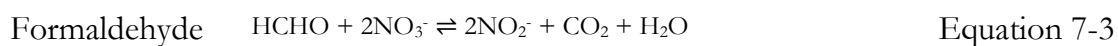
(Lloyd et al., 2000; Burke et al., 2005; Burke et al., 2010; Senko et al., 2005; Morris et al., 2008), therefore biostimulation is considered a treatment option for these radionuclides whereby an electron donor is added to groundwater to stimulate the indigenous microbial community and create a reducing environment (Lloyd and Renshaw, 2005). This microbial activity can result in the production of  $\text{HCO}_3^-$  which would increase pH and promote supersaturation of carbonate mineral phases such as calcite. During microbial reduction of Fe(III) siderite ( $\text{Fe(II)CO}_3$ ) can form (Parmar et al., 2000; Roden et al., 2002) both of which have the potential to incorporate  $^{14}\text{C}$  as  $^{14}\text{CO}_3^{2-}$ . As  $^{14}\text{C}$  can be found as a co-contaminant with Tc and U at nuclear sites (Stamper et al., 2012) studying its behaviour under these redox conditions is essential to understanding the fate of this radionuclide in existing and engineered reducing conditions.

$^{14}\text{C}$  is produced at each stage of the nuclear power generation process, in both inorganic and organic forms. It is of interest due to its long half-life of  $5730 \pm 40\text{a}$  (Godwin, 1962), its ability to bioaccumulate (Begg et al., 1992; Cook et al., 1998; Yim and Caron, 2006) and its position as a key radionuclide in safety assessment for geological disposal (NDA, 2012). Inorganic  $^{14}\text{C}$  behaviour in groundwater environments is influenced mainly by pH and the availability of divalent cations (Krauskopf and Bird, 1995, Boylan et al., 2016).  $^{14}\text{C}$ -labelled low molecular weight organic (LMWO) substances are predicted to form under geological disposal conditions (Wieland and Hummel, 2015), but there is growing concern over their formation in intermediate waste storage facilities due to the corrosion of activated fuel and fuel cladding (Kaneko et al., 2003; Wieland and

Hummel, 2015). In interim storage at nuclear sites, such as the silos at Sellafield nuclear reprocessing site, UK, reducing conditions may occur due to the lack of oxygen penetration with increasing depth (see Chapter 6, Figure 6-1). Under completely oxic or reducing conditions  $^{14}\text{CO}_2$  and  $^{14}\text{CH}_4$  are expected to be produced at the highest concentrations respectively (Wieland and Hummel, 2015), but this redox stratification with depth also allows for the formation of intermediate  $^{14}\text{C}$ -labelled LMWO substances which are partly oxidised. Radiolysis can also cause the formation of organic compounds within these environments (Hudson and Moore, 1999). The four compounds expected to form at significant concentrations due to the corrosion of fuel cladding are acetate, formate, formaldehyde and methanol (Kaneko et al., 2003; Wieland and Hummel, 2015). Acetate consumption has been previously studied (Rifle, CO, USA, Anderson et al., 2003; Sellafield, UK, Newsome et al., 2014, Thorpe et al., 2012) but little is understood on the impacts of reducing conditions on the behaviour of formate, formaldehyde and methanol.

Balanced equations for the oxidation of these four LMWO substances are shown below under nitrate reducing conditions (Equation 7-1 to 7-4) and under iron reducing conditions (Equation 7-5 to 7-8). All of these reactions convert organic carbon in to inorganic forms, with acetate producing  $\text{HCO}_3^-$  which may increase groundwater pH.





This study aims to define the behaviour of  $^{14}\text{C}$  in the form of four LMWO substances (acetate, formate, formaldehyde and methanol) in environments which have active denitrification and iron reduction. The specific objectives of this study were: 1) to investigate the behaviour of aqueous, organic  $^{14}\text{C}$  under denitrification and iron-reducing conditions in contact with sediment; 2) to establish the extent of transformation of organic  $^{14}\text{C}$  to  $^{14}\text{CO}_2(\text{g})$ ; 3) to quantify the amount of  $^{14}\text{C}$  retained in the organic and inorganic fractions in solid; 4) to determine the active microbial populations which utilise the organic compounds under reducing conditions; and 5) to assess the implications of these processes for  $^{14}\text{C}$  in the form of dissolved organic carbon (DOC) release into shallow subsurface environments.

## **7.3 Materials and Methods**

### **7.3.1 Sediment**

Sediment collection took place in July 2016 in the River Calder valley, Cumbria, UK (Lat 54°26.3'N, Long 3°28.2'W). This sediment is representative of the glacial/fluviol quaternary deposits underlying the UK Sellafield nuclear reprocessing site (Law et al., 2010; Wallace et al., 2012). Sediment was collected in sterile HDPE bags and stored at 4°C. Prior to use the soil was sieved and the 2mm fraction retained for use.

### **7.3.2 Bioreduction microcosms**

Sediment microcosms were prepared with 10 ±0.1 g of sediment mixed with 100 ±1 mL of a representative synthetic groundwater media (Wilkins et al., 2007) in sterile 120 mL glass serum bottles (Wheaton Scientific, U.S.). Two artificial groundwater compositions were used, A) unamended (used for iron-reducing conditions) and B) high nitrate, producing a final nitrate concentration of 10 mM L<sup>-1</sup>(used for denitrifying conditions)(see Table7- 1). Groundwater was filtered (0.2 µm), sparged with N<sub>2</sub>(g) and pH adjusted after deoxygenation prior to addition to microcosm. Experiments were run in triplicate excepting sterilised control microcosms which were single experiments.

To stimulate redox conditions no additional electron donor was added to the microcosms prior to amendment with <sup>14</sup>C-LMWO substance. Microcosms were conditioned to simulate two differing redox conditions: denitrifying and iron-reducing using organic substrates from the sediment. Denitrifying microcosms were incubated for 7 days prior to the addition of the organic <sup>14</sup>C-labelled spike.

Iron-reducing microcosms were incubated for 28 days prior to  $^{14}\text{C}$  addition, for both denitrification and iron-reducing conditions the microcosm headspace was sparged with  $\text{N}_2(\text{g})$  before sealing with butyl rubber septa and crimp.

After incubation one of the LMWO substances (acetate, formate, formaldehyde or methanol) was added to give a concentration of  $10^{-5}$  M. To this, 100  $\mu\text{L}$  of LMWO  $^{14}\text{C}$ -tracer was added in the same organic form as the non-labelled addition (producing a final  $^{14}\text{C}$  activity of 100  $\text{Bq ml}^{-1}$ , or  $5 \times 10^{-7}$  M, in each bottle). Formate and acetate were added in sodium salt form and acetate was  $\text{C}^2$  labelled (methyl group) (ARC Ltd., USA). After incubation sterile control microcosms were autoclaved for 30 minutes at  $120^\circ\text{C}$  before spiking with  $^{14}\text{C}$  compounds.

Table 7-1 Solution composition for synthetic groundwater A) unamended and B) high nitrate, both adjusted to pH 7.2 modified from Wilkins et al (2007).

Compound	g/L in DIW
KCl	0.006
$\text{MgSO}_4 \cdot 7\text{H}_2\text{O}$	0.0976
$\text{MgCl}_2 \cdot 6\text{H}_2\text{O}$	0.081
NaCl	0.0094
* $\text{NaNO}_3$	0.868

\* $\text{NaNO}_3$  only added to high nitrate solution composition

### 7.3.3 Geochemical methods

Fe(II) in solid fraction was determined using an acid extraction based on the method of Lovley and Philips (1986) whereby the amount of Fe(II) in the solid is expressed as a percentage of the total Fe in sediment. Approximately 0.1 g of sediment was added to 5 mL of 5 M HCl and left for 60 minutes, followed by

colorimetric assay of Fe(II) by ferrozine and total Fe (after reduction of any extracted Fe(III) to Fe(II) by addition of hydroxylamine HCl). Total Fe in solution determined colorimetrically using ferrozine method from Viollier et al., 2000. At circumneutral pH Fe(III) has limited solubility and so total Fe is assumed to represent the Fe(II) fraction in solution. The limit of detection for this method is ~20 ppb. pH was determined using a Thermo Scientific Orion benchtop ultrimeter and electrodes calibrated daily at pH 4, 7 and 10. Nitrate and nitrite concentrations were determined colorimetrically using on a continuous segmented flow analyzer (III) (SEAL Autoanalyzer 3HR, SEAL, UK), which measures nitrite and total nitrogen (by reduction of nitrate). Nitrate reduction is achieved using a copper-cadmium redactor column. Aqueous  $^{14}\text{C}$ -DOC was measured by mixing 800  $\mu\text{L}$  of filtered (0.2  $\mu\text{m}$ ) sample with 10 mL of EcoScint A liquid scintillation cocktail. Samples were dark adjusted for 24 hours before counting on the liquid scintillation counter.

#### **7.3.4 $^{14}\text{C}$ associated with sediment**

To separate the inorganic (carbonates and  $\text{CO}_2$ ) and organic fraction (hydrocarbons and organic acids) a two-step method was adapted from Magnusson et al., 2007 where acidification and then oxidation of all  $^{14}\text{C}$  associated with sediment was transformed to  $^{14}\text{CO}_2(\text{g})$  and captured (see Chapter 6, Figure 6-2). In to a 250 mL reaction vessel  $1 \pm 0.01\text{g}$  of sediment was added with a magnetic stirrer. The system was sparged with  $\text{N}_2(\text{g})$  prior to and during the extraction process, gas flow rate was set to 40 mL/min. Once sparged the reaction vessel was attached to two 125 mL gas washing bottles, the first of which

contained 100 mL of Carbo-Sorb E and the second 100 mL of 1 M NaOH (acting as a safety bottle to ensure no release of  $^{14}\text{CO}_2(\text{g})$ ). 20 mL of 2 M  $\text{H}_2\text{SO}_4$  was added to the reaction vessel to achieve a pH  $\sim 3$  when buffered by sediment. It was left to react for 30 minutes before disconnecting the gas washing bottles and exchanging for duplicate wash bottles. For the oxidation step 20 mL of 5% potassium persulfate and 4 mL 4%  $\text{AgNO}_3$  were added to the container and heated to 80-90°. Further additions of  $\text{K}_2\text{S}_2\text{O}_8$  and  $\text{AgNO}_3$  at the same concentration and volume were made after one and two hours of reaction. The system was left for another hour to give a total oxidation reaction time of 3 hours. Triplicate samples of 1 mL were collected from wash bottles containing Carbo-Sorb E and mixed with 10 mL of PermaFluor E (Ahn et al., 2003; Magnusson et al., 2007). All samples were left to dark adjust for 24 hours prior to counting on the liquid scintillation counter. The values recorded represent minimum values as the method is 85-95% efficient at recovering  $^{14}\text{C}$  (as measured by Magnusson et al., 2007).

### 7.3.5 Microbiology

Eleven soil samples were selected for next-generation sequencing, one of each organic compound under each redox condition were sampled (eight total) and three unamended samples were sequenced, representing the sediment collected at the field site and frozen on the same day. DNA was extracted from soil samples ( $\sim 0.5\text{g}$ ) using the Fast DNA spin kit for soil (MP Bio). DNA fragments in the size range 3 kb to approximately 20 kb were isolated on a 1% agarose “1x” Tris-borate-EDTA (TBE) gel stained with ethidium bromide for viewing under UV light (10x TBE solution supplied by Invitrogen Ltd., UK). The DNA was extracted from the gel using a QIAquick gel extraction kit (QIAGEN

Ltd, UK); final elution was by 1/10th strength elution buffer (unless explicitly stated, the manufacturer's protocols supplied with all kits employed were followed precisely). DNA concentration was quantified fluorometrically using a Qubit dsDNA HS Assay (Thermo Fisher Scientific Inc., USA).

DNA samples (1ng/ $\mu$ L in 20  $\mu$ L aqueous solution) were sent for sequencing at the Centre for Genomic Research, University of Liverpool, where Illumina TruSeq adapters and indices were attached to DNA fragments in a two-step PCR amplification targeting the 16S rRNA gene. Pooled amplicons were paired-end sequenced on the Illumina MiSeq platform (2x250 bp). Illumina adapter sequences were removed, and the trimmed reads were processed using the UPARSE pipeline (Edgar, 2013) within the USEARCH software (version 9.2) on a Linux platform. Overlapping paired end reads were merged prior to quality filtering and relabelling. The entire sequence run was clustered, with chimeras and singletons removed for generation of the operational taxonomic units (OTUs) which were defined by minimum of 97% sequence identity between the putative OTU members. Taxonomy was defined using a confidence value of more than 0.7 to balance sensitivity and error rate in the prediction using the online Ribosomal Database Project (Wang et al., 2007). The entire set (~7M reads) was then allocated to the OTUs and reported in the OTU table with the taxonomy and abundance of the OTUs.

Statistical analysis was performed to determine the bacterial diversity. In this study the alpha diversity was defined using Hill numbers,  $D_q$ , (Hill, 1973; Jost,

2006). Hill numbers define the biodiversity as the reciprocal mean of proportional abundance and compensate for the disproportionate impact of rare taxa by weighting taxa based on abundance. The degree of weighting is controlled by the index  $q$  where increasing  $q$  places progressively more weight on the high-abundance species in a population (Hill, 1973; Jost, 2006, 2007; Kang et al., 2016).  $D_0$  is the unweighted Hill number and is equal to the species richness.  $D_1$  is a measure of the common species and is equivalent to the exponential of Shannon entropy.  $D_2$  is a measure of the number of dominant species and is equivalent to the inverse of Simpson concentration (Hill, 1973; Jost, 2006, 2007).

## **7.4 Results**

### **7.4.1 Sediment characterisation**

Sediment from this location has been extensively characterised in previous studies (e.g Law et al., 2010; Wallace et al., 2012). In summary the sediment is described as poorly sorted sandy loam. The fine fraction is dominated by quartz, albite, microcline, chlorite and mica (see Chapter 6, section 3-1). The approximate particle composition is 53% sand, 42% silt and 5% clay (Law et al., 2010), sediment pH is 5.5.

### **7.4.2 Microcosm geochemical conditions**

Geochemical conditions of the microcosms were recorded within one hour of establishment (see Table 7-2) prior to any amendment to establish pH and concentration of iron and nitrate/nitrite at the start of incubation.

Table 7-2 Geochemical conditions measured in unaltered microcosms within one hour of establishment.

<b>Geochemical conditions prior to amendments</b>	
<b>pH</b>	5.1-6.6
<b>Fe(II) (as % of total Fe in solid)</b>	0.5 ±0.5%
<b>Fe in solution (ppb)</b>	<20 ppb*
<b>Nitrate (mM)</b>	0.8 ±0.01
<b>Nitrite (mM)</b>	0.08 ±0.01

\* LOD = Limit of detection (20 ppb)

#### 7.4.3 The behaviour of <sup>14</sup>C-labelled LMWO compounds under denitrifying conditions

For all denitrification experiments 10 mM of nitrate was added and microcosms were left for 7 days to allow denitrifying conditions to develop prior to the addition of the <sup>14</sup>C-LMWO substances. 7 to 14 days shown in Figure 7-1, therefore, refers to the post-incubation stage when the <sup>14</sup>C-LMWO substance is added i.e. after 7 days have elapsed for preconditioning. Experiments were run from day 7 to day 14 (acetate and formate) continuing to day 22 for formaldehyde and methanol (data not shown; see Appendix C, Figure C1).

In the acetate experiments pH increased from 5.2 on day 7 to 6 over the duration of the experiment (14 days). For the formate experiments the pH decreased from an initial value of 5.7 on day 7 to 5.2 at the end of the experiment (14 days). The pH of the formaldehyde experiments decreased from an initial pH

of 6.7 on day 7 to 6.2 at the end of the experiment (14 days). In the methanol experiment the pH remained at  $6.7 \pm 0.3$  for the duration of the experiment (7-14 days)(Figure 7-1a).

In the acetate experiments the percentage of aqueous  $^{14}\text{C}$  decreased from 100% on day 7 to 3% at the 8 day sample point. It remained at  $3 \pm 1.5\%$  for the duration of the experiment (14 days). The percentage of  $^{14}\text{C}$  in solution in the formate experiment decreased from 100% on day 7 to 1% at the 8 day sample point, remaining at  $3 \pm 2\%$  for the duration of the experiment (14 days). The formaldehyde experiments showed a decrease from 100% on day 7 to 85% at the 8 day sampling point. It reduced to 6% after 14 days and remained at 6% for the duration of the experiment (22 days). In the methanol experiments the percentage of  $^{14}\text{C}$  in solution decreased from 100% on day 7 to 90% at the 8 day sampling point. The percentage of  $^{14}\text{C}$  decreased to 30% after 14 days, with 6% remaining in solution at the end of the experiment (22 days)(Figure 7-1b).

The percentage of acid extractable Fe present as Fe(II) in the acetate experiments increased from 0% on day 7 to 7% on day 10, 0% is recorded at the end of the experiment (14 days). The formate experiment also shows a decrease from 11.6 on day 7 to 8.6% at the 10 day sample point. At the end of the experiment 0.1% Fe(II) is measured (14 days). Fe(II) in the formaldehyde experiment decreased from 5.2% on day 7 to 3% on day 10, this continued to decrease to 0.5% at the end of the experiment (22 days). In the methanol experiment the percentage of Fe(II) increased from 2.7% on day 7 to 10.4% at the 10 day sample point. This decreased to 1% at the end of the experiment (22 days).

For all denitrification experiments aqueous Fe measurements were <20 ppb and so below limit of detection.

In all experiments the concentration of nitrate on day 0 was 10 mM. In the acetate experiment the concentration of nitrate in solution decreased from 1.3 mM on day 7 to 0.7 mM at the final sample point (14 days). The nitrite concentration rose from 2.6 mM on day 7 to 3.3 mM on day 8, before decreasing to a minimum of 2.5 mM at the final sample point (14 days). For the formaldehyde experiment the nitrate concentration was 0.8 mM on day 7 decreasing to 0.4 mM at day 14, it was measured at 0.2 mM at the end of the experiment (day 22). The nitrite concentration was 2.1 mM on day 7 which increased to a maximum of 2.6 at the day 10 sample point before decreasing to 2.2 mM at the end of the experiment (22 days). In the methanol experiment the nitrate concentration was 0.6 mM on day 7 which decreased to 0.5 mM after 7 days reaching a minimum of 0.2 mM at the end of the experiment (22 days). Nitrite concentrations increased from 2.1 mM on day 7 to 2.2 mM at the 8 day sample point and maintained this concentration until day 14 where the concentration decreased to 1.5 mM. It remained 1.5 mM for the duration of the experiment (22 days)(Figure 7-1c,d).

In the control experiments the pH for the acetate experiments was 5.1 on day 7, increasing to 5.8 at the end of the experiment (day 14). For all other electron donors the pH remained relatively constant at  $5.6 \pm 0.2$  for the duration (7-14 days). The percentage of  $^{14}\text{C}$  in solution remained at  $99 \pm 1\%$  throughout the experiment for each electron donor. The amount of Fe(II) in solid fraction remained below 10% for each electron donor and the amount of Fe in solution

was below the limit of detection for the duration of the experiment. In all experiments the concentration of nitrate on day 0 was 10 mM. The amount of nitrate in solution was measured at  $2.2 \pm 0.3$  mM for all electron donors from day 7 to day 14 and the amount of nitrite remained almost constant at 0.5 mM for the duration of the experiment (see Appendix C, Figure C-3).

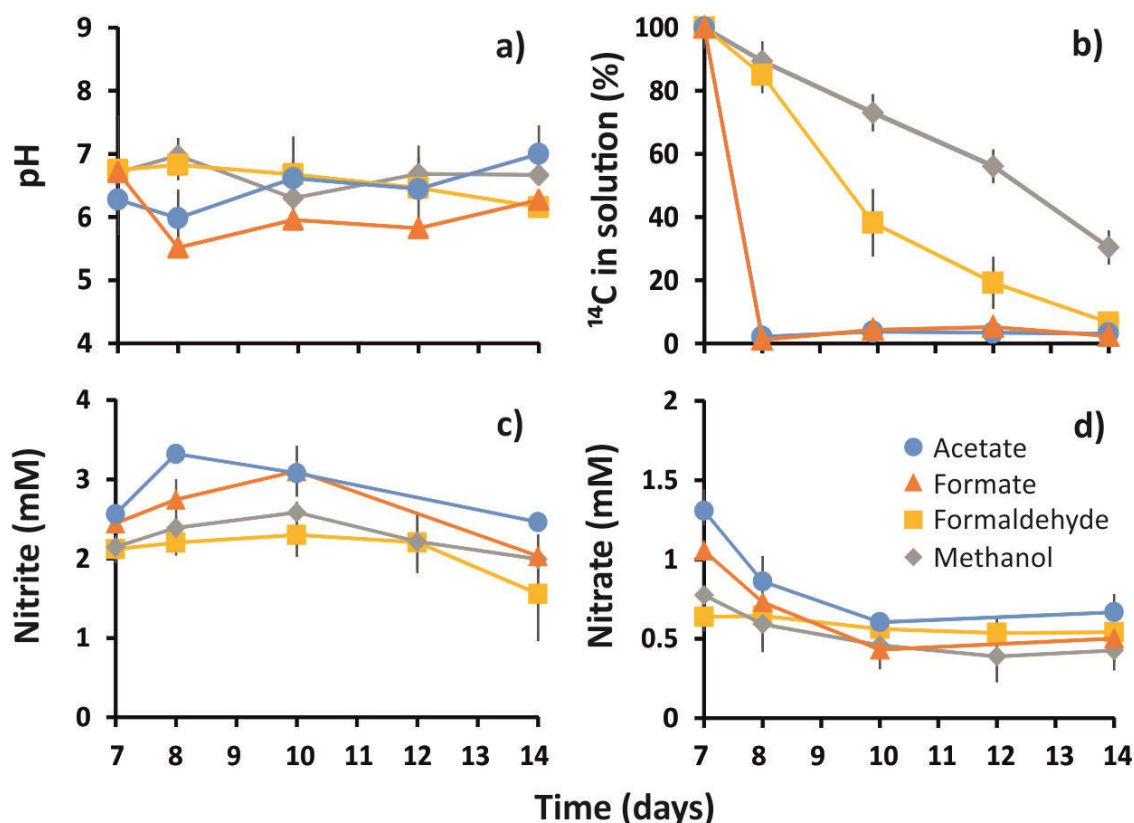


Figure 7-1 The results of the denitrification experiments a) pH; b) percentage of <sup>14</sup>C in solution; c) concentration of nitrite in solution; d) concentration of nitrate in solution (original nitrate addition = 10mM, t=7 indicates time of <sup>14</sup>C addition). Experiment duration from day 7 to day 14 (acetate and formate) continuing to day 22 for formaldehyde and methanol (data not shown). Error bars denote one standard deviation of triplicate measurements; where not shown error bars are less than the size of the symbol used.

#### 7.4.3.1 <sup>14</sup>C speciation at the end of denitrification experiments

Table 7-3 shows the results of the measurement of <sup>14</sup>CO<sub>2</sub>(g) in the microcosm headspace and the percentage of <sup>14</sup>C associated with the inorganic and

organic solid fractions as a percentage of the original  $^{14}\text{C}$  activity added to the experiment. Measureable  $^{14}\text{CO}_2(\text{g})$  was recorded from each experiment with the lowest value of 25.7% found in the acetate experiment and the maximum recovery at 72.5% from the methanol experiment. For the solid fraction in both inorganic and organic fractions the maximum recovery was 3.7% of the original  $^{14}\text{C}$  activity suggesting very little  $^{14}\text{C}$  is retained in any solid fraction under these conditions.

Table 7-3 The results of the  $\text{CO}_2(\text{g})$  measurement and solid fraction sequential extraction expressed as a percentage of the original activity addition for denitrification experiments. All measurements were based on one sample; where error measurement is recorded this corresponds to the standard deviation of replicate samples taken from an individual gas wash bottle. DIC – dissolved inorganic carbon; TIC – total inorganic carbon; TOC – total organic carbon.

	Acetate	Formate	Formaldehyde	Methanol
	14d	14d	22d	22d
$^{14}\text{C}$ -DOC	3.8%	2.4%	7.9%	8.3%
$^{14}\text{CO}_2(\text{g})$	25.7%	49.9%	70.3%	72.5%
$^{14}\text{C}$ -TIC	1.0 $\pm$ 1.5%	2.6 $\pm$ 4.0%	3.6 $\pm$ 2.5%	1.6 $\pm$ 2.4%
$^{14}\text{C}$ -TOC	3.0 $\pm$ 0.1%	3.0 $\pm$ 4.1%	3.7 $\pm$ 2.7%	1.7 $\pm$ 2.6%
Sum	33.5%	58%	85.5%	84.2%
Balance (by difference)*	66.5%	42%	14.5%	15.8%

\* Balance (by difference) is attributed to the  $^{14}\text{C}$ -DIC fraction which is not measured.

#### 7.4.4 The behaviour of <sup>14</sup>C-labelled LMWO compounds under iron-reducing conditions

For all iron reducing experiments microcosms were incubated for 28 days to allow iron reducing conditions to develop prior to the addition of <sup>14</sup>C-LMWO substances. T=28-35 days shown in Figure 7-2, therefore, refers to the post-incubation stage when the <sup>14</sup>C-LMWO substance is added i.e. after 28 days have elapsed for preconditioning. Experiments were run from day 28 to day 35 (acetate and formate) continuing to day 60 for formaldehyde and methanol (see Appendix C, Figure C2).

Nitrate concentrations prior to the incubation were  $0.8 \pm 0.08$  mM and initial nitrite concentrations were  $0.08 \pm 0.01$ . Prior to the incubation period the fraction of Fe(II) in solid was 0.5% and Fe in solution was below the limit of detection (20 ppb)(see Table 7-2).

The pH of the acetate experiment is 6.3 at 28 days. It decreases to 5.6 at 30 days, before increasing to 6.2 at the end of the experiment (35 days). For the formate experiment the pH is 5.8 at 28 days, it increases to a maximum of 6.2 at 30 days, pH is measured at 5.5 at the end of the experiment (35 days). In the formaldehyde experiment the pH is 6.4 at 28 days. At 29 days this has decreased to 6, before increasing to pH 6.3 at the end of the experiment (60 days). The methanol pH is 6.1 on day 28. It decreases to a minimum of 5.5 at 29 days, before increasing to 6.9 at the end of the experiment (60 days)(Figure 7-2a).

<sup>14</sup>C-acetate decreases from 100% in solution on day 28 to 6.2% on day 29, 5.4% remains in solution at the end of the experiment (35 days). The percentage

of  $^{14}\text{C}$  in solution in the formate experiments decreased from 100% on day 28 to 48% at 29 days, further reducing to 3% at the end of the experiment (35 days). The percentage of  $^{14}\text{C}$ -formaldehyde in solution decreased from 100% at day 28 to 31% at the 35 day sample point. It continued to decrease with 19.3% remaining in solution at the end of the experiment (60 days).  $^{14}\text{C}$ -methanol decreased from 100% at day 28 to 75% at 35 days, it continued to decrease over the experimental run with 11% left in solution after 60 days (Figure 7-2b).

The percentage of Fe(II) in solid for acetate experiment was  $9.4 \pm 0.5\%$  at 28 days, with  $14.5 \pm 8\%$  recorded at the end of the experiment (35 days). The formate experiment showed increasing Fe(II) in solid fraction, from  $7.6 \pm 2\%$  at day 28 it increased to  $20 \pm 8\%$  at the end of the experiment (35 days). The formaldehyde fraction of Fe(II) also increased from  $5.5 \pm 2\%$  on day 28 to  $32.7 \pm 7\%$  at the end of the experiment (60 days). The methanol Fe(II) fraction increased from  $6.4 \pm 3\%$  on day 28 to  $29 \pm 0.5\%$  at the end of the experiment (60 days)(Figure 7-2c).

The concentration of Fe in solution in the acetate experiment is  $96 \pm 33$  ppb on day 28 and  $110 \pm 10$ ppb at the end of the experiment (35 days). In the formate experiment the initial Fe concentration in solution is  $102 \pm 10$  ppb on day 28, with  $153 \pm 59$ ppb measured on day 35. In the formaldehyde experiment the concentration of Fe in solution increases from  $69 \pm 30$  ppb on day 28 to  $90 \pm 6$  ppb at the end of the experiment (60 days). Fe(II) concentrations in solution for methanol increases from  $31 \pm 15$  ppb on day 28 to  $76 \pm 5$  at the end of the experiment (60 days)(Figure 7-2e).

For all iron-reducing experiments nitrate concentrations remained at  $0.06 \pm 0.02$  mM for the duration of the experiments. Nitrite concentrations were measured at  $0.02 \pm 0.02$  mM on day 7 decreasing to 0 at the end of the experiments (35/60 days)(Figure 7-2d,f).

In the control experiments the pH for all electron donors remained relatively constant at  $5.6 \pm 0.2$  for the duration (28-35 days). The percentage of  $^{14}\text{C}$  in solution remained at  $100 \pm 2\%$  throughout the experiment for each electron donor. At the point of  $^{14}\text{C}$  addition (28 days) the amount of Fe(II) in solid fraction was between 13 and 20% for each electron donor, in all experiments the amount decreased at the 31 day samples point before increasing with all experiments showing between 13 and 18% Fe(II) in solid fraction. The concentration of Fe in solution at 28 days is 105 ppb for the acetate experiment, decreasing to 100 ppb at the ends of the experiment (35 days). For the formate experiment the concentration at 28 days is 47 ppb which decreases to 30 ppb on day 31 before increasing slightly to 40 ppb. The formaldehyde experiment has 70 ppb of Fe in solution at 28 days, this decreases to 40 ppb at 35 days. The methanol experiment has 47 ppb in solution on day 28, with 35 ppb in solution at the end of the experiment (35 days). The amount of nitrate in solution was measured at  $<0.06$  mM for all electron donors and the amount of nitrite remained almost constant at 0.02 mM for the duration of the experiment (see Appendix C, Figure C-4).

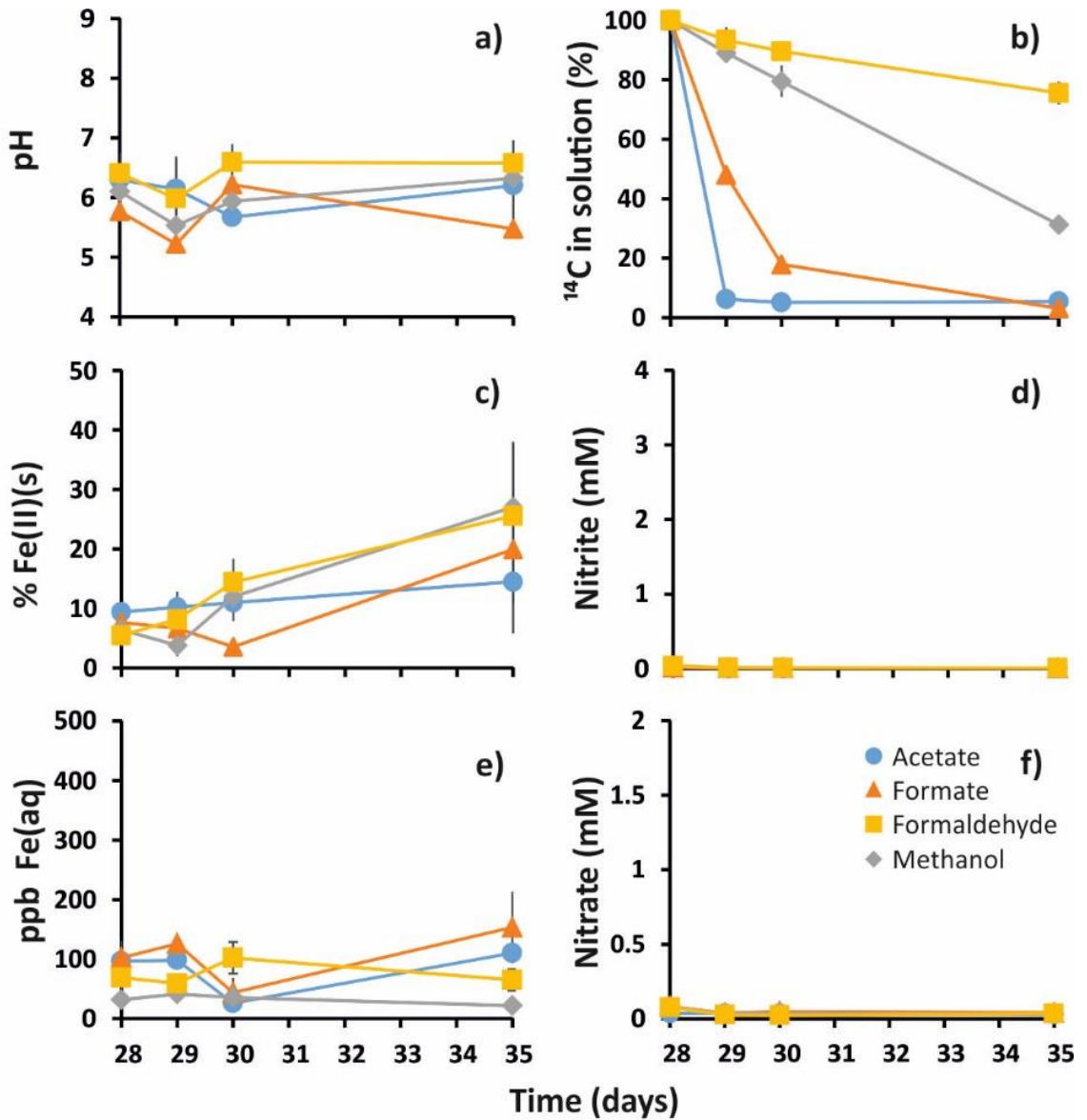


Figure 7-2 The results of the iron-reducing experiments a) pH; b) percentage of <sup>14</sup>C remaining in solution; c) fraction of Fe(II) in solids; d) concentration of nitrite; e) concentration of Fe(II) in solution; f) concentration of nitrate. Experiment duration from day 28 to day 35 (acetate and formate) continuing to day 60 for formaldehyde and methanol (data not shown) Error bars denote one standard deviation of triplicate measurements; where not shown error bars are less than the size of the symbol used.

#### 7.4.4.1 <sup>14</sup>C speciation at the end of the iron-reducing experiments

Table 7-4 summarises the <sup>14</sup>CO<sub>2</sub>(g) production measured at the end of the experiments, with a minimum of 44.6% associated with the formaldehyde experiment to a maximum of 64.9% associated with the methanol experiment. Association with solid fraction was low with all values for both inorganic and organic below 5.2%.

Table 7-4 The results of the CO<sub>2</sub>(g) measurement and solid fraction sequential extraction expressed as a percentage of the original activity addition for iron-reducing experiments. All measurements were based on one sample; where error measurement is recorded this corresponds to the standard deviation of replicate samples taken from the gas wash bottle.

	Acetate	Formate	Formaldehyde	Methanol
	35d	35d	60d	60d
<sup>14</sup> C-DOC	5.5%	3.2%	19.3%	11%
<sup>14</sup> CO <sub>2</sub> (g)	51.7%	64.5%	44.6%	64.9%
<sup>14</sup> C-TIC	2.3 ± 2.4%	5.0 ± 0.2%	1.5 ± 2.3%	5.1 ± 0.3%
<sup>14</sup> C-TOC	5.2 ± 0.1%	2.8 ± 2.4%	4.9 ± 0.1%	5.2 ± 0.4%
Sum	64.6%	75.5%	70.3%	86.2%
Balance (by difference)*	35.4%	24.5%	29.7%	13.8%

\* Balance (by difference) is attributed to the <sup>14</sup>C-DIC fraction which is not measured.

#### 7.4.5 Microbial community composition

Illumina MiSeq analysis gave >100,000 paired-end reads per sample after quality control. The combined pool was used to identify the characteristic OTUs. 8,763,879 reads passed the chimera check and these were clustered in to OTUs (>97% sequence identity) in the UPARSE pipeline and assigned to taxonomic

groups. OTUs classified as archaea (8% of non-chimeric reads) and bacteria which were not classified at phylum level with a confidence of  $>0.7$  (38% of non-chimeric reads) were excluded from further analysis. This resulted in 7792 OTUs classified to bacteria phylum with a confidence greater than 0.7 which were used to characterise the impact of  $^{14}\text{C}$ -labelled electron donors on microbial populations under varying redox conditions.

OTUs classified at the level of a phylum with a confidence were grouped to identify those phyla that represented  $<1\%$  of the total number of pair-end reads from this study. There were 11 phyla that individually represented more than 1% of the total population. The unaltered sediment samples contained between 10 and 11 individually identified phyla at more than 1% of the total population. OTUs classified in a phylum which individually represented  $<1\%$  of the total reads of the microbial population were grouped and classified as other phylum. Acidobacteria was the most abundant phylum ( $28 \pm 2\%$  of the reads), followed by Proteobacteria ( $27 \pm 2\%$ ), Actinobacteria ( $10 \pm 3\%$ ) and Verrucomicrobia ( $10 \pm 3\%$ ; Figure 7-3).

Under nitrate reducing conditions for acetate, formate and formaldehyde the number of individual phyla was 10. Acidobacteria is the most abundant phylum (28-35%). The relative abundance of Proteobacteria is between 29 and 30%, with the largest relative contribution from the Betaproteobacteria class (11-13%) and the Gammaproteobacteria class (3-4%)(Figure 7-3). The number of individual phyla in the methanol sample is reduced to 7, the relative abundance of Proteobacteria is 72% of which 35% is associated with the Betaproteobacteria class and 30% with the Gammaproteobacteria class. Within the Betaproteobacteria

class the order of Burkholderiales is the most abundant accounting for more than 92% of the Betaproteobacteria in the methanol sample. 98% of the Gammaproteobacteria are associated with the Xanthomonadales order and particularly the Rhodanobacter genus.

The number of individual phyla represented under iron reducing conditions is 9 for the acetate and formate systems. The most abundant phylum was Proteobacteria (39 ±1%), Acidobacteria (24%) and Actinobacteria (13 ±1%). The most abundant class within Proteobacteria was Betaproteobacteria (22%). The number of phyla represented in the formaldehyde system was 8. The most abundant of which was Proteobacteria (61%), followed by Acidobacteria (11%) and Actinobacteria (9%). The most abundant class within the Proteobacteria was the Betaproteobacteria (38%). In the methanol system 9 phyla were individually identified. The most abundant of these was Proteobacteria (52%), followed by Acidobacteria (19%) and Planctomycetes (5%). The most abundant class within Proteobacteria was Betaproteobacteria (22%). The Gammaproteobacteria class accounted for 11% of total reads (Figure 7-3).

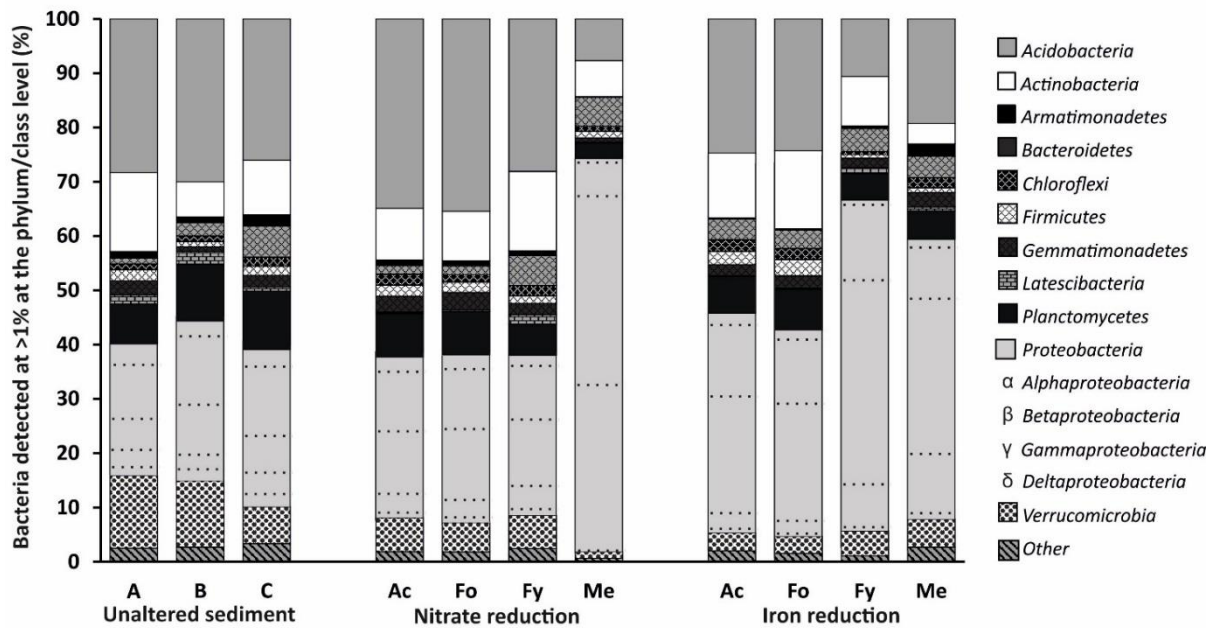


Figure 7-3 Bacterial phylogenetic diversity within the unaltered sediment (A-C) and under denitrification and iron reduction (Ac- acetate; Fo- formate; Fy- formaldehyde; Me-methanol). Phyla with relative abundance less than 1% of the community are grouped as “Other”. Dashed line denotes classes of Proteobacteria descending as follows: unclassified;  $\alpha$ ;  $\beta$ ;  $\gamma$ ;  $\delta$ .

The OTU richness ( $D_0^\alpha$ ) for each sample is shown below in Table 7-5. The average richness for the unaltered sediment is  $5790 \pm 598$  OTUs, under both reducing conditions this value is reduced by between 31% and 44%. The species richness does not take account of the relative abundance of the OTUs. The average value of  $D_1^\alpha$  for the unaltered sediment is  $922 \pm 336$  OTUs. Under both reducing conditions there are fewer common species,  $D_1^\alpha$  values are reduced in comparison to the unaltered sediment with values ranging between 105 and 360 OTUs.  $D_2^\alpha$  for unaltered sediment is  $218 \pm 114$ . There are fewer dominant species under reducing conditions with  $D_2^\alpha$  values ranging between 17.9 and 68.8. Common OTUs accounted for more than 78% of total sequence reads in all samples, and dominant OTUs account for at least 48% of total reads. Therefore the decrease in the number of common and dominant OTUs in the reducing

systems represents a shift towards fewer, but more abundant OTUs under these conditions.

Table 7-5 Alpha-diversity measurements,  $D_0^\alpha$ , species richness,  $D_1^\alpha$ , exponential of Shannon entropy,  $D_2^\alpha$ , inverse of the Simpson index for samples under denitrification (Ac- acetate; Fo- formate; Fy- formaldehyde; Me-methanol).

Unaltered sediment				Denitrification				Iron reduction				
				7d	7d	15d	15d	7d	7d	32d	32d	
A	B	C	Average	Ac	Fo	Fy	Me	Ac	Fo	Fy	Me	
$D_0^\alpha$	5640	6590	5150	5790	3820	3950	3400	3520	3840	3460	3230	3510
			$\pm 598$									
$D_1^\alpha$	495	1320	960	922	360	342	256	105	348	280	210	126
			$\pm 336$									
$D_2^\alpha$	80.8	360	212	218	68.8	64.6	53.7	17.9	66.6	53.9	53.7	52.3
			$\pm 114$									

## 7.5 Discussion

### 7.5.1 The behaviour of aqueous $^{14}\text{C}$ -LMWO substances during denitrification

The geochemical conditions recorded in these experiments (Figure 7-1) suggest active nitrate reduction occurring at the same time as the acetate and formate are being removed from solution via microbial processes. The formaldehyde and methanol are not removed from solution as rapidly as acetate and formate. Their removal from solution coincides with decreasing nitrite concentrations which suggests that the removal of these LMWO substances is linked to nitrite reduction rather than nitrate. There is some fluctuation in the percentage of Fe(II)(s) but less than 1% is recovered for any electron donor at the end of the experiments suggesting that there is no active iron reduction for the duration of these experiments. Nitrite concentrations are recorded at between 2

and 3 mM for these experiments, which is higher than recovery in the iron-reducing systems and the measurements recorded in the unaltered microcosms (see Table 7-2). In combination with the decreasing nitrate concentrations these geochemical results confirm that denitrification processes are occurring prior to addition of electron donors. After 15 days the  $^{14}\text{C}$  in solution has reduced to 6% for all electron donors with over 70% of the activity recovered in the gas phase as  $^{14}\text{CO}_2(\text{g})$  for formaldehyde and methanol.

The phylogenetic microbial composition is similar to unaltered sediment with the relative abundance of Proteobacteria remaining around 30%, but the relevant contribution of the Betaproteobacteria and Gammaproteobacteria classes both increase. The extent of microbial community changes are not as pronounced as previous work using sediment from the same location (Thorpe et al., 2012; Law et al., 2010), especially for acetate and formate experiments which remain broadly similar to the unaltered sediment in phylogenetic composition. This is attributed to the shorter duration for the experiments compared to previous studies. The methanol system shows the largest compositional changes to the phylogenetic diversity. The number of individually identified phyla reduces from 11 in unaltered sediment to 7, 30% of reads are associated with the Gammaproteobacteria class, with the majority of those associated with the Xanthomonadales order. The large increase in the Xanthomonadales order is particularly associated with the *Rhodanobacter* genus which is associated with denitrification. This genus is present in all the samples from the denitrification system, but is much increased in the methanol sample and has been identified at other nuclear contaminated sites as

having an important role in denitrification (e.g. Oak Ridge, TN, USA; Green et al., 2012). 35% of reads are associated with the Betaproteobacteria class in this system, with most of those associated with the Burkholderiales order (>32% total reads) which contains methylotrophic representatives (Kalyuzhnaya et al., 2008). Methylotrophic bacteria are recognised for their ability to utilise single carbon organic compounds (those which do not contain a C to C bond), in particular Burkholderiales has been noted as it is also able to utilise organic both compounds which do contain C to C bonds as well as those which do not. This may explain why there is an increase in the proportion of reads associated with this order for every  $^{14}\text{C}$ -LMWO substance including the two carbon compound acetate (Kalyuzhnaya et al., 2008; Chistoserdova et al., 2009).

### **7.5.2 The behaviour of aqueous $^{14}\text{C}$ -LMWO substances under iron reducing conditions**

The increasing levels of Fe(II) in solid fraction and in solution suggest that metal-reducing processes are established prior to addition of  $^{14}\text{C}$ -labelled electron donors. Nitrate and nitrite concentrations remain very low throughout the duration of the experiments with little fluctuation and were lower than those measured in unaltered microcosms (see Table 7-2) suggesting that any denitrification processes occurred prior to the addition of  $^{14}\text{C}$  and therefore these experiments represent early onset iron reduction. At the end of all experiments more than 44% of  $^{14}\text{C}$  is recovered as  $^{14}\text{CO}_2(\text{g})$  irrespective of incubation time suggesting microbial utilisation is occurring in all systems, this is supported by control experiments where no  $^{14}\text{C}$  removal from solution occurs (see Appendix C3), however unlike acetate and formate which are removed rapidly (~5%

remaining on day 35), some  $^{14}\text{C}$ -formaldehyde and  $^{14}\text{C}$ -methanol remain in solution on day 60 (19% and 11% respectively). These compounds are therefore the most likely LMWO substances to be more mobile in subsurface environments under iron-reducing conditions relative to both oxic and denitrifying conditions (see Chapter 6 for discussion on  $^{14}\text{C}$ -LMWOs behaviour in subsurface environments).

Although all measured  $^{14}\text{C}$  concentrations in solid fraction are low there is slightly higher percentage of  $^{14}\text{C}$  associated with solid fraction under iron reducing conditions compared to denitrification (maximum retention 5.2% and 3.7% respectively). For both formate and methanol the retention is 5% in the TIC fraction which may suggest that there is some retention of  $^{14}\text{C}$  in carbonate solids as siderite is known to precipitate under microbially induced iron-reducing conditions (Thorpe et al., 2012; Wieland and Hummel, 2014) and can also occur in low pH environments where microbially mediated iron reduction is occurring (Sanchez-Roman et al., 2014). A simple PHREEQC calculation suggests that siderite can be supersaturated under iron reducing conditions at  $\text{pH} > 6.7$  if there is sufficient  $\text{Fe(II)}$  and carbonate (see Appendix C.3), therefore siderite precipitation may be possible in the methanol system where the pH reaches 6.9. In the  $^{14}\text{C}$ -TOC acetate, formaldehyde and methanol all show around 5% retention in this fraction. This suggests that there is some retention of  $^{14}\text{C}$  as TOC under iron-reducing conditions either through sorption reactions or assimilation, regardless of the electron donor being utilised.

Under iron-reducing conditions the phylogenetic microbial composition is different to that of the unaltered sediment with all samples showing an increase in

the relative abundance of the Proteobacteria, particularly the Betaproteobacteria class. The largest increase is associated with the formaldehyde sample where 37% of total reads are associated with Betaproteobacteria compared to  $7.2 \pm 1.5\%$  of the unaltered sediment. Most of these reads are associated with the Burkholderiales order (>34% total reads) which contains methylotrophic bacteria (Kalyuzhnaya et al., 2008).

There is a decrease in dominant diversity values ( $D_2^z$ ) as the electron donor becomes more reduced (acetate > formate > formaldehyde > methanol), but an increase in the proportion of reads assigned to these OTUs, from a minimum of 48% for acetate to 73% for methanol, this impact is replicated in the denitrifying experiments, although to a lesser degree (minimum of 48% for acetate to a maximum of 65% for methanol). This suggests that the microbial population has shifted towards fewer, but more abundant OTUs and this impact is enhanced by the electron donor being utilised, with the most reduced species (methanol) showing the largest decrease in  $D_2^z$  values.

### **7.5.3 Implications for persistence of $^{14}\text{C}$ -containing LMWO compounds in anaerobic subsurface environments**

$^{14}\text{C}$ -labelled carboxylates (acetate and formate) do not persist in aqueous form under denitrification and iron-reducing conditions in sediment with an active microbial population exhibiting a rapid transformation from organic to inorganic  $^{14}\text{C}$ .  $^{14}\text{C}$ -formaldehyde and  $^{14}\text{C}$ -methanol appear to be more sensitive to redox condition, where the rate of utilisation is slower under both denitrification and iron reduction than for the acetate and formate which may suggest that fewer microbes are adapted to use these substrates as diversity values are also reduced.

Retention of  $^{14}\text{C}$  in solid phase is minimal across all electron donors and redox conditions (<5% of original activity) suggesting that in subsurface environments there will be little retention in solid fraction at circumneutral pH. However both the inorganic and organic solid phase association will be affected by changes in groundwater pH (Boylan et al., 2016; Gu and Schulz, 1991; Krauskopf and Bird, 1995; Sposito, 1989) with the potential to increase the  $^{14}\text{C}$  retention. These results imply that aqueous  $^{14}\text{C}$  may remain in groundwater under iron reducing conditions in the form of simple  $^{14}\text{C}$ -containing alcohol and aldehyde compounds, but this is unlikely to persist in the long term as these compounds were still being utilised (albeit at a slower rate).

## 7.6 Conclusions

This study shows that across most redox and electron donor systems  $^{14}\text{C}$ -LMWO substances are removed rapidly from solution. The production of  $^{14}\text{CO}_2$  is attributed to microbial utilisation of the  $^{14}\text{C}$ -LMWO substances. The production of inorganic  $^{14}\text{C}$  in subsurface environments would increase the  $^{14}\text{C}$  associated with the dissolved inorganic pool (see Boylan et al., 2016 for discussion of inorganic  $^{14}\text{C}$  behaviour). The retention in solid phase is minimal in both organic and inorganic phases reaching a maximum of ~5% of total  $^{14}\text{C}$  activity with sorption of the organic species limited at circumneutral pH values as the anion exchange capacity is restricted (Gu and Schulz, 1991; Sposito, 1989). The indigenous microbial population in this study represent a diverse mix of phyla which are ubiquitous in terrestrial environments and are likely to be similar to those found in the subsurface of nuclear sites, e.g. Sellafield reprocessing site, UK. They are able to

utilise  $^{14}\text{C}$ -labelled carboxylate electron donors (acetate and formate) rapidly under reducing conditions, formaldehyde and methanol are both utilised quickly under denitrification conditions, but under iron-reducing conditions both  $^{14}\text{C}$ -formaldehyde and  $^{14}\text{C}$ -methanol may persist for longer in subsurface environments and be transported with groundwater flow.

## 7.7 References

- Ahn, H.J., Song, B.C., Sohn, S.C., Lee, M.H., Song, K., Jee, K.Y., 2013. Application of a wet oxidation method for the quantification of  $^3\text{H}$  and  $^{14}\text{C}$  in low-level radwastes. *Applied Radiation and Isotopes* 81, 62-66.
- Anderson, R.T., Vrionis, H.A., Ortiz-Bernad, I., Resch, C.T., Long, P.E., Dayvault, R., Karp, K., Marutzky, S., Metzler, D.R., Peacock, A., 2003. Stimulating the in situ activity of *Geobacter* species to remove uranium from the groundwater of a uranium-contaminated aquifer. *Applied and environmental microbiology* 69, 5884-5891.
- Begg, F.H., Cook, G.T., Baxter, M.S., Scott, E.M., McCartney, M., 1992. Anthropogenic radiocarbon in the eastern Irish Sea and Scottish coastal waters. *Radiocarbon* 34, 707-716.
- Begg, J.D., Burke, I.T., Morris, K., 2007. The behaviour of technetium during microbial reduction in amended soils from Dounreay, UK. *Science of the Total Environment* 373, 297-304.
- Boylan, A.A., Stewart, D.I., Graham, J.T., Trivedi, D., Burke, I.T., 2016. Mechanisms of inorganic carbon-14 attenuation in contaminated groundwater:

Effect of solution pH on isotopic exchange and carbonate precipitation reactions. *Applied Geochemistry*. <https://doi.org/10.1016/j.apgeochem.2016.12.006>.

Burke, I.T., Boothman, C., Lloyd, J.R., Livens, F.R., Charnock, J.M., McBeth, J.M., Mortimer, R.J.G., Morris, K., 2006. Reoxidation behavior of technetium, iron, and sulfur in estuarine sediments. *Environmental Science and Technology* 40, 3529-3535.

Burke, I.T., Livens, F.R., Lloyd, J.R., Brown, A.P., Law, G.T.W., McBeth, J.M., Ellis, B.L., Lawson, R.S., Morris, K., 2010. The fate of technetium in reduced estuarine sediments: Combining direct and indirect analyses. *Applied Geochemistry* 25, 233-241.

Chistoserdova, L., Kalyuzhnaya, M.G., Lidstrom, M.E., 2009. The expanding world of methylotrophic metabolism. *Annual review of microbiology* 63, 477-499.

Cook, G.T., MacKenzie, A.B., Naysmith, P., Anderson, R., 1998. Natural and anthropogenic <sup>14</sup>C in the UK coastal marine environment. *Journal of Environmental Radioactivity* 40, 89-111.

Edgar, R.C., 2013. UPARSE: highly accurate OTU sequences from microbial amplicon reads. *Nature methods* 10, 996-998.

Edwards, L., Küsel, K., Drake, H., Kostka, J.E., 2007. Electron flow in acidic subsurface sediments co-contaminated with nitrate and uranium. *Geochimica et Cosmochimica Acta* 71, 643-654.

Finneran, K.T., Housewright, M.E., Lovley, D.R., 2002. Multiple influences of nitrate on uranium solubility during bioremediation of uranium-contaminated subsurface sediments. *Environmental Microbiology* 4, 510-516.

Fredrickson, J.K., Zachara, J.M., Balkwill, D.L., Kennedy, D., Shu-mei, W.L., Kostandarithes, H.M., Daly, M.J., Romine, M.F., Brockman, F.J., 2004. Geomicrobiology of high-level nuclear waste-contaminated vadose sediments at the Hanford Site, Washington State. *Applied and environmental microbiology* 70, 4230-4241.

Godwin, H., 1962. Half-life of radiocarbon. *Nature* 195, 984.

Green, S.J., Prakash, O., Jasrotia, P., Overholt, W.A., Cardenas, E., Hubbard, D., Tiedje, J.M., Watson, D.B., Schadt, C.W., Brooks, S.C., 2012. Denitrifying bacteria from the genus *Rhodanobacter* dominate bacterial communities in the highly contaminated subsurface of a nuclear legacy waste site. *Applied and environmental microbiology* 78, 1039-1047.

Gu, B., Schulz, R.K., 1991. Anion retention in soil: possible application to reduce migration of buried technetium and iodine. Nuclear Regulatory Commission, Washington, DC (United States). Div. of Regulatory Applications; California Univ., Berkeley, CA (United States). Dept. of Soil Science.

Hill, M.O., 1973. Diversity and evenness: a unifying notation and its consequences. *Ecology* 54, 427-432.

Hudson, R., Moore, M., 1999. Laboratory studies of the formation of methanol and other organic molecules by water+ carbon monoxide radiolysis: Relevance to comets, icy satellites, and interstellar ices. *Icarus* 140, 451-461.

Istok, J.D., Senko, J.M., Krumholz, L.R., Watson, D., Bogle, M.A., Peacock, A., Chang, Y.J., White, D.C., 2004. In Situ Bioreduction of Technetium and Uranium

in a Nitrate-Contaminated Aquifer. *Environmental Science & Technology* 38, 468-475.

Jost, L., 2006. Entropy and diversity. *Oikos* 113, 363-375.

Jost, L., 2007. Partitioning diversity into independent alpha and beta components. *Ecology* 88, 2427-2439.

Kalyuzhnaya, M.G., Hristova, K.R., Lidstrom, M.E., Chistoserdova, L., 2008. Characterization of a novel methanol dehydrogenase in representatives of Burkholderiales: implications for environmental detection of methylotrophy and evidence for convergent evolution. *Journal of bacteriology* 190, 3817-3823.

Kaneko, S., Tanabe, H., Sasoh, M., Takahashi, R., Shibano, T., Tateyama, S., 2003. A study on the chemical forms and migration behavior of carbon-14 leached from the simulated hull waste in the underground condition, *Materials Research Society Symposium Proceedings*. Warrendale, Pa.; Materials Research Society; 1999, pp. 621-628.

Kang, S., Rodrigues, J.L., Ng, J.P., Gentry, T.J., 2016. Hill number as a bacterial diversity measure framework with high-throughput sequence data. *Scientific Reports* 6.

Krauskopf, K.B., Bird, D.K., 1995. *Introduction to geochemistry*. McGraw-Hill.

Law, G.T.W., Geissler, A., Boothman, C., Burke, I.T., Livens, F.R., Lloyd, J.R., Morris, K., 2010. Role of nitrate in conditioning aquifer sediments for technetium bioreduction. *Environmental Science and Technology* 44, 150-155.

Lloyd, J., Sole, V., Van Praagh, C., Lovley, D., 2000. Direct and Fe (II)-mediated reduction of technetium by Fe (III)-reducing bacteria. *Applied and Environmental Microbiology* 66, 3743-3749.

Lloyd, J.R., Renshaw, J.C., 2005. Microbial transformations of radionuclides: Fundamental mechanisms and biogeochemical implications, *Metal Ions in Biological Systems*, pp. 205-240.

Lovley, D.R., Phillips, E.J., 1986. Organic matter mineralization with reduction of ferric iron in anaerobic sediments. *Applied and Environmental Microbiology* 51, 683-689.

Magnusson, Å., Stenström, K., Aronsson, P.-O., 2007. <sup>14</sup>C in spent ion-exchange resins and process water from nuclear reactors: A method for quantitative determination of organic and inorganic fractions. *Journal of Radioanalytical and Nuclear Chemistry* 275, 261-273.

Marshall, A., Coughlin, D., Laws, F., 2015. Groundwater monitoring at Sellafield: Annual data review 2014.

McBeth, J.M., Lear, G., Lloyd, J.R., Livens, F.R., Morris, K., Burke, I.T., 2007. Technetium reduction and reoxidation in aquifer sediments. *Geomicrobiology Journal* 24, 189-197.

McKenzie, H., Armstrong-Pope, N., 2010. Groundwater Annual Report 2010. Sellafield Ltd.

Morris, K., Livens, F., Charnock, J., Burke, I., McBeth, J., Begg, J., Boothman, C., Lloyd, J., 2008. An X-ray absorption study of the fate of technetium in reduced and reoxidised sediments and mineral phases. *Applied Geochemistry* 23, 603-617.

NDA, 2012. Geological Disposal: Carbon-14 Project - Phase 1 Report. Nuclear Decommissioning Authority.

- Parmar, N., Warren, L.A., Roden, E.E., Ferris, F.G., 2000. Solid phase capture of strontium by the iron reducing bacteria *Shewanella* alga strain BrY. *Chemical Geology* 169, 281-288.
- Parry, S.A., O'Brien, L., Fellerman, A.S., Eaves, C.J., Milestone, N.B., Bryan, N.D., Livens, F.R., 2011. Plutonium behaviour in nuclear fuel storage pond effluents. *Energy & Environmental Science* 4, 1457-1464.
- Roden, E.E., Leonardo, M.R., Ferris, F.G., 2002. Immobilization of strontium during iron biomineralization coupled to dissimilatory hydrous ferric oxide reduction. *Geochimica et Cosmochimica Acta* 66, 2823-2839.
- Sánchez-Román, M., Fernández-Remolar, D., Amils, R., Sánchez-Navas, A., Schmid, T., Martín-Uriz, P.S., Rodríguez, N., McKenzie, J.A., Vasconcelos, C., 2014. Microbial mediated formation of Fe-carbonate minerals under extreme acidic conditions. *Scientific Reports* 4, 4767.
- Senko, J.M., Mohamed, Y., Dewers, T.A., Krumholz, L.R., 2005. Role for Fe(III) Minerals in Nitrate-Dependent Microbial U(IV) Oxidation. *Environmental Science & Technology* 39, 2529-2536.
- Singleton, M.J., Woods, K.N., Conrad, M.E., DePaolo, D.J., Dresel, P.E., 2005. Tracking sources of unsaturated zone and groundwater nitrate contamination using nitrogen and oxygen stable isotopes at the Hanford Site, Washington. *Environmental science & technology* 39, 3563-3570.
- Sposito, G., 1989. *The Chemistry of Soils*. Oxford University Press.
- Stamper, A., McKinlay, C., Coughlin, D., Laws, F., 2012. *Land Quality Programme Groundwater Monitoring at Sellafield*. Sellafield Ltd.

Thorpe, C.L., Law, G.T.W., Boothman, C., Lloyd, J.R., Burke, I.T., Morris, K., 2012. The Synergistic Effects of High Nitrate Concentrations on Sediment Bioreduction. *Geomicrobiology Journal* 29, 484-493.

Viollier, E., Inglett, P.W., Hunter, K., Roychoudhury, A.N., Van Cappellen, P., 2000. The ferrozine method revisited: Fe(II)/Fe(III) determination in natural waters. *Applied Geochemistry* 15, 785-790.

Wallace, S.H., Shaw, S., Morris, K., Small, J.S., Fuller, A.J., Burke, I.T., 2012. Effect of groundwater pH and ionic strength on strontium sorption in aquifer sediments: Implications for <sup>90</sup>Sr mobility at contaminated nuclear sites. *Applied Geochemistry* 27, 1482-1491.

Wang, Q, G. M. Garrity, J. M. Tiedje, and J. R. Cole. 2007. Naïve Bayesian Classifier for Rapid Assignment of rRNA Sequences into the New Bacterial Taxonomy. *Appl Environ Microbiol.* 73(16), 261-7.

Wieland, E., Hummel, W., 2015. Formation and stability of <sup>14</sup>C-containing organic compounds in alkaline iron-water systems: Preliminary assessment based on a literature survey and thermodynamic modelling. *Mineralogical Magazine* 79, 1275-1286.

Wilkins, M.J., Livens, F.R., Vaughan, D.J., Beadle, I., Lloyd, J.R., 2007. The influence of microbial redox cycling on radionuclide mobility in the subsurface at a low-level radioactive waste storage site. *Geobiology* 5, 293-301.

Yim, M.-S., Caron, F., 2006. Life cycle and management of carbon-14 from nuclear power generation. *Progress in Nuclear Energy* 48, 2-36.

## Chapter 8 Conclusions

This chapter presents a summary of the overall findings of this thesis. The main results of each data chapter are summarised and the chapter concludes with the implications of this work and suggestions for future research.

### 8.1 Summary of results

$^{14}\text{C}$  is a radioactive contaminant found at numerous nuclear sites worldwide (Yim and Caron, 2006), for the successful remediation and management of these sites it is essential to understand the processes which govern  $^{14}\text{C}$  behaviour. This thesis has presented a comprehensive study of  $^{14}\text{C}$  behaviour in subsurface environments looking at both inorganic and organic  $^{14}\text{C}$  forms. The behaviour of inorganic  $^{14}\text{C}$  in subsurface environments is governed principally by the pH and availability of divalent cations (Langmuir, 1997), whereas the behaviour of organic  $^{14}\text{C}$  species in subsurface environments is typically governed by their utilisation by microbial communities (Fischer et al., 2010). This thesis investigates the role of these processes in affecting the behaviour of  $^{14}\text{C}$  and the implications of these findings for contaminated nuclear sites.

Chapter 5 presents the first results of this thesis focussing on the retention mechanisms of aqueous inorganic  $^{14}\text{C}$  in subsurface environments. This work used both batch experiments and modelling to determine the influence of pH and extent of supersaturation on the formation of calcite, before studying the impacts

of isotopic exchange with solid carbonates and atmospheric CO<sub>2</sub>. The results suggest that precipitation of calcite minerals is likely in subsurface environments where the saturation index of calcite is greater than 0.5, with increases in the pH and/or Ca<sup>2+</sup> concentrations also acting to increase the saturation index of a solution. Laboratory experiments suggest that maximum isotopic exchange with solid carbonate is reached after two weeks of equilibration and that the loss of <sup>14</sup>C from solution is proportional to the surface area of calcite present. The removal from solution is equivalent to the rapid equalisation of the isotope ratio in an active 8-10 Å active surface layer. Atmospheric isotopic exchange proceeded very rapidly at pH values below 9.3 with complete loss of <sup>14</sup>C from solution occurring on a timescale of 10's of hours. This loss is characterised as a pseudo-first order rate reaction due to a rapid exchange of dissolved <sup>14</sup>C species with <sup>12</sup>CO<sub>2</sub>(g), the kinetics of <sup>14</sup>C removal increased as pH values were lowered.

Chapter 6 examines the behaviour of low molecular weight <sup>14</sup>C-labelled organic substances under aerobic conditions. A series of batch experiments determined that microbial utilisation is the primary mechanism of removal of <sup>14</sup>C from solution, although the loss of methanol may be partially attributed to volatilisation. The highest retention of <sup>14</sup>C in solid fraction is associated with acetate, particularly the inorganic fraction which suggests that precipitation may occur after microbial utilisation. Phylogenetic diversity remained similar to unaltered sediment at environmentally relevant concentrations.

Finally Chapter 7 expanded the work of Chapter 6 to consider the impact of different redox conditions on the behaviour of aqueous  $^{14}\text{C}$ -LMWO substances. In this chapter denitrification and iron reduction are considered as both are known to occur in the subsurface of nuclear sites. Using batch microcosm experiments it was shown that all aqueous  $^{14}\text{C}$ -LMWO substances behave similarly under denitrification as in aerobic systems with rapid loss from solution, however both  $^{14}\text{C}$ -formaldehyde and  $^{14}\text{C}$ -methanol show much slower rates of utilisation under iron reduction. The generation of  $^{14}\text{CO}_2(\text{g})$  in all experiments confirmed that microbial utilisation is the primary removal mechanism in these experiments and retention in solid fractions is limited (<5%).

## 8.2 Implications

This thesis represents an advance in understanding the fundamental processes which govern the behaviour of  $^{14}\text{C}$  in subsurface environments. It has highlighted the importance of precipitation and isotopic exchange in inorganic  $^{14}\text{C}$  behaviour, with particular reference to the retention of  $^{14}\text{C}$  in the subsurface of Sellafield reprocessing site, UK, as well as the significant role of microbial communities in transforming organic  $^{14}\text{C}$  to inorganic  $^{14}\text{C}$ .

Chapter 5 presents new insights in to the mechanisms for aqueous inorganic  $^{14}\text{C}$  retention in groundwater environments. Atmospheric isotopic exchange is likely to be limited in subsurface environments due to the limited connectivity with atmosphere, but upon authorised and accidental release to surface waters atmospheric isotopic exchange is likely to contribute to the rapid loss of enriched  $^{14}\text{C}$ -DIC which has previously been attributed to the impact of

mixing of the surface waters (Ahad et al., 2006; Wang et al., 2014). The results suggest that precipitation of  $^{14}\text{C}$ -bearing carbonate is likely to occur in subsurface environments where the nucleation sites are abundant. The models of leak and groundwater interactions at Sellafield site, UK, also suggest that precipitation of  $^{14}\text{C}$ -carbonate is likely to occur when an alkali leachate plume intersects with groundwater containing  $\text{Ca}^{2+}$  as is thought to be the case at Sellafield reprocessing site, UK (Marshall et al., 2015; Parry et al., 2011; Wallace et al., 2012). This result also emphasises the importance of understanding the geochemical conditions that exist in the subsurface at nuclear sites to be better able to predict the behaviour of  $^{14}\text{C}$  and other radionuclides. This study suggests isotopic exchange with solids will be an important  $^{14}\text{C}$  retardation mechanism in subsurface environments, as exchange occurs even when the sediments contain low total inorganic carbon concentrations. These results imply that aqueous, inorganic  $^{14}\text{C}$  released to subsurface environments may persist close to the site of accidental release due to precipitation and solid phase exchange reactions retarding the transport of inorganic  $^{14}\text{C}$  with groundwater.

The results of Chapters 6 and 7 suggest that the ubiquitous and diverse indigenous bacterial phyla are able to utilise  $^{14}\text{C}$ - carboxylates very rapidly under aerobic and denitrification conditions and so will not persist in groundwater environments. However alcohol and aldehyde groups show slightly varied behaviour dependent on the redox condition. Under both aerobic and denitrifying conditions the loss of  $^{14}\text{C}$  from solution was at a similar rate to the carboxylates,

conversely during iron reduction the rate of microbial utilisation appeared reduced implying that it is possible for both  $^{14}\text{C}$ -alcohol and  $^{14}\text{C}$ -aldehyde substances to persist for longer in groundwater environments under those reducing conditions. A further implication is the retention of  $^{14}\text{C}$  in solid fraction, although generally minimal in each fraction ( $\sim 5\%$ ), this mechanism may retard some  $^{14}\text{C}$  movement in groundwater.

### **8.3 Future research**

This project has revealed several areas of possible future research. Due to the long half-life of  $^{14}\text{C}$  this radionuclide has the potential to have a significant impact on site management and particularly the expected site closure dates. The incorporation of the findings of Chapter 5 in to site models at Sellafield site, UK, and elsewhere would allow more accurate prediction of the movement of aqueous, inorganic  $^{14}\text{C}$  plumes by incorporating retention mechanisms which are often overlooked. This work has highlighted the need for analytical improvements, particularly regarding samples which contain both  $^{14}\text{C}$ -DIC and  $^{14}\text{C}$ -DOC as currently there is no direct approach to differentiate between these two aqueous  $^{14}\text{C}$  forms, but it may be possible to exploit their differing chemical properties to allow quantification of both forms from a single aqueous sample.

The consideration of organic  $^{14}\text{C}$  is also an important part of site management, although they are produced at much lower yield than inorganic in waste storage, they have the potential to be a much larger component of waste in geological disposal as well as possibly the more mobile form of  $^{14}\text{C}$  contamination (Jackson and Yates, 2011). This makes understanding their behaviour all the more

essential. To this end an extension of this work may be to consider the impacts of geological disposal conditions on the  $^{14}\text{C}$ -LMWO substances. In the geological disposal environment alternative redox conditions, particularly methanogenesis are likely to dominate, as this project has shown the redox condition does affect the behaviour and persistence of  $^{14}\text{C}$ -LMWO substances.

#### **8.4 References**

Ahad, J.M., Ganeshram, R.S., Spencer, R.G., Uher, G., Gulliver, P., Bryant, C.L., 2006. Evidence for anthropogenic  $^{14}\text{C}$ -enrichment in estuarine waters adjacent to the North Sea. *Geophysical Research Letters* 33.

Fischer, H., Ingwersen, J., Kuzyakov, Y., 2010. Microbial uptake of low-molecular-weight organic substances out-competes sorption in soil. *European Journal of Soil Science* 61, 504-513.

Jackson, C.P., Yates, H., 2011. Key processes and data for the migration of  $^{14}\text{C}$  released from a cementitious repository, Serco Report.

Langmuir, D., 1997. *Aqueous Environmental Geochemistry*. Prentice Hall.

Marshall, A., Coughlin, D., Laws, F., 2015. Groundwater monitoring at Sellafield: Annual data review 2014.

Parry, S.A., O'Brien, L., Fellerman, A.S., Eaves, C.J., Milestone, N.B., Bryan, N.D., Livens, F.R., 2011. Plutonium behaviour in nuclear fuel storage pond effluents. *Energy & Environmental Science* 4, 1457-1464.

Wallace, S.H., Shaw, S., Morris, K., Small, J.S., Fuller, A.J., Burke, I.T., 2012. Effect of groundwater pH and ionic strength on strontium sorption in aquifer

sediments: Implications for  $^{90}\text{Sr}$  mobility at contaminated nuclear sites. *Applied Geochemistry* 27, 1482-1491.

Wang, Z., Hu, D., Xu, H., Guo, Q., 2014.  $^{14}\text{C}$  Distribution in Atmospheric and Aquatic Environments Around Qinshan Nuclear Power Plant, China. *Radiocarbon* 56, 1107-1114.

Yim, M.-S., Caron, F., 2006. Life cycle and management of carbon-14 from nuclear power generation. *Progress in Nuclear Energy* 48, 2-36.

## Appendix A Supporting Information for Chapter 5

### A.1 Tables

Table A-1 Input solution compositions for PHREEQC precipitation modelling.

Predicted Saturation Index	PHREEQC input
+2.92	Temp 20; pH 9; 0.03 M Na <sub>2</sub> CO <sub>3</sub> equilibrated with atmospheric CO <sub>2</sub> (g), 0.02 M CaCl <sub>2</sub>
+2.51	Temp 20; pH 9; 0.015 M Na <sub>2</sub> CO <sub>3</sub> equilibrated with atmospheric CO <sub>2</sub> (g), 0.015 M CaCl <sub>2</sub>
+2.12	Temp 20; pH 9; 0.0075 M Na <sub>2</sub> CO <sub>3</sub> , 0.005 M NaOH equilibrated with atmospheric CO <sub>2</sub> (g), 0.006 M CaCl <sub>2</sub>
+1.58	Temp 20; pH 9; 0.005 M Na <sub>2</sub> CO <sub>3</sub> , 0.005 M NaOH equilibrated with atmospheric CO <sub>2</sub> (g), 0.0015 M CaCl <sub>2</sub>
+0.96	Temp 20; pH 9; 0.0025 M Na <sub>2</sub> CO <sub>3</sub> , 0.005 M NaOH equilibrated with atmospheric CO <sub>2</sub> (g), 0.0005 M CaCl <sub>2</sub>
+0.48	Temp 20; pH 9; 0.0025 M Na <sub>2</sub> CO <sub>3</sub> , 0.005 M NaOH equilibrated with atmospheric CO <sub>2</sub> (g), 0.00015 M CaCl <sub>2</sub>
+0.01	Temp 20; pH 9; 0.0025 M Na <sub>2</sub> CO <sub>3</sub> , 0.005 M NaOH equilibrated with atmospheric CO <sub>2</sub> (g), 0.00005 M CaCl <sub>2</sub>
-0.98	Temp 20; pH 9; 0.0025 M Na <sub>2</sub> CO <sub>3</sub> , 0.005 M NaOH equilibrated with atmospheric CO <sub>2</sub> (g), 0.000005 M CaCl <sub>2</sub>

### A.2 Determining the value of the rate constant ( $k_{r2}$ )

The key equation, Equation S1 below, allows a  $k_{obs}$  value to be calculated for different pH using the rate constant which is then substituted into the first

order rate equation to find values for  $[^{14}\text{C}]$  at defined time points. The experimental data are plotted with the modelled loss curves (main text, Section 4.2, Figure 5) using this technique.

$$k_{\text{obs}} = \frac{k_{r2}}{\left(1 + \frac{K_{a1}}{[\text{H}^+]} + \frac{K_{a1}K_{a2}}{[\text{H}^+]^2}\right)} \quad \text{Equation A-1}$$

$K_{\text{obs}}$  is a function of the outgassing rate and pH dependent partitioning of  $^{14}\text{C}$  between the aqueous carbonate phases

$$k_{r2} = k_{\text{obs}} \cdot \left(1 + \frac{K_{a1}}{[\text{H}^+]} + \frac{K_{a1}K_{a2}}{[\text{H}^+]^2}\right) \quad \text{Equation A-2}$$

Table A-2 Calculated values of  $k_{r2}$  using Equation S2 and  $k_{\text{obs}}$  values.

pH	$K_{\text{obs}}$	Calculated values	$k_{r2}$
7.2	0.254	1000	
7.8	0.060	1000	
8.8	0.028	5000	
9.3	0.008	5000	
10.5	0.004	10,000	
12.6	0.002	$2 \times 10^8$	

By inputting the  $k_{\text{obs}}$  values from the experimental data into Equation S2 a series of possible  $k_{r2}$  values were obtained, for the purpose of this study  $k_{r2} = 4500 \text{ hr}^{-1}$  has been applied to model the experimental data (see main text, Section 4.2).

### **A.3 Solution compositions for input files for PHREEQC modelling**

SOLUTION 1 SWALLACE et al (2012) – site data

pH 9 charge;units g/L; Na 0.31;N 0.57;C 0.12 CO2(g) -3.5;S 0.02;end

SOLUTION 2 Theoretical composition when groundwater equilibrated with MgCO<sub>3</sub>

pH 9 charge;units g/L; Na 0.31;N 0.57;C 0.18 CO2(g) -3.5;S 0.02; Mg 0.03; end

SOLUTION 3 Groundwater composition of well near to leak source – site data

Ph 6.5 ;UNITS mg/L; K 4.3; Na 25;Ca 38; Mg 5; Cl 57 charge ; S 20; N 20; C 75 CO2(g)

-3.5;end

### **A.4 Calculating the thickness of the calcite surface layer**

Isotopic exchange between a solution and a solid phase is likely to be surface, or near surface phenomena. The nominal thickness of the surface layer of calcite involved in isotope exchange with DIC has been estimated by assuming that, at equilibrium, the isotope ratio in the active layer is equal to the isotope ratio in the solution. Further it is assumed that net exchange of a proportion,  $X$ , of the <sup>14</sup>C initially in solution corresponds to net exchange of same proportion of the carbonate species initially in solution (i.e. isotope exchange across the solid solution boundary occurs as a result of dynamic equilibrium between dissolution and precipitation reactions).

If the concentration of aqueous carbonate species in isotope exchange experiments is  $[C_{(aq,carb)}]$ , then net exchange of the proportion,  $X$ , of the <sup>14</sup>C initially in solution corresponds to net exchange of  $X \cdot [C_{(aq,carb)}]$  mM of carbonate. This corresponds to  $X \cdot [C_{(aq,carb)}] \cdot m_w$  g/L of calcium carbonate (where  $m_w$  is the molar mass of calcium carbonate in g/mol). If that calcium carbonate precipitates as calcite it will have a volume of  $X \cdot [C_{(aq,carb)}] \cdot m_w / \rho_{calcite}$  cm<sup>3</sup>/L (where  $\rho_{calcite}$  is the density of calcite in g/cm<sup>3</sup>). If the mass of calcite per unit volume of solution is  $m_{calcite}$  (g/L), and this has a specific surface area of  $A_{calcite}$  (cm<sup>2</sup>/g), then the calcite surface area per unit volume is  $m_{calcite} \cdot A_{calcite}$  (cm<sup>2</sup>/L). Thus, the thickness,  $\delta$  (cm), of the active layer involved in solid phase isotope exchange is:

$$\delta = (X \cdot [C_{(\text{aq,carb})}] \cdot m_w) / (\rho_{\text{calcite}} \cdot m_{\text{calcite}} \cdot A_{\text{calcite}})$$

The isotope exchange experiments were equilibrated with a solution containing 1.25 mM  $\text{HCO}_3^-/\text{CO}_3^{2-}$ . This concentration was substantially unchanged by addition of the  $^{14}\text{C}$  spike. Calcite has a density of 2.711 g/cm<sup>3</sup> and molecular weight of 100.09 g/mol. The measure SSA of the calcite,  $A_{\text{calcite}}$ , used in the solid phase isotopic exchange experiments is 2900 cm<sup>2</sup>/g. Thus, in the systems containing 20 and 50 g/L of calcite, where 10% and 30% of the  $^{14}\text{C}$  DIC was exchanged onto the solid, the nominal thickness of the surface layer of calcite involved in isotope exchange is  $0.80 \times 10^{-7}$  cm = 8.0 Å and  $0.95 \times 10^{-7}$  cm = 9.5 Å.

## Appendix B Supporting information for Chapter 6

### B.1 Experimental results for open flask experiments

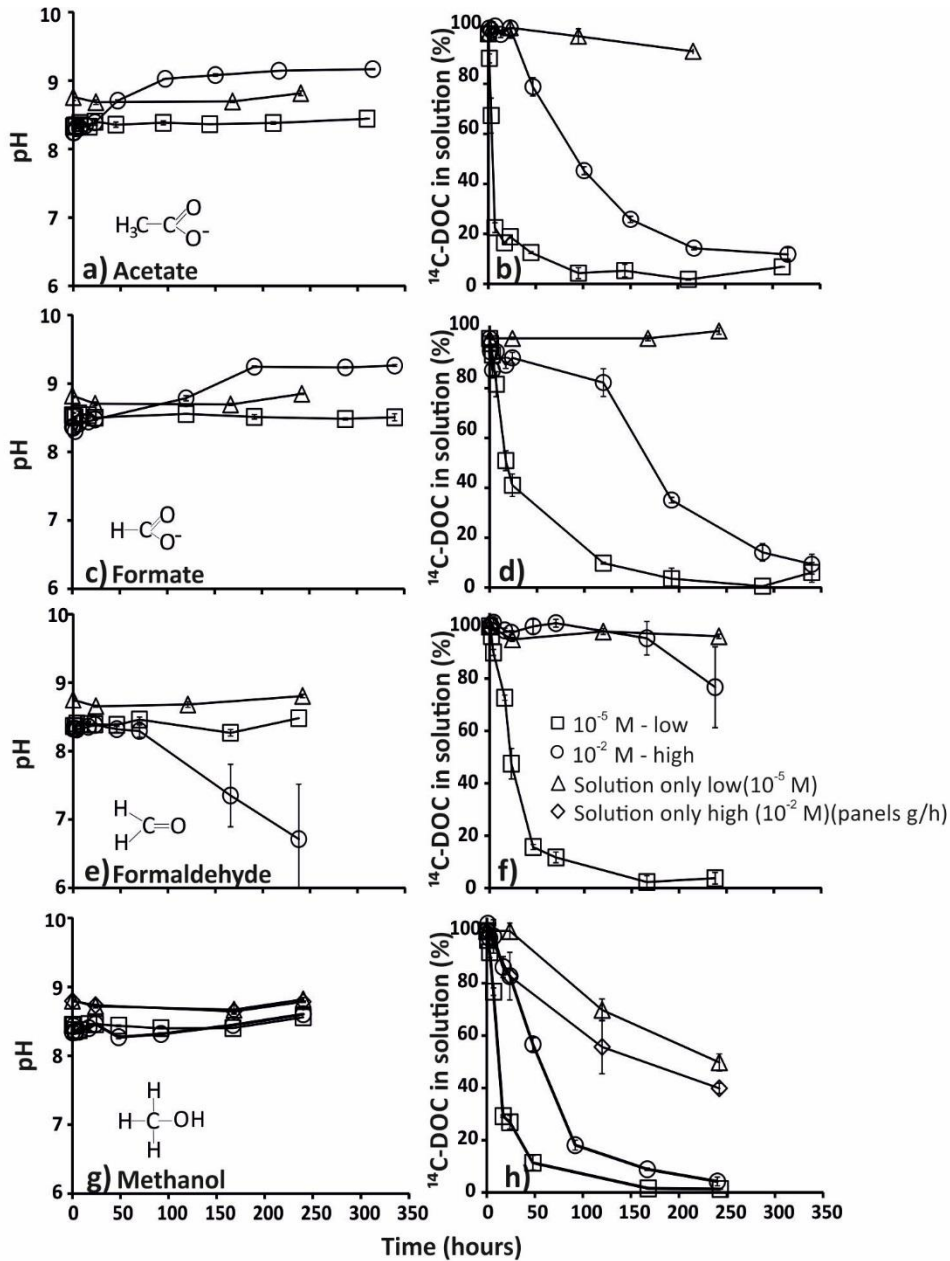


Figure B 1 Experimental results from open flask experiments showing the evolution of pH and <sup>14</sup>C-DOC activity with time in (a, b) <sup>14</sup>C-acetate amended experiments; (c, d) <sup>14</sup>C-formate amended experiments; (e, f) <sup>14</sup>C-formaldehyde amended experiments and, (g, h) <sup>14</sup>C-methanol amended experiments. Error bars denote one standard deviation of triplicate measurements; where not shown, error bars are less than the size of the symbols used.

## Appendix C Supporting information for Chapter 7

### C.1 Experimental results for complete experimental run

#### C.1.1 Nitrate amended microcosms

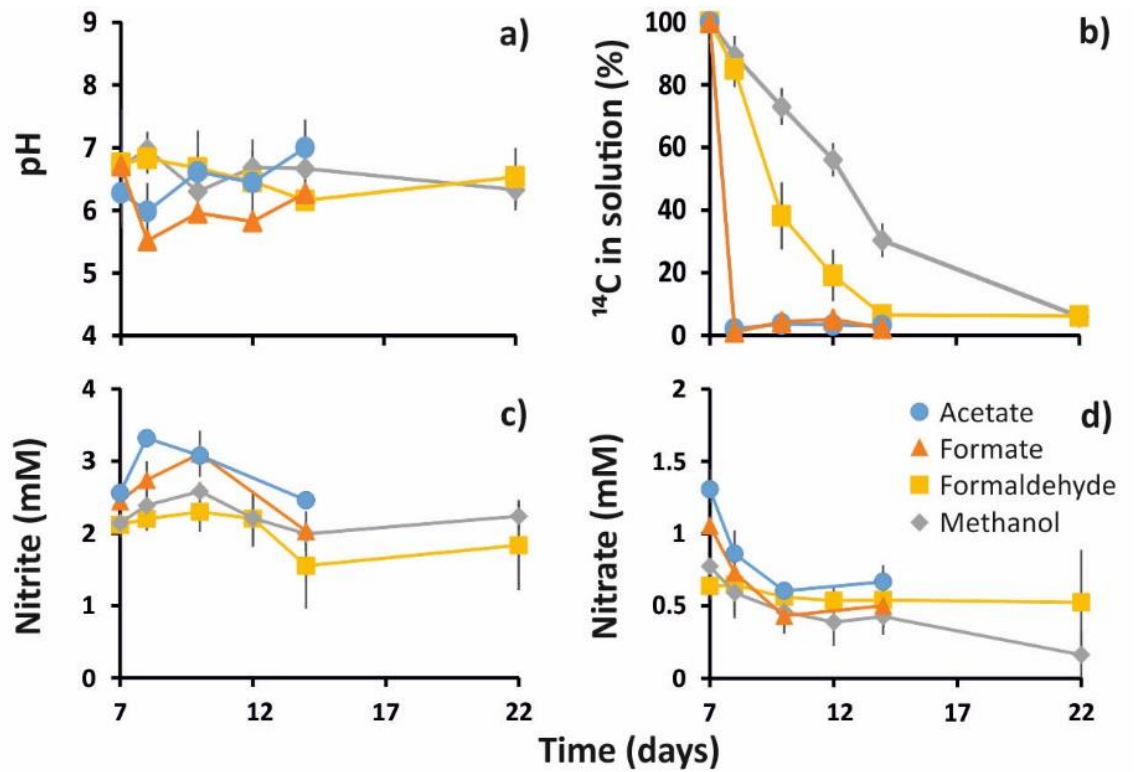


Figure C 1 The results of the denitrification experiments a) pH; b) percentage of <sup>14</sup>C in solution; c) concentration of nitrite in solution; d) concentration of nitrate in solution (original nitrate addition = 10mM, t=7 indicates time of <sup>14</sup>C addition). Experiment duration from day 7 to day 14 (acetate and formate) continuing to day 22 for formaldehyde and methanol. Error bars denote one standard deviation of triplicate measurements; where not shown error bars are less than the size of the symbol used.

C.1.2 Iron reducing microcosms

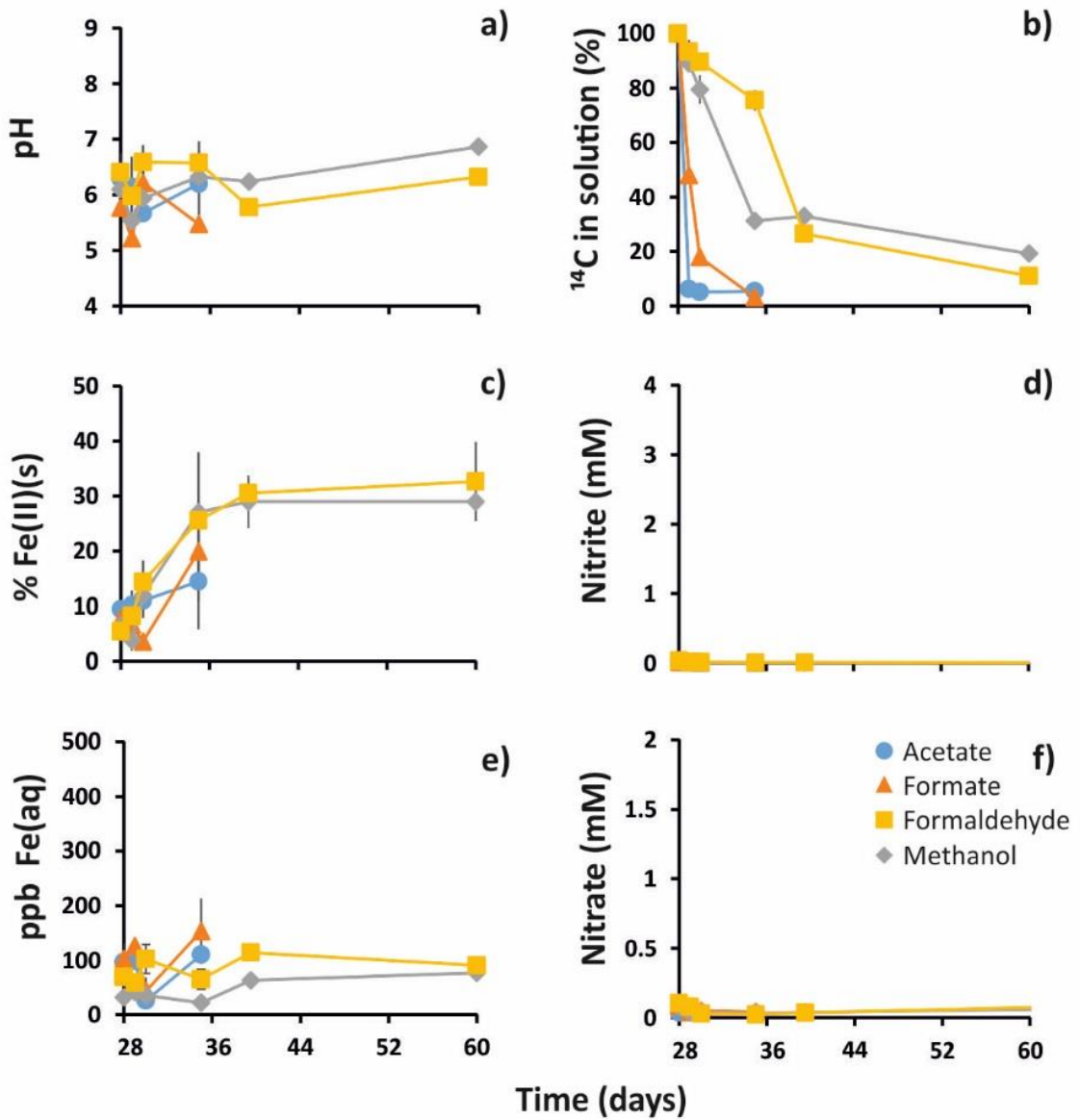


Figure C 2 The results of the iron-reducing experiments a) pH; b) percentage of <sup>14</sup>C remaining in solution; c) fraction of Fe(II) in solids; d) concentration of nitrite; e) concentration of Fe(II) in solution; f) concentration of nitrate. Experiment duration from day 28 to day 35 (acetate and formate) continuing to day 60 for formaldehyde and methanol. Error bars denote one standard deviation of triplicate measurements; where not shown error bars are less than the size of the symbol used.

## C.2 Sterile control figures

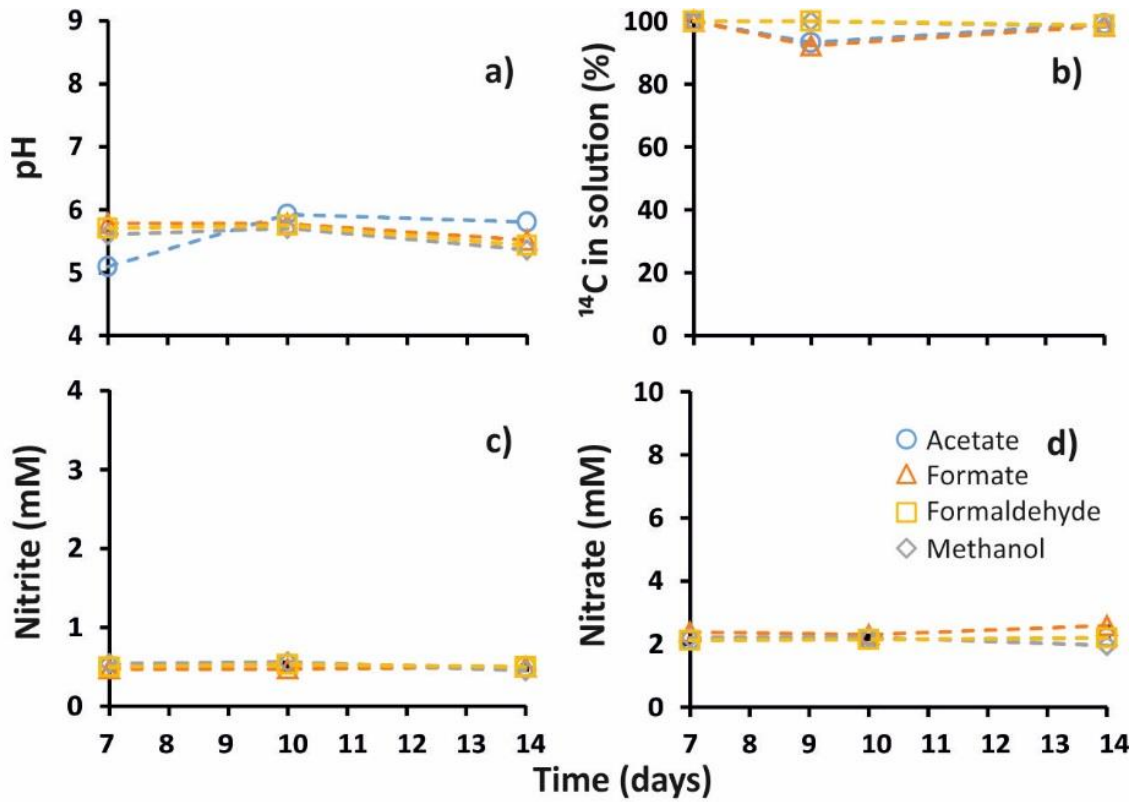


Figure C-3 The results of the denitrification control experiments a) pH; b) percentage of <sup>14</sup>C in solution; c) concentration of nitrite in solution; d) concentration of nitrate in solution (original nitrate addition = 10mM, t=7 indicates time of <sup>14</sup>C addition). Experiment duration from day 7 to day 14.

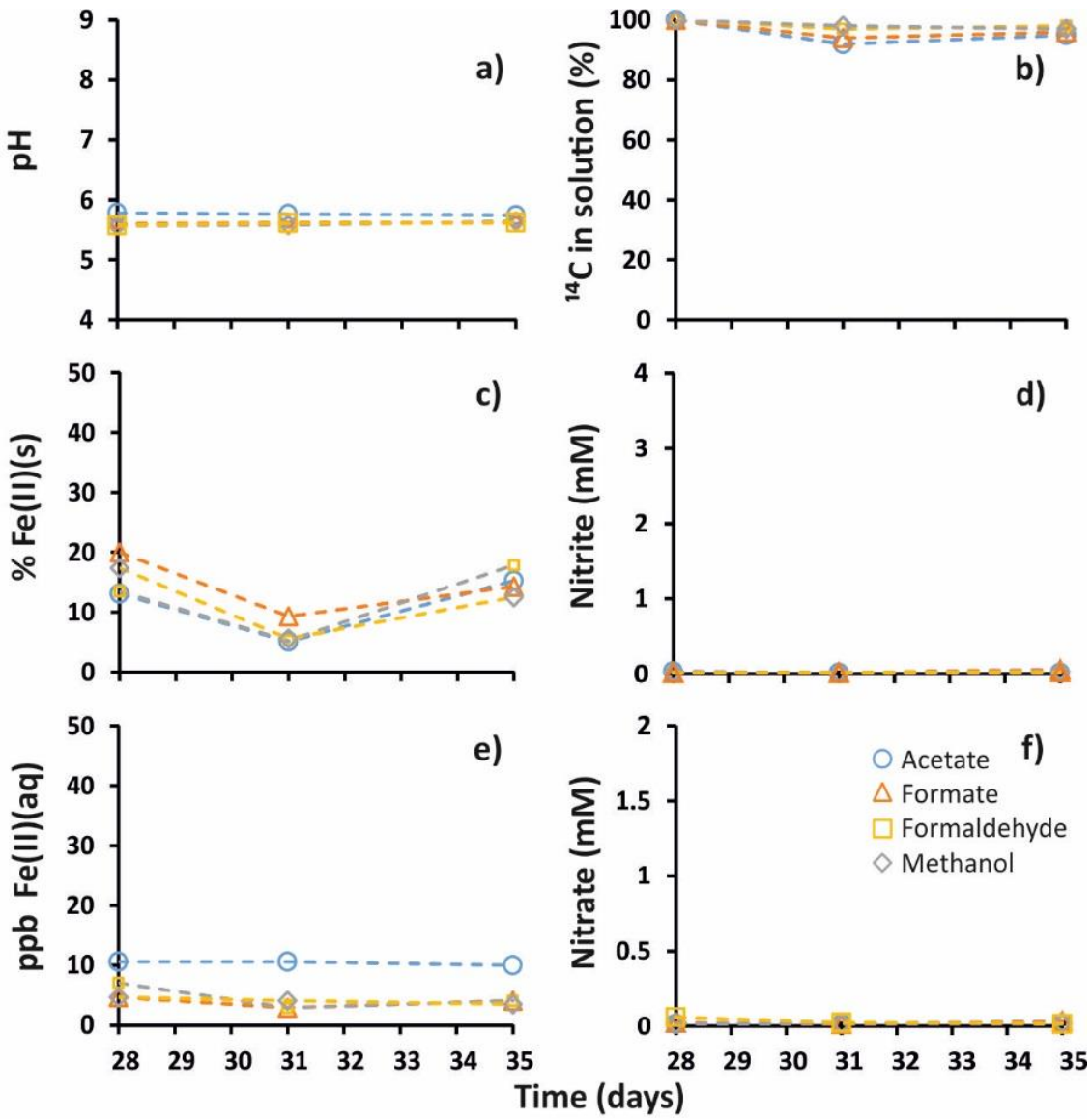


Figure C-4 The results of the iron-reducing control experiments a) pH; b) percentage of  $^{14}\text{C}$  remaining in solution; c) fraction of Fe(II) in solids; d) concentration of nitrite; e) concentration of Fe(II) in solution; f) concentration of nitrate. Experiment duration from day 28 to day 35.

### C.3 Siderite precipitation

Table C-1 Input solution composition for siderite precipitation model.

Solution composition	g/L in DIW
pH	6.7
pe	0
KCl	0.006
MgSO <sub>4</sub> ·7H <sub>2</sub> O	0.0976
MgCl <sub>2</sub> ·6H <sub>2</sub> O	0.081
NaCl	0.0094
Fe(II)	0.02
C as CO <sub>3</sub> <sup>2-</sup>	0.02

Geochemical modelling was undertaken using the PHREEQC (version 3) geochemical speciation program (Parkhurst and Appelo, 2013) and the Hatches database (version 18) (Cross and Ewart, 1991). Siderite saturation index predicted to be +0.02 under these conditions.

### C.4 References

Cross, J.E., Ewart, F.T., 1991. Hatches — A Thermodynamic Database And Management System. *Radiochimica Acta* 52-53, 421-422.

Parkhurst, D.L., Appelo, C.A.J., 2013. Description of input and examples for PHREEQC version 3- A computer program for speciation, batch-reaction, one-dimensional transport, and inverse geochemical calculations, U.S. Geological Survey Techniques and Methods, p. 497.

## Appendix D PHREEQC modelling code

### D.1 Note for users

The following input files are designed to be run in PHREEQC (version 3) (Parkhurst and Appelo, 2013) with the Hatches database (version 18) (Cross and Ewart, 1991). They can be copied and pasted to produce the data which has been used in Chapters 5 and 7.

### D.2 PHREEQC code

#### D.2.1 To establish the solution compositions required to obtain the desired $SI_{CAL}$ values

```
PRINT
```

```
SELECTED_OUTPUT 1
```

```
-reset false;-file Hoppt.xl;-si calcite;-pH; totals Na Ca Cl C(4);-pe;-alkalinity;
```

```
SOLUTION 1;TEMP 20; pH 9 CHARGE;units mol/L;Na 0.06;C(4) 0.03 CO2(g) -3.5;end
```

```
SOLUTION 2;temp 20;pH 9 charge; units mol/L;Ca 0.02;Cl 0.04;end
```

```
MIX 10 3.0
```

```
19 0.5;20 0.5;end
```

```
SOLUTION 3;temp 20;pH 9 charge; units mol/L;Na 0.03;C(4) 0.015 CO2(g) -3.5;end
```

```
SOLUTION 4;temp 20;pH 9 charge;units mol/L;Ca 0.015;Cl 0.03;end
```

```
MIX 11 2.5
```

```
21 0.5;22 0.5;end
```

```
SOLUTION 5;temp 20;pH 9 charge;units mol/L;Na 0.02;C(4) 0.0075 CO2(g) -3.5;end
```

```
SOLUTION 6;temp 20;pH 9 charge;units mol/L;Ca 0.006;Cl 0.012;end
```

```
MIX 12 2.0
```

```
23 0.5;24 0.5;end
```

SOLUTION 7;TEMP 20;pH 9 charge;units mol/L;Na 0.015;C(4) 0.005 CO2(g) -3.5;end

SOLUTION 8;temp 20;pH 9 charge;units mol/L;Ca 0.0015;Cl 0.003;end

MIX 13 1.5

25 0.5; 26 0.5;end

SOLUTION 9;temp 20;pH 9 charge;units mol/L;Na 0.01;C(4) 0.0025 CO2(g) -3.5;end

SOLUTION 10;temp 20;pH 9 charge;units mol/L;Ca 0.0005;Cl 0.001;end

MIX 14 1.0

27 0.5; 28 0.5;end

SOLUTION 11;temp 20;pH 9 charge;units mol/L;Na 0.01;C(4) 0.0025 CO2(g) -3.5;end

SOLUTION 12;temp 20;pH 9 charge;units mol/L;Ca 0.00015; Cl 0.0003;end

MIX 15 0.5

29 0.5; 30 0.5;end

SOLUTION 13;temp 20;pH 9 charge; units mol/L;Na 0.01;C(4) 0.0025 CO2(g) -3.5;end

SOLUTION 34;temp 20;pH 9 charge;units mol/L;Ca 0.00005;Cl 0.0001;end

MIX 16 0.0

31 0.5;32 0.5;end

SOLUTION 15 ;temp 20;pH 9 charge;units mol/L;Na 0.01;C(4) 0.0025 CO2(g) -3.5;end

SOLUTION 16;temp 20;pH 9 charge;units mol/L;Ca 0.000005;Cl 0.00001;end

MIX 17 -1.0

33 0.5;34 0.5;end

**D.2.2 To investigate the variation of  $SI_{CAL}$  with calcium concentration, carbonate alkalinity and pH**

PRINT

SELECTED\_OUTPUT 1;-reset false

-file TalkCa.xl;-totals Ca C(4);-alkalinity;-pH;-percent error;END

PHASES

Fix\_ph;H+ = H+;log\_k 0.0

#pH 7

#SI 0

solution 1;temp 20; pH 7 ;units mol/L;Na 0.02;C(4) 0.01 ;Ca 0.1;Cl 0.2;

equilibrium\_phases

calcite 0 0 precipitate\_only

-force\_equality

Fix\_ph -7.0 HCl

end

solution 2;temp 20; pH 7 ;units mol/L;Na 0.035;C(4) 0.0175 ;Ca 0.1;Cl 0.2;

equilibrium\_phases

calcite 0 0 precipitate\_only

-force\_equality

Fix\_ph -7.0 HCl

end

solution 3;temp 20; pH 7 ;units mol/L;Na 0.2;C(4) 0.1 ;Ca 0.01;Cl 0.12;

equilibrium\_phases

calcite 0 0 precipitate\_only

-force\_equality

Fix\_ph -7.0 HCl

end

#SI 1.5

solution 4;temp 20;pH 7;units mol/L;Na 0.2;C(4) 0.1;Ca 1;Cl 2;

equilibrium\_phases

calcite 1.5 0 precipitate\_only

-force\_equality

Fix\_ph -7.0 HCl

end

solution 5;temp 20;pH 7;units mol/L;Na 2;C(4) 1;Ca 0.01;Cl 0.02;

equilibrium\_phases

calcite 1.5 0 precipitate\_only

-force\_equality

Fix\_ph -7.0 HCl

end

#pH 9

#SI 0

solution 2;temp 20; pH 9 ;units mol/L;Na 0.11;C(4) 0.1 ;Ca 0.00001;Cl 0.00002;

equilibrium\_phases

calcite 0 0 precipitate\_only

-force\_equality

Fix\_ph -9.0 NaOH

end

solution 3;temp 20; pH 9 ;units mol/L;Na 0.01;C(4) 0.01 ;Ca 0.0001;Cl 0.0002;

equilibrium\_phases

```
calcite 0 0 precipitate_only  
-force_equality  
Fix_ph -9.0 NaOH  
end
```

```
solution 3.1;temp 20; pH 9 ;units mol/L;Na 0.005;C(4) 0.005 ;Ca 0.0005;Cl 0.001;  
equilibrium_phases  
calcite 0 0 precipitate_only  
-force_equality  
Fix_ph -9.0 NaOH  
end
```

```
solution 4;temp 20; pH 9 ;units mol/L;Na 0.001;C(4) 0.001 ;Ca 0.001;Cl 0.002;  
equilibrium_phases  
calcite 0 0 precipitate_only  
-force_equality  
Fix_ph -9.0 NaOH  
end
```

```
solution 4.1;temp 20; pH 9 ;units mol/L;Na 0.0005;C(4) 0.0005 ;Ca 0.005;Cl 0.01;  
equilibrium_phases  
calcite 0 0 precipitate_only  
-force_equality  
Fix_ph -9.0 NaOH  
end
```

```
solution 5;temp 20; pH 9 ;units mol/L;Na 0.0001;C(4) 0.0001 ;Ca 0.01;Cl 0.02;  
equilibrium_phases
```

calcite 0 0 precipitate\_only

-force\_equality

Fix\_ph -9.0 NaOH

end

solution 6;temp 20; pH 9 ;units mol/L;Na 0.00001;C(4) 0.00001 ;Ca 0.1;Cl 0.2;

equilibrium\_phases

calcite 0 0 precipitate\_only

-force\_equality

Fix\_ph -9.0 NaOH

#SI 1.5

solution 2;temp 20; pH 9 ;units mol/L;Na 0.11;C(4) 0.1 ;Ca 0.001;Cl 0.002;

equilibrium\_phases

calcite 1.5 0 precipitate\_only

-force\_equality

Fix\_ph -9.0 NaOH

end

solution 2.5;temp 20; pH 9 ;units mol/L;Na 0.05;C(4) 0.05 ;Ca 0.0005;Cl 0.001;

equilibrium\_phases

calcite 1.5 0 precipitate\_only

-force\_equality

Fix\_ph -9.0 NaOH

end

solution 3;temp 20; pH 9 ;units mol/L;Na 0.011;C(4) 0.01 ;Ca 0.01;Cl 0.02;

equilibrium\_phases

calcite 1.5 0 precipitate\_only

-force\_equality

Fix\_ph -9.0 NaOH

end

solution 3.1;temp 20; pH 9 ;units mol/L;Na 0.0075;C(4) 0.0075 ;Ca 0.025;Cl 0.05;

equilibrium\_phases

calcite 1.5 0 precipitate\_only

-force\_equality

Fix\_ph -9.0 NaOH

end

solution 3.2;temp 20; pH 9 ;units mol/L;Na 0.005;C(4) 0.005 ;Ca 0.05;Cl 0.1;

equilibrium\_phases

calcite 1.5 0 precipitate\_only

-force\_equality

Fix\_ph -9.0 NaOH

end

solution 4;temp 20; pH 9 ;units mol/L;Na 0.002;C(4) 0.001 ;Ca 0.1;Cl 0.2;

equilibrium\_phases

calcite 1.5 0 precipitate\_only

-force\_equality

Fix\_ph -9.0 NaOH

end

#pH 11

#SI 0

solution 3 ;temp 20; pH 11;units mol/L;Na 0.00012;C(4) 0.00001 ;Ca 1;Cl 2;

equilibrium\_phases

calcite 0 0 precipitate\_only

-force\_equality

Fix\_ph -11.0 NaOH

end

solution 4 ;temp 20; pH 11;units mol/L;Na 0.0002;C(4) 0.0001 ;Ca 0.01;Cl 0.02;

equilibrium\_phases

calcite 0 0 precipitate\_only

-force\_equality

Fix\_ph -11.0 NaOH

end

solution 5 ;temp 20; pH 11;units mol/L;Na 0.0025;C(4) 0.001 ;Ca 0.001;Cl 0.002;

equilibrium\_phases

calcite 0 0 precipitate\_only

-force\_equality

Fix\_ph -11.0 NaOH

end

solution 6 ;temp 20; pH 11;units mol/L;Na 0.02;C(4) 0.01 ;Ca 0.0001;Cl 0.0002;

equilibrium\_phases

calcite 0 0 precipitate\_only

-force\_equality

Fix\_ph -11.0 NaOH

end

solution 7;temp 20; pH 11;units mol/L;Na 0.2;C(4) 0.1 ;Ca 0.0001;Cl 0.0002;

equilibrium\_phases

calcite 0 0 precipitate\_only

-force\_equality

Fix\_ph -11.0 NaOH

end

### **D.2.3 To model potential leach scenarios relevant to Sellafield Reprocessing site, UK**

solution 1 SWALLACE et al (2012)

pH 9 charge;units g/L; Na 0.31;N 0.57;C 0.12 CO2(g) -3.5;S 0.02;end

solution 3 Theoretical composition when groundwater equilibrated with MgCO3

pH 9 charge;units g/L; Na 0.31;N 0.57;C 0.18 CO2(g) -3.0;S 0.02;

equilibrium\_phases

MgCO3 0 10

save solution 3

end

SOLUTION 2 10202 GW

Ph 6.5 ;UNITS mg/L; K 4.3; Na 25;Ca 38; Mg 5; Cl 57 charge ; S 20; N 20; C 75 CO2(g) -3.5;end

MIX 1;1 0.00;2 1.0;end

MIX 2;1 0.01;2 0.99;end

MIX 3;1 0.05;2 0.95;end

MIX 4;1 0.10;2 0.90;end

MIX 5;1 0.2;2 0.8;end

MIX 6;1 0.3;2 0.7;end

MIX 7;1 0.4;2 0.6;end

MIX 8;1 0.5;2 0.5;end

MIX 9;1 0.6;2 0.4;end

MIX 10;1 0.7;2 0.3;end

MIX 11;1 0.8;2 0.2;end

MIX 12;1 0.9;2 0.1;end

MIX 13;1 0.95;2 0.05;end

MIX 14;1 0.99;2 0.01;end

MIX 15;1 1.0;2 0.0;end

MIX 1;3 0.00;2 1.0;end

MIX 2;3 0.01;2 0.99;end

MIX 3;3 0.05;2 0.95;end

MIX 4;3 0.10;2 0.90;end

MIX 5;3 0.2;2 0.8;end

MIX 6;3 0.3;2 0.7;end

MIX 7;3 0.4;2 0.6;end

MIX 8;3 0.5;2 0.5;end

MIX 9;3 0.6;2 0.4;end

MIX 10;3 0.7;2 0.3;end

MIX 11;3 0.8;2 0.2;end

MIX 12;3 0.9;2 0.1;end

MIX 13;3 0.95;2 0.05;end

MIX 14;3 0.99;2 0.01;end

MIX 15;3 1.0;2 0.0;end

## **D.2.4 Modelling siderite precipitation**

solution 1

pH 6.7 ;pe 0;units g/L; K 0.003; Mg 0.03; Cl 0.07; S(6) 0.04; Na 0.004; C 0.02 ; Fe(2) 0.02;  
end

#use solution 1

### **D.3       References**

Cross, J.E., Ewart, F.T., 1991. Hatches — A Thermodynamic Database And Management System. *Radiochimica Acta* 52-53, 421-422.

Parkhurst, D., Appelo, C., 2013. PHREEQC (Version 3)—A computer program for speciation, batch-reaction, one-dimensional transport, and inverse geochemical calculations. US Geological Survey: The United States.

## **Appendix E      Presentations**

This appendix gives a summary of all presentations given during the course of the tenure of this PhD.

### **E.1              Oral presentations**

June 2016 Yokohama, Japan – **Invited talk at Goldschmidt international geochemistry conference**

January 2016 Burlington House, London RSC Radiochemistry group, – **Frontiers of Environmental Radioactivity** – Talk given as part of a wide-ranging series giving an overview of work currently undertaken in Environmental Radioactivity.

April 2016 Glasgow University – Talk given to **Coordinating Group of Environmental Radioactivity (COGER)**

March 2016 **Geochemistry Group Research in Progress meeting**, University of Leeds – Talk given to non-specialist audience

May 2015, Manchester – Talk given at the **Young Researcher's Meeting of the Environmental Radioactivity Network**

April 2015, British Geological Society, Nottingham – Talk given at the **Coordinating Group of Environmental Radioactivity (COGER)**

June 2015 **National Nuclear Laboratory, Birchwood, UK** – Talk given to non-specialists from all departments of the company.

## **E.2 Poster presentations**

October 2016 Burlington House, London - Poster presentation **Radio Chem50**

June 2015 **Mineralogical Society**, University of Leeds – Poster presentation given at Research in Progress meeting

September 2014 Bath, UK – Poster presentation at **ERA12 conference** on radioactivity in the environment